Durham E-Theses

Photobiomodulation with IR1072nm in the murine CNS: in vitro and in vivo studies

BURROUGHS, STEPHANIE,LOUISE

Photobiomodulation with IR1072nm in the murine CNS:

in vitro and *in vivo* studies

Stephanie Louise Burroughs

A thesis submitted to the University of Durham in accordance with the requirements for the degree of Doctor of Philosophy

School of Biological and Biomedical Sciences

2010

Supervisor: Dr. Paul Chazot

Abstract

Photobiomodulation refers to low-intensity light therapy (LILT) in the far-red to near-infrared (IR) region of the spectrum (630-1000nm). A peak wavelength, 1072nm (IR1072), in the IR transmission spectrum has been previously shown to have protective effects against UVA toxicity in human lymphocytes and beneficial effects on working memory in IR-treated 12 month old CD-1 mice. The aim of this investigation was to establish the beneficial effects of IR1072 in the murine mammalian CNS utilising a range of *in vivo* and *in vitro* model systems. Acute treatment of primary rat neuronal cultures with IR1072 endowed an insult severity-dependent protective effect; the less severe the insult the more profound the protection. An age-dependent (3 month to 12 month) reduction in brain derived neurotrophic factor (BDNF) and heat shock protein HSP27, and HSP40 and HSP90 was observed in both CD-1 and TASTPM Alzheimer disease mice, which may underlie the severe learning deficits seen in these mice. Acute whole body treatments of CD-1 mice *in vivo* comprising ten consecutive daily 6 minute sessions of IR1072 elicited increased mitochondrial complex II enzyme activity. Long-term chronic *in vivo* IR1072 treatments in CD-1 mice, consisting of biweekly 6 minutes sessions spanning a 5 month period, increased expression of selective HSPs, notably HSP27 in cortical and hippocampal regions. Following chronic IR1072 treatment, a profound reduction of AMPA receptor binding sites in CD-1 mice, and reduced total $A\beta_{1-42}$ expression and small amyloid plaque counts (in cortex and dentate gyrus) in TASTPM mice, was observed. Overall, this thesis reveals new mechanisms of photobiomodulation with IR1072 which involves restoring cellular homeostasis for optimal functional operation of a neuron.

<u>Acknowledgements</u>

This thesis would not have been possible without the help and support of my colleagues in the University of Durham.

I am especially indebted to Dr. Paul Chazot, whose seemingly inexhaustible encouragement, guidance and long hours of supervision proved invaluable throughout the course of this research.

I would also like to express my appreciation to Dr. Abdel Ennaceur and my fellow lab members, and in particular to Natasha Lethbridge, both for acting as an extra pair of hands and for our many conversations whilst undertaking long hours of laboratory work.

Finally, I wish to thank my family and friends for their enduring patience and support over the past four years.

Declaration

I confirm that no part of the material presented has previously been submitted for a degree in this or any other university. If material has been generated through joint work, my independant contribution has been clearly indicated. In all other cases, material from the work of others has been clearly indicated, acknowledged and quotations and paragraphs indicated.

The copyright of this thesis rests with the author. No quotation from it should be published without prior consent and information derived from it should be acknowledged.

Table of Contents

Abbreviations

2α-amino-3-hydroxy-5-methyl-4-isoxazolepropionic acid	AMPA
3,3-Diaminobenzidine	DAB
90 kDa ribosomal protein S6 kinases	RSK90
β-amyloid	Aβ
Adenosine 5'Diphosphate	ADP
Adenosine 5'Triphosphate	ATP
Adrenocorticotrophic Hormone	ACTH
Alzheimer's Disease	AD
Amyloid Precursor Protein	APP
Antibody	Ab
Apoptosis Antigen-1	FAS
Apoptosis Inducing factor	AIF
B-cell Lymphoma 2	Bcl-2
Bcl-2 Associated Death Protein	BAD
Bcl-2 Associated X Protein	BAX
BH3-only Proteins	BIM/jBID
Bovine Serum Albumin	BSA
Brain Derived Neurotrophic Factor	BDNF
c-Jun N-terminal Kinase	JNK
Ca2+/calmodulin-dependent kinase II	CAMKII
cAMP Response Element Binding Protein	CREB
Caudate Putamen	CPu
CD-1 Age Timeline	CD-1 TL
Central Nervous System	CNS
Cerebral cortex	Ctx
Cerebellum	Cb
Cornu Ammonis	CA
Cyclic Adenosine Monophosphate	cAMP
Cysteine Aspartic Specific Proteases	Caspases

Cytochrome *c*	Cyt *c*
Days *In Vitro*	DIV
Dentate Gyrus	DG
Deoxyribonucleic Acid	DNA
Dithiothreitol	DTT
Drosophila Melanogaster Homologue	DIABLO
Electromagnetic	EM
Electron Transport Chain	ETC
Ethylenediaminetetraacetic Acid	EDTA
Ethyleneglycotetraacetic Acid	EGTA
Exposure Buffer Solution	EBS
Extracellular Signal Regulated Kinase	ERK
Fas-associated Death Domain	FADD
Fas Ligand	FasL
Flavine Adenine Dinucleotide	FAD
Foetal Calf Serum	FCS
Forkhead	FKHRL1
G-protein Coupled Receptors	GPCRs
Gamma-aminobutyric Acid	GABA
Glial Derived Neurotrophic Factor	GDNF
Glutamate Receptor 2	GluR2
Glutathione	GSH
Glycogen Synthase Kinase	GSK3
Hank's Buffered Saline Solution	HBSS
Heat Shock Factors	HSF
Heat Shock Protein	HSP
Horse Radish Peroxidase	HRP
Inducible NO-Synthase	iNOS
Infrared	IR
IR Wavelength 1072nm	IR1072
Potassium Thiocyanate	KSCN
Light Emmiting Diodes	LED

Long Term Potentiation	LTP
Low-intensity Light Therapy	LILT
Mammalian Target of Rapamycin	mTOR
MAPK/ERK Kinase	MEK
Messenger RNA	mRNA
Misfolded Proteins	MF
Mitochondria Permeability Transition Pore	MPTP
Mitochondrial DNA	mtDNA
Mitochondrial Membrane Potential	MMP
Mitogen Activated Protein Kinase	MAPK
N-methyl-D-aspartate	NMDA
Neurofibrillary Tangles	NFT
Nicotinamide Adenine Dinucleotide	NAD
Nitric Oxide	NO
Nitric Oxide Synthase	NOS
Olfactory Ensheathing Cells	OEC
Phosphate Buffered Saline	PBS
Phosphatidylinositol 3-Kinase	PI3K
Phosphoinositide-dependent Kinase 1 and 2	PDK1/2,
Phospholipase Cg	PLC-g
Potassium Thiocyanate	KSCN
Poylmerase Chain Reaction	PCR
Protease Inhibitor Cocktail III	PICIII
Protein Kinase B	AKT
Rabbit	Rb
Reactive Oxygen Species	ROS
Reduction-oxidation	Redox
Respiratory Control Index	RCI
Ribonucleic Acid	RNA
Room Temperature	RT
S-6 Kinase	RSK
Sea, Air and Land	SEAL

Second Mitochondrial-derived Activator of Caspases	SMAC
Serum Amyoid Assay	SAA
Sodium Dodecyl Sulphate	SDS
Sprague-Dawley	SEM
TASTPM Age Timeline	ADTL
Tetramethylethylenediamine	TEMED
Toxin 2,3,7,8-tetrachlorodibenzo-p-dioxin	TCDD
Tricarboxylic Acid	TCA
Tris Buffered Saline	TBS
Tumour Necrosis Factor Receptors	TNFR
Tyrosine Protein Kinase Receptor	TRK
Ubiquitin-proteasome System	UPS
Ultraviolet	UV
Wild Type	WT

Chapter 1: Literature Review and aims

1.1 Photobiomodulation

1.1.1 EM spectrum

Electromagnetic (EM) waves are photons of light that exhibit electrical and magnetic properties that vibrate at different rates resulting in differing photon energy and wavelengths (Enwemeka, 2004). The EM spectrum includes radio waves, infrared (IR) radiation, visible light, ultraviolet rays, x-rays, gamma rays, and cosmic radiation.
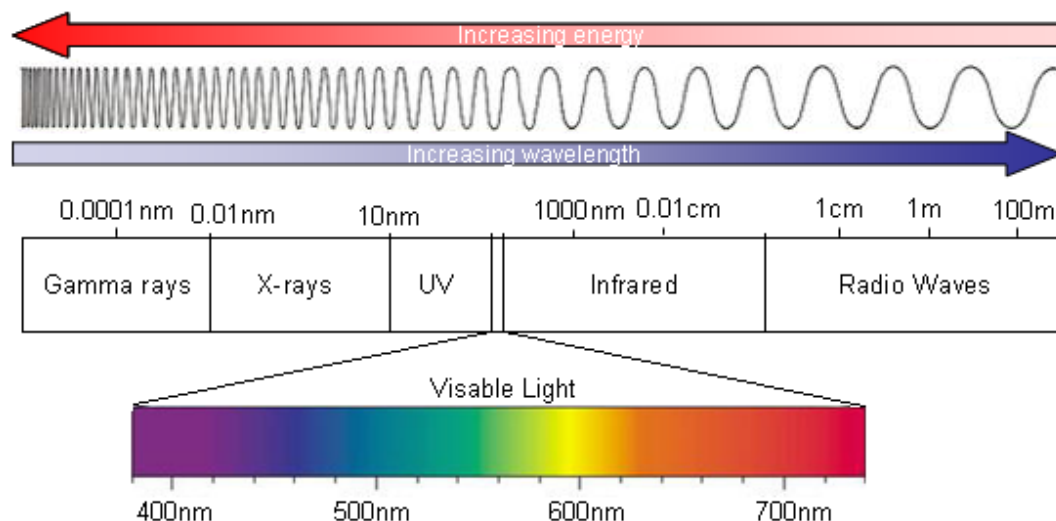
Figure 1-1: Electromagnetic spectrum of light. Abbreviations: UV, Ultraviolet.

As photons of differing regions in the EM spectrum possess varying energy and wavelengths, they have been shown to produce varying effects in cells e.g. Gamma rays, X-rays, and UV rays are high energy photons with short wavelengths and produce ionising damage in tissue, whereas radio waves are fairly low energy photons with long wavelengths and are relatively harmless (Enwemeka, 2004). Near-IR and visible light are in between these two

opposing ends of the spectrum. Evidence shows that red and IR light have therapeutic benefits, where research to characterise the effects of unique wavelengths in these regions of the EM spectrum are plenteous. The development of single colour (monochromatic) light sources occurred in 1960 when Theodore Maiman developed a device that produced red light at a unique wavelength (Maiman, 1960; Enwemeka, 2004). The device was called a Light Amplification by Stimulated Emission of Radiation or LASER, which led to early research focused on high powered laser techniques and therapies, where later in the decade an accidental discovery by a Hungarian physician, Endre Mester, paved the way for research into low-powered or low-intensity light therapy (LILT) (Enwemeka, 2004).

1.1.2 Photobiomodulation

Photobiomodulation refers to LILT in the far-red to near-IR region of the spectrum (630-1000nm), which modulates numerous cellular functions in various *in vitro* and *in vivo* models (Eells et al., 2004; Barolet, 2008). As early as 1968, Endre Mester was studying the stimulating effects of photobiomodulation on biological systems (Mester et al., 1968). Mester hypothesised that "high power" lasers could be used to destroy tumours, where he irradiated tumours implanted into rats with a customized ruby laser thought to be high powered, but was later discovered to be a low powered red light. Mester's experiments showed that tumour cells were not destroyed by this red light but, however, observed the skin incisions he made had appeared to heal faster in treated animals compared control animals (Mester et al., 1968; Enwemeka, 2004). These findings led Mester to conduct further experiments using this LILT on skin defects, burns, and human cases of

ulcers arising from diabetes, venous insufficiency, infected wounds, and bedsores, where the LILT appeared to aid the healing process in all groups compared to controls (Enwemeka, 2004).

These pioneering experiments by Mester led to an array of fascinating *in vitro* and *in vivo* research on photobiomodulation, mostly by using laser therapy. Lasers have some limitations when used in a clinical environmental, including exact wavelength capabilities and beam width, production of multiple wavelengths optimal for wound healing, treatment area i.e. excessive hardware and bulky equipment are needed for large area wounds, heat production from the laser light causing tissue damage, and retinal damage if inadvertently exposed to the laser beam (Whelan et al., 2001; Eells et al., 2004; Brawn and Kwong-Hing, 2007). Light Emmiting Diodes (LED) have become a favourable and effective alternative to lasers, as they can be configured to produce single or multiple wavelengths with a narrow bandwidth, require smaller hardware packages, can be arranged in large arrays allowing treatment of large areas and do not produce heat as they have a lower energy density and therefore reduced risk of eye damage compared to laser light (Whelan et al., 2001; Eells et al., 2004; Brawn and Kwong-Hing, 2007), where experiments at the cellular level have provided evidence that laser and LED, or coherent and non-coherent light, respectively, with the same wavelength, intensity, and irradiation time provide the same biological effect (Karu, 2003). LEDs also have the Food and Drug Administration (FDA) approval for light therapy, as they are deemed as a non-

significant risk in humans (Whelan et al., 2001; Eells et al., 2004; Brawn and Kwong-Hing, 2007).

Tissue penetration using red to near- IR light is an issue that should be brought to attention when dealing with LILT. Spectra from photons at the red to near-IR 630–800 nm wavelengths have been shown to travel approximately 23 cm through the skin surface (light input) and muscle of wrist flexor muscles in the forearm and muscles in the calf of the leg (Whelan et al., 2001). Young et al. (2000) conducted a study to determine the near-IR transmission in the human head. Sterile probes for emitting and detecting IR light at a fixed separation of 40 mm were placed in turn on intact skin, skull, dura and cerebral cortex of patients undergoing elective neurosurgery, where the detecting probe was moved through successive extracereberal layers with the emitter (776.5, 819, 871 or 909nm wavelength) on the skin surface, or vice versa (Young et al., 2000). They found that removal of bone and dura from the light path caused a 14-fold significant reduction in detected intensity, therefore suggesting the skull and/or its interface with other layers may act as an optical 'channel', distorting the behaviour of near-IR light (Young et al., 2000). These results show that photons in the red to near-IR can travel distances in the brain and other tissue, therefore photobiological effects of wavelengths in these regions are plausible.

1.2 Therapeutic effects of photobiomodulation

1.2.1 General

Various effects of LED and laser LILT have been reported, some of which confirm Mester's evidence of improved wound healing (Mester et al., 1971; Deriabin, 1997; Yu et al., 1997b; Schaffer et al., 2000a; Pugliese et al., 2003; Byrnes et al., 2004), show increases in mitochondrial respiration or adenosine triphosphate (ATP) synthesis (Passarella et al., 1984; Morimoto et al., 1994; Karu et al., 1995; Yu et al., 1997a; Wilden and Karthein, 1998; Mochizuki-Oda et al., 2002) and promotion of cell proliferation and cell survival (Yu et al., 1997a; Carnevalli et al., 2003; Brondon et al., 2005; Hawkins and Abrahamse, 2006).

Reports detailing the beneficial effects of various wavelengths and treatment protocols of LILT on wound types are plentiful and show improved healing time, stimulated re-epithelialization, granulation tissue and collagen fibre deposition, local microcirculation and decreased inflammation and edema in the early phases of the wound healing using laser LILT in the 630nm-690nm (Yu et al., 1997b; Pugliese et al., 2003; Medrado et al., 2008; Meireles et al., 2008; Meirelles et al., 2008; Oliveira et al., 2008; Chung et al., 2009; Freddo et al., 2009; Gonzaga Ribeiro et al., 2009; Santos et al., 2009), 780nm-790nm (Schaffer et al., 2000b; Oliveira et al., 2008; Santos et al., 2009), and 830nm (Freddo et al., 2009) wavelength range. Using LED LILT, Deriabin et al. (1997) showed a decrease in inflammation at the injured site of mandilar bone defects in rabbits following LILT at 890nm compared to sham controls. Interestingly, Whelan et al. (2001) studied LED LILT at combined wavelengths

(670nm, 728nm & 880nm) in *in vitro* and *in vivo* models and showed an increase of cell growth of 140-200% in mouse-derived fibroblasts, rat-derived osteoblasts, and rat-derived skeletal muscle cells, and increases in growth of 155-171% in normal human epithelial cells. In the same study, LILT in conjunction with hyperbaric oxygen, showed wound size was decreased by 36% in an *in vivo* ischemic rat model and in clinical studies, LILT showed greater than 40% improvement of in musculoskeletal training injuries and decreased wound healing time in Navy sea, air and land (SEAL) team members, suggesting the combined wavelengths in this range may be optimal for accelerated wound healing using LED LILT.

Dentistry has also used low-power lasers in the treatment of dentin hypersensitivity, gingivitis, periodontitis, and oral ulcers (Pereira et al., 2002). Whelan et al. (2002) treated bone marrow transplant patients, who are susceptible to oral mucositis following chemotherapy, with daily 670nm LED LILT to the left extraoral epithelium and found ulcerated oral mucositis to be decreased compared to the sham (right extraoral epithelium), where left and right buccal pain was also improved (Whelan et al., 2002). Also, LILT reduced pain by 47% in children suffering from oral mucositis suggesting that LILT, overall improves the wound healing process (Whelan et al., 2001).

Laser LILT has been shown to increase bone resorption and formation at 660nm (Nicola et al., 2003), 685nm (Freddo et al., 2009), and 830nm (Blaya et al., 2008; Gerbi et al., 2008), to increase calcium and phosphorus mineralisation and percentage crystallinity at 830nm (Hubler et al., 2009) as

well as to increase calcium and alkaline phosphotase in osteoblastic cell lines at 632.8nm and 830nm, respectively (Yamada, 1991; Ueda and Shimizu, 2003). Brawn and Kwong-Hing (2007) grafted sockets, created from tooth extraction, with hydroxyapatite, a calcium phosphate ceramic, and used LED LILT 605nm-631nm for 21 days post-extraction, and found increased bone formation and particle resorption compared to the non-LILT treated socket. A similar study in rabbit dental implants confirmed increased calcium hydroxyapatite following laser LILT at 880nm (Lopes et al., 2007).

LILT research has been used for various other applications, in order to try and elucidate any therapeutic benefits. Further other effects using laser LILT have included decreased myocardial tissue loss in rats following myocardial infarction at 804nm (Ad and Oron, 2001), preventing signs of brain damage in mannitol-induced blood brain barrier breakdown in rats receiving 770nm, 850nm or 905nm laser treatments (Keller et al., 2002), preventing tumour growth acceleration and increasing life span in tumour-bearing mice using chronic 632.8nm laser treatments (Glushkov et al., 2006), selective nanoshell-assisted thermal ablation of tumour cells in mice using a 808nm laser (Schwartz et al., 2009), and increasing axonal number and distance of regrowth, suppressing immune cell activation and decreasing cytokine/chemokine expression in rats during spinal cord injury using an 810nm laser (Byrnes et al., 2005a). Barolet et al. (2009) demonstrated that LED 660nm LILT reduced rhytid depth and surface roughness in 90% of individuals taking part in a split-face single blinded study. Furthermore, his study showed LED LILT reversed age-related collagen downregulation and

matrix metalloproteinase-1 upregulation (an enzyme involved in the breakdown of interstitial collagens) compared to sham controls using human reconstructed skin (Barolet et al., 2009). Yeager and colleagues conducted a series of experiments using LED 670nm LILT in fertile chicken eggs to demonstrate the effect on embryonic mortality, as well as various other parameters. Yeager et al. (2005) showed that treatments on embryonic days 0-20 decreased mortality rates, increased body weight, crown-rump length and liver weight in hatchlings (Yeager et al., 2005). Upon injection with a sub-lethal dose of toxin 2,3,7,8-tetrachlorodibenzo-p-dioxin (TCDD) at 200ppt, Yeager showed that LILT attenuated the toxic effects of TCDD by increasing hatchling size and weight, decreasing hepatic oxidised:reduced glutathione ratio and hepatic glutathione and catalase, therefore restoring hepatic enzyme activities to control levels (Yeager et al., 2006a; Yeager et al., 2006b; Yeager et al., 2006c). Eells et al. (2003) showed that LED LILT at 670nm wavelength reduced the methanol-derived formate, a mitochondrial toxin formed following methanol intoxication. Significant recovery of rod- and cone-mediated function was also determined using an electroretinogram as a sensitive indicator of retinal function (Eells et al., 2003)

Overall, these results demonstrate that photobiomodulation in the red to near-IR spectrum changes recovery pathways to promote cellular proliferation and restore cellular function following injury. This present study focuses on LED photobiomodulation at the infra-red wavelength 1072nm (IR1072).

1.2.2 Infrared 1072nm

Most of the published work to date to establish the therapeutic effects and mechanisms underpinning photobiomodulation has centred around the 600-900nm wavelength range. Much work using 1064nm wavelength lasers have been used mainly for skin resurfacing (Trelles and Allones, 2006; Berlin et al., 2007), dental cavities or decay (Harazaki et al., 2001; Zezell et al., 2009) and wrinkle treatment (Karabudak et al., 2008).

The narrow waveband of IR light centred at 1072 nm (IR1072) is a peak wavelength in the transmission spectrum through water (Figure 1-2) therefore it has been reasoned that tissue penetration would be influenced by light transmitted by water, which represents the major component of the human body (Dougal and Kelly, 2001). LED IR1072 LILT has been previously reported to show an improved healing time of *Herpes labialis* (Dougal and Kelly, 2001), had protective effects against UVA toxicity in human lymphocytes (Bradford et al., 2005) and beneficial effects on the acquisition of working memory in IR-treated 12 month old CD-1 mice (Michalikova et al., 2008).

Bradford et al. (2005) examined the effects of various protocols and wavelength in the red to near-IR spectrum (660nm, 880nm, 950nm, 1072nm and 1267nm) on human lymphocytes and found cell viability to be highest for the 1072nm wavelength-treated cells compared to other wavelengths and the untreated controls. These findings correlate data reported from other red to IR

wavelengths of light, therefore the establishment of any further beneficial effects following IR1072 treatment *in vivo* and *in vitro* was essential.
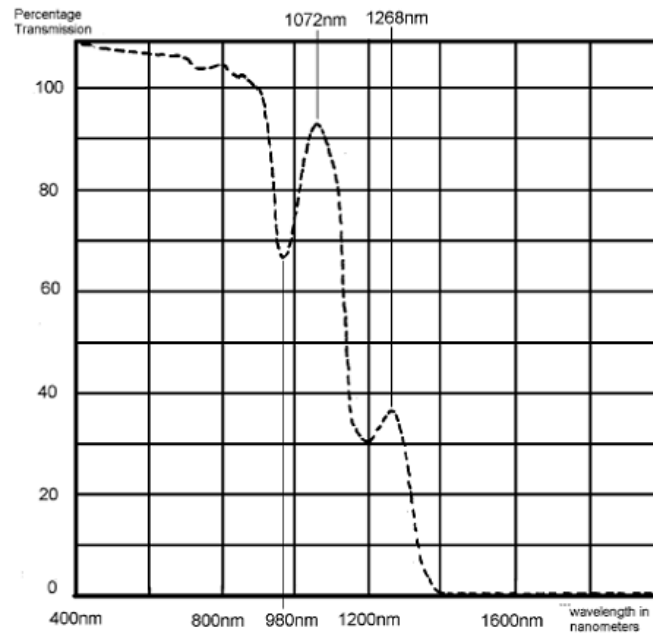
Figure 1-2: Percentage transmission of IR through pure water (Figure based on Bradford et al., 2005).

1.3 Molecular Mechanisms of Photobiomodulation

LED and laser LILT in the red to near-IR spectrum appear to have beneficial effects in diverse range of *in vitro* and *in vivo* experimental models.

Increased cellular proliferation has been a common reported effect of LILT in multiple cell culture systems, including; fibroblasts at 570nm LED (Vinck et al., 2003) 632.8nm laser (Hawkins and Abrahamse, 2006) 660-670nm laser (Taniguchi et al., 2009) and LED (Vinck et al., 2003; Brondon et al., 2005), 900-950nm laser (Pereira et al., 2002) and LED (Vinck et al., 2003); osteoblast cells at 800-830nm (Kreisler et al., 2003a; Ueda and Shimizu, 2003; Pires Oliveira et al., 2008); olfactory ensheathing cells at 810nm

(Byrnes et al., 2005b), human larynx carcinoma cells at 808nm (Kreisler et al., 2003b); CHO K-1 cells at 830nm (Carnevalli et al., 2003); and rabbit aortic endothelial cells at 685nm (Ricci et al., 2009). These findings show that wavelengths in the red to near-IR region have an effect on cellular proliferation, although the energy density and treatment regime may be important in eliciting these effects (Hawkins and Abrahamse, 2006; Pinheiro and Gerbi, 2006). It has been postulated that many of the therapeutic effects seen with LILT i.e. tissue repair, is due to an increase in cellular proliferation following red to IR irradiation.

Oxidative phosphorylation in mitochondria is the main process by which ATP is produced in excitable and non-excitable mammalian tissue, whereby hydrolysis of ATP drives cellular processes such as protein synthesis, DNA/RNA synthesis, ion (Na^+, K^+, Ca^{2+}) transport through the cell membrane, gluconeogenesis, ureagenesis, relative movement of myosin and actin filaments during muscle contraction (Korzeniewski, 2001). In 1960, Gordon & Surrey investigated the effect of red light in isolated rat liver mitochondria and found that red light at 670nm reversed far red light (725nm)-induced ATP reduction. Over 20 years later, Passarella et al. (1984) irradiated isolated rat liver mitochondria with a low-powered 632.8nm laser, and found an increase in mitochondrial membrane potential, proton gradient and an increase in ATP. They correlated this effect to the mitochondrial ETC, as complex chain inhibitors appeared to block the effects elicited by LILT, and suggested that the increase in ATP synthesis is due to a laser-induced increase in proton-motive force, where the electrochemical potential is discharged through ATP

synthesis (Passarella et al., 1984). Supporting evidence show rises in ATP levels following LILT, some of which include 602nm lasers (Vekshin and Mironov, 1982) 632.8nm lasers (Karu et al., 1995; Zungu et al., 2009) and 830nm lasers (Mochizuki-Oda et al., 2002). These findings have become the basis for continuing research on LILT-induced ATP synthesis, and has led to the idea that the mitochondrial ETC is the primary photoacceptor for LILT resulting in a cascade of signalling events, proposed as secondary mechanisms, involved in promoting cellular proliferation and cytoprotection (Eells et al., 2004; Gao and Xing, 2009).
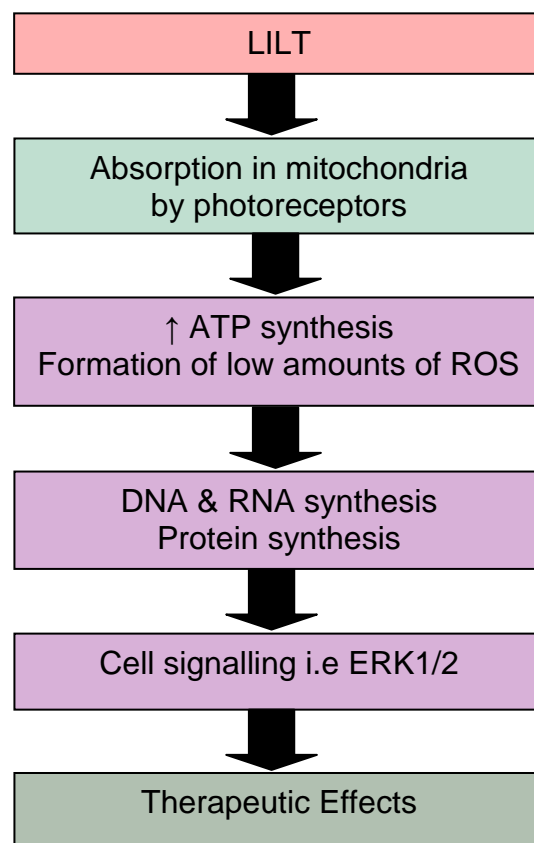

Figure 1-3: Cascade of events proposed to be elicited by LILT Abbreviations: LILT, Low Intensity Light Therapy; ATP, Adenosine Triphosphate; DNA, Deoxyribonucleic Acid; RNA, Ribonucleic Acid; ERK1/2, Extracellular Signal-regulated Kinase 1 and 2 (Figure based on Enwemeka, 2004).

1.3.1 Photoreceptors for red to near-IR light

All photoreceptors known to date consist of the following: A protein moiety and one or several chromophores which are covalently or non-covalently bound to the protein (Batschauer, 2003). Light in the visible region of the spectrum requires a chromophore in order to absorb light, thus if additional photoreceptors are identified in the future, it is unlikely that they will divert from this rule, however bare in mind the same may not be true of light in other regions of the spectrum i.e. IR (Batschauer, 2003). The chromophore, with its conjugated π electron system, can be excited with photons of longer wavelengths and lower energy, such as those present in the red to near-IR region (600-1000 nm) where photon absorption causes a shift in the molecular configuration of the protein moiety that is required to transduce the primary light signal to downstream components (Batschauer, 2003; Gao and Xing, 2009). Photoreceptors are present on the most metabolically active cells in the body, and the energy required for phototransduction is derived primarily from oxidative metabolism (Eells et al., 2003).

A growing body of evidence suggests cytochrome c oxidase, the terminal enzyme of the electron transport chain (ETC), to be the key photoacceptor of light in the far red to near-IR spectral range (Karu, 1999; Eells et al., 2004; Barolet, 2008; Gao and Xing, 2009). It has been generally accepted that cytochrome c oxidase acts as the primary mechanism for red to near-IR photobiomodulation and subsequent signalling is the secondary mechanism of LILT, however some other photoacceptors have been suggested. Complex II and IV activity of the ETC has been shown to be increased following LILT

using 904nm wavelength laser suggesting a possible photoacceptor of IR light (Silveira et al., 2007) and phosphorylation of tyrosine protein kinase receptor (TPKR) following LILT using 632.8nm laser has been shown also (Shefer et al., 2001), suggesting the receptor to be in the "right energetic state" to accept laser energy and autophosphorylate to activate signalling pathways such as the ERK1/2 pathway, which in turn promote cell proliferation and cytoprotection in cells (Gao and Xing, 2009). Cytochrome c and Ubiquinone, mobile electron transporters in the electron transport chain (ETC), have also been suggested as possible photoacceptors.

These would be interesting alternate photoacceptors, however more evidence is required in order to define the possible role of these photoacceptors, albeit to establish whether these are wavelength-specific photoacceptors or possess combined photoabsorbing activity - either way evidence for cytochrome c oxidase to be the primary photoacceptor is compelling and confirms a likely role for this enzyme upon red to IR photobiomodulation.

1.4 Mitochondria: Primary mechanism

Mitochondria are organelles found in the cytoplasm of most eukaryotic cells. They are spherical or elliptical in shape, with general dimensions of 1-2μm in length by 0.5-1μm in width (Scheffler, 2001; Burroughs and French, 2007). Structurally, mitochondria are bound by two membranes that create two distinct compartments separated by an intermembrane space (Scheffler, 2001; Burroughs and French, 2007). The outer membrane encloses the entire

organelle and is permeable to small molecules and ionic species, but recent studies suggest that it might form a more important and potentially regulated barrier via specific transporters (Duchen, 2004; Burroughs and French, 2007). The inner membrane forms an invaginated high surface area containing cristae that project into and enclose the matrix (Duchen, 2004; Burroughs and French, 2007).

The central role of mitochondria in respiring cells of eukaryotic organisms is aerobic catabolism of dietary intermediates, i.e. fatty acids and amino acids, to the three carbon intermediate, pyruvate (Duchen, 2004; Burroughs and French, 2007). Pyruvate is transported into the mitochondrial matrix by pyruvate dehydrogenase and subsequently undergoes oxidative decarboxylation to the two carbon intermediate, acetyl CoA, (Duchen, 2004; Burroughs and French, 2007). Acetyl CoA enters the tricarboxylic acid (TCA) cycle and combines with oxaloacetate which is further oxidised generating carbon dioxide and water (Duchen, 2004; Burroughs and French, 2007). Oxidation of respiratory substrates, NADH to NAD^+ and $FADH_2$ to FAD^+, is coupled to phosphorylation of adenosine diphosphate (ADP) and inorganic phosphate (Pi) to ATP via the ETC (Duchen, 2004; Burroughs and French, 2007). Anaerobic glycolysis can provide enough ATP for some cells, but energetically active cells such as cardiomyocytes and neurons require a more efficient ATP supply, which can only be provided by mitochondrial oxidative phosphorylation via ETC (Trounce, 2000; Burroughs and French, 2007).

The cristae of the inner mitochondrial membrane are the site at which the components of the ETC are localized (Scheffler, 2001; Duchen, 2004; Burroughs and French, 2007). The ETC is composed of five multi subunit enzyme complexes: NADH-ubiquinone reductase, (complex I), succinate-ubiquinone reductase, (Complex II), ubiquinone-cytochrome c reductase (complex III), cytochrome *c* oxidase (Complex IV) and ATP synthase (complex V). The chain also includes lipid soluble mobile electron carriers: ubiquinone (coenzyme Q) is responsible for shuttling electrons from both complex I and II to complex III, whilst cytochrome *c* transports electrons from complex III to IV (Nicholls and Budd, 2000; Duchen, 2004; Burroughs and French, 2007).
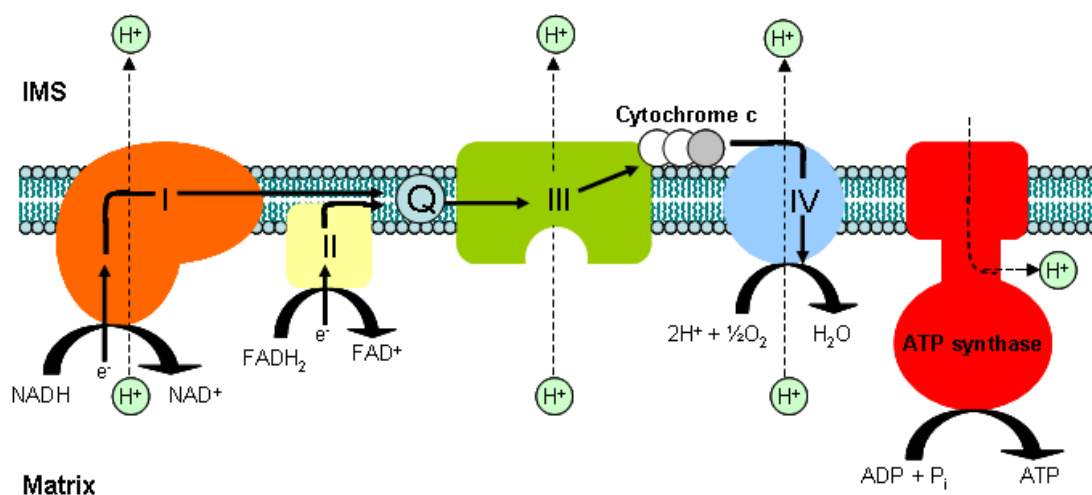

Figure 1-4: The Electron Transport Chain. NADH-ubiquinone reductase, (complex I), succinate-ubiquinone reductase, (Complex II), ubiquinone-cytochrome c reductase (complex III), cytochrome *c* oxidase (Complex IV) and ATP synthase (complex V). Abbreviations: FAD, Flavin Adenine Dinucleotide; NAD, Nicotinamide Adenine Dinucleotide ; ADP, Adenosine Diphosphate; ATP, Adenosine Triphosphate; e⁻, electron; H⁺, hydrogen ion (Figure based on Ow et al., 2008).

According to the chemio-osmotic principle (Mitchell, 1961), a series of successive exergonic (energy releasing) redox reactions transfers electrons through the flavin mono nucleotides (FMN) and iron-sulphur (FeS) centres within the ETC towards compounds with more oxidative potentials, providing complexes with enough energy to translocate protons from the matrix to the inter-membrane space (IMS) (Bratic and Trifunovic; Nicholls and Budd, 2000; Burroughs and French, 2007). The transfer of protons across the mitochondrial matrix to the inner membrane space at complexes I, III and IV establishes a trans-membrane electrochemical gradient of 180-220 mV negative to the cytosol (Bratic and Trifunovic; Bernardi et al., 1999; Nicholls and Budd, 2000; Duchen, 2004; Van Houten et al., 2006; Burroughs and French, 2007). This proton gradient drives the phosphorylation of ADP to ATP, whereby the extruded protons re-enter the mitochondria via the Complex V (ATP synthase), coupling their transfer to the synthesis of a high energy intermediate, ATP (Kadenbach, 2003; Murphy et al., 2005; Van Houten et al., 2006; Burroughs and French, 2007). The final electron acceptor is molecular oxygen, which is reduced through a four electron addition to water (Van Houten et al., 2006; Burroughs and French, 2007).

Cytochrome c oxidase, (complex IV) of the electron transport chain is a large multicomponent membrane protein (200 kDa) in the mitochondrial electron-transport chain and has been shown to have absorption bands in the red to near-IR spectrum (Huang et al., 2009). In addition to the LILT-induced ATP synthesis in isolated mitochondria discussed earlier (Passarella et al., 1984), the 660–680 nm wavelength range has been shown to increase electron transfer in purified cytochrome oxidase with laser LILT (Gordon and Surrey,

1960; Pastore et al., 2000) and to upregulate cytochrome oxidase activity in cultured neuronal cells with LED LILT (Wong-Riley et al., 2001). It's centre comprises of two heme moieties (heme a and heme a3), two redox-active copper sites (CuA, and CuB,), one zinc, and one magnesium, all of which have been suggested as possible chromophores for red to near-IR light (Figure 1-5) (Eells et al., 2004; Gao and Xing, 2009).
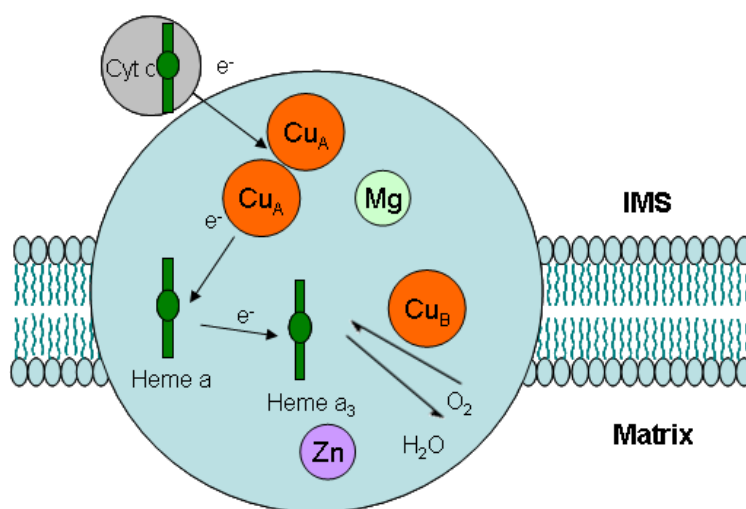

Figure 1-5: Cytochrome *c* oxidase centre. Abbreviations: Cyt c, Cytochrome c; heme a and heme a3, heme moieties; CuA, and CuB; redox-active copper sites; Zn, Zinc; Mg, magnesium; e⁻, electron (Figure based on Karu et al., 1995).

During respiration, the pair of Cu_A chromophore of cytochrome c oxidase accepts electrons from the cytochrome c molecule, where internal electron transfer between Cu_A, heme a, and the heme a_3-Cu_B centre results in reduction of molecular oxygen via at least seven redox intermediates (Karu, 1999; Gao and Xing, 2009). Action spectra investigations on biological responses following LILT on HeLa cells conducted by Karu et al. (1995) suggested that reduced form of Cu_A accepts 620nm light, oxidised Cu_B

accepts 680nm, reduced Cu_B accepts 760nm and oxidised Cu_A accepts the near infra red spectrum of 825nm. They further confirmed cytochrome c cannot be considered as a primary photoacceptor when it is in a fully oxidised or fully reduced state (Karu et al., 1995; Karu and Kolyakov, 2005), however it is still unclear which one of the cytochromes *c* oxidase intermediates is the primary photoacceptor (Gao and Xing, 2009).

1.5 Cell signalling: Secondary mechanism

Mitochondria are at the centre of many diverse cellular functions integrating signals between the organelle and the nucleus (Gao and Xing, 2009). The changes in pH, ATP, mitochondrial membrane potential (MMP) following LILT described previously (Passarella et al., 1984), can initiate mitochondrial retrograde signalling process, which is the communication in cells from mitochondria to the nucleus that influences many cellular activities under both physiological and pathophysiological conditions (Karu, 1999; Gao and Xing, 2009). Mitochondrial retrograde signalling is thought to be the initiator of several pathways following LILT, including the Mitogen-activated protein kinase (MAPK) cascade and extracellular signal regulated kinase 1/2 (ERK1/2) signalling.

1.5.1 MAPK Cascade

MAPK is one of three components that regulate a number of key intracellular signalling events including cell proliferation, differentiation, survival and apoptosis, which are activated by an enormous array of stimuli (Schmitz et al.,

2007; May and Hill, 2008; Gao and Xing, 2009). Downstream of the activating stimuli, the kinases themselves may be stimulated by combinations of small G proteins, MAP4Ks, scaffolds, or oligomerization of the MAP3K in a pathway (Lawrence et al., 2008). Each of the three major mammalian MAPK pathways, ERK1/2, p38 and c-Jun N-terminal Kinase (JNK) pathways, contains a three-tiered kinase cascade comprising a MAP kinase kinase kinase (MAPKKK), a MAP kinase kinase (MAPKK) and MAPK, which are involved in the phosphorylation and activation of numerous proteins, including transcription factors, cytoskeletal proteins, kinases and other enzymes (Schmitz et al., 2007). The ATP site is common to all of the protein kinases and is coupled to their dual phosphorylation of the conserved threonine and tyrosine residues, which promotes a conformational change in the kinase in order to elicit activation of transcription factors i.e. Brain derived neurotrophic factor (BDNF) activation of the ERK1/2 signalling pathway can result in the phosphorylation and activation of cyclic adenosine monophosphate (cAMP) response element binding (CREB) protein (Johnson, 2009).

1.5.2 ERK1/2 pathway

 BDNF is a member of the growth factor family and is highly implicated in neuroprotection with a major role in cell proliferation, cell survival and resilience via activation of the ERK1/2 pathway (Schloesser et al., 2007). A study by Byrnes et al. (2005b) showed BDNF gene expression to be increased following IR LILT. RNA extraction and real-time poylmerase chain reaction (PCR) techniques were used to analyse the level of gene expression following 810 nm laser LILT in olfactory ensheathing cells (OEC), where

irradiated cells showed a significant increase in BDNF and glial derived neurotrophic factor (GDNF) gene expression compared to control groups. OEC proliferation was also significantly increased in LILT treated groups compared to control groups, suggesting a possible role for BDNF in IR LILT-induced cell proliferation (Byrnes et al., 2005b).
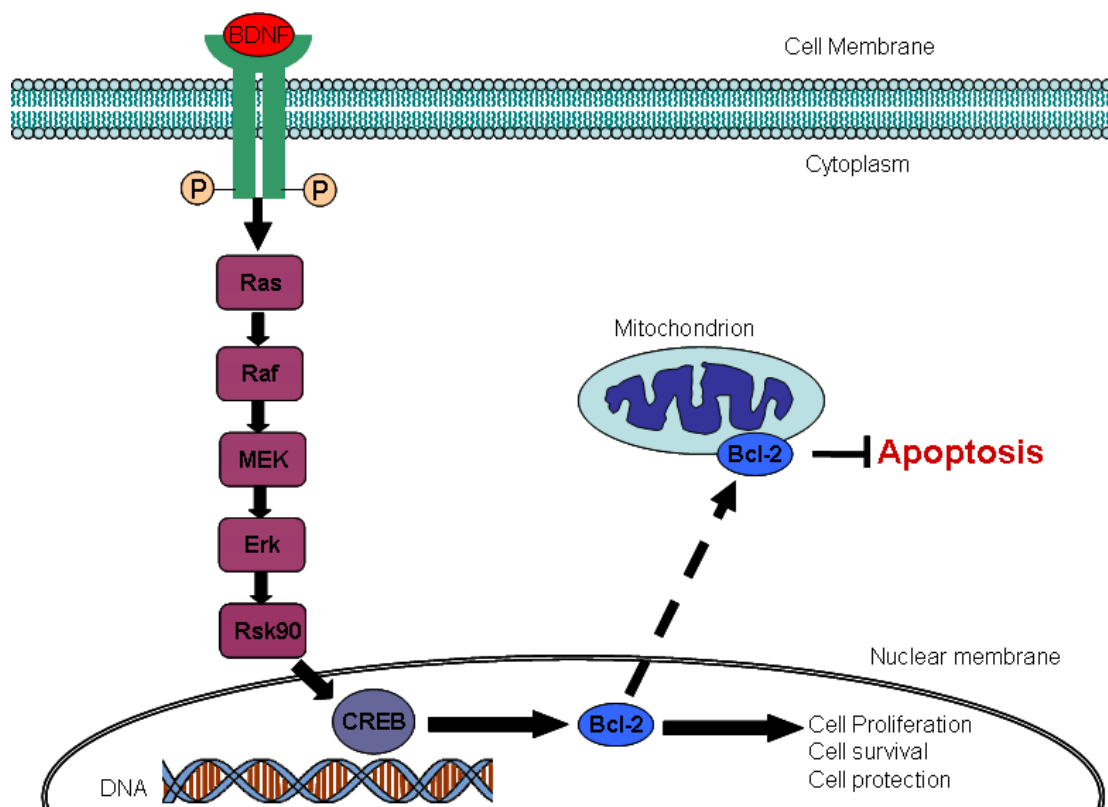

Figure 1-6: ERK1/2 signalling. Abbreviations: BDNF, Brain Derived Neurotrophoc Factor; MEK, MAPK/ERK kinase; ERK1/2, Extracellular Signal-regulated Kinase 1 or 2; Rsk90, 90 kDa Ribosomal Protein S6 Kinases; CREB, Cyclic Adenosine Monophosphate (AMP) Response Element Binding; Bcl-2, B-cell CLL/lymphoma 2; BAD, Bcl-2 Associated Death Factor; P, Phosphate; DNA, Deoxyribonucleic Acid (Schloesser et al., 2007).

BDNF binds to the high affinity tyrosine kinase B receptor (TRKB) (Huang and Reichardt, 2003; Charney and Manji, 2004; Markham et al., 2004; Nagappan

and Lu, 2005), resulting in postsynaptic rises in cyclic adenosine monophosphate (cAMP) concentrations that facilitate translocation of TRKB into the postsynaptic density (Nagappan and Lu, 2005), subsequently triggering autophosphorylation of tyrosine residue in its intracellular domain leading to downstream activation of signalling events i.e. ERK1/2 activation (Mattson et al., 2004a; Burroughs and French, 2007).

ERK1/2 is the major signalling pathway implicated in LILT. Shefer et al (2001) irradiated myoblasts with laser LILT at 632.8nm used phospho-specific antibodies to identify an upregulation of phospho-ERK1/2 following irradiation, with no effect on phospho-p38 or phospho-JNK. They also showed that Hepatocyte growth factor receptor, a member of the TRK family, was phosphorylated following irradiation whereas phosphorylated TNFα receptor, known to activate the stress pathways p38 and JNK, was unaffected by irradiation, suggesting these stress pathways are not involved in LILT (Shefer et al., 2001; Gao and Xing, 2009). The activation of ERK1/2 pathways are induced by stimuli such as TRKs or G-protein coupled receptors (Lawrence et al., 2008) which results in the sequential phosphorylation of Ras-Raf, MAPK/ERK kinase (MEK) and ERK (May and Hill, 2008). Depending upon the intensity and duration of stimulation, ERK1/2 can activate a diverse variety of substrates, both directly and indirectly by including several key transcription factors which can result in cell proliferation and cytoprotection (Lawrence et al., 2008). Regulation of transcription factors indirectly can occur by phosphorylation of the 90 kDa ribosomal protein S6 kinases (RSK90; Lawrence et al., 2008). Active RSK90 can mediate the actions of the ERK1/2

cascade and neurotrophic factors and appears to play a major role in transcriptional regulation, translocation to the nucleus and phosphorylating transcription factors such as CREB, at Ser133 (Lawrence et al., 2008).

CREB is an important regulatory transcription factor for immediate early gene transcription and has been implicated in cell proliferation and survival, and upregulates the anti-apoptotic protein B-cell Lymphoma 2 (Bcl-2) (Frödin and Gammeltoft, 1999). The Bcl-2 family consists of anti-apoptotic members (including Bcl-2 and Bcl-x_L) and pro-apoptotic members (such as BAD and BAX) (Beere, 2004; Einat et al., 2005). Studies have shown that an overexpression of Bcl-2 in mitochondria of cultured cells suppresses apoptosis by inhibiting calcium activation of the permeability transition pore of mitochondria (Murphy et al., 2005) thus protecting mitochondrial membrane integrity and preventing the release of cytochrome *c* (Einat et al., 2005). The release of cytochrome *c* from the mitochondria is an essential positive signal engaging the last phase of apoptosis, inducing the binding of apoptotic protease activating factor 1 (Apaf1) to cytochrome *c* and dATP to form an apoptosome thus initiating the caspases (cysteine aspartate-specific proteases) cascade pathway, resulting in the proteolysis of the various protein substrates of caspases, subsequently leading to intrinsic apoptosis (Dubois-Dauphin et al., 2001).

1.5.3 AKT signalling

Phosphatidylinositol 3-kinase (PI3K) or AKT (Protein Kinase B; PKB) signalling is a critical pathway in cell metabolism, cell survival, motility, cell cycle progression and transcription survival and many stimuli, including neurotrophins, via TRKB receptor phosphorylation, which are reported to activate this pathway (Martin et al., 2001; Nakagami, 2004; Akbar et al., 2005; Schmitz et al., 2007; Nie et al., 2009).
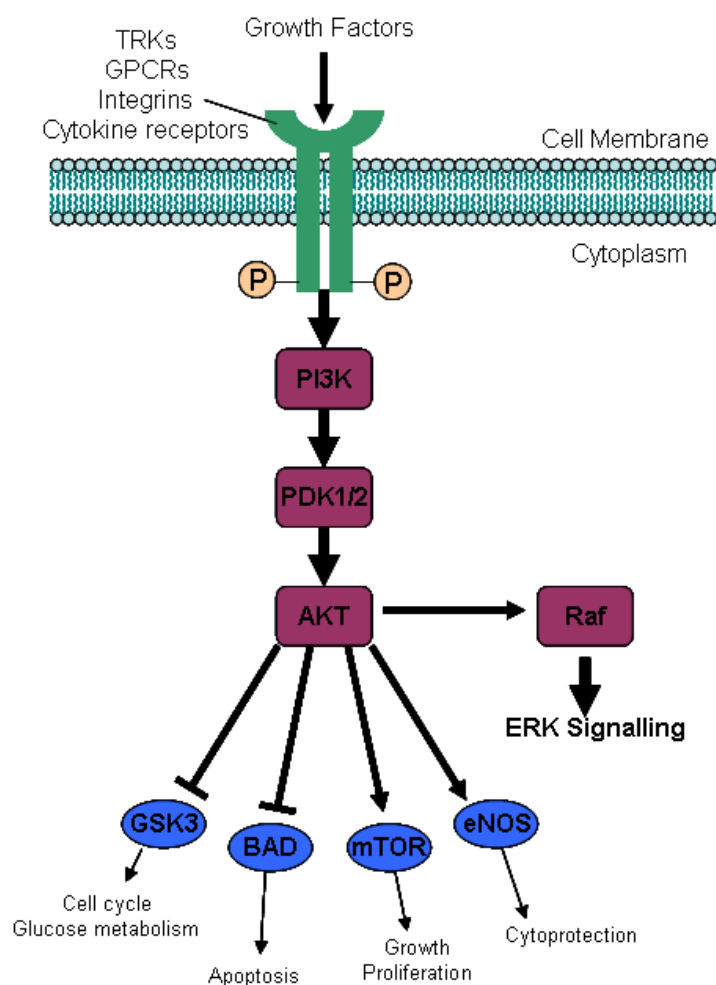

Figure 1-7: AKT signalling pathway. Abbreviations: AKT, Protein Kinase B; TRKs, Tyrosine Kinase Receptors; GPCRs, G-protein Coupled Receptors; PI3K, Phosphatidylinositol-3 Kinase; PDK1/2, Phosphoinositide-dependent Kinase 1 and 2; ERK1/2, Extracellular Signal-Regulated Kinase; GSK3, Glycogen Synthase Kinase; BAD, Bcl-2-associated Death Promoter; mTOR, Mammalian Target of Rapamycin.

AKT is a serine/threonine kinase and its activation is induced by phosphorylation mediated by the upstream localised PI3K, which is essential for activation of AKT, in association with TRKs (Schmitz et al., 2007). Activation of the PI3K pathway include stimuli such as autophosphorylation of receptor tyrosine kinases induced by ligands such as growth factors; activation of cytokine receptors; stimulation of G-Protein coupled receptors, or activation of integrin signaling (Schmitz et al., 2007). Upon PI3K mediated generation of the second messenger PTEN, AKT is translocated from the cytoplasm to the plasma membrane where sequential phosphorylation of AKT by a phosphoinositide-dependent kinase 1 and 2 (PDK1, PDK2) occurs. Phosphorylation of both Threonine 308 and Serine 473 residues results in full AKT activation leading to modulation of a variety of central cellular processes both in the cytoplasm and in the nucleus (Schmitz et al., 2007). AKT is responsible for phosphoryation of a diverse variety of substrates to inhibit (pro-apoptotic proteins) or activate (anti-apoptotic proteins) including Glycogen Synthase Kinase (GSK3) BAD, caspase 9, Mammalian Target of Rapamycin (mTOR) endothelial nitric oxide synthase (eNOS) and Raf protein kinase (Figure 1-7) (Datta et al., 1997; Beere, 2004; Schmitz et al., 2007). AKT also regulates transcription factors that direct the expression of several cell death genes. AKT-mediated phosphorylation of forkhead (FKHRL1) prevents its translocation to the nucleus and therefore prevents the induced expression of its target genes including the Fas ligand (FasL) (Beere, 2004).

1.6 Heat Shock Proteins

The heat shock protein (HSP) family are molecular chaperones that function to prevent the misfolding of proteins by facilitating folding into the native conformation that are specified by their primary sequences, and by suppressing subsequent protein aggregation, where HSPs are also responsible for transportation of misfolded proteins or aggregates to the ubiquitin-proteasome system (UPS) for degradation (Benn and Woolf, 2004; Wilhelmus et al., 2007; Gao and Hu, 2008; Li et al., 2009). HSP induction is thought to protect cells against the harmful consequences of a diverse array of stresses, some of which include heat shock (Hahn and Li, 1982; Mailhos et al., 1993) UV irradiation (Simon et al., 1995; Trautinger et al., 1995; Zhou et al., 1998) polyglutamine repeat expansion (Hansson et al., 2003; Iijima-Ando et al., 2005; Huen et al., 2007) and tumour necrosis factor (TNF) (Mailhos et al., 1993; Vietor and Vilcek, 1994; Engel et al., 1995; Heimbach et al., 2001; Miura et al., 2003). Originally, HSPs where thought to be induced solely for controlling protein misfolding and aggregation as a consequence of heat stress, but recent evidence demonstrates HSP participation in an array of cellular processes, including cytoprotection, and suggest they have two main cellular functions: promoting the UPS function and inhibiting pro-apoptotic activity; where HSPs, UPS, mitochondria and other organelles may work in conjunction to keep the cell in a stabilized state (Yenari, 2002; Arya et al., 2007; Luo et al., 2007). HSP are broadly categorized according to their size and include the HSP27, HSP40, HSP60, HSP70, HSP90 and HSP100 families (Beere, 2004).

1.6.1 HSPs in the control of protein misfolding

HSPs are normally bound to heat shock factors (HSF) but dissociate in the presence of denatured or misfolded proteins (MP) (Yenari, 2002). Once dissociated, the controlled chaperone activity of the HSPs acts via an ATP binding, hydrolysis and nucleotide exchange cycle which mediates rapid association-dissociation cycles between the HSP and its target MP (Beere, 2004; Arya et al., 2007). The unbound HSFs are phosphorylated and trimerize to produce trimers that bind to heat shock elements (HSE) that are contained within the promoters of the HSP that lead to upregulation of HSPs (Figure 1-8).
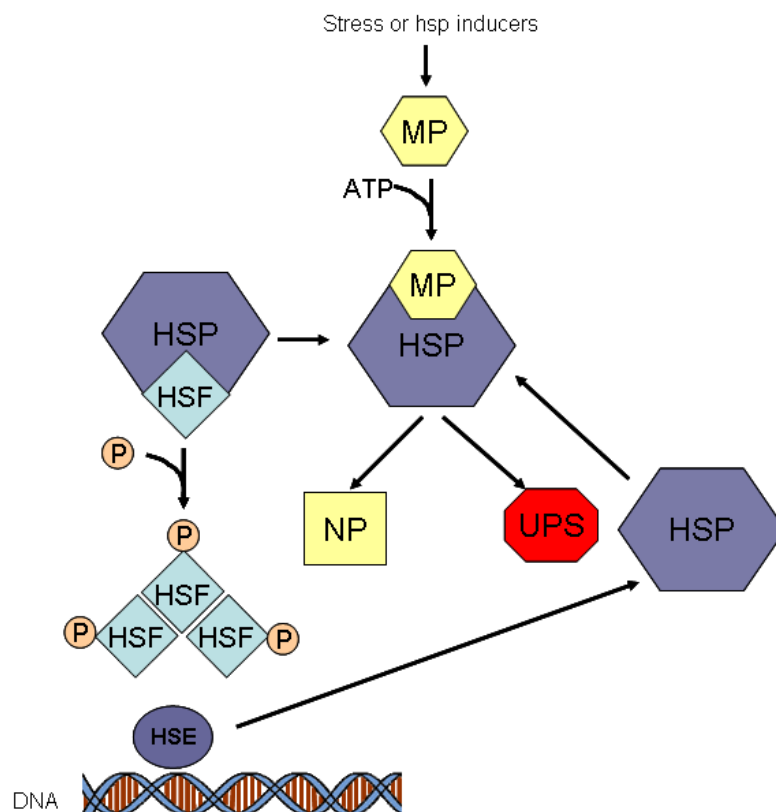
Figure 1-8: Mechanism of HSP activation and protein misfolding. Abbreviations: MP, Misfolded Protein; HSP, Heat Shock Protein; HSF, Heat Shock Factor; HSE, Heat Shock Element; NP, Normal Protein; UPS, Ubiquitin-proteasome System; DNA, Deoxyribonucleic Acid (Figure based on Yenari, 2002).

1.6.2 Role of HSP in the regulation of apoptosis

Cell death can occur by apoptosis or necrosis. Necrosis typically occurs in response to acute cellular dysfunction which leads to the release of intracellular contents into the extracellular space initiating the activation of a marked inflammatory response (Bree et al., 2002; Beere, 2004). Apoptosis is a highly regulated energy-dependent, active form of cell death that occurs normally during development, in the immune system and in response to injury (Bree et al., 2002; Beere, 2004). There are two pathways leading to apoptosis: the mitochondrial (intrinsic) pathway and the "death receptor" (extrinsic) pathway (Bree et al., 2002; Beere, 2004; Benn and Woolf, 2004; Arya et al., 2007).

Tumour necrosis factor receptors (TNFR) are known as "death receptors" and are the major players in extracellular signals initiating apoptosis (Benn and Woolf, 2004; Andera, 2009). Receptors of this family include TNFR-1 and TNFR-2 and apoptosis antigen-1 (FAS) (Benn and Woolf, 2004). The FAS ligand (FASL) is a member of the TNF superfamily of cytokines, where FASL-activation of the FASL/FAS pathway leads recruitment of Fas-associated death domain (FADD), thus promoting caspase-8 activation and subsequent cleavage of BID to tBID, a pro-apoptotic member of the Bcl-2 family (Bree et al., 2002; Benn and Woolf, 2004; Andera, 2009). Activation of tBid results in translocation to the mitochondrial membrane where its binds and initiates conformational changes and oligomerisation of BAX and BAK, resulting in membrane permeabilisation, promoting pore formation and releasing a cavalry of pro-apoptotic proteins from the mitochondrial cristae and the inter-

membrane space, such as cytochrome c, apoptosis inducing factor (AIF) and Smac/DIABLO (Benn and Woolf, 2004; Andera, 2009).

Tumor necrosis factor (TNF) is a multifunctional cytokine that plays important roles in diverse cellular events such as cell survival, proliferation, differentiation, and death (Wang and Lin, 2008). TNF activates the nuclear factor-kappaB (NF-kappaB) cellular survival pathway, or the JNK death pathway (Benn and Woolf, 2004; Wang and Lin, 2008). Binding of TNF results in trimerization of TNFR-1 and recruitment of the TNFR associated death domain (TADD), which promotes caspase-8 cleavage, as with FADD, but also leads to the recruitment of TNFR-2, where binding results in the activation of the JNK pathway (Benn and Woolf, 2004). JNK initiates apoptosis by phosphorylating (inactivating) anti-apoptotic Bcl-2 proteins, and by inducing and phosphorylating (activating) the expression of the pro-apoptotic BH3-only protein, BIM (Benn and Woolf, 2004). JNK modification of BID to jBid, results in jBID translocation to mitochondria to selectively release SMAC/DIABLO (second mitochondrial-derived activator of caspases and the *Drosophila melanogaster* homologue), a mitochondrial protein that promotes apoptosis (Benn and Woolf, 2004).

HSP-mediated regulation of apoptotic pathways has been proposed to be a fundamental protective mechanism that decreases cellular sensitivity to damaging events to allow cells to escape the otherwise inevitable apoptotic pathway (Novoselova et al., 2006). The role of HSPs in the control of apoptosis, both extrinsic and intrinsic, include the regulation of signalling

pathways such as JNK and FAS/FASL pathway (preventing apoptosis) and AKT signalling (promoting cell survival; Beere, 2004; Gao and Hu, 2008).
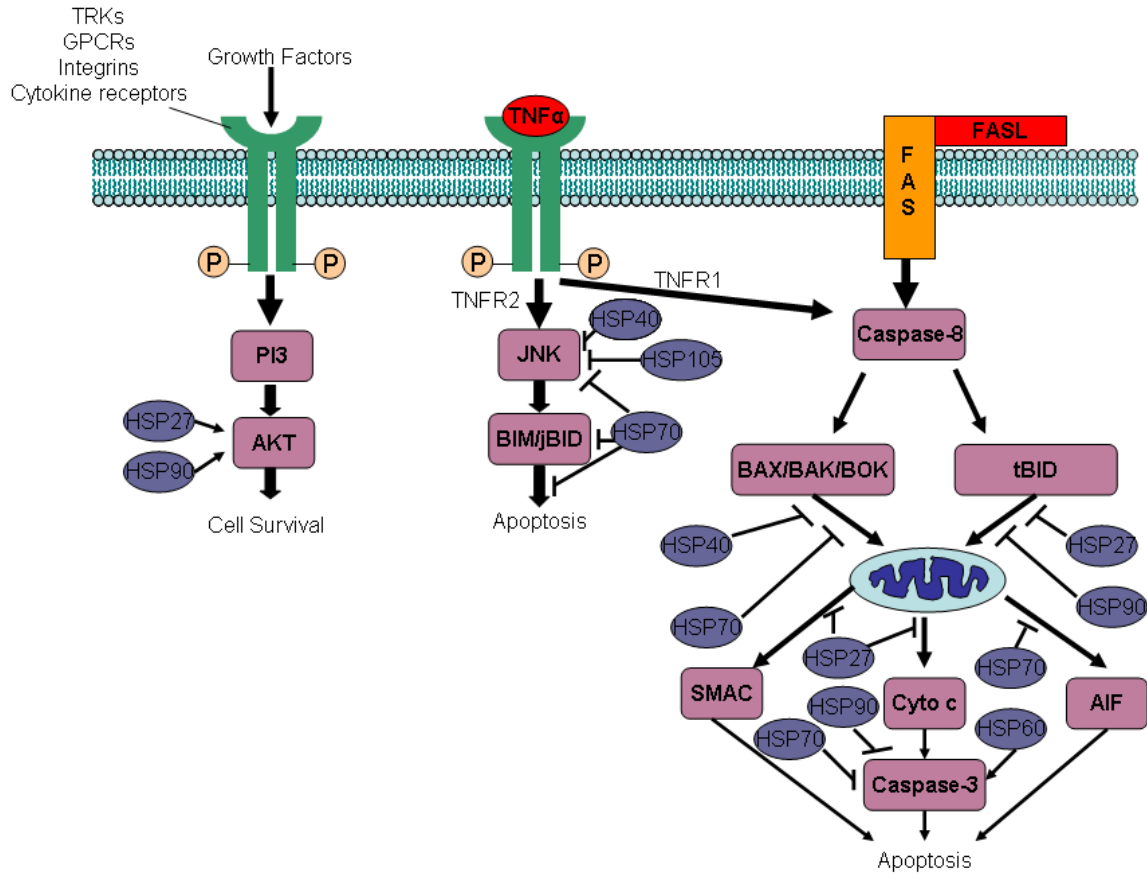

Figure 1-9: Some roles of HSPs in the control of apoptosis. Abbreviations: TRKs, Tyrosine Kinase Receptors; GPCRs, G-protein Coupled Receptors; PI3, Phosphatidylinositol 3-Kinase; TNF, Tumour Necrosis Factor; TNFR1 or 2, Tumour Necrosis Factor 1 or 2; JNK, c-Jun N-terminal Kinase; BIM/jBID, BH3-only proteins; FASL, FAS ligand; BAX/BAK/BOK/tBID, Bcl-2 family proteins; SMAC, Second Mitochondrial-derived Activator of Caspases; Cyto c; cytochome c; AIF, Apoptosis Inducing Factor; HSP, Heat Shock Protein; P, phosphate (Figure based on Beere, 2004).

1.6.2.1 HSP27

The small heat shock protein HSP27, acts as an ATP-independent chaperone in protein-protein interactions such as folding, translocation, and prevention of inappropriate protein aggregation, where they undergo self-oligomerization and MAPK-dependant phosphorylation (activation) (Mese et al., 2002; Kostenko and Moens, 2009). HSP27 has been shown to form complexes with pathological hyperphosphorylated and paired helical filaments tau which alters it's conformation, degrades and dephosphorylates the protein. This complex formation can lead to a reduction in pathological tau levels, thus rescuing the cell from tau-mediated apoptosis, therefore eliciting a neuroprotective effect in Alzheimer's Disease (AD) and other tauopathies (Shimura et al., 2004). HSP27 has also been implicated in regulation and architecture of the cytoskeleton (Zhu et al., 1994; Schafer et al., 1999; Coss et al., 2002; Keezer et al., 2003; Hargis et al., 2004), cell migration (Piotrowicz et al., 1998; Rust et al., 1999), metabolism, cell survival (Latchman, 2005; Wang et al., 2007), cell differentiation (Takahashi-Horiuchi et al., 2008), mRNA stabilization (Sinsimer et al., 2008), and tumor progression (Lambot et al., 2000).

HSP27 is involved in anti-apoptotic and cell survival pathways, including interacting and forming complexes with AKT to promote cell survival. Experiments by Konishi et al. (1997) suggested that HSP27 is involved in the activation process of AKT in the signal transduction pathway of various forms of stress (Konishi et al., 1997). Mearow et al. (2002) confirmed this by subjecting PC12 cells and a stable cell line overexpressing HSP27 (HSPC cells) to heat shock which resulted in the rapid activation of AKT followed by

p38 mitogen-activated protein kinase (MAPK) signalling, where HSP27 was phosphorylated and translocated intracellularly. HSP27 was found to form a complex with AKT and p38 MAPK in both heat shocked and sham control cells, whereby dissociation of AKT and p38 from the HSP27 occured during the latter. NGF differentiated cells were subjected to NGF withdrawal, where cell death in HSPC cells was reduced and AKT remained phosphorylated or activated compared to parental PC12 cells. These data suggest that HSP27 may stabilize the AKT protein and prevent it from dephosphorylation therefore promoting the cell survival pathway (Mearow et al., 2002; Beere, 2004; Luo et al., 2007). HSP27 can also block the mitochondrial pro-apoptotic protein tBID from translocation in to the mitochondria, can reduce SMAC and can bind to cytochrome c to prevent apoptotic peptidase activating factor 1, (Apaf-1) oligomerization, so as to block the apoptotic process (Figure1-9) (Paul et al., 2002; Beere, 2004; Benn and Woolf, 2004)

1.6.2.2 HSP60

HSP60 proteins are classified as chaperonins, proteins that "oligomerize to form large structures that can engulf their clients and function as folding chambers" (Calderwood et al., 2009). HSP60 resides in the mitochondrial matrix as a homomultimer where roles include aiding protein folding and transport of mitochondrial proteins, where it has been proposed to have a role during the late stages of apoptosis as, following mitochondrial degradation and cytochome c release during the late stages of apoptosis (Beere, 2004). Samali et al. (1999) demonstrated that recombinant HSP60 and HSP10 cells accelerated the activation of pro-caspase-3 by cytochrome c release in an

ATP-dependent manner, suggesting that the release of mitochondrial HSP60 may act as a feed-forward mechanism to accelerate and ensure optimal caspase activation in the cytoplasm of cells (Figure 1-9) (Samali et al., 1999; Beere, 2004).

1.6.2.3 HSP40 and HSP70

HSP40 protein functions as a pair with HSP70 protein to promote protein folding, protein transport and degradation (Li et al., 2009). Gotoh et al. (2004) showed that macrophages stably co-expressing HSP40 and 70 prevented NO-mediated apoptosis and pro-apoptotic mitochondrial protein BAX translocation from the cytosol to the mitochondria compared to wild-type control cells, suggesting that this co-chaperone anti-apoptotic action is through prevention of BAX translocation to the mitochondria (Beere, 2004; Gotoh et al., 2004).

Gabai et al. (2000a) showed, using an *in vitro* model of myocardial ischemia, transient energy deprivation of H9c2 myogenic cells, that HSP72 specifically down-regulates JNK activity by accelerating its dephosphorylation properties, and that UV- or TNF-induced JNK activation was suppressed by HSP72 accumulation (Gabai et al., 2000a; Gabai et al., 2000b). Park et al (2001) correlated this by demonstrating that overexpression of HSP72 in NIH3T3 cells suppresses UV-induced JNK activity, where *in vitro* binding and kinase studies suggested HSP72 binds to JNK to elicit this effect (Park et al., 2001). Gabai et al. (2002) showed that HSP72 blocked TNF-activation of the JNK pathway which temporarily blocked Bid activation and the subsequent apoptotic events, suggesting in TNF-induced apoptosis, HSP72 specifically

interferes with the Bid-dependent apoptotic pathway via inhibition of JNK (Gabai et al., 2002). HSP70, and its co-chaperone HSP40 partner, also inhibit JNK-mediated apoptosis by direct protein–protein interactions, which result in prevention of cleavage and activation of BID to tBID (Figure 1-9) (Benn and Woolf, 2004).

HSP70 prevents nuclear import of apoptosis inducing factor (AIF) following its release from mitochondria and, as a consequence, neutralizes its death inducing activity in Apaf-1-null cells (Beere, 2004; Benn and Woolf, 2004). In a study by Novoselova et al. (2006), macrophages and splenic lymphocytes irradiated with 632.8nm laser increased HSP70, but reduced HSP90 expression (Novoselova et al., 2006), providing preliminary evidence that HSP, 70 and 90 at least, may be involved in the neuroprotective effects seen with LILT.

1.6.2.4 HSP90

HSP90 play an important role in conformational protein regulation and cell signalling (Beere, 2004; Benn and Woolf, 2004). Sato et al. (2000) constructed deletion mutants and identified that amino acid residues 229-309 of AKT were involved in the binding to HSP90 and amino acid residues 327-340 of HSP90β were involved in the binding to AKT, whereby inhibition of these binding residues resulted in dephosphorylation and inactivation of AKT, indicating that HSP90 plays an important role in maintaining AKT kinase activity by preventing the dephosphorylation of AKT (Figure 1-9) (Sato et al., 2000; Beere, 2004; Benn and Woolf, 2004). Furthermore, HSP90 has also

been reported to prevent Apaf-1 oligomerization by directly associating with Apaf-1 (Beere, 2004)

1.6.2.5 HSP105

HSP105 is constitutively expressed and concentrated in the brain whereby synthesis is enhanced by the various stress stimuli, suggesting a specific role for HSP105 in stress responses within the nervous system (Wang and Bag, 2008). HSP105 is essential for cell survival in eukaryotes, however over-expression of HSP105 has been shown to have an anti-apoptotic effect in cultured neuronal PC12 cells (Hatayama et al., 2001). Ishihara et al. (2003) showed that HSP105 suppresses apoptosis in a cell culture model of polyglutamine disease, a neurodegenerative disease caused by the toxicity that is derived from a misfolded mutant protein. These findings suggest that overexpression of HSP105α suppresses cell death caused by expansion of the polyglutamine tract without chaperone activity, and the enhanced expression of the essential domains of HSP105α in brain may provide an effective therapeutic approach for CAG repeat diseases (Yamashita et al., 2007). HSP105 has also been shown to prevent caspase-activation induced by proteasomal inhibition with lactacystin in neuroblastoma cell line (Ishihara et al., 2003).

1.7 Ageing and signalling deficits

Ageing is a complex process by which organisms undergo cell deterioration within vital organs and is associated with alterations in skeletal, muscular, gastrointestinal, neuronal and metabolic processes (Harrison and

Pierzynowski, 2008; Calderwood et al., 2009). Mitochondrial dysfunction and decreased levels of neurotrophic factors and HSP that occur during the ageing process can result in decreased anti-apoptotic factor upregulation and disregulation of misfolded proteins that may contribute towards the neuronal loss which occurs in the ageing organism.

A proton leak, or mitochondrial uncoupling, occurs when protons re-enter into the mitochondrial matrix without contributing towards ATP synthesis, where the energy of the proton electrochemical gradient is released as heat, consequently leading to low ATP production associated with high levels of electron transfer and respiration (Bratic and Trifunovic).
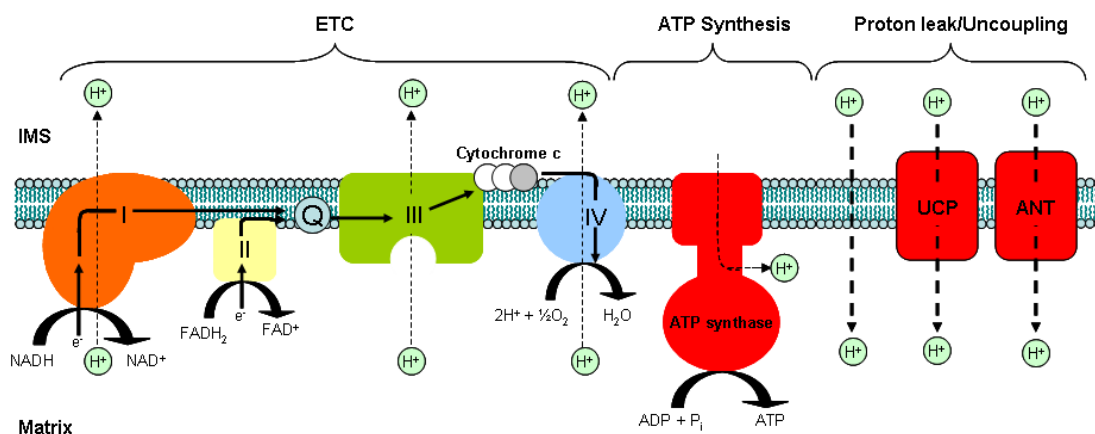
Figure 1-10: Proton leak during ageing Abbreviations: UCP, Uncoupling Protein; ANT, Adenine Nucleotide Translocator (Figure based on Conley et al., 2007).

This uncoupling can result in the reduction of oxygen production and the formation of reactive oxygen species (ROS), thus producing free radicals that cause oxidative damage (Bratic and Trifunovic). In 1956, Denham Harman proposed what is now known as the "free radical theory of ageing", proposing that oxidative damage accumulates in tissues over time which contributes to

the decline of physiological function in cells with age, and has become the most prevalent theories in ageing research to date (Harman, 1956; Van Remmen and Richardson, 2001). Low levels of ROS production has been implicated in initiating cell survival signalling, however excessive ROS production can cause lipid peroxidation damage to cell membranes and to DNA, this includes mitochondrial DNA (mtDNA) which has no associated histones and is therefore less protected against radical damage than nuclear DNA (Duchen, 2004; Burroughs and French, 2007). A consequence of the oxidative phosphorylation process is the generation of unpaired electrons that interact with O_2 resulting in the generation of superoxide ions, highly reactive free radical species (Duchen, 2004; Burroughs and French, 2007). These are readily converted to other free radical species, such as hydrogen peroxide (H_2O_2) and hydroxyl ions (OH^-) where excessive levels are thought to damage the ETC of the mitochondria (Duchen, 2004; Burroughs and French, 2007). As age increases, the accumulated ROS and therefore free radical production is proposed to contribute to decreased mitochondrial function, leading to further increased of ROS production due to the electron transport chain (ETC) uncoupling, increased mtDNA mutations, and decreased ATP synthesis, all of which contribute to declining physiological function as a consequence of ageing (Huang and Manton, 2004).

BDNF signal transduction pathways in the brain are important mediators of both genetic and environmental influences upon the ageing process (Mattson et al., 2004b). Decreased neuronal plasticity during the adult life span has been correlated with a reduction in the level of effectors i.e. BDNF, of

plasticity responses (Ruttiger et al., 2007). Croll et al. (1998) showed that BDNF mRNA is decreased in the pons and BDNF protein decreases in the midbrain of aged rats, and proposed that memory ability and impaired learning as measured with the Morris water maze resulted as a consequence of these reductions (Croll et al., 1998). Previous publications have suggested an involvement of BDNF in the pathogenesis of AD (Holsinger et al., 2000; Roka et al., 2000; Laske et al., 2006). Using western blotting and immunohistochemical techniques, Ferrer et al. (1999) demonstrated the selective decline of the BDNF and TRKB signaling pathway in the frontal cortex and hippocampus of individuals affected by long-lasting severe AD and age-matched controls. These data suggest that the decrease in BDNF and subsequent signalling may play a role in the cognitive decline that occurs during ageing (Ferrer et al., 1999). The reduction of BDNF as the ageing process occurs suggests that there would be a decrease in the ERK1/2 signalling pathways and phosphorylation of RSK90, and therefore a reduction of CREB phosphorylation which activates the Bcl-2, anti-apoptotic mitochondrial protein, discussed earlier.

The PI3-Kinase pathway is responsible for phosphorylating AKT to initiate cell survival actions following stimulation. Recent studies have shown a phosphorylation of AKT decreases as age increases. Nie et al. (2009) investigated the effects of ageing on AKT signalling in hippocampal tissue senescence-accelerated mice (SAMP10) and age-matched control mice. This study found whilst AKT mRNA remained constant during ageing, phosphorylated AKT was reduced in aged SAMP10 mice we, which was

accompanied by deterioration in performance of learning and memory tasks from 6 months of age (Nie et al., 2009). This suggests a potential decline in AKT may contribute to the learning and memory deficits seen during ageing.

An increase in protein damage has been shown to occur during ageing whereby HSP induction is reduced, resulting in the disregulation of mis-folded proteins and reduction of anti-apoptotic effects (Calderwood et al., 2009). Induction of HSP in response to heat shock declines in ageing cells, where cells lose the capacity to activate the transcriptional pathways leading to HSP synthesis (Keller et al., 2008; Calderwood et al., 2009). This attenuation of HSP induction can lead insufficient levels of HSPs available to regulate abnormal polypeptides, resulting in toxic accumulation which can initiate the apoptotic pathway (Sherman and Goldberg, 2001; Calderwood et al., 2009). There is plenty of evidence showing age increased accumulation of abnormal proteins, damaged by processes such as oxidative damage, isomerised residues and inactivation due to conformational change, where the reduction in HSP limits the ability of cells to deal with abnormal or misfolded proteins (Sherman and Goldberg, 2001). In addition to ageing, this has been suggested to indirectly contribute towards the progression of neurodegenerative diseases e.g. AD (Sherman and Goldberg, 2001).

1.8 Major Aims

The aim of this project was to determine whether IR1072 has neuroprotective effects, if any, in *in vitro* and behavioural or molecular beneficial effects in ageing CD-1 and TASTPM mice (*in vivo*). We used molecular i.e. immunoblotting, immunohistochemistry and behavioural techniques in order to address the following areas to achieve our overall aim:

1) to confirm behavioural cognitive benefits of IR1072 in aged CD-1 mice

2) to determine the effects of IR1072 in an Alzheimer disease mouse model (TASTPM)

3) to delineate the mechanisms underpinning the photomodulatory effects of IR1072 in CD-1 and TASTPM mice

4) to define the influence of age upon the photomodulatory effects of IR1072.

1.8.1 Primary hypothesis

IR1072 treatment elicits a beneficial effect in the ageing mammalian CNS via a multiple-step mechanism

Chapter 2: Materials and Methods

2.1 Animals

All mouse strains were maintained in the Life Sciences Support Unit (LSSU) located at the University of Durham. All animals had unlimited access to food and water until behavioural experiments commenced, and were maintained on a 12 hour light/dark cycle.

CD-1 mice were the in-house, inbred mouse strain used in this study, and were maintained at the University of Durham.

TASTPM mice (heterozygous double transgenic mice (TASTPM) with the Swedish (K670N; M671L) double familial mutation (Thy-1-APP695Sw, Line 10 (TAS10)) and the PS1 (M146V) mutation (Thy-1-PS-1M146V)) were backcrossed onto a pure C57BL/6 background originally obtained from GlaxoSmithKline (Harlow, Essex, UK) where a breeding programme was set up at the University of Durham and has continued for 2 years.

Pregnant (Embryonic day 17) Sprague-Dawley female rats were obtained from Harlem (UK). The rats were maintained in the LSSU at the University of Durham.

All animal husbandry, breeding and experimental procedures was performed in accordance with the Animals (Scientific Procedures) Act 1986.

2.2 Pure Cortical neuronal Cultures

All neuronal cultures were seeded and maintained in sterile Iwaki 24 well plates. The 24 well plates were coated using a poly-D-lysine solution (50µg/ml) and incubated for 1 hour at room temperature (RT). The poly-D-lysine solution was removed from the wells and subsequently rinsed with sterile water to remove any excess poly-D-lysine. The plates were left to air-dry for a further 1 hour at RT.

Pregnant female Sprague-Dawley rats at embryonic stage 17 (E17) were stunned and killed by neck dislocation (schedule 1). The embryonic sack was dissected and rinsed in ice-cold Hank's buffered saline solution (HBSS (-)) buffer (5mM KCl, 0.4mM KH_2PO_4, 137mM NaCl, 4mM $NaHCO_3$, 5mM Glucose, 5mM HEPES, 1mM Sodium Pyruvate, pH 7.4). The rat pups were decapitated and the heads rinsed in fresh HBSS (-) buffer, where the cortices were dissected and any visible blood vessels were removed.

The cortices were triturated 20 times in ~2mls of HBSS (-) using a wide-mouthed fire polished pipette, made up to a final volume of 10ml HBSS (+) (HBSS plus 1.25mM $CaCl_2$, 0.5mM $MgCl_2$, 0.85mM $MgSO_4$, pH 7.4) and left for 90 seconds to settle and remove any non-dispersed tissue.

The suspension was centrifuged at 500rpm for 1min, and the pellet was discarded. The supernatent was further triturated 10-20 times using a small-mouthed fire polished pipette and made up to a final volume of ~5mls with HBSS (+) buffer.

Cell population was determined using a haemocytometer, and a final cell density of 3000cells/mm^2 in Neurobasal culture medium containing, 2% B27 supplement, 20 units/ml penicillin, 20µg/ml streptomycin, 2.5µM Glutamate, 0.5mM Glutamax-1 was achieved.

Cultures were fed on DIV3, using Neurobasal culture medium absent of glutamate. Experiments were carried out on DIV 7 (Figure 2-1).
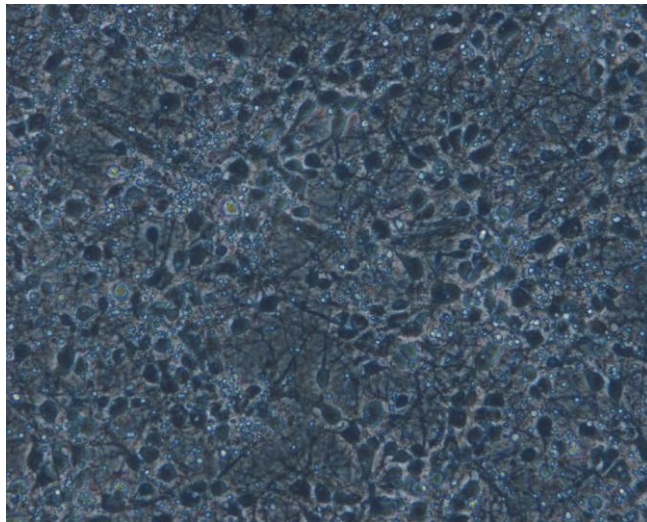
Figure 2-1: Pure cortical neuronal cultures produced in this study (DIV 7).

2.3 IR1072 Treatments

2.3.1 IR1072 Treatment Apparatus

The IR1072 treatment apparatus consists of 1072nm IR LED array which encloses the animals under investigation on all 6 sides facilitating irradiation of the target from every conceivable direction. The 1072nm LEDs are pulsed at 600 Hz with a duty cycle of 300 microseconds. The temperature of the LEDs are kept as close to room temperature as possible by a standard cooling fan, which reduces potential for thermal drift of the peak wavelength. The same specification and duty cycle for the 1072nm LEDs used in the panel for cell lines was the same. The treatment cycle for *in vivo* experiments is 6 minutes and 3 minutes for *in vitro* experiments. The LEDs were supplied by Virulite Distribution Limited.

2.3.1.1 *In Vitro*

Pure neuronal cultures (DIV7) received 5 x 3 minute sham- or IR1072-treatments and incubated in a 37ºC, 5%CO_2, 95% O_2 incubator. After 4 hours, the media was removed and the sham- or IR-treated cultures were subjected to a 10 minute incubation with exposure buffer solution (EBS) buffer (2.5mM $CaCl_2$, 5mM KCl, 137mM NaCl, 0.3mM KH_2PO_4, 4mM $NaHCO_3$, 0.3mM Na_2HPO_4, 5.6mM glucose, 0.01mM glycine, 10mM HEPES, pH7.4) alone (sham; n=6) or EBS containing 1mM glutamate (insult; n=6) for 10 minutes at RT, where the buffer was replaced with fresh media and incubated at 37ºC, 5%CO_2, 95% O_2. Twenty-four hours following the sham or insult treatment, an MTT assay (Mosmann, 1983) was performed by adding 0.5 mM MTT (3-(4,5-

Dimethylthiazol-2-YI)-2,5-diphenyltetrazolium bromide) to all treated cultures in order to determine cell viability.

2.3.1.2 *In Vivo*

2.3.1.2.1 Acute IR Treatments

CD-1 male mice or TASTPM male mice were exposed to IR1072 treatment box for 6 minute daily sessions over a 10 day period. Brains were dissected immediately following the final IR1072 treatment and prepared for immunoblotting or mitochondrial studies.

2.3.1.2.2 Chronic IR Treatments

CD-1 male mice or TASTPM mice were exposed to sham or IR1072 treatments for 6 minute sessions for two consecutive days, biweekly over 5-6 months, during which time weights of the mice and internal box temperatures for sham and IR treatments were monitored. Sham treatments were carried out using a replica IR treatment box that did not emit infra-red light. Following IR treatments, mice were subjected to 12 day behavioural testing on the 3-D radial maze, as described in Chapter 4. Brains were dissected immediately following the final behavioural test and prepared for immunoblotting, immunohistochemistry, or ligand autoradiography purposes.

2.4 Behavioural Paradigm: 9-arm 3D Radial Maze

2.4.1 Food Deprivation

Chronically treated Sham or IR1072-treated CD-1 mice or TASTPM mice were food-deprived for 24hrs prior to behavioural testing, and subsequently given 5g of food daily. TASTPM mice required food pellets to be soaked in water beforehand in order to soften the food, otherwise mice were unable to feed properly. Water availability remained *ad libitum* for all mice. During behavioural testing, 1 small food pellet was available on the end of each arm. One sham and one IR-treated TASTPM female mouse died before behavioural testing (cause unknown).

2.4.2 9-arm 3-D Radial maze

The maze is made from grey PVC (5 mm thick). It consists of 9 arms radiating from a central platform. Each arm (51 x 11.2 cm) is made from two segments, extended from an octagonal shaped central hub (43 cm in diameter) and can be manipulated independently. The first segment of an arm (15.2 x 11.2 cm) directly attached to the central platform was tilted to form a 60º slope and constitutes a bridge that allows access to the second segment (35 x 11.2 cm) of the arm which is presented horizontally either at the same (flat arm configuration), below (lowered arm configuration) or above (raised arm configuration) the level of a central platform. In order to change the configurations of the maze, the central platform can be raised or lowered. Each entry to a bridge is narrowed with a short wire mesh wall (8 x 4 cm) either on the left or on the right side. The narrowing of the entries to and exits from the bridges are designed to prevent mice relying entirely on sequential

arm choices. The end of each arm is extended with panels of identical size (20.2 x 11.2 cm). These panels are used for holding intra-maze cues made of distinctive pattern drawings designed on plastic adhesive material and attached to a PVC board (18 x 11.2 cm). Sidewalls, about 1 cm high, extended the length of each arm. There are no enclosures surrounding the central platform, bridges or arms. The maze is totally surrounded with a heavy beige-light colored curtain. A camera is centered 180 cm above the central platform. The ambient light at the surface of the central platform is 180 Lux.

Testing procedures: Naïve food deprived mice were introduced to the maze to acquire a spatial working memory task. They had no previous experience or habituation to the maze. They are placed in the central platform and let free to explore the maze until 9 arm choices are made or 10 minute elapsed. One food pellet is available at the end of each arm. A first visit to an arm is a recorded as unique visit (correct choice) and any subsequent visit is considered as a repeated choice or incorrect choice. A mouse can make up to 8 repeated visits to the same arm. Animals are tested one session a day on 12 consecutive days.

Tools and recording measures: During the test, mice were observed on a screen monitor connected to a video camera suspended above the test arena. The video record of the experiment is run on a computer screen monitor through a capture card. The experiment is also video taped, the experimenter can review the VCR tape and check the accuracy of the recording at any time.

An in-house computer program is used to record the frequency of entries as well as the duration and latencies of entries of pre-defined areas of the maze.

Measurements and statistical analysis: Several measurements were considered. A session last until 9 choices are made or 10 minute elapsed. An entry to an arm or a bridge is recorded whenever a mouse crosses with all four paws the line that delimits these areas.

1) **Number of repeated visits to arms:** This measure refers to incorrect choices or errors. An arm that is visited only once during a session is considered as a unique entry to that arm (a correct choice). A session last until 9 choices are made or 10 minute elapsed. Each entry to an arm is considered as one choice. An animal can make up to 9 visits to the same arm. The first visit is considered a unique visit or a correct choice and subsequent visits are considered repeated choice or incorrect choices. In the first few sessions a mouse may visit a few arms or may not visit any arms. In this case, a mouse that did not visit any arm would receive a penalty of 9 repeated visits. For a mouse that made less than 9 choices, the number of the remaining arm choices is added to their actual number of repeated arm visits. For example, a mouse that has made 5 choices and 2 repeat visits to arms will be recorded having made 3 unique visits and 6 repeated visited (the actual 2 repeats + the remaining 4 arm choices). A mouse that has made 5 choices and 0 repeat visit to arms will be recorded having made 5 unique visits and 4 repeated visited.

2) **Number of arm entries before first repeated arm visit:** An arm that is visited only once during a session is considered as a unique entry to that arm *(see number of repeated visits to arms below).* A mouse that did not visit any arm will be recorded as having made 0 unique visits before first repeat. A mouse that made less than 9 choices with no repeat was recorded as having made the first repeated choice after the last arm visit. This measurement indicates whether an animal made an arm repeat earlier or later in a session.

3) **Number of bridge and arm entries:** An entry to a bridge was recorded only once if a mouse entered a bridge and continued to an arm. A return from an arm to a bridge within the same visit was not recorded.

4) **Arm/Bridge ratio for number of entries:** Number of arm entries divided by the number of bridges entries. A ratio close to 1 describes an animal that continued to an arm each time it visited a bridge. A ratio close to 0 described an animal that made numerous visits to bridges before engaging onto an arm. In the former, the animal showed no hesitations or fewer hesitations to engage fully onto an arm whereas in the latter the animal demonstrated more hesitations before adventuring on an arm.

5) **Arm/Bridge ratio for duration of entries:** Duration of arm entries divided by duration of bridge entries. A ratio close to 1 described an animal that spent an approximate equal amount of time on the arms and the bridges. A ratio close to 0 described an animal that spent less time on the arms than on the bridges while a ratio above 1 indicated the opposite. The former could have indicated that animals are reluctant to spent longer time in the arms (brief entries).

6) **Number of bridge entries before first arm visit:** Animals that did not visit any arm in a session received the highest recorded number of bridges visited before first entry from any mouse in that session.

7) **Latency of first entry to a bridge:** The time spent by a mouse in the central platform before it entered one of the bridges for the first time with all four paws. A mouse that did not enter a bridge received the highest score which was 10 minute.

8) **Latency of first entry to an arm:** The time spent by a mouse in the central platform and bridges before entering the arm for the first time. A mouse that did not enter any arm received the highest score which was 10 minute.

9) **Total time spent in the central platform:** The time was recorded from the entry of a mouse with all four paws in the central platform until it exited to a bridge.

10) **Total time spent on the bridges:** The time recorded from the entry of a mouse with all four paws in a bridge until exiting the central platform or to an arm. If a mouse entered a bridge and continued to an arm, then the time on an arm was subtracted from the time spent on a bridge.

11) **Total time spent on the arms:** The time recorded from the entry of a mouse with all four paws in an arm until it exiting to the bridge.

12) **Session duration:** Animals were removed from the maze at the end of a session when 10 minute elapsed or when the animal returned to the central platform after 9 choices were made. A choice was considered any visit or repeated visit to an arm.

2.5 Immunoblotting

2.5.1 Sample Preparation

CD-1 or TASTPM mice were sacrificed by CO_2 narcosis and brains were rapidly dissected, where the left hemisphere was separated and snap frozen to be stored at -20ºC in preparation for homogenisation. The brains were individually homogenised in 5ml of homogenisation buffer (50mM Tris-Base, 5mM ethylenediaminetetraacetic acid (EDTA), 5mM ethyleneglycotetraacetic acid (EGTA) and 150μM protease inhibitor cocktail III (PICIII), pH7.4) per cortices, where protein concentration was determined spectrophotometrically by the Lowry Protein Assay (Lowry et al., 1951). Protein (10-50μg) was prepared for immunoblotting in 3X sample buffer (30mM NaH_2PO_4, 30% (v/v) glycerol, 0.05% (w/v) Bromophenol blue, 7.5% (w/v) sodium dodecyl sulphate (SDS), made up in dH_2O) made up to a final volume of 15μl with dH_2O and applied to an SDS-PAGE gel or stored at -20ºC.

Dithiothreitol (DTT; 23.5mM final concentration, from a 200mM stock solution made with dH_2O) was added to the samples and mixed thoroughly, pulsed at 13000rpm, incubated for 5 minutes at 95°C, pulsed again at 13000rpm, and mixed thoroughly in preparation for electrophoresis.

2.5.2 Immunoblotting

Samples for immunoblotting were subjected to SDS-PAGE (Chazot et al., 2002). For sample loading, wells were formed in a 6.5% SDS-PAGE stacking gel (56.9% (v/v) dH_2O, 24.7% (v/v) stacking gel buffer (1M Tris, 1% (w/v) SDS), 16.1% (v/v) acrylamide (40%), 2% ammonium persulphate (APS; 1mM

stock made with dH$_2$O) and 0.25% TEMED) using a 0.75mm 10 well comb, set above 10%-15% acrylamide resolving gels (47.6% (v/v) dH$_2$O, 23.8% (v/v) acrylamide (40%), 23.8% running gel buffer (0.5M Tris, 8mM EDTA, pH6.8, 0.4% SDS (w/v), pH 8.8), 4.8% APS (1mM stock made with dH$_2$O), and 0.8% TEMED). Once set, Hoefer Mighty small II vertical slab gel electrophoresis tanks were filled with electrode buffer (5mM Tris, 0.38mM Glycine, 2mM EDTA, pH 8.8) and prepared samples or a pre-stained standard (10-250kDa) were loaded in to the wells using a 50µl syringe.

Electrophoresis was conducted at 180V and 10mA, until the samples had entered the resolving gel, and subsequently increased to 15mA until electrophoresis has finished.

The protein from the resolving gel was then transferred to a nitrocellulose membrane using a Hoefer TE series transfer unit, set at 50V, <200mA for 2.5hrs in transfer buffer (25mM Tris, 192mM Glycine, 20% Methanol (v/v)).

2.5.3 Antibody labelling of immunoblots

The nitrocellulose was incubated in a block buffer consisting of 5% Marvel (dried skimmed milk (w/v)), 0.2% Tween 20 (v/v), and NaOH (4mM) made up with TBS (50mM Tris, 0.9% sodium chloride (w/v), pH7.4) for 1 hour at RT. Following blocking, the nitrocellulose was probed with a primary antibody in incubation buffer (2.5% Marvel (w/v) in TBS) at antibody-specific incubation times at 4°C (see Table 2-1). Following primary antibody incubation, the nitrocellulose was subjected to four 10 minute washes (5% Marvel (w/v), 0.2%

Tween 20 (v/v) made up with TBS) and incubated with HRP-linked anti-rabbit secondary antibody for 1hr, after which further four 10 minute washes followed, and finally rinsed in TBS buffer.

Following antibody labelling, the nitrocellulose was incubated in a luminol solution (100mM Tris, pH8.5, 1.25M Luminol) containing 1mM p-coumaric acid, and 0.5% (v/v) hydrogen peroxide (30% stock) for 1 minute and exposed to ECL hyperfilm (Amersham) at varying exposure times depending on the primary antibody being used. The hyperfilm was developed manually using Kodak GBX fixer and developer solutions.

The signal volumes from each lane were scanned and analysed using Image J to quantify the optical density of the labelled bands compared to the background. Protein levels were standardised using mouse β-actin primary antibody (1:5000 dilution, purchased from Sigma).

2.6 Immunohistochemistry

2.6.1 Tissue preparation

CD-1 or TASTPM mice were sacrificed by CO_2 narcosis and brains were rapidly dissected, where the right hemisphere was separated and placed in fixative solution (4% paraformaldehyde, 0.1M Na_2PO_4, 0.1M NaH_2PO_4, pH adjusted with NaOH). Samples were post-fixed for one week in fixative solution, and subsequently dehydrated using sucrose infiltration, where the tissue is placed in 10% sucrose, then 20% sucrose made up with Phosphate

Buffered Saline (PBS diluted from a 10X stock purchased from Sigma). Once dehydrated, the tissue was snap frozen in iso-pentane -70⁰C for 1 minute and stored at -80⁰C. Samples were sliced sagitally into 25µm thick sections at -25⁰C using a Leica model CM 3050S Cryostat. Sections were transferred into a 24 well plate, with each well containing PBS 0.05% (w/v) sodium azide and stored at 4⁰C.

2.6.2 Immunohistochemistry

In order to inhibit endogenous peroxidase activity, samples were incubated in a solution consisting of 10% (v/v) methanol, 3% (v/v) hydrogen peroxide (30% stock), made up in TBS, and incubated for 30 minutes at RT.

The samples were subjected to three 5 minute washes in 0.2% (v/v) Triton-X-100 in TBS (TBS-T), and incubated in 0.2% (w/v) glycine in TBS for 30 minutes at room temperature in order to quench any excess paraformaldehyde.

The samples were further incubated in a blocking solution consisting of 10% foetal calf serum (FCS) in TBS-T, after which a primary antibody was added at the respective concentration and incubation time (see Table 2-1) in 1% FCS in TBS at 4⁰C.

Following the primary antibody incubation, the samples were left to equilibrate to RT for 1 hour. Once the samples had reached RT, TBS-T washes followed as previous and samples were incubated with 50µl of anti-rabbit biotinylated

secondary antibody (from Vectastain ABC kit, purchased from Vector Laboratories) diluted in 10ml of 1% Fotal Calf Serum (FCS) in TBS for 2 hours at RT.

Following another wash stage, the samples were incubated with ABC reagent (100µl reagent A and 100µl reagent B (from Vectastain ABC kit) diluted in 5ml TBS; made up 30 minutes prior to use) for one hour at RT. Samples were subjected to another wash stage as previous, with a further two 5 minute washes with TBS alone.

Samples were allowed to develop in 3,3-Diaminobenzidine (DAB) solution (200µl TBS, 100µl DAB and 100µl H_2O_2 in 5ml dH_2O; DAB peroxidase substrate kit obtained from Vector Laboratories) until the optimal signal had been achieved (see Table 2-1), where the DAB solution was removed and the reaction stopped with dH_2O and further rinsed. Sections were dehydration mounted and set with DPX mountant. Stained sections were viewed on a Nikon Eclipse E400 microscope, where images were photographed using Progen Eyepeice 1.3 and 3M Pixel camera.

2.7 AMPA Autoradiography

2.7.1 Tissue Preparation

CD-1 or TASTPM mice were sacrificed by CO_2 narcosis and brains were rapidly dissected, where the brain underwent sucrose infiltration, as per immunohistochemical tissue preparation. Once the brains had been dehydrated, they were snap frozen in iso-pentane -40ºC for 3 minutes and

stored at -80ºC. Samples were sliced horizontally into 20µm thick sections at -25ºC using a Leica Cryostat model CM 3050S. Sections were collected on to poly-D-lysine coated glass slides and stored at -20ºC.

2.7.2 Ligand Autoradiography with [3H] AMPA

Sections were left to reach RT for at least 1 hour before the protocol commenced. The sections were then pre-incubated for 20 minutes in pre-incubation buffer (30mM Tris, pH 7.4) on ice.

Following pre-incubation, sections were transferred to radioligand buffer (30mM Tris pH7.4, 20nM [3H] AMPA and 100mM KSCN) and incubated on ice for 1 hour. For non-specific binding, sections followed the same protocol as radiolabelled sections except with the addition of 1mM glutamate into the radioligand buffer.

After incubation with the radioligand or non-specific buffer, sections were subjected to three 15 second washes with wash buffer (30mM Tris, pH7.4, 100mM KSCN) and a final wash of dH_2O; all conducted on ice.

After the washes, sections were left overnight to dry before being placed in an autoradiography cassette exposed to [3H] Hyperfilm (Amersham), prepared in a darkroom and left for 5 weeks before manual developing using the Kodak GBX fixer solutions as per immunoblots.

2.8 Mitochondrial Respiratory Studies

2.8.1 Mitochondrial isolation

TASTPM or CD-1 mice were stunned and decapitated, where the forebrain and liver were dissected and immediately placed in ice-cold brain or liver isolation buffer (220mM Mannitol, 60mM Sucrose, 5mM Tris-HCl, 0.5mM (EGTA), and 1mg/ml Bovine Serum Albumin, pH 7.4 or 250mM sucrose, 3.4mM Tris-HCl pH7.4, respectively). The tissue was rinsed several times in isolation buffer to remove any excess blood, and finely chopped in a small volume (~5ml) of isolation buffer.

A glass dounce homogeniser, in a 7ml mortar with a loose pestle was used to homogenise the tissue gently 3-4 times, then 7-8 times with a tight pestle where a smooth suspension was achieved. The homogenate was transferred to a centrifuge tube and centrifuged at 500g (0-4°C) Beckman J20 rotor for 10 minutes. Following centrifugation, the pellet was discarded and the supernatant centrifuged for a further 10 minutes at 12,000g (0-4°C). This remaining pellet is the crude mitochondrial pellet which contains mitochondrial synaptosomes and other membranous material.

The supernatant from the liver preparation was discarded and the pellet resuspended in 0.5ml isolation buffer in preparation for oxidative phosphorylation studies.

The supernatant from the brain preparation was discarded and the pellet was resuspended in 9ml of isolation buffer and aliquoted in layers on to 10ml ice

cold Percoll solution (250mM sucrose, 5mM Tris-HCl, 0.1mM EGTA, and 18% Percoll, pH7.4) and centrifuged at 12,000g for 45 minutes.

A loose mitochondrial pellet, free from most contamination was formed at the bottom of the tube and a synaptosomal layer on the top. The mitochondrial layer was isolated and resuspended in chamber buffer (220mM Mannitol, 60mM Sucrose, 5mM Tris-HCl, and 1mg/ml Bovine Serum Albumin, pH 7.4) and centrifuged twice at 12,000g for 10 minutes to remove the Percoll. The final pellet was resuspended in ~100µl chamber buffer for respiration studies. protein concentration was determined spectrophotometrically by the Lowry Protein Assay (Lowry et al., 1951).

2.8.2 Oxidative Phosphorylation Protocol

A Clark-type oxygen electrode was used to measure mitochondrial oxygen consumption polargraphically (Sweetman and Weetman, 1969) with a maximum bath volume of 1ml (Rank bros, Bottisham, UK). A Kipp and Zonen Flat bed recorder was calibrated to give a full scale deflection of 10mV and a chart speed of 0.5mm/sec, and used to record the changes in oxygen consumption.

A reaction chamber with a final volume of 0.3ml containing incubation buffer plus 5mM KH_2PO_4 was produced, where the buffer was saturated with oxygen (139ng O atoms/ml), and the experiment began with the addition of brain (0.3-0.5mg) or liver (0.9-1.2mg) mitochondrial protein was used to measure mitochondrial respiration. After the endogenous respiration of substrates was

recorded for 1 minute, substrate (5mM glutamate plus 5mM malate, or 5mM succinate) was added in order to record state 4 respiration, where the mitochondria would respire in the presence of excess amount of oxygen and substrate, and the absence of ADP. After 1min, ADP (167µM) was added creating a reaction where ADP, substrate and oxygen are present in excess and so measuring state 3 respiration. Once all ADP had been phosphorylated, the respiration returned to state 4 where substrate and oxygen were found in excess, absent of ADP (Chance and Williams, 1956).

Respiratory rates were calculated as nanoatoms of oxygen consumed per minute per mg mitochondrial protein. RCI was calculated by dividing the state 3 respiration rate by the return to state 4 respiration rate. This value gives an indication of the integrity of the mitochondria, and is a measure of the coupling of oxidation in the ETC to ATP synthesis. Values greater than 3 and 2, for glutamate plus malate and succinate respectively, indicate tightly coupled mitochondria (Chance and Williams, 1956).

2.8.3 Electron Microscopy

An electron micrograph (Figure 2-2) was obtained to prove the presence of intact mitochondria from the mitochondrial isolation protocol detailed. Electron Microscopy was conducted by Mrs. Christine Richardson in the Histology laboratory at the University of Durham.

Following mitochondrial isolation, the pellet was resuspended in Karnovsky fixative (2% paraformaldehyde, 2.5% glutaraldehyde in 0.1M phosphate

buffer, pH7.4) for 2 hours, after which the suspension was divided into 1.5ml eppendorf tubes and centrifuged at 2,000g for 1 minute. The supernatant (fixative) was removed and the pellet received 3 x 5 minute washes in 0.1M phosphate buffer. The pellet was then resuspended and post-fixed in 1% Osmium Tetroxide in 0.1M phosphate buffer for 1 hr. The supernatant was removed and the pellet was again washed 3 x 5 minute washes in 0.1M phosphate buffer. The pellet was then dehydrated through a series of alcohols:

50%, 70%, 95% alcohol 3 x 5min

100% alcohol 3 x 10min

The pellet was then resuspended in a 50:50 mixture of 100% alcohol:propylene oxide 3 x 5min incubations. The pellet then received 3 x 10 minute incubations with propylene oxide, and a further 3 x 1hr incubations with the 50:50 mixture of propylene oxide:araldite. The pellet was then incubated overnight with araldite, where the following day the pellet was subjected to two changes of araldite and polymerised at 60ºC for 24hrs.

The mitochondrial samples were received ultrathin sectioning at 60nm, where sections were picked up on to 200 mesh copper grids and stained with 1% uranyl acetate made in 70% alcohol for 10 minutes, and Reynold's lead citrate for 10 minutes. Sections were viewed using a Hitachi S7600 Transmission Electron Microscope.

A

B
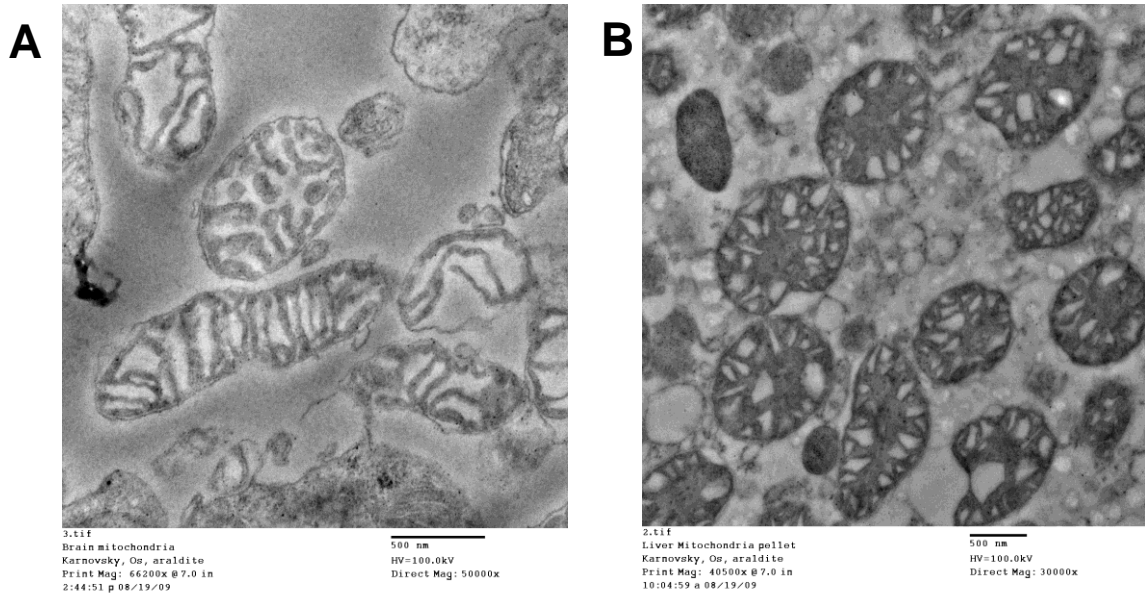
Figure 2-2: A representative electron micrograph image of A) brain and B) liver mitochondria prepared from the isolation protocol. The scale bar represents 500nm, at a A) 50,000X magnification and a B) 30,000X magnification.

Sample Sets	Commercial Antibody Information			Immunoblotting				Immunohistochemistry		
	Antibody	2º Ab	Company	SDS Gel (%)	1º Ab Dilution	Days Inc	Exposure time (min)	1º Ab Conc.	Days Inc.	Dev Time
CD-1 & TASTPM	BDNF	Rb	AbCam	10	1:1000	1	1-3	1:2000	1	5
	ERK1/2	Rb	Cell Signalling	10	1:1000	1	1-3	1:4000	1	5
	ERK1/2-P	Rb	Cell Signalling	10	1:125	2-3	10	1:250	2-3	10
	CREB	Rb	Cell Signalling	10	1:125	2-3	10	1:1000	1	5
	CREB-P	Rb	Cell Signalling	-	-	-	-	1:250	2-3	5
	AKT	Rb	Cell Signalling	10	1:2000	1	1-3	1:1000	1	5
	AKT-P	Rb	Cell Signalling	10	1:1000	2-3	1-3	1:1000	1	5
	HSP27	Rb	Cell Signalling	15	1:125	2-3	10	1:200	2-3	10
	HSP40	Rb	Cell Signalling	10	1:125	1-2	7-10	1:200	2-3	10
	HSP60	Rb	Cell Signalling	10	1:125	1-2	5-10	1:200	2-3	10
	HSP70	Rb	Cell Signalling	10	1:125	1-2	5-10	1:200	2-3	10
	HSP90	Rb	Cell Signalling	10	1:125	1-2	5-10	1:200	2-3	10
	HSP105	Rb	Cell Signalling	10	1:250	1-2	5-10	1:200	2-3	10
TASTPM	βA_{1-42}	Rb	Chemicon	-	-	-	-	1:250	1	5
	$\beta A_{1-40/42}$	Rb	Chemicon	10	1:250	1-2	1-5	1:4000	1	5
	APP	Rb	Chemicon	10	1:1000	1-2	1-5	1:2000	1	5

Table 2-1: Table depicting the varying antibodies and concentrations for differing protocols used in this study. BDNF; Brain Derived Neurotrophic Factor; ERK1/2 or ERK1/2-P; unphosphorylated or phosphorylated extracellular-signal regulated kinase 1 or 2, respectively; AKT, Protein Kinase B; CREB, Cyclic Adenosine Monophosphate (AMP) Response Element Binding; HSP, Heat Shock Protein; Aβ, β-amyloid; APP, Amyloid Precursor Protein; SDS, Sodium Dodecyl Dulphate; Rb, rabbit; Ab, antibody.

Chapter 3: Acute IR1072 Treatment: Effects in rat neuronal cultures (*in vitro*) and CD-1 mice *(in vivo)*

3.1 Introduction

3.1.1 *In vitro* model system - neuronal cultures

Neuronal cultures are a useful *in vitro* experimental model for studying all aspects of neuronal processes including therapies that may influence neuronal differentiation, excitability, and synapse formation and/or function *in vivo* (Sicaeros and O'Dowd, 2007; van Rensburg et al., 2009). Where *n*-numbers in *in vivo* experimental protocols are counted as one *n*-number per single animal, *in vitro* models class one n-number as a population of cells in a growth vessel, as the process of de-differentiation commences immediately after the tissue has been extracted from the parent tissue therefore establishing a unique model system in a constant state of change (Hartung et al., 2002), ensuing the possibility of hundreds of *n*-numbers per single animal, and consequently a cheaper and more ethical, i.e. reduction in animals, approach to establishing data preceding more expensive *in vivo* investigations.

For this investigation, a treatment regime for an *in vitro* neuronal culture system was devised based on a previous study by Bradford et al. (2005) who tested a range of IR treatment protocols on cell viability in human lymphocytes, and found that cells irradiated with IR1072 using a 5 x 3 minute treatment protocol was significantly higher than that of cells irradiated with other IR wavelengths using the same protocol. The preliminary aim was to

establish whether IR1072 preconditioning had any protective effect on cell viability in a neuronal *in vitro* model system of excitotoxicity before establishing any molecular changes of IR1072 preconditioning in an *in vivo* animal model of premature ageing.

3.1.2 *In vivo* model system - CD-1 mice

CD-1 mice have a high mortality rate at approximately 2 years of age, and have been shown to have learning deficits at a premature age, as young as 3 months old, where circulating amyloidosis has been implicated as a major contributing factor (Ennaceur et al., 2008). Ennaceur et al. (2008) performed detailed behavioural analysis of male and female 4 month old and 13 month old CD-1 mice, and found that 4 month old male CD-1 mice make significantly more errors in the behavioural task compared to young female CD-1 mice. This correlates with previous reports that 3 month old male CD-1 mice were unable to acquire a working memory task in a continuous choice procedure (Mizumori et al., 1982). As CD-1 mice show learning deficits at as early an age as 3 month old (Mizumori et al., 1982), another preliminary aim was to investigate protein expression or mitochondrial respiratory changes in young CD-1 mice following acute exposure to IR1072, before instigating more costly and time consuming chronic IR1072 exposure protocols.

Previously, 10 daily sessions of 6 minute IR1072 exposures has been shown to improve overall cognitive performance in middle-aged mice (12 monh old) compared to young 3 month old CD-1 mice. This study has undertaken the

same treatment protocol, 10 daily 6 minute sessions of IR1072, in CD-1 mice in order to obtain our objectives.

The aim of this chapter was to establish preliminary data pertaining to the neuroprotective effect of IR1072 on *in vitro* (neuronal cultures) and *in vivo* (CD-1 mice) systems, and to investigate proposed primary (mitochondria) and secondary (signalling) mechanisms of IR1072 LILT.

3.2 Results

3.2.1 IR1072-preconditioning of pure neuronal cultures: Cell viability

Glutamate excitotoxicity, has been hypothesized to play a key role in neuronal dysfunction and neuronal death in several neurological disease states in the CNS (Akaike, 1994; Skaper et al., 2001; Canzoniero and Snider, 2005). Glutamate excitotoxicity is generally accepted to act through the glutamate NMDA subtype receptors in cortical neurons, since the excitotoxic event can be abolished by addition of NMDA receptor antagonists (Meldrum, 1990; Santos et al., 2001; Skaper et al., 2001; van Rensburg et al., 2009). Overstimulation of these receptors can result in calcium overload which may compromise mitochondrial integrity, accelerating free radical production and can ultimately lead to cell death (de Bock et al., 1998; Skaper et al., 2001). A reproducible and reliable *in vitro* model of excitotoxicity is critical to understanding the cellular and molecular mechanisms of neurodegenerative processes *in vivo* (van Rensburg et al., 2009).

An *in vitro* excitotoxic model was used in this study, which was adapted for pure neuronal cultures in a study conducted by Van Rensburg et al. (2009) where pure neuronal cultures were treated with an insult of 1mM glutamate for 10 minute, to achieve approximately 10-30% neuronal loss, determined 24 hours following the insult using an MTT assay. Preceding the excitotoxic insult, neuronal cultures were preconditioned with 5 x 3 minute IR1072 exposure and incubated for four hours at 37ºC.

Data was analysed using a one-way ANOVA followed by Bonferroni post-test. Data represent mean ± SEM. The experiments can be divided into three types in terms of severity of insult: Mild, moderate, and severe.

Formulation used to calculate the increase in neuronal cell viability following IR1072 irradiation was as follows:

Increase in % cell viability following IR x 100= % neuroprotection
            Total % neuronal loss

i.e Sham % insult - IR % insult X 100
            Sham % insult

(100 - [-IR-G]) - (100 - [+IR+G]) x 100 = % neuroprotection
            (100 - [-IR-G])

e.g. Mild Insult: (100 - 85.99) - (100 - 98.61) = 14.01 - 1.39 x 100 = 90.08%
            (100-85.99)   14.01

3.2.1.1 Mild insult

In the presence of glutamate (n=6, 85.99 ± 8.18%), sham-preconditioned neuronal cultures displayed a significant decrease in cell viability (14.01%) compared to control insults absent of glutamate (n=6, 100.0 ± 7.56 p<0.01%). In the presence of glutamate (n=6, 96.32 ± 2.78%), IR1072-preconditioned neuronal cultures displayed no change in cell viability, compared to control insults absent of glutamate (n=6, 98.61 ± 4.26%, Figure 3-1) Cell viability in IR1072-treated neuronal cultures that received a glutamate insult (n=6, 96.32 ± 2.78%) was significantly increased (90.08%, p<0.01) compared to sham-preconditioned cultures (n=6, 85.99 ± 8.178) which had received the same insult.
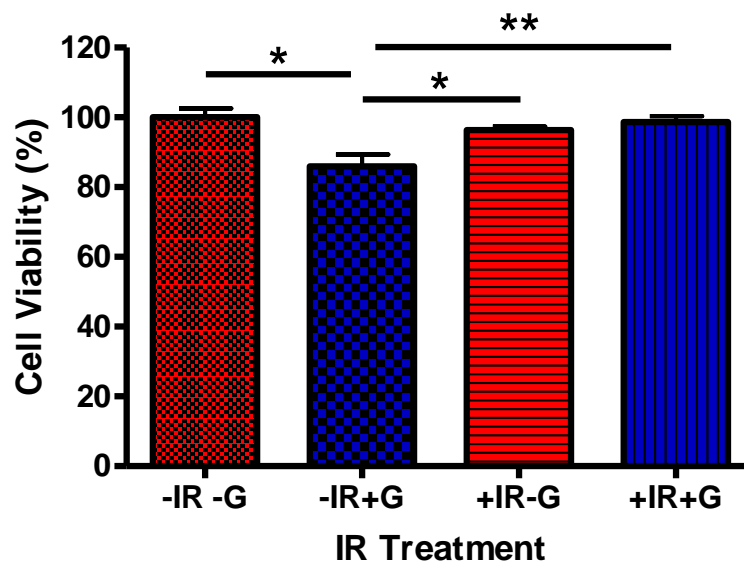
Figure 3-1: Column graph showing the effects of IR1072 on cell viability in DIV7 mixed cortical cultures following a mild excitotoxic insult. Abbreviations: -IR-G, sham pre-treatment and sham insult (representing 100%); -IR+G, sham pre-treatment and glutamate insult; +IR-G, IR pre-treatment and sham insult; +IR+G, IR pre-treatment and glutamate insult. Cell viability determined via an MTT assay. Mean values +/- SEM for n = 6 replicates from one culture, *p < 0.05, **p < 0.01.

3.2.1.2 Modest insult

In the presence of glutamate (n=6, 75.29 ± 5.43%), sham-preconditioned neuronal cultures displayed a significant decrease in cell viability (24.7%, $p < 0.001$) in sham-preconditioned cultures, compared to control insults absent of glutamate (n=6, 99.99 ± 4.26%). In the presence of glutamate (n=6, 86.33 ± 5.14%), IR1072-preconditioned neuronal cultures displayed a significant decrease in cell viability (19.4%, $p < 0.001$), compared to control insults absent of glutamate (n=6, 107.2 ± 7.03%, Figure 3-2). Cell viability in IR1072-preconditioned neuronal cultures that received a glutamate insult (n=6, 75.29 ± 5.43%) was significantly increased (44.7%, $p < 0.01$) compared to sham-preconditioned cultures (n=6, 86.33 ± 5.14%) which had received the same insult.
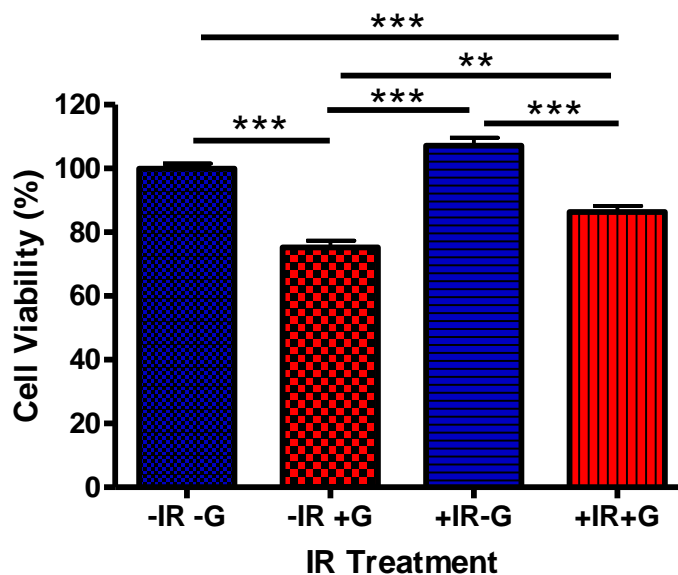
Figure 3-2: Column graph showing the effects of IR1072 on cell viability in DIV7 mixed cortical cultures following a moderate excitotoxic insult. Abbreviations: -IR-G, sham pre-treatment and sham insult (also representing 100%); -IR+G, sham pre-treatment and glutamate insult; +IR-G, IR pre-treatment and sham insult; +IR+G, IR pre-treatment and glutamate insult. Cell viability determined via an MTT assay. Mean values +/- SEM for n = 6 replicates from one culture, ** $p < 0.01$, ***$p < 0.001$.

3.2.1.3 Severe insult

In the presence of glutamate (n=6, 66.29 ± 5.55%), sham-preconditioned neuronal cultures displayed a significant decrease in cell viability (33.71%, p<0.001), compared to control insults absent of glutamate (n=6, 100.0± 8.39%). In the presence of glutamate (n=6, 66.37 ± 8.54%), IR1072-preconditioned neuronal cultures displayed a significant decrease in cell viability (27.1%, p<0.001), compared to control insults absent of glutamate (n=6, 91.27 ± 7.58%, Figure 3-3). No difference in cell viability in IR1072-preconditioned neuronal cultures that received a glutamate insult (n=6, 66.37 ± 8.537%) was shown (0.002%) compared to sham-preconditioned cultures (n=6, 66.29 ± 5.55%) which had received the same insult.
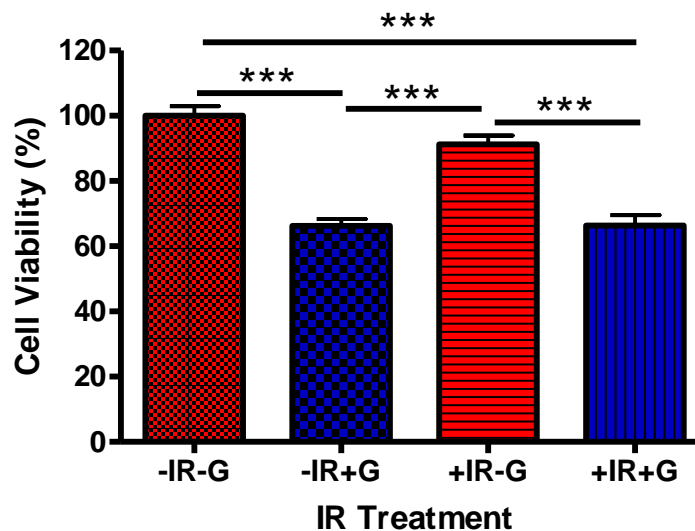
Figure 3-3: Column graph showing the effects of IR1072 on cell viability in DIV7 mixed cortical cultures following a severe excitotoxic insult. Abbreviations: -IR-G, sham pre-treatment and sham insult (also representing 100%); -IR+G, sham pre-treatment and glutamate insult; +IR-G, IR pre-treatment and sham insult; +IR+G, IR pre-treatment and glutamate insult. Cell viability determined via an MTT assay. Mean values +/- SEM for n = 6 replicates from one culture, ***p< 0.001

3.2.2 IR1072-preconditioning in CD-1 mice: Mitochondrial respiratory studies.

Chance and Williams (1956) developed the polarographic method using an oxygen electrode for measuring respiratory rates in cells and subcellular systems including isolated mitochondria (Ernster, 1993) which has been used in this study (Chance and Williams, 1956). The ratio between the respiratory rate during state 3 (active state of respiration) and the return to state 4 (controlled respiratory rate after all ADP is phosphorylated) is called the respiratory control index (RCI); this gives a ratio which allows one to ascertain the integrity of coupling of oxidation and reduction within the ETC to phosphorylation of ADP to ATP (Campello et al., 1964). In order to assess the impact, if any, of IR1072 on Complex I and II of the ETC, respiration studies using the polarographic method were performed on isolated sham or IR1072-preconditioned (*in vivo*) CD-1 mouse brain and liver mitochondria.

All Data were statistically analysed using a two tailed student t-test. Data represent mean ± SEM.

In the presence of glutamate (5mM) plus malate (5mM), IR1072 treated 7 month old CD-1 mice (n=2) brain showed no significant differences in endogenous (66.62 ± 1.783 ng O min^{-1} mg^{-1} protein) , state 4 (80.08 ± 5.425 ng O min^{-1} mg^{-1} protein), state 3 (171.5 ± 16.63 ng O min^{-1} mg^{-1} protein) and return to state 4 (73.32 ± 4.917 ng O min^{-1} mg^{-1} protein) respiratory rates compared to age-matched sham controls (n=3) endogenous (48.91 ± 13.98 ng O min^{-1} mg^{-1} protein), state 4 (66.38 ± 10.48 ng O min^{-1} mg^{-1} protein), state 3 (136.3 ± 3.494 ng O min^{-1} mg^{-1} protein) and return to state 4 (52.41 ± 17.47 ng O min^{-1} mg^{-1} protein) respiratory rates (Figure 3-4).
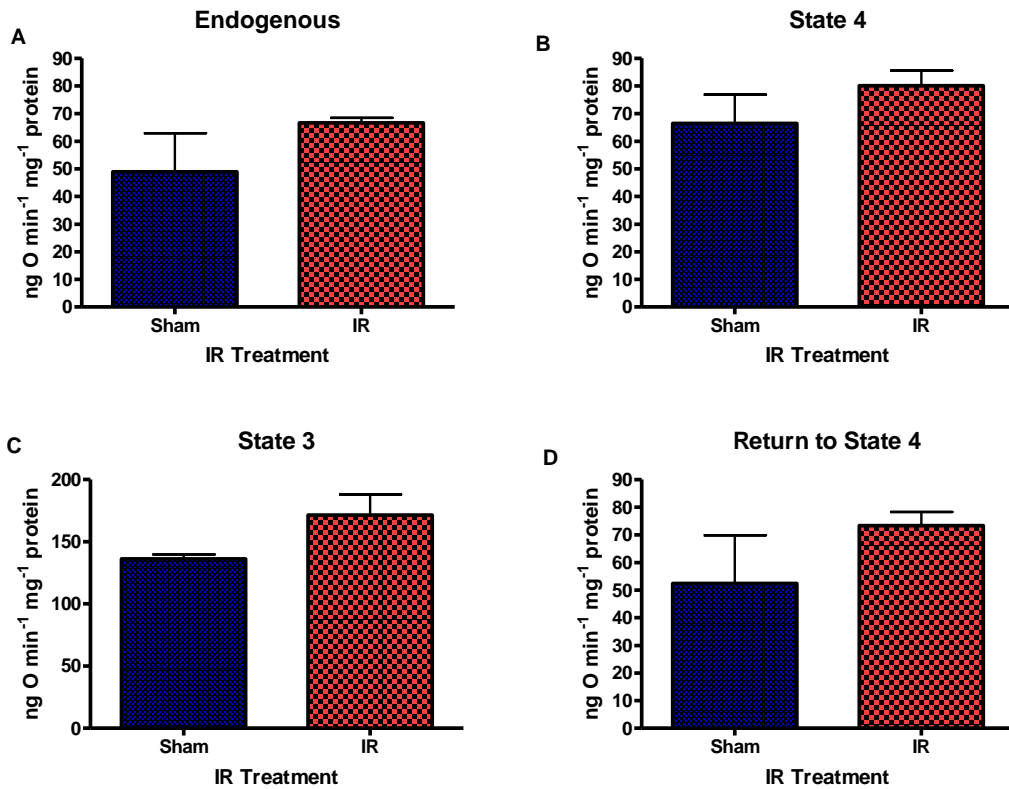
Figure 3-4: The effect of acute sham- or IR- treatment on glutamate plus malate respiratory rates in male 7m old CD-1 mouse *(in vivo)* brain mitochondria. Respiratory rates of glutamate plus malate at A) endogenous state B) state 4 C) state 3 and D) the return to state 4. Mean values ± SEM, n = 2 for each group.

In the presence of glutamate (5mM) plus malate (5mM), the RCI of IR1072 treated 7 month old CD-1 mice brain (n=2, 2.775 ± 0.4124) shows no significant difference compared to RCI of age-matched sham controls (2.701 ± 0.0764) (Figure 3-5).
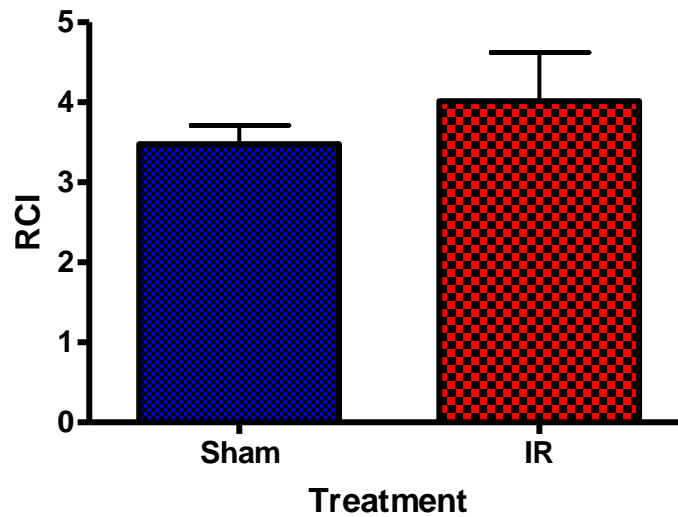
Figure 3-5: The effect of acute sham- or IR- treatment on glutamate plus malate RCI in male 7m old CD-1 mouse (*in vivo*) brain mitochondria Mean values ± SEM, n = 2 for each group.

In the presence of succinate (5mM), IR1072 treated 7 month old CD-1 mice brain (n=3) displayed higher state 4 (193.2 ± 10.79 ng O min^{-1} mg^{-1} protein, p<0.05) , state 3 (684.6 ± 40.59 ng O min^{-1} mg^{-1} protein, p<0.05), and return to state 4 (208.8 ± 11.31 ng O min^{-1} mg^{-1} protein, p <0.05) respiratory rates compared age-matched sham controls (n=3) state 4 (125.6 ± 13.79 ng O min^{-1} mg^{-1} protein), state 3 (492.6 ± 31.39 ng O min^{-1} mg^{-1} protein) and return to state 4 (140.7 ± 14.96 ng O min^{-1} mg^{-1} protein) respiratory rates. No significant differences were found between IR1072 treated CD-1 mice endogenous rate (60.59 ± 11.67 ng O min^{-1} mg^{-1} protein) and sham treated mice (60.08 ± 5.446 ng O min^{-1} mg^{-1} protein) (Figure 3-6).
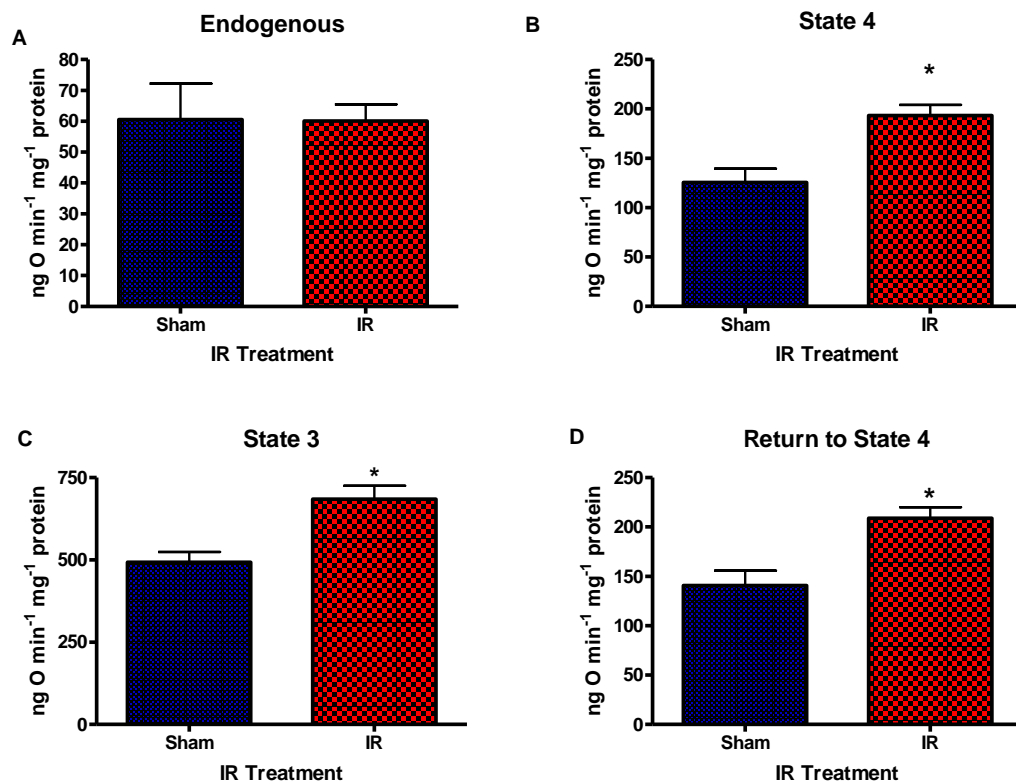
Figure 3-6: The effect of acute sham- or IR- treatment on succinate RCI in male 7m old CD-1 mouse (*in vivo*) brain mitochondria. Respiratory rates of succinate at A) endogenous state B) state 4 C) state 3 and D) the return to state 4. Mean values ± SEM, n = 3 for each group, *p<0.05.

In the presence of succinate (5mM), the RCI of IR1072 treated 7 month old CD-1 mice brain (n=3, 4.016 ± 0.6048) showed no significant differences compared to age-matched sham controls (n=3, 3.477 ± 0.233) (Figure 3-7).
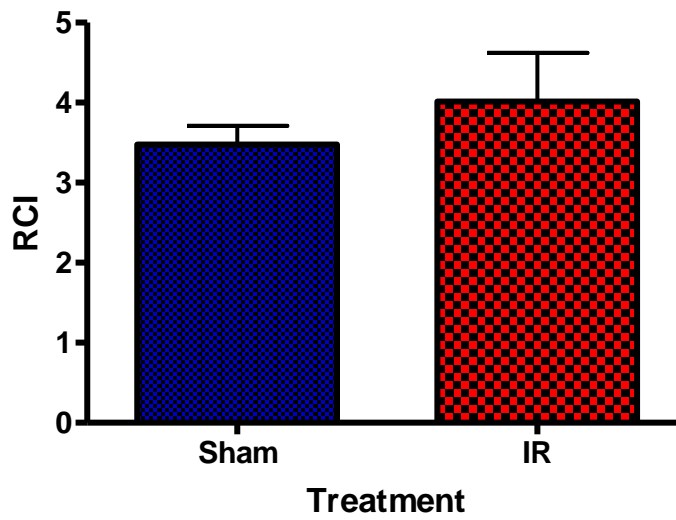
Figure 3-7: The effect of acute sham- or IR- treatment on succinate RCI in male 7m old CD-1 mouse (*in vivo*) brain mitochondria. Mean values ± SEM, n = 3 for each group.

In the presence of glutamate (5mM) plus malate (5mM), IR1072 treated 7 month old CD-1 mice liver (n=3) showed no significant differences in endogenous (36.15 ± 1.347 ng O min^{-1} mg^{-1} protein) , state 4 (17.28 ± 0.802 ng O min^{-1} mg^{-1} protein), state 3 (197.2 ± 11.24 ng O min^{-1} mg^{-1} protein) and return to state 4 (17.87 ± 2.524 ng O min^{-1} mg^{-1} protein) respiratory rates compared to age-matched sham controls (n=3) endogenous (37.39 ± 0.797 ng O min^{-1} mg^{-1} protein), state 4 (15.36 ± 2.827 ng O min^{-1} mg^{-1} protein), state 3 (217.2 ± 7.707 ng O min^{-1} mg^{-1} protein) and return to state 4 (16.33 ± 2.162 ng O min^{-1} mg^{-1} protein) respiratory rates (Figure 3-8).
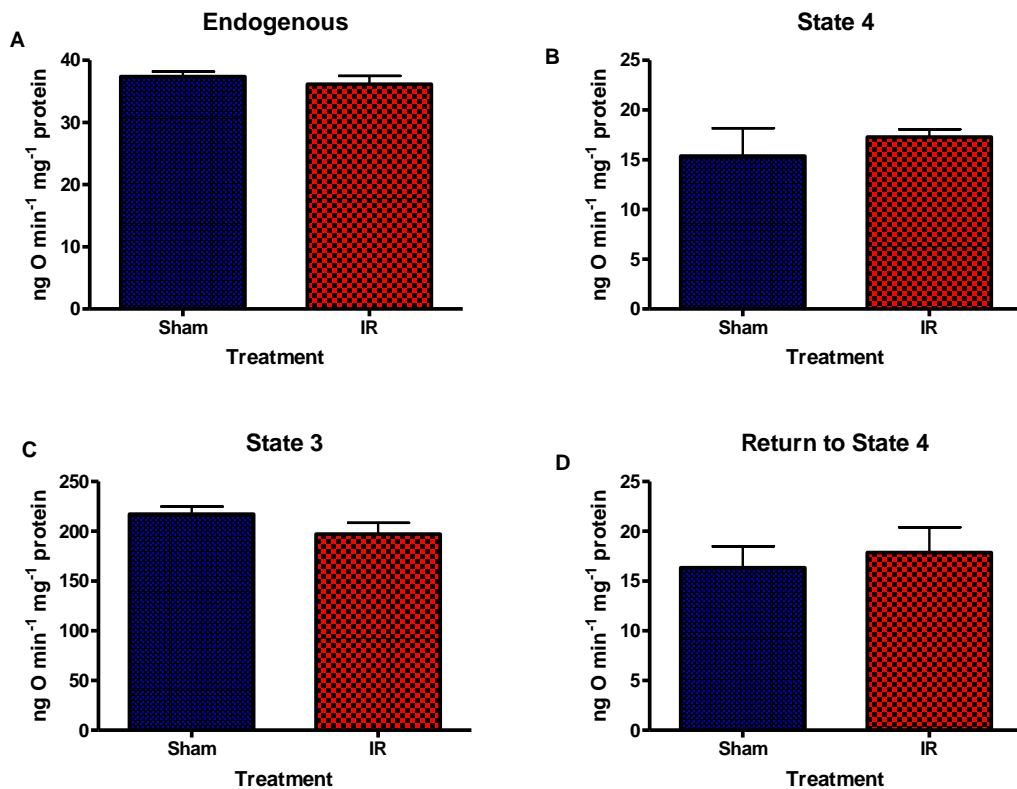
Figure 3-8: The effect of acute sham- or IR- treatment on glutamate plus malate RCI in male 7m old CD-1 mouse (*in vivo*) liver mitochondria. Respiratory rates of glutamate plus malate at A) endogenous state B) state 4 C) state 3 and D) the return to state 4. Mean values ± SEM, n = 3 for each group.

In the presence of glutamate (5mM) plus malate (5mM), IR1072 treated 7 month old CD-1 mice liver (n=3, 4.187 ± 0.0827) showed a trend toward a decrease in RCI (p= 0.0532) compared to age-matched sham controls (n=3, 4.735 ± 0.1842) (Figure 3-9).
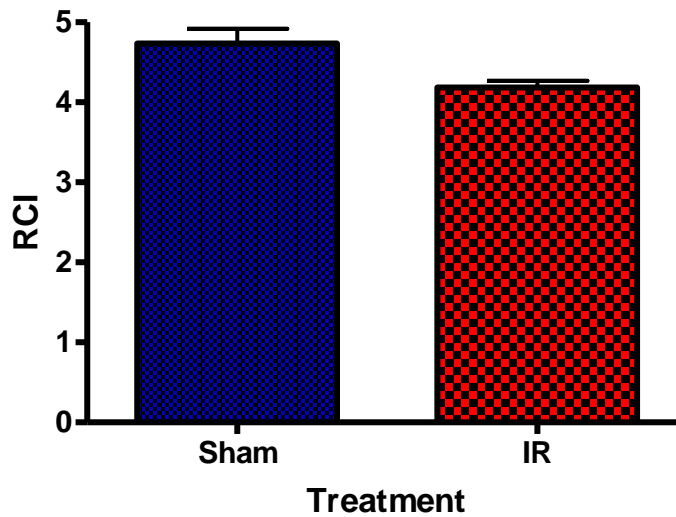
Figure 3-9: The effect of acute sham- or IR- treatment on glutamate plus malate RCI in male 7m old CD-1 mouse (*in vivo*) liver mitochondria. Mean values ± SEM, n = 3 for each group.

In the presence of succinate (5mM), IR1072 treated 7 month old CD-1 mice liver (n=3) showed no significant differences in endogenous (39.86 ± 1.188 ng O min^{-1} mg^{-1} protein), state 4 (75.14 ± 5.578 ng O min^{-1} mg^{-1} protein), state 3 (352.4 ± 9.790 ng O min^{-1} mg^{-1} protein) and return to state 4 (70.93 ± 3.951 ng O min^{-1} mg^{-1} protein) respiratory rates compared to age-matched sham controls (n=3) endogenous (37.86 ± 2.526 ng O min^{-1} mg^{-1} protein) , state 4 (62.20 ± 3.530 ng O min^{-1} mg^{-1} protein), state 3 (370.7 ± 19.89 ng O min^{-1} mg^{-1} protein) and return to state 4 (56.88 ± 5.746 ng O min^{-1} mg^{-1} protein) respiratory rates (Figure 3-10).
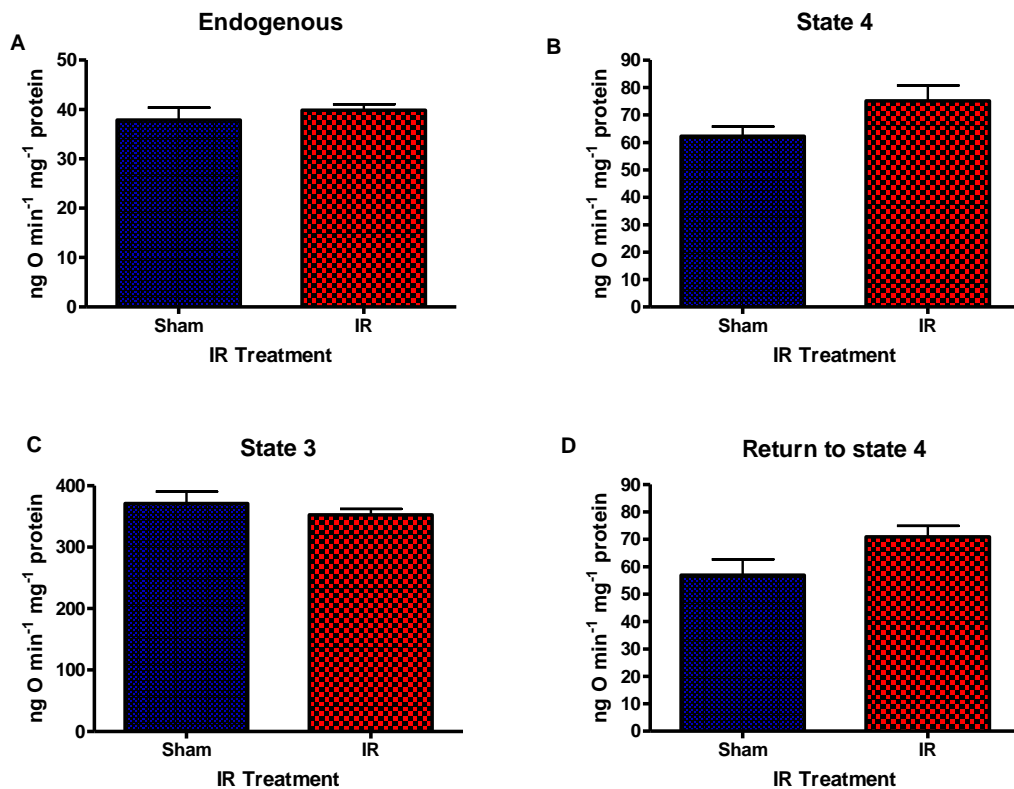
Figure 3-10: The effect of acute sham- or IR- treatment on succinate RCI in male 7m old CD-1 mouse (*in vivo*) liver mitochondria. Respiratory rates of succinate at A) endogenous state B) state 4 C) state 3 and D) the return to state 4. Mean values ± SEM, n = 3 for each group.

In the presence of succinate (5mM), IR1072 treated 7 month old CD-1 mice liver (n=3, 4.323 ± 0.1452) showed a trend toward a decrease in RCI (p<0.05) age-matched sham controls (n=3, 3.559 ± 0.1105) (Figure 3-11).
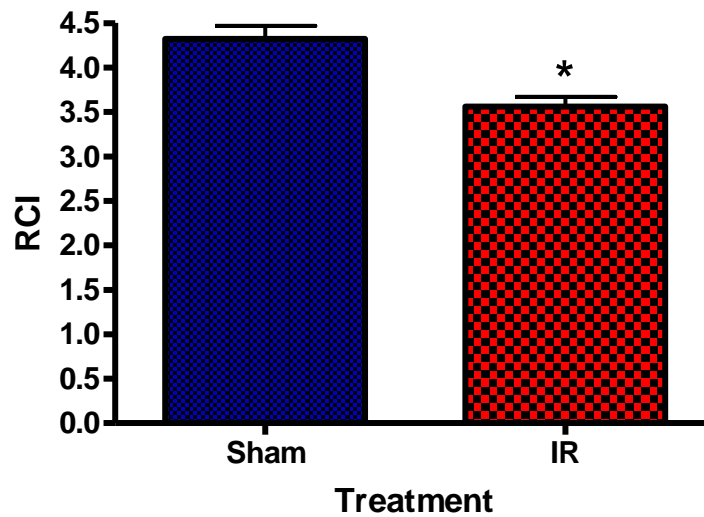
Figure 3-11: The effect of acute sham- or IR- treatment on succinate RCI in male 7m old CD-1 mouse (*in vivo*) liver mitochondria. Mean values ± SEM, n = 3 for each group, *p<0.05.

Glutamate (5mM) plus Malate (5mM)
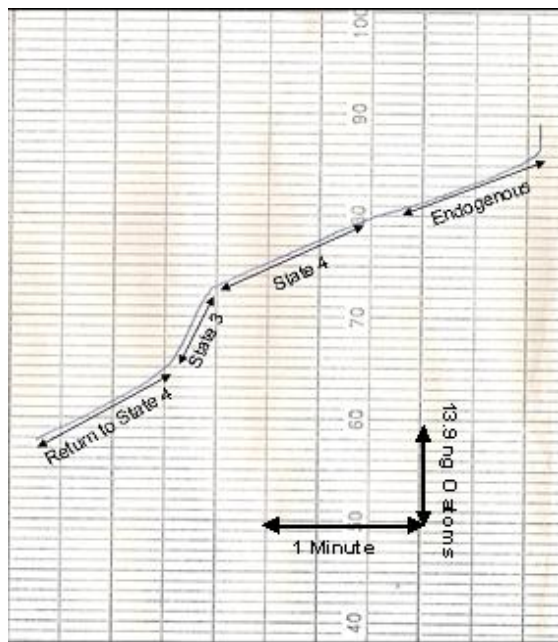
Succinate (5mM)
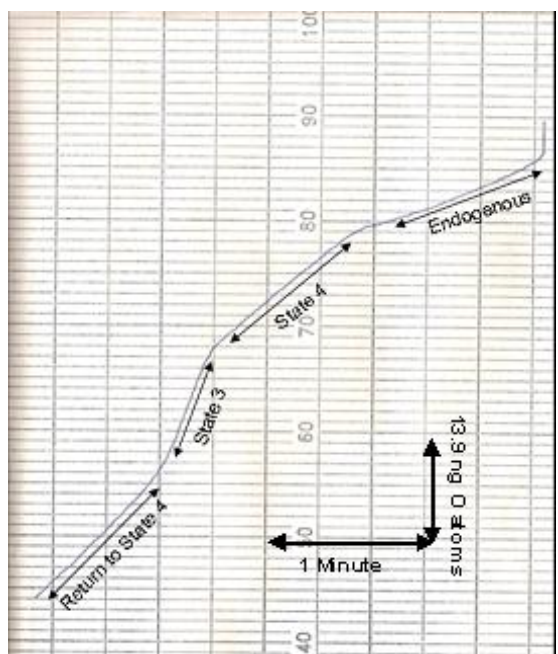
Figure 3-12: A typical trace showing Oxidative Phosphorylation for Complex I & II. Traces generated by measuring the respiratory rate of mitochondria alone (endogenous) for 1 minute, after adding glutamate (5mM) plus malate (5mM; Complex I) or succinate (5mM; Complex II) for 1 minute (State 4), by adding ADP (167μM; State 3) and allowing all the ADP to be phosphorylated (Return to State 4).

3.2.3 IR1072-preconditioning in CD-1 mice: ERK1/2 and HSP expression

It has been proposed that low-powered laser irradiation (red and near infra-red spectrum) does not work via the stress signal pathway i.e. p38 and JNK pathways, but rather through the ERK1/2 signalling pathway heavily implicated in neuroprotection (Gao and Xing, 2009). A possible primary mechanism of low power laser irradiation is activation through dimerization of receptors, i.e. TRKB receptors, that are in the "right energetic state" to accept the laser energy, leading to their autophosphorylation and downstream effects (Karu, 1999; Gao and Xing, 2009). However, the mitochondrial ETC appears to be the primary photoacceptor, therefore through changes in respiration, MMP and/or mitochondrial retrograde signalling, ERK1/2 signalling is more likely to be the secondary mechanism associated with near IR irradiation (Gao and Xing, 2009). Although HSP are implicated in activation of the stress signal pathways rather than ERK1/2 signalling, they are also heavily implicated in neuroprotection, where induction of HSP expression is associated with aiding protein misfolding and improved healing of damaged tissues in animal models and in humans. HSP also act by inhibiting various pro-apoptotic factors associated with mitochondrial dysfunction.

Age matched sham- or IR1072-preconditioned CD-1 mouse brain tissue was subjected to quantitative immunoblot analysis to assess the protein expression of phosphorylated and unphosphorylated ERK1/2, BDNF, another protein heavily implicated in neuroprotection mainly via the ERK1/2 pathway, CREB, a transcription factor subsequently upregulated by ERK1/2 activation, and selected HSP associated with neuroprotection. Although AKT acts via the

PI3 kinase pathway, it is associated with cell survival and, as a neuroprotective effect was shown previously in cell viability in neuronal cultures, it seemed apt to investigate any possible upregulation of this cell survival protein.

Protein levels were standardised using mouse β-actin primary antibody. Data were statistically analysed using a two tailed student t-test. Data represent mean ± SEM.

Table 3-1: Protein expression profile of 4 month old CD-1 mice following acute IR1072 treatment compared to age-matched sham-treated CD-1 mice. Arrows represent an increase (↑) or decrease (↓) in protein expression in IR-treated CD-1 compared to age-matched sham controls, and respective figure numbers. Abbreviations; BDNF, Brain Deived Neurotrophic Factor; ERK1/2, Extracellular Signal-regulated Kinase; CREB, Cyclic Adenosine Monophosphate (AMP) Response Element Binding; AKT, Protein Kinase B; HSP, Heat Shock Protein. Data were statistically analysed using a two tailed student t-test. Pink cells represent significant results and blue cells represent a trend. n=4 for each group, *p<0.05, **p<0.01.

Effect of Acute IR1072 treatment on protein expression in 4 month old CD-1 mice			
1º Ab	**p value**	**Result**	**Figure**
BDNF	***0.0096**	↓	**3-13**
ERK1	0.0511	↓	**3-14**
ERK2	0.1021	NS	
ERK1-P	0.8107	NS	Data not shown
ERK2-P	0.5372	NS	
CREB	0.4082	NS	Data not shown
AKT	0.1839	NS	Data not shown
HSP60	0.0816	↑	**3-15**
HSP70	*0.011	↑	**3-16**
HSP90	0.1069	NS	Data not shown

IR1072-treated CD-1 mice (n=5) showed a significant decrease (0.6050 ± 0.108, p<0.01) in BDNF expression compared to age-matched sham controls (n=5, 0.7786 ± 0.039; Figure 3-13).

A
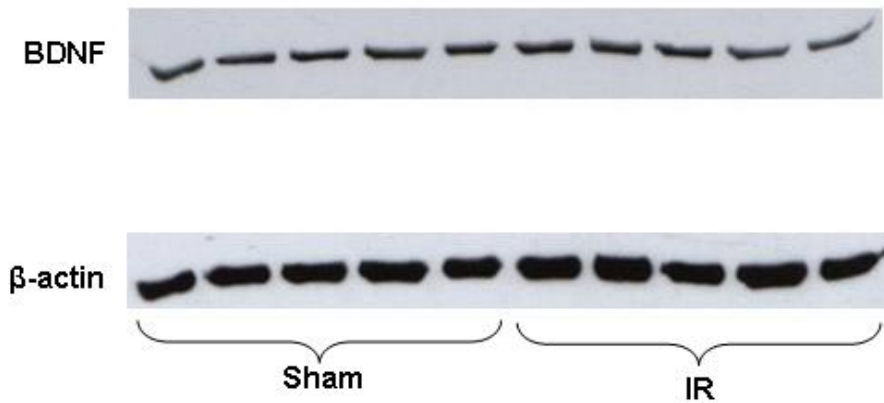
B
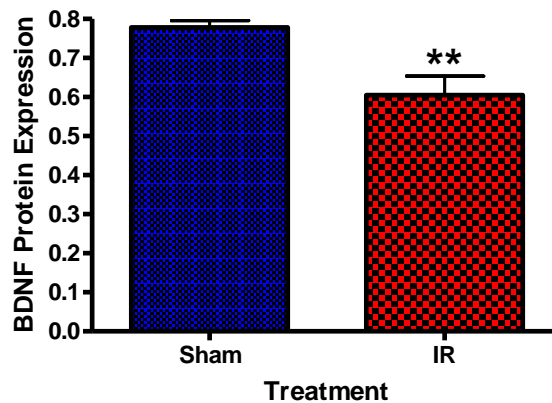
Figure 3-13: Effects of BDNF expression in acutely sham or IR1072 treated 4 month old CD-1 mouse brain (*in vivo*) where A) is an Immunoblot representation where each lane represents an individual mouse, therefore one n number and B) is a column graph showing the quantitative results of BDNF expression from the immunoblot. Abbreviations: BDNF, Brain Derived Neurotrophic Factor. Mean values ± SEM, n = 5 for each group, **p<0.01.

IR1072-treated CD-1 mice (n=4) showed a trend for decreased ERK1 and 2 expression (0.377 ± 0.064, p=0.0511 and 0.888 ± 0.036, p=0.1021, respectively) compared to age-matched sham controls (n=4, 0.5725 ± 0.148 and 1.005 ± 0.115, respectively) (Figure 3-14).

A
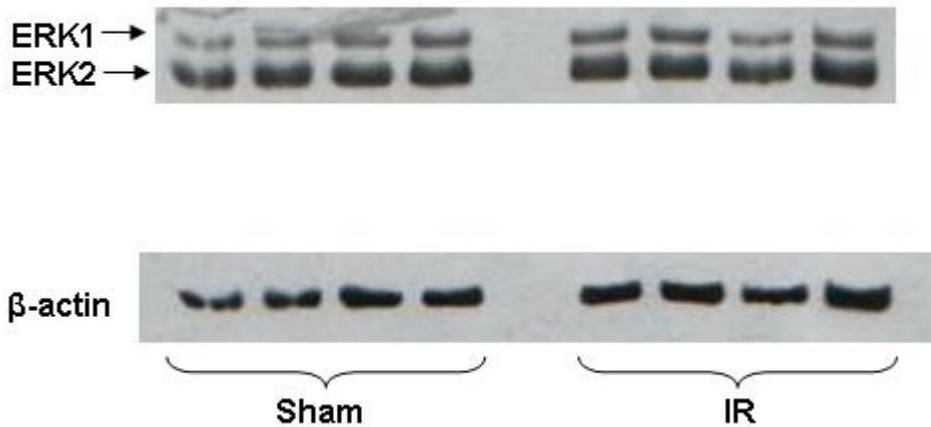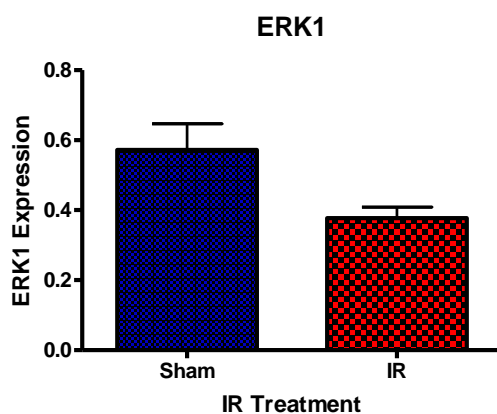
B i)   **ii)**
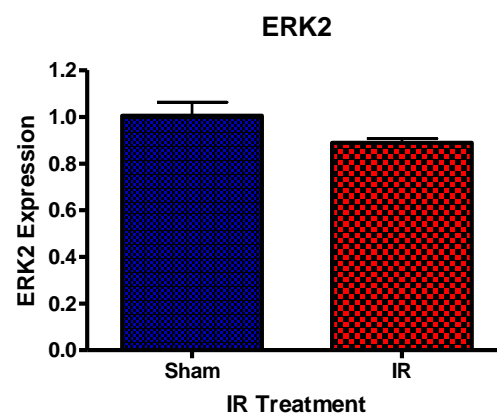
Figure 3-14: Effects of ERK1/2 expression in acutely sham or IR1072 treated 4 month old CD-1 mouse brain (*in vivo*) where A) is an Immunoblot representation, each lane represents an individual mouse therefore one n number and B) is a column graph showing the quantitative results of a) ERK1 and ii) ERK 2 expression. Abbreviations: BDNF, extracellular signal regulating kinase. Mean values ± SEM, n = 4 for each group.

IR1072-treated CD-1 mice (n=4) showed a trend for decreased HSP60 expression (0.263 ± 0.042, p= 0.0816) compared to age-matched sham controls (n=4, 0.4730 ± 0.196) (Figure 3-15).

A
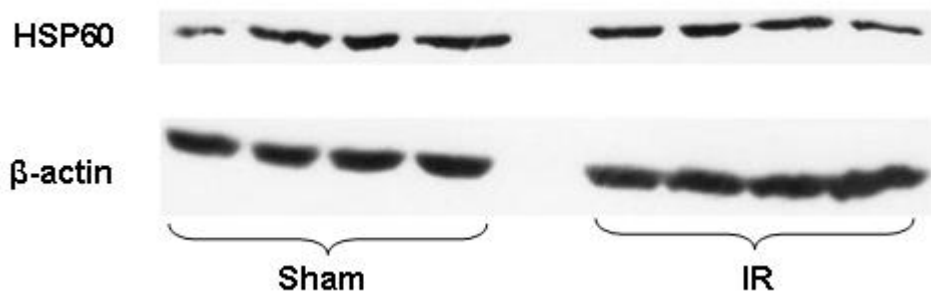
B
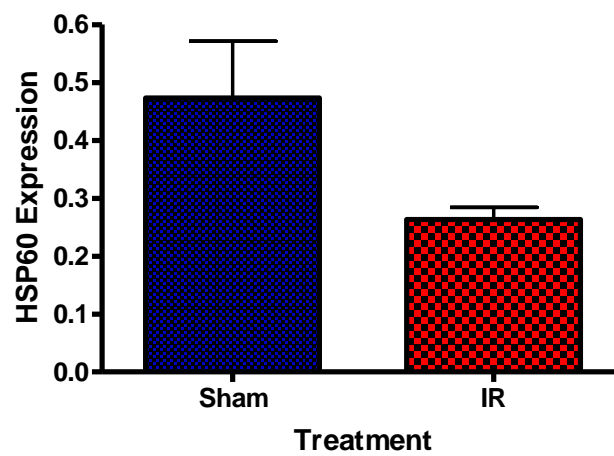
Figure 3-15: Effects of HSP60 expression in acutely sham or IR1072 treated 4 month old CD-1 mouse brain (*in vivo*) where A) is an Immunoblot representation where each lane represents an individual mouse, therefore one n number and B) is a column graph showing the quantitative results of HSP60 expression. Abbreviations: HSP, Heat Shock Protein. Mean values ± SEM, n = 4 for each group.

IR1072-treated CD-1 mice (n=4) showed a significant increase (2.285 ± 0.686, p<0.05) in HSP70 expression compared to age-matched sham controls (n=4, 0.9321 ± 0.293; Figure 3-16).

A
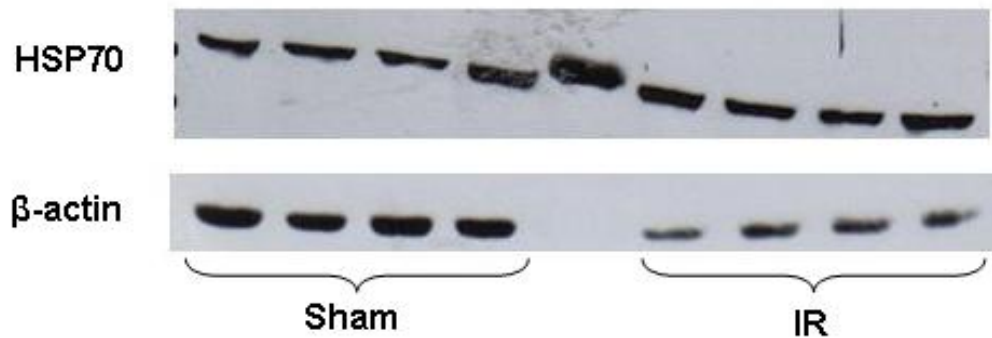
B
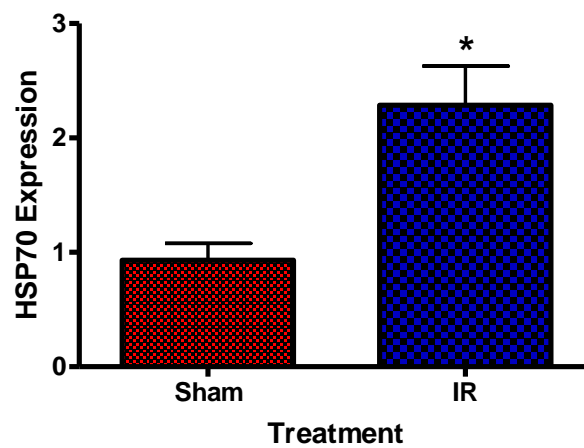
Figure 3-16: Effects of acute sham or IR1072 treatments on HSP70 expression in treated 4 month old CD-1 mouse brain (*in vivo*) where A) is an Immunoblot representation where each lane represents an individual mouse, therefore one n number and B) is a column graph showing the quantitative results of HSP70 expression. Abbreviations: HSP, Heat Shock Protein. Mean values ± SEM, n = 4 for each group, *p<0.05.

3.3 Discussion

The aim of this chapter was to establish the neuroprotective effects, if any, of acute IR1072-preconditioning using *in vitro* and *in vivo* methodologies, and if so, propose a mechanism relating to IR1072 in order to warrant further investigations.

The pure neuronal cultures produced in this study are evenly dispersed with a minimal presence of glial cells (<5%). Variations in glutamate cell death is dependant on cultures prepared on various dates and therefore may be due to quality of culture preparation as well as total duration of the culture preparation. Despite this, the cultures were consistently seeded at a density of 3000 cells/mm^2. Due to these variations in cell death, the results were divided in to three classes of insult, mild, moderate and severe depending on the neuronal loss achieved. The level of protection following IR1072-preconditioning in the pure neuronal cultures was dependent on the level of neuronal loss, where the more severe the insult the neuronal cultures received, the less, if any, the protection. However, in the minor insult of approximately 14% neuronal loss, a 90% protection was achieved with IR treatment. In fact, the cell viability in the mild glutamate insult group of the IR1072-preconditioned cultures was higher than the control insult, possibly indicating a potentiated effect of IR1072-preconditioning. Lin et al. (2008) preconditioned, rather than insulted, rat cortical cultures with glutamate before subjecting the cultures to oxygen-glucose deprivation, in an *in vitro* model of ischemia. They showed that pre-treatment with N-methyl-D-aspartate (NMDA)

receptor antagonists prevented OGD-induced cell death, whereas alpha-amino-3-hydroxy-5-methyl-4-isoxazole propionate (AMPA) receptor did not. However, protective efficacy of glutamate preconditioning was blocked by NMDA or AMPA receptor blockers, and if extracellular calcium was removed the neuroprotective effect was abolished. Also, glutamate preconditioning increased levels of phosphorylated CREB and Bcl-2. They demonstrated that low levels of glutamate, 120µM for 40 minutes, produced the maximal protective effect at a minimal cost to neuronal loss (10%). They proposed that glutamate preconditioning protected neurons via AMPA receptor and NMDA receptor activation, where an influx of intracellular calcium induced Ca2+/calmodulin-dependent kinase II (CAMKII) autophosphorylation which activated CREB and led to upregulation of Bcl-2 and ultimately preventing apoptosis (Lin et al., 2008). Although this study used a 10 minute 1mM glutamate insult (rather than preconditioning) only a 14% neuronal loss occurred in the mild insult group which, combined with IR1072 pre-treatment, could have lead to an upregulation of CREB therefore elicited neuroprotective effects rather than neurotoxic events seen in sham controls. The more severe insults of 25% and 33% neuronal loss may have resulted in high level of calcium toxicity that was unable to recover from just CREB activation alone, therefore resulting in little or no neuroprotective effect. LILT has also been shown to have an insult-dependant neuroprotective effect. Liang et al. (2006) pre-treated primary neuronal cultures from postnatal rat visual cortex with LED LILT (670nm) before being subjected to a potassium cyanide insult for 28h, in order to induce cell death via the apoptotic pathway. Liang showed LILT pretreatment reduced apoptosis from 36% to 17.9% (100µM potassium

cyanide) and from 58.9% to 39.6% (300µM potassium cyanide), representing a 50.3% and 32.8% reduction, respectively. Liang also showed that LILT significantly decreased potassium cyanide-induced caspase-3 and Bax expression and increased Bcl-2 levels, indicating that LILT partially protects neurons from cyanide-induced apoptosis by down-regulating apoptosis and upregulation anti-apoptotic proteins (Liang et al., 2006). These results indicate that the level of insult achieved is influential on LILT-induced neuroprotection. Similar results have been obtained with anaesthetic precondition (results not shown)

Naturally, mitochondrial studies were a focus of this primary investigation since mitochondria have been postulated to be the primary photo-targets during IR irradiation. Mitochondria are sensitive to irradiation with near-IR, 50% of which is reportedly absorbed in the liver by mitochondrial chromophores, such as cytochrome c oxidase (Liang et al., 2006). As the IR1072-preconditioning *in vivo* apparatus irradiated the entire body of the CD-1 mice, the brain and liver were the primary targets for mitochondrial respiratory studies. The electron micrograph (Figure 2-2) confirms isolation of in-tact liver and brain mitochondria from the protocol implicated. The RCI value has been shown to give an indication on whether a mitochondrial preparation is tightly or loosely coupled (Campello et al., 1964)

Glutamate plus malate or succinate can be used to stimulate the complex activity in the oxidative phosphorylation assay in order to measure complex I or II activity, respectively (Figure 3-12) (Chance and Williams, 1956; Markham et al., 2004). Thus, not only is this a useful tool to measure the coupling and

therefore the reliability of a mitochondrial preparation at different complexes, it is also a procedure to evaluate where the physiological changes may take place in mitochondria when examining various parameters i.e. IR1072-preconditoning *in vivo*.

Table 3-2: Comparison of RCI values produced in this investigation and that performed by Chance & Williams (1956). Abbreviations: RCI, respiratory control index, G&M, gluatmate and malate.

	Tissue	G&M RCI	Succinate RCI
This investigation	**CD-1 brain**	2.70 ± 0.08	3.48 ± 0.23
	CD-1 Liver	4.74 ± 0.18	3.56 ± 0.11
Chance & Williams (1956)		>3	>2

Mitochondrial complex II of the ETC in complex II was affected in both brain and liver mitochondria following 10 day *in vivo* treatment IR1072. Reports show that low-level laser therapy (wavelength of 904 nm) significantly increases the activities of complexes II and IV of mitochondrial respiratory chain components, but does not affect succinate dehydrogenase activity and has been discussed as a possible photacceptor for near-IR light. Changes occur in complex II, albeit RCI or respiratory rates following LILT. IR1072-preconditioning had no effect for both respiration and RCI for complex I in liver and brain mitochondria, probably because complex I has been shown to act as a photoacceptor for the blue spectral region, but not for the red or near infra-red light (Gao and Xing, 2009). Another possible reason is that the RCI of the glutamate plus malate for brain mitochondria was lower than 3, indicating loosely coupled mitochondria and therefore a less reliable mitochondrial preparation, although this is unlikely as the RCI was only 0.3

units lower than the recommended RCI. These results confirm previous reports of increased complex II activity in laser LILT treated ulcerations created in wistar rats (Silveira et al., 2007) and may show that complex II in the mitochondrial respiratory chain may be acting as a photoacceptor for IR LILT, therefore increasing the respiratory activity.

Due to time constraints and cost effectiveness i.e. one mitochondrial preparation of approximately 50-100µl requires at least 3 mouse brains, we have only investigated the effects of acute IR1072 treatment in 7 month old CD-1 mice. Further investigations to assess the effect of chronic exposure of IR1072 in younger and older CD-1 mice, on individual complex activity would be required to try to determine the mechanistic nature of IR1072 exposure on the mitochondrial respiratory chain.

This increase in complex activity could be contributing to the rise in MMP, & ATP generation seen in previous studies. As discussed previously, these can lead to cell signalling pathways involved in neuroprotection. Surprisingly, we found that 10 day IR1072 treatment reduced BDNF and ERK1/2 levels in 4 month old CD-1 mice, which does not correlate with previous findings of increased BDNF gene expression following IR LILT (Byrnes et al., 2005b), although ERK1/2 phosphorylated, therefore activated ERK1/2 and CREB, is unchanged. This could be due to differences in wavelength, as Byrnes et al. (2005b) used an 810nm wavelength which has been suggested to act through cytochrome c oxidase where 904nm, and now 1072nm, has been shown to

increase activity in complex II, which could possibly elicit differential effects. These differences may also simply be due to species or protocol differences.

However, despite inducing a downregulation in ERK1/2 signalling pathways, IR1072 produced different effects in HSP expression. IR1072, appeared to reduce the expression of HSP60, which plays a role in inducing caspase-3, an enzyme involved in cleaving and therefore activating the caspases involved in the apoptotic caspase cascade, and increase HSP70 expression, a well-studied HSP involved in several anti-apoptotic actions. In a study by Novoselova et al. (2006) irradiated macrophages and splenic lymphocytes with 632.8nm laser increased HSP70, but reduced HSP90 expression (Novoselova et al., 2006), suggesting upregulation of HSP70, at least, may be involved in the neuroprotective effects seen with LILT.

Chapter 4: Effect of chronic IR1072 *(in vivo)* treatment on behaviour: 3D radial maze

4.1 Introduction

The nine-arm 3D radial maze is a modification of an eight-arm radial maze, where an animal's response to the novelty of an open space environment are assessed in either a single session (emotional) or multiple sessions (learning, memory and emotional; Ennaceur et al., 2006b). It has been proposed that the first few exposures to the maze are likely to induce fear of novelty-induced anxiety, therefore these initial sessions were assessed for emotional responses as well as working memory, following which repeated exposures are thought to diminish anxiety as learning improves (Ennaceur et al., 2006b). In this study, the food-deprived mice were introduced to the maze without prior habituation, where food pellets were placed at the end of each arm and mice are subjected to daily sessions in order to test working memory (Michalikova et al., 2008). Therefore, this behavioural paradigm is able to assess the motor activity, emotional responses and working memory performance of an animal within the same experimental settings and testing conditions (Ennaceur et al., 2006b). The mice were placed in the central platform and required to cross a bridge to reach the end of the arm that contains the food pellet. This study used the raised arm configuration, as previous results find that rats and mice show a preference for this configuration as the visual cue may need to be above the horizontal plane of their snouts in order for them see which arm they need to access to retrieve a pellet (Ennaceur et al., 2006b).
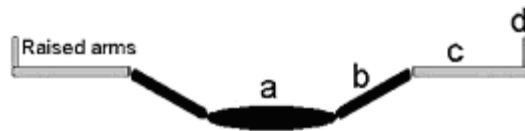
Figure 4-1: 3D radial maze where a) central platform b) bridge c) arm and d) visual cue.

A perfect working memory would consist of a mouse moving from one arm to the next, completing one visit to each arm without repeats or errors. Hesitation or reluctance to move to different areas of the maze is an emotional response, not memory impairment (Ennaceur et al., 2008), therefore various parameters are recorded in order to assess emotional responses and working memory.

Previous studies have shown IR1072 to have a beneficial effect in learning and memory following a 10-minute treatment. Michalikova et al. (2008) subjected young (3 months old) and middle-aged (12 months old) mice to 10 daily sessions of 6 minute IR1072 exposures, and found IR1072 to improve overall cognitive performance in middle-aged mice comparable to young 3 month old CD-1 mice. We have altered this protocol to use a chronic form of IR1072 treatment, whereby mice received 10 minute IR1072 sessions, over two consecutive days, bi-weekly for 5-6 months.

The aim of this chapter was to determine whether a chronic form of IR1072 treatment in younger (7 month old) and older (13 month old) male CD-1 mice would confirm previous findings of improved cognitive performance following short term IR1072 irradiation.

4.2 Results

4.2.1 Chronic IR1072-preconditioning in 7 month old CD-1 mice: 3D radial maze

Group means were tested for significance with a two-way ANOVA repeated measures. This was followed up with Newman-Keuls post-hoc comparisons. Statistics were calculated using the statistical package Statistica for Windows (version 5.5). Results were considered significant when $p \leq 0.05$.

There were no significant differences in the number of repeated visits to arms between sham or IR1072 treated 7 month old CD-1 mice ($F_{1,14}=0.07$, $p>0.10$), significant differences between sessions ($F_{9,140}=4.93$, $p<0.0001$) but no significant interactions between groups and sessions ($F_{9,140}=0.82$, $p>0.10$; Figure 4-2).
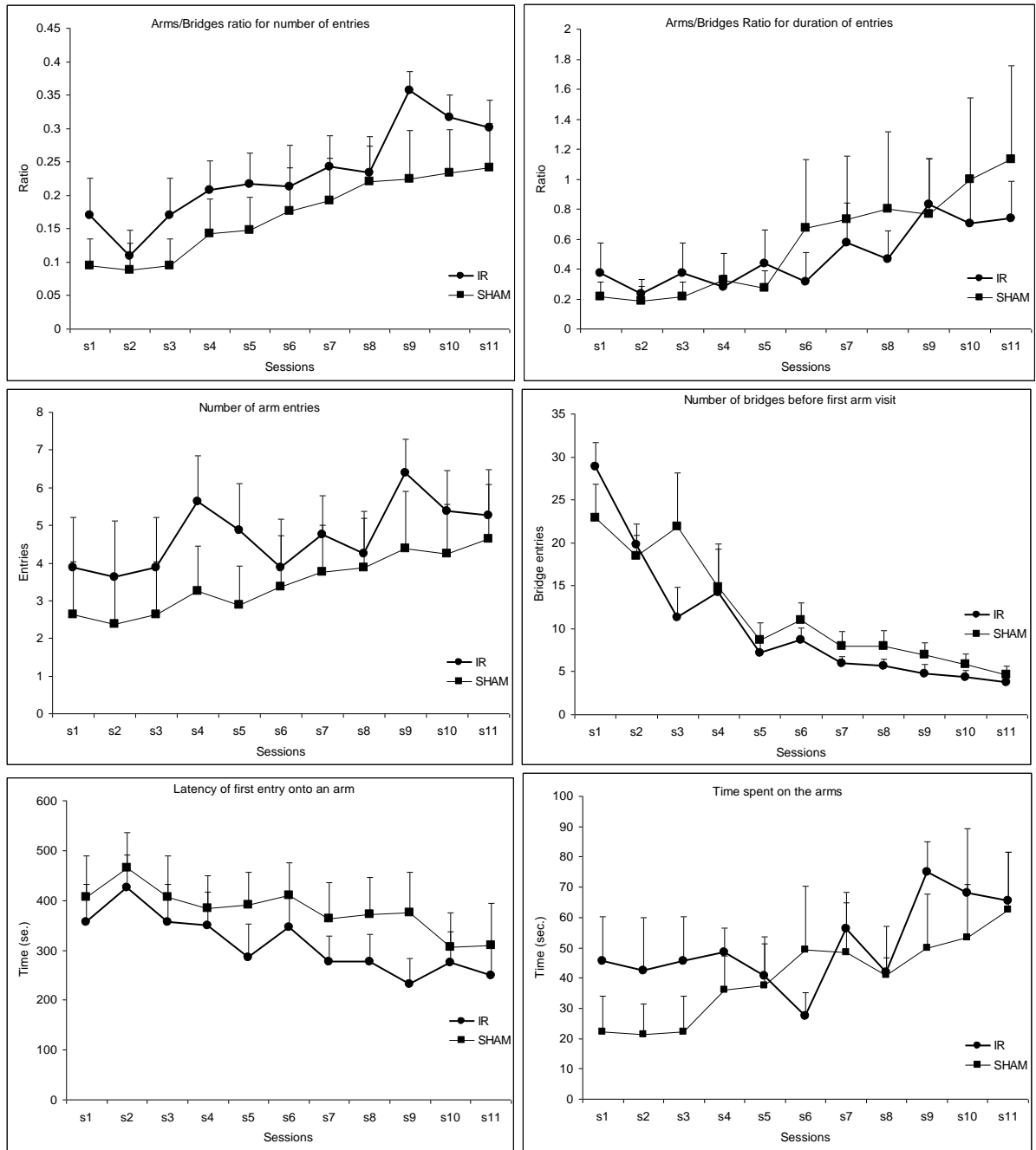
There were no significant differences in the number of arm entries before first repeated arm visit, between sham or IR1072 treated 7 month old CD-1 mice ($F_{1,14}=0.31$, $p>0.10$), significant differences between sessions ($F_{9,140}=3.76$, $p<0.0001$) but no significant interactions between groups and sessions ($F_{9,140}=1.38$, $p>0.10$; Figure 4-2).
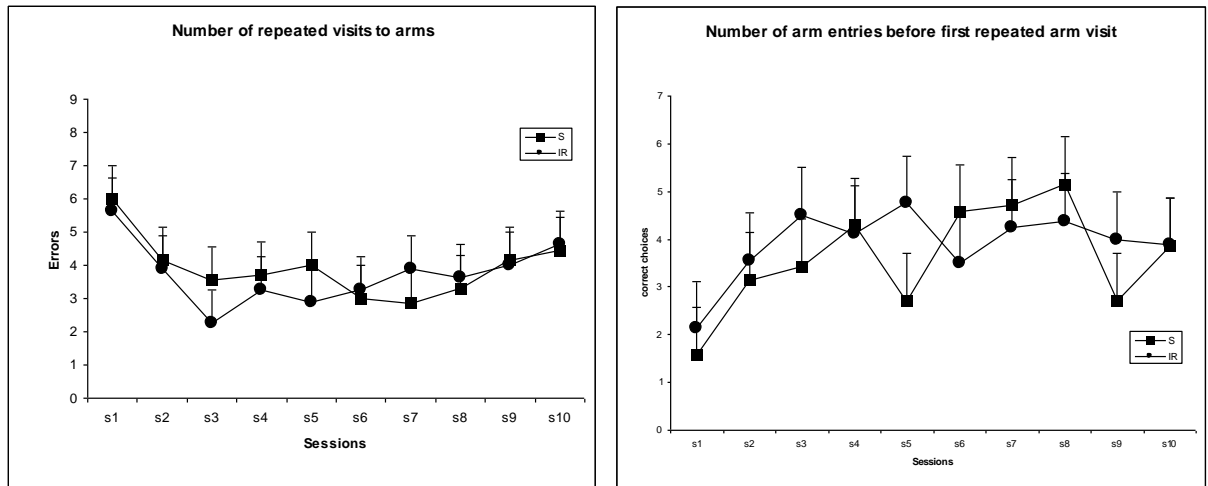
Figure 4-2: Graphs depicting the learning and memory in 7 month old IR1072-treated CD-1 mice and age-matched sham controls. Behavioural parameters; number of repeated arm visits and the number of arm visits before first repeated arm visit. Sessions refer to daily 10 minute 3D radial maze testing over 10 days, S1-10. Group means were tested for significance with a two-way ANOVA repeated measures. This was followed up with Newman-Keuls post-hoc comparisons, n=8 for each group.

There were no significant differences in the number of arm entries, between sham or IR1072 treated 7 month old CD-1 mice ($F_{1,14} < 0.64$, $p > 0.10$), significant differences between sessions ($F_{9,140} > 6.40$, $p < 0.0001$) but no significant interactions between groups and sessions ($F_{9,140} < 1.47$, $p > 0.10$; Figure 4-3).

There were no significant differences in the arm/bridge ratio for number of entries between sham or IR1072 treated 7 month old CD-1 mice ($F_{1,14} = 0.75$, $p > 0.10$), no significant differences between sessions ($F_{9,140} = 0.54$, $p > 0.10$) and no significant interactions between groups and sessions ($F_{9,140} = 0.84$, $p > 0.10$; Figure 4-3).

There were no significant differences in the arm/bridge ratio for duration of entries between sham or IR1072 treated 7 month old CD-1 mice ($F_{1,14} = 052$, $p > 0.10$), no significant differences between sessions ($F_{9,140} = 0.98$, $p > 0.10$) and no significant interactions between groups and sessions ($F_{9,140} = 0.95$, $p > 0.10$; Figure 4-3).

There were no significant differences in the number of bridge entries before first arm visit between sham or IR1072 treated 7 month old CD-1 mice ($F_{1,14} = 0.58$, $p > 0.10$), significant differences between sessions ($F_{9,140} = 11.27$, $p < 0.0001$) but no significant interactions between groups and sessions ($F_{9,140} = 0.80$, $p > 0.10$; Figure 4-3).

There were no significant differences in the latency of first entry to an arm between sham or IR1072 treated 7 month old CD-1 mice ($F_{1,14}=1.20$, $p>0.10$), no significant differences between sessions ($F_{9,140}=1.33$, $p>0.10$) and no significant interactions between groups and sessions ($F_{10,140}=1.17$, $p>0.10$; Figure 4-3).

There were no significant differences in the total time spent on the bridges between sham or IR1072 treated 7 month old CD-1 mice ($F_{1,14}=0.26$, $p>0.10$), no significant differences between sessions ($F_{9,140}=1.41$, $p>0.10$) and no significant interactions between groups and sessions ($F_{9,140}=0.28$, $p>0.10$; Figure 4-3).
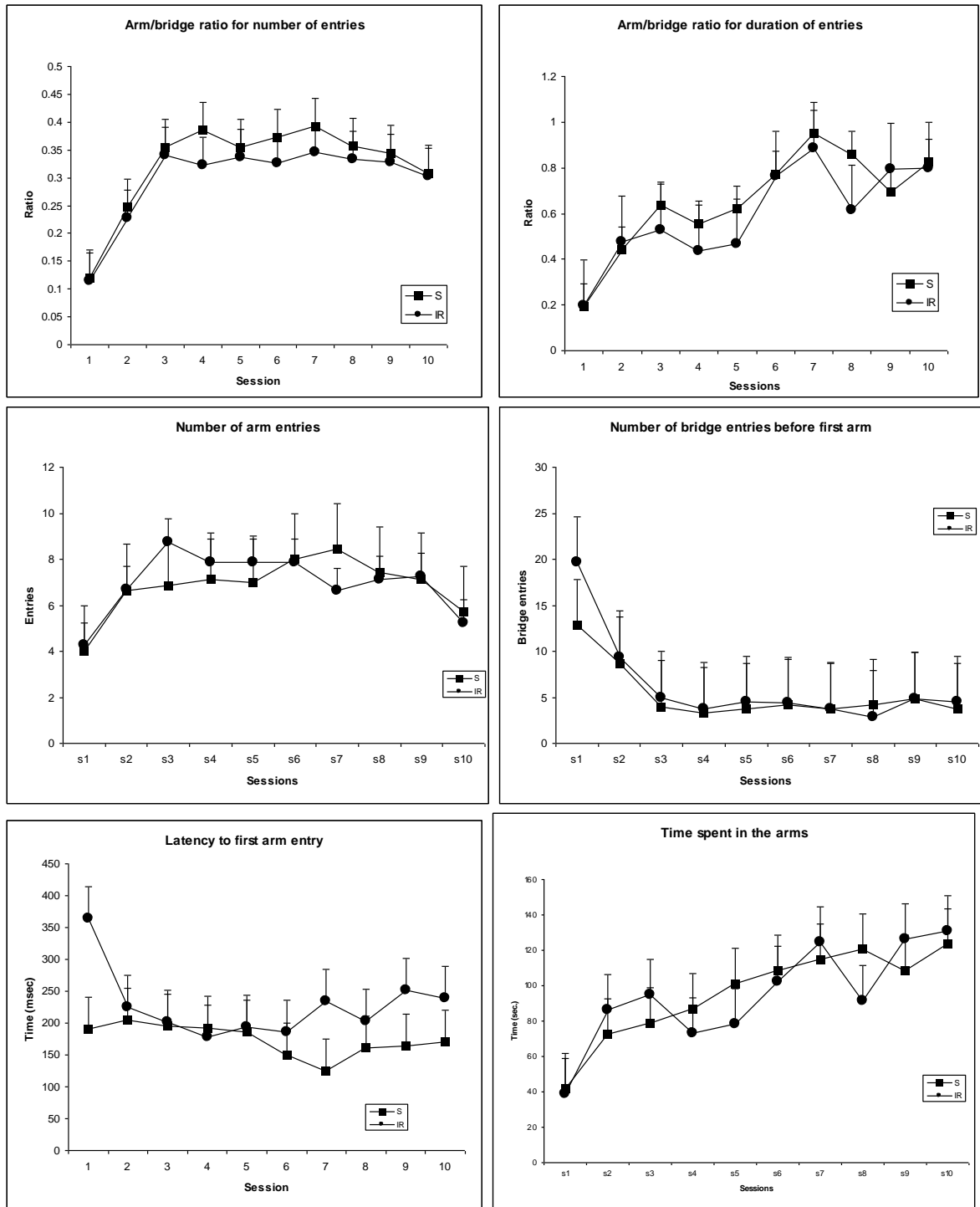
Figure 4-3: Graphs depicting emotional responses in 7 month old IR1072-treated CD-1 mice and age-matched sham controls. Behavioural parameters; arm/bridge ratio of number of entries or duration of entries, number of arm or bridge entries, latency to first entry onto an arm and time spent on an arm. Sessions refer to daily 10 minute 3D radial maze testing over 10 days, S1-10. Group means were tested for significance with a two-way ANOVA repeated measures. This was followed up with Newman-Keuls post-hoc comparisons, n=8 for each group.

There were no significant differences in the total time spent on the arms between sham or IR1072 treated 7 month old CD-1 mice ($F_{1,14}=0.001$, p>0.10), significant differences between sessions ($F_{9,140}=3.58$, p<0.0001) but no significant interactions between groups and sessions ($F_{9,140}=0.37$, p>0.10; Figure 4-4).

There were no significant differences in the total time spent in the central platform between sham or IR1072 treated 7 month old CD-1 mice ($F_{1,14}=3.47$, p<0.09), significant differences between sessions ($F_{9,140}=6.77$, p<0.0001), but no significant interactions between groups and sessions ($F_{9,140}=1.32$, p>0.10; Figure 4-4).

There were no significant differences in the session duration between sham or IR1072 treated 7 month old CD-1 mice ($F_{1,14}=4.17$, p<0.06), significant differences between sessions ($F_{9,140}=7.88$, p<0.0001), but no significant interactions between groups and sessions ($F_{9,140}=1.54$, p>0.10; Figure 4-4).
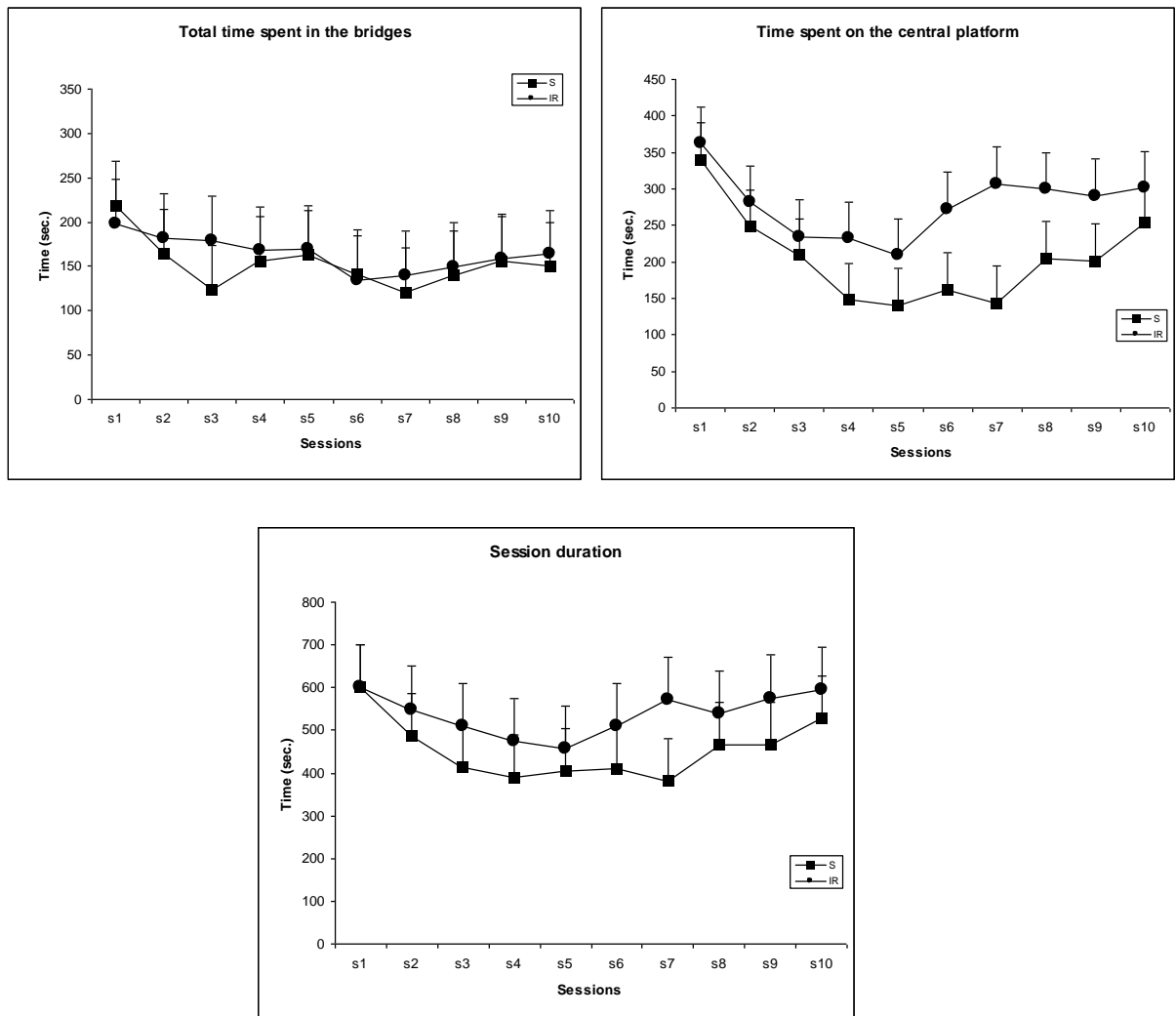
Figure 4-4: Graphs depicting general mobility responses in 7 month old IR1072-treated CD-1 mice and age-matched sham controls. Behavioural parameters; Time spent on the bridges, time spent on the central platform and sessions' duration. Sessions refer to daily 10 minute 3D radial maze testing over 10 days, S1-10. Group means were tested for significance with a two-way ANOVA repeated measures. This was followed up with Newman-Keuls post-hoc comparisons, n=8 for each group.

4.2.2 Chronic IR1072-preconditioning in 13 month old CD-1 mice: 3D radial maze

Group means were tested for significance with a two-way ANOVA repeated measures. This was followed up with Newman-Keuls post-hoc comparisons. Statistics were calculated using the statistical package Statistica for Windows (version 5.5). Results were considered significant when $p \leq 0.05$.

There were no significant differences in the number of repeated visits to arms between sham or IR1072 treated 13 month old CD-1 mice ($F_{1,14}=1.06$, $p>0.10$), there were significant differences between sessions ($F_{10,140}=2.64$, $p<0.009$) but no significant interactions between groups and sessions ($F_{10,140}=0.49$, $p>0.10$; Figure 4-5).

There were no significant differences in the number of arm entries before first repeated arm visit, between sham or IR1072 treated 13 month old CD-1 mice ($F_{1,14}=0.98$, $p>0.10$), significant differences between sessions ($F_{10,140}=3.63$, $p<0.0001$) but no significant interactions between groups and sessions ($F_{10,140}=0.83$, $p>0.10$; Figure 4-5).
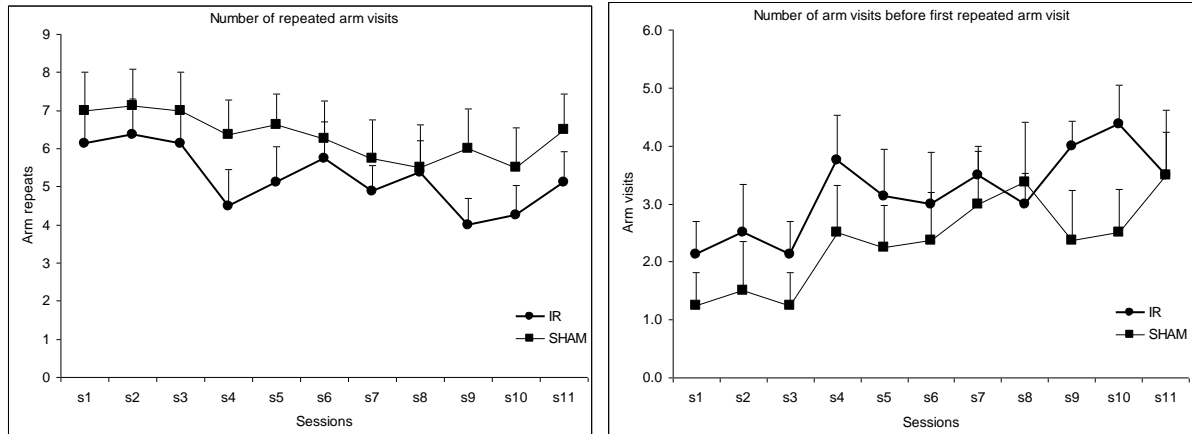
Figure 4-5: Graphs depicting the learning and memory in 13 month old IR1072-treated CD-1 mice and age-matched sham controls. Behavioural parameters; number of repeated arm visits and the number of arm visits before first repeated arm visit. Sessions refer to daily 10 minute 3D radial maze testing over 11 days, S1-11. Group means were tested for significance with a two-way ANOVA repeated measures. This was followed up with Newman-Keuls post-hoc comparisons, n=8 for each group.

There were no significant differences in the number of arm entries, between sham or IR1072 treated 13 month old CD-1 mice ($F_{1,14} < 0.71$, $p > 0.10$), significant differences between sessions ($F_{10,140} > 2.65$, $p < 0.005$) but no significant interactions between groups and sessions ($F_{10,140} < 0.47$, $p > 0.10$; Figure 4-6).

There were no significant differences in the arm/Bridge ratio for number of entries between sham or IR1072 treated 13 month old CD-1 mice ($F_{1,14} = 1.05$, $p > 0.10$), significant differences between sessions ($F_{10,140} = 8.19$, $p < 0.0001$) but no significant interactions between groups and sessions ($F_{10,140} = 0.54$, $p > 0.10$; Figure 4-6).

There were no significant differences in the arm/Bridge ratio for duration of entries between sham or IR1072 treated 13 month old CD-1 mice ($F_{1,14} = 0.06$, $p > 0.10$), significant differences between sessions ($F_{10,140} = 4.41$, $p < 0.0001$) but no significant interactions between groups and sessions ($F_{10,140} = 0.84$, $p > 0.10$; Figure 4-6).

There were no significant differences in the number of bridge entries before first arm visit between sham or IR1072 treated 13 month old CD-1 mice ($F_{1,14} = 0.49$, $p > 0.10$), significant differences between sessions ($F_{10,140} = 17.44$, $p < 0.0001$) but no significant interactions between groups and sessions ($F_{10,140} = 1.36$, $p > 0.10$; Figure 4-6).

There were no significant differences in the latency of first entry to an arm between sham or IR1072 treated 13 month old CD-1 mice ($F_{1,14}=0.66$, $p>0.10$), significant differences between sessions ($F_{10,140}=3.36$, $p<0.0006$) but no significant interactions between groups and sessions ($F_{10,140}=0.43$, $p>0.10$; Figure 4-6).

There were no significant differences in the total time spent on the bridges between sham or IR1072 treated 13 month old CD-1 mice ($F_{1,14}=1.89$, $p>0.10$), significant differences between sessions ($F_{10,140}=5.23$, $p<0.0001$) but no significant interactions between groups and sessions ($F_{10,140}=0.80$, $p>0.10$; Figure 4-6).

Figure 4-6: Graphs depicting emotional responses in 13 month old IR1072-treated CD-1 mice and age-matched sham controls. Behavioural parameters; arm/bridge ratio of number of entries or duration of entries, number of arm or bridge entries, latency to first entry onto an arm and time spent on an arm. Sessions refer to daily 10 minute 3D radial maze testing over 11 days, S1-11. Group means were tested for significance with a two-way ANOVA repeated measures. This was followed up with Newman-Keuls post-hoc comparisons, n=8 for each group.

There were no significant differences in the total time spent on the arms between sham or IR1072 treated 13 month old CD-1 mice ($F_{1,14}=0.39$, $p>0.10$), significant differences between sessions ($F_{10,140}=3.18$, $p<0.001$) but no significant interactions between groups and sessions ($F_{10,140}=1.03$, $p>0.10$; Figure 4-7).

There were no significant differences in the total time spent in the central platform between sham or IR1072 treated 13 month old CD-1 mice ($F_{1,14}=2.75$, $p>0.10$), no significant differences between sessions ($F_{10,140}=1.04$, $p>0.10$), and no significant interactions between groups and sessions ($F_{10,140}=0.64$, $p>0.10$; Figure 4-7).

There were no significant differences in the session duration between sham or IR1072 treated 13 month old CD-1 mice ($F_{1,14}=0.31$, $p>0.10$), no significant differences between sessions ($F_{10,140}=1.80$, $p>0.10$), and no significant interactions between groups and sessions ($F_{10,140}=0.69$, $p>0.10$; Figure 4-7).
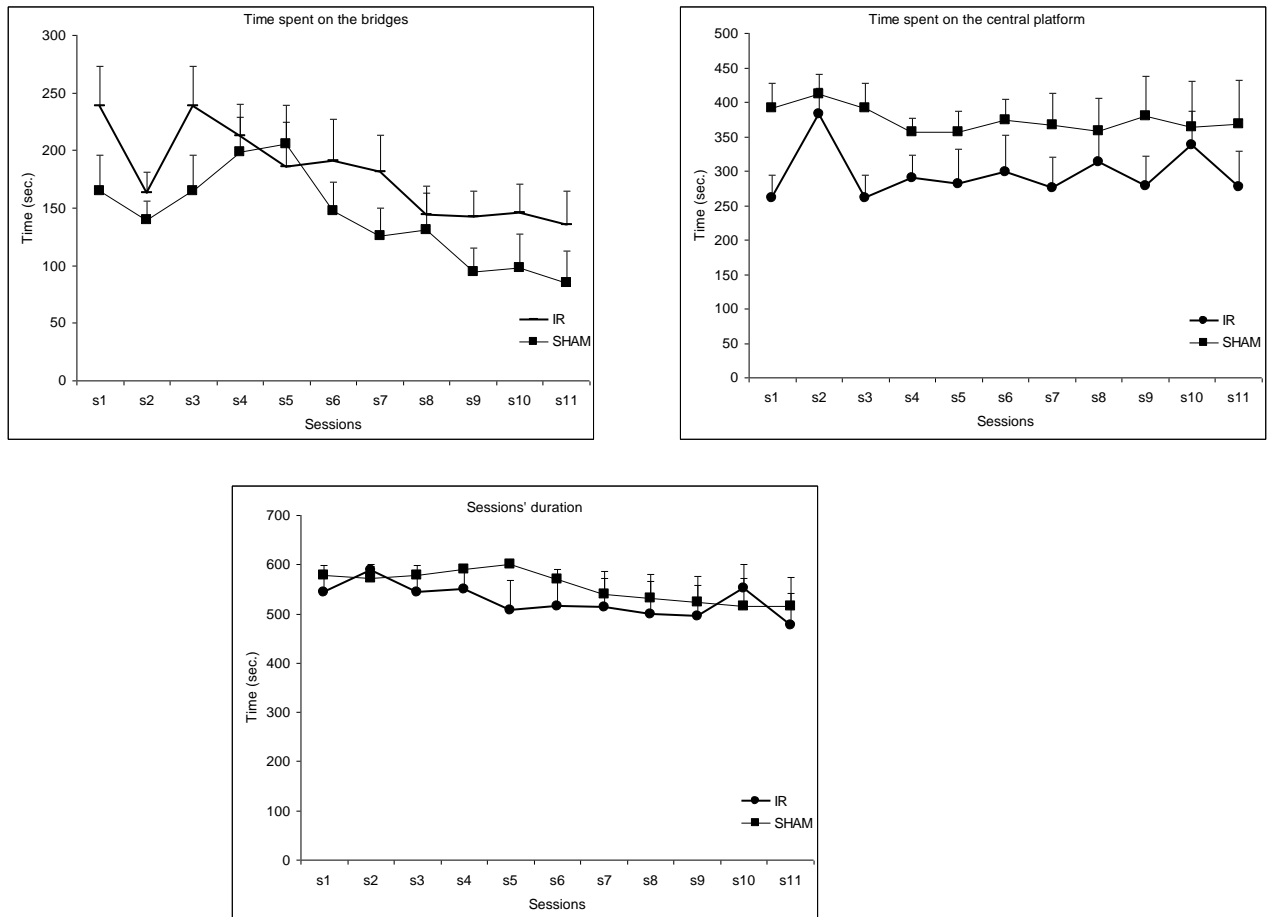
Figure 4-7: Graphs depicting general mobility responses in 13 month old IR1072-treated CD-1 mice and age-matched sham controls. Behavioural parameters; Time spent on the bridges, time spent on the central platform and sessions' duration. Sessions refer to daily 10 minute 3D radial maze testing over 11 days, S1-11. Group means were tested for significance with a two-way ANOVA repeated measures. This was followed up with Newman-Keuls post-hoc comparisons, n=8 for each group.

4.3 Discussion

In the present study, 3 or 7 month old CD-1 mice received chronic IR1072 irradiation which consisted of 10 minutes exposures over two consecutive days, bi-weekly for 5 months where behaviour was tested using the 3D radial maze. This behavioural paradigm examined emotional responses to novelty and open spaces in initial exposures to the test, in addition to learning and memory performance which continued throughout the successive testing sessions. Although these results are insignificant statistically, there appears to be a trend in the older 13 month old mice as the IR and sham mean values are consistently separated apart in each data set. There was significance between sessions but this was to be expected, as once the mouse appears to overcome the anxiety of the novelty and open space environment, learning should commence therefore test parameters would differ between sessions.

Number of repeated arm visits and number of arm visits before arm repeats are a measure of learning and memory on the 3D maze. Repeated arm visits are classed as an error made by the animal, where the decision to visit a unique arm in order to receive a pellet is the correct choice. The animals should learn a repeat arm visit is an error as the arm would be without a pellet as they have already visited the arm to retrieve the pellet. In younger mice, the sham and IR-treated mice appeared to make a similar amount of errors throughout the sessions. The amount of correct choices before an error or repeated arm visit was made was variable throughout the sessions in the younger sham or IR treated mice, where no real pattern emerged. IR-treated

CD-1 mice appeared to commit less errors on the 3D behavioural maze throughout all 10 sessions compared to sham treated CD-1 mice. Number of arm visits before an arm repeat measures how many correct or unique choices the mouse makes before an error is committed. Again, the amount of correct choices the IR-treated CD-1 mice made before an error was committed was greater than the sham-treated mice, throughout the sessions, particularly in sessions 9-11. However, it is important to note that the errors made by the sham and IR-treated younger mice was between 2 and 6 throughout the sessions, averaging at around 4, whereas in the older mice the amount of errors committed by the sham treated mice was between 6 and 7 (demonstrating a severe learning impairment) and the IR-treated mice was between 4 and 6, which is lower than the sham-treated mice however towards the end of the session the errors committed by the IR-treated older mice had lowered to around 4-5 errors, similar to the average errors made in the younger mice. The correct or unique arm visits made by younger mice before an error was committed was between 1 and 5 for both sham and IR -treated mice, whereas older sham treated mice was between 1 and 3 and IR-treated older mice was between 2 and 4 on average, which is also higher than the sham-treated mice and more similar to the younger mice, where more correct choices were made before an error occurred. Not only does this show a age-dependant memory impairment in the older sham-treated mice compared to the younger mice, but this also implies that IR1072 may have an effect on the acquisition of working memory and possibly reverses the memory impairment shown during ageing. The severity of learning deficits (due to excessive

anxiety) at both ages is perhaps to extreme to reverse robustly by IR1072 treatments.

The emotional response or anxiety measures for an animal on the 3D radial maze consisted of the number of arms entered, the number of bridges entered before the first arm visit, the time spent on the arm, arm/bridge ratio for the number of entries or duration of entries, and the latency of first entry on to an arm.

The index arm/bridge ratio is used to assess the difference in anxiety between sham and IR-treated groups, where the lower the ratio the higher the anxiety and vice versa. For the younger sham or IR-treated mice the ratio was low in the first session of the test for both number of entries and duration of entries, but sharply increased as sessions commenced where this increase levelled off at session 3-4 for both entry numbers and duration. The arm/bridge ratio for number of entries in older sham and IR-treated CD-1 mice began low but increased much slower than the younger CD-1 mice. This suggests that the younger mice recover from anxiety induced by the novel, open-spaced environment faster than the older mice. Sham and IR groups in the younger mice appeared to be the same almost, and the same can be said about the arm/bridge ratio for duration of entries in older sham and IR-treated, however the IR-treated mice displayed higher arm/bridge ratio for the number of entries compared to sham-treated mice, suggesting IR1072 treatment may have a beneficial effect on the anxiety state in older CD-1 mice (although again this did not reach significance).

CD-1 mice for both young and old groups did not make all eight arm choices on the first sessions, but this steadily improved as sessions commenced. Younger CD-1 mice appeared to make similar arm entries in sham or IR-treated groups, however IR-treated older CD-1 mice made more entries in to the arms in the initial sessions and throughout, suggesting the IR-treated group displayed lower anxiety response than sham-treated groups. The younger mice made more arm entries in general compared to older mice, which may suggest that aged CD-1 mice express a higher anxiety response compared to younger mice, where IR1072 could potentially reverse this response. Again this was only a trend rather than a robust significant effect.

A high number of entries to bridges before first arm visit is thought reflect the hesitations or reluctance of mice to engage onto an arm. The younger CD-1 mice showed a high number of bridge sessions in the initial "anxiety phase" of the test, where by session 3 the number of bridge entries before the first arm entry had stabilised to around for 4 or 5 entries per session, and there was no real difference between sham and IR groups. Older mice made more bridge entries before first arm visit, and appeared to have a longer anxiety phase where numbers stabilised at session 5 to around 7 or 8 bridge entries before first arm visit, however improvement was shown in every session. Apart for the initial session, IR-treated mice appeared to make less bridge entries before the first arm visit than sham, suggesting less hesitation to enter a bridge. These results show an age-dependant difference in CD-1 mice, where older mice appear to be more hesitant than the younger mice, and that IR appears to improve this somewhat (trend yet not significant).

Measures of latencies, and duration are not specific indices of memory function (Ennaceur et al., 2008). Making a fast decision or choice does not guarantee an accurate or a correct response, and taking longer time to make a decision or a choice can be equivalent to increasing a memory retention interval leading to confusion between choices (Ennaceur et al., 2008). They are likely to reflect a physical or physiological state of animals as well as the exploratory strategy or pattern of responses adopted by animals (Ennaceur et al., 2008). The latency of young CD-1 mice to make the first arm entry seemed to be lower than the older CD-1 mice in general, suggesting again that younger mice are less hesitant to engage in initial arm entry, however the latency times gradually improved or reduced in the older CD-1 mice as sessions commenced, whereas the younger mice appeared to stabilise at around 150-200msec. There was no apparent difference between sham and IR groups in the younger CD-1 mice, but the IR-treated mice in the older group took less time to engage in the first arm visit compared to sham-treated mice, suggesting IR1072 treated mice to be less hesitant than sham-treated.

The time spent in the arms is another indicator of emotional response. The younger and older mice appeared to spend longer in the arms as the sessions commenced, where there was no real differences shown between sham and IR groups in the younger or older mice.

The central platform and the bridges are the two places were a decision can be made about the choice of an arm (Ennaceur et al., 2008). The amount of time the younger mice spent on the central platform began high where a

steady decrease in time spent on the platform occurred, where the time increased slightly then levelled off. In the older mice the time spent in the central platform was pretty much constant throughout all sessions. The IR-treated group showed a trend to spend less time in the central platform in both younger and older mice compared to sham-treated groups. The younger mice appeared to spend a similar amount of time in the bridges throughout the sessions, and regardless of if they were sham- or IR-treated. The older IR-treated mice appeared to spend more time on the bridges compared to sham-treated mice. Lengthy duration on the central platform may reflect the hesitation and reluctance of mice to engage onto the bridges (Ennaceur et al., 2008). The older IR-treated mice spend less time on the central platform and more time on the bridges and arms compared to sham-treated mice, suggesting that sham treated groups may be more hesitant than the IR-treated groups.

The sessions duration is an indication of how long the animal takes to complete the maze. The younger mice showed a slight fall in session time from sessions 1-5, but slightly increased in sessions 5-10. The IR-treated younger mice appeared to have longer session times compared to the sham-treated group. In contrast, session time in the older sham and IR-treated group did not vary between sessions or groups.

Previous experiments have shown that all mice of different strains and ages are able to climb the bridges to reach the raised arms (Ennaceur et al., 2008). In fact, mice seem to prefer climbing, and the raised arm configuration

appears more attractive to mice than the flat or lowered arm configurations (Ennaceur et al., 2008). In addition, the bridge floors are covered with wire mesh to provide mice with further grip on the floor though our experiments demonstrate that mice can climb the bridges tilted by 60⁰ without wire mesh, therefore mobility or inability of the mouse to complete the maze due maze design is not an issue (Ennaceur et al., 2006a).

Notably, the level of anxiety (arm/bridge ratio of < 0.4) displayed by both mice age groups was excessively high compared to other mice strains and simpler tests, which may account for the poor learning performance seen in both age groups. The limited performance is distinct from the previous findings and may reflect distinct animal husbandry or inexperienced animal handling (Michalikova et al., 2009)

As the time spent on bridges and arms are higher in younger mice and the sessions duration is lower than older mice, this suggests that most of the time younger mice enter the bridges and continue to arms while the older mice remain in the central platform for longer without venturing to bridges, suggesting that general mobility and decision making may be affected with age in CD-1 mice.

In conclusion, older subjects were found to require more time to solve a 3D spatial navigation task and to acquire spatial information in a novel environment compared to younger adults. The IR1072 treatment in older mice appeared to trend to an improvement in the anxious state and cognitive

performance of the CD-1 mice, although not significantly compared to sham-treated CD-1 mice. These findings display modest effects less robust than previous data showing overall cognitive improvement following 10 daily sessions of IR1072 in 12 month old CD-1 mice, performed by highly experienced behaviourists.

Chapter 5: Age-dependant molecular changes in CD-1 mice: Effect of chronic IR1072 *(in vivo)* treatment

5.1 Introduction

5.1.1 Animal model of premature ageing: CD-1-mice

Mizumori et al. (1982) tested S-1 rats versus CD-1 mice on the radial maze behavioural test and found that rats were able to readily solve this behavioural paradigm but CD-1 mice were not, and suggested that mice in general may have limited learning capacity, but stressed that testing the performance of other strains is of great importance in order to determine if it is in fact a strain difference rather than a species difference. Since then, CD-1 mice have been shown to develop early behavioural and learning deficits (Parmigiani et al., 1999; Ennaceur et al., 2008) and amyloidosis with age, where the latter is thought to be the cause of premature death repeatedly reported in this strain of mouse (Conner et al., 1983; Frith and Chandra, 1991; Engelhardt et al., 1993; Gruys et al., 1996). Chen et al. (2006) compared brain volumes of C57 mice compared to the age-matched CD-1 mice in order to relate the improved performance of the C57 strain over the other mouse strains as seen in previous studies (Rogers et al., 1999). They found that C57 mice had consistently larger total brain volumes, despite their substantially smaller gross body weight compared to CD-1 mice, where the cerebral cortex and ventricular compartments (lateral and 3rd and 4th ventricles) had increases of 10% and 13%, respectively, in C57 mice compared to CD-1 (Chen et al., 2006). Sunyer et al. (2009) showed that C57 had decreased $GABA_B$ receptor subunit 2 compared to age-matched CD-1 mice, whereby activation of

presynaptic GABA$_B$ receptors inhibits neurotransmitter release of several neurotransmitters and postsynaptic GABA$_B$ receptors induce a slow inhibitory current through activation of inwardly rectifying K+ channels (Sunyer et al., 2009). These results may contribute toward a better understanding of the early learning deficits shown in the CD-1 mouse strain.

There is little evidence showing changes in protein changes involved in the CD-1 mice as they age, so one aim of this chapter was to establish any changes in protein expression involved in learning and memory processes that may be contributing to the severe age-dependent learning deficits and premature ageing seen in this mouse strain. Another aim was to establish any protein changes, age-dependant or otherwise, that may occur following chronic IR1072 treatment in younger (7 month old) and older (13 month old) CD-1 mice using immunoblotting, immunohistochemical and autoradiographical techniques.

5.2 Results

5.2.1 CD-1 Age Timeline: Immunoblot analysis

Protein levels were standardised using mouse β-actin primary antibody. Data were statistically analysed using a two tailed student t-test. Data represent mean ± SEM.

Table 5-1: Protein expression profile in 3, 10 or 12 month old CD-1 mice. Arrows represent an increase (↑) or decrease (↓) in protein expression in IR-treated CD-1 mice compared to age-matched sham controls. Abbreviations; BDNF, Brain Deived Neurotrophic Factor; ERK1/2, Extracellular Signal-regulated Kinase; CREB, Cyclic Adenosine Monophosphate (AMP) Response Element Binding; AKT, Protein Kinase B; HSP, Heat Shock Protein. Data were statistically analysed using a two tailed student t-test. Pink cells represent significant results and blue cells represent a trend. n=3 for each group, *p<0.05.

	CD-1 TL					
	3mv10m		3mv12m		10mv12m	
	p value	result	p value	result	p value	result
BDNF	0.0768	10m↓	*0.0227	12m↓	0.0165	12m↓
ERK1	0.5864	NS	0.9919	NS	0.6573	NS
ERK2	0.3524	NS	0.3203	NS	0.8201	NS
ERK1-P						
ERK2-P						
CREB	0.0652	10m↑	0.3317	NS	0.103	NS
CREB-P						
AKT	0.6451	NS	0.8324	NS	0.8605	NS
AKT-P						
HSP27	0.5561	NS	0.0831	12m↓	*0.0325	12m↓
HSP40	0.3146	NS	0.5798	NS	0.2531	NS
HSP60	0.5345	NS	0.2807	NS	0.5012	NS
HSP70	0.8596	NS	0.6737	NS	0.325	NS
HSP90	0.3666	NS	0.05	12m↓	0.4053	NS
HSP105	0.112	NS	0.1206	NS	0.8299	NS

CD-1 mice at 12 months of age (n=3, 0.341 ± 0.181) showed significantly decreased BDNF expression compared to mice at 3 months (n=3, 2.578 ± 0.5938, $p<0.05$) and 10 months of age (n=3, 1.153 ± 0.096, $p<0.05$). CD-1 mice at 10 months of age showed a trend for decreased BDNF expression compared to 3 month old mice (n=3, $p<0.1$) (Figure 5-1).

A

B
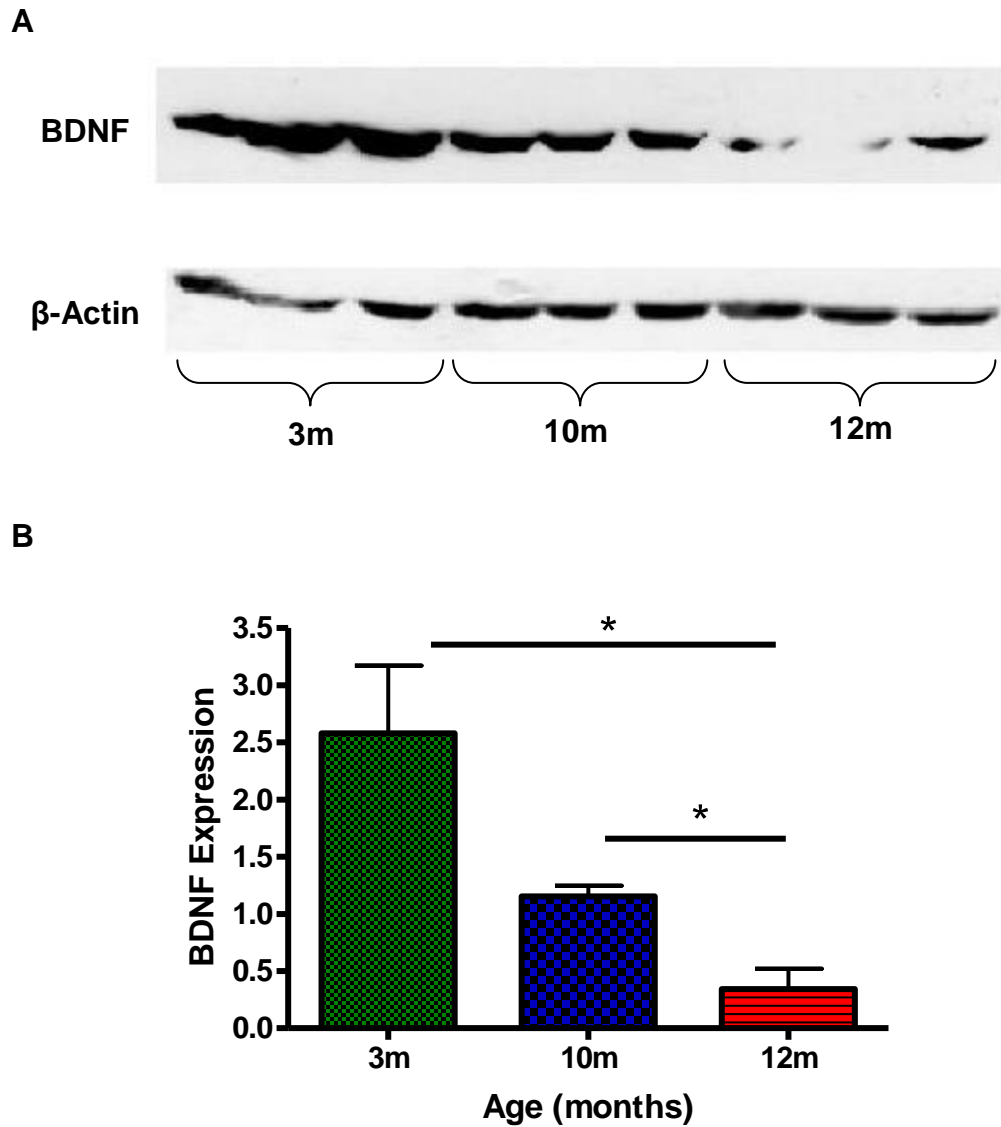
Figure 5-1: Age-dependent changes in BDNF expression in 3, 10 and 12m old CD-1 mouse brain where A) is an Immunoblot representation where each lane represents an individual mouse and B) is a column graph showing the quantitative results of BDNF expression from the immunoblot. Abbreviations: BDNF, Brain Derived Neurotrophic Factor. Mean values ± SEM, n = 3 for each group, *$p<0.05$.

CD-1 mice at 10 months of age (n=3, 0.5913 ± 0.1145) showed a trend for increased CREB expression compared to mice at 3 months (n=3, 0.244 ± 0.076, p<0.1). CD-1 mice at 3 or 10 months showed no difference in CREB expression compared to 12 month old mice (n=3, 0.338 ± 0.037) (Figure 5-2).

A
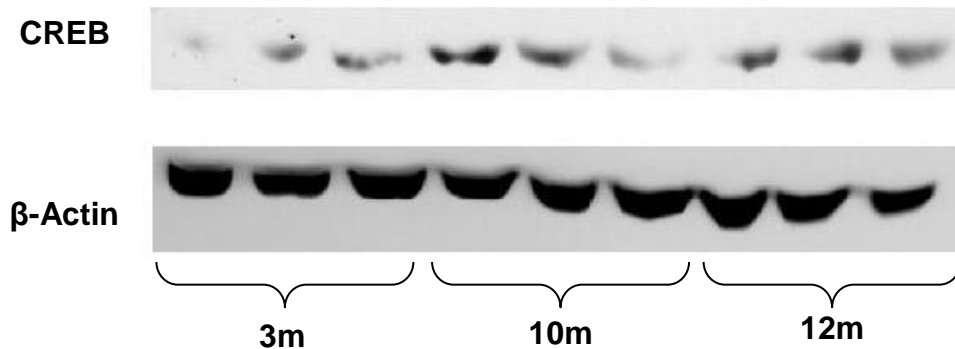
B
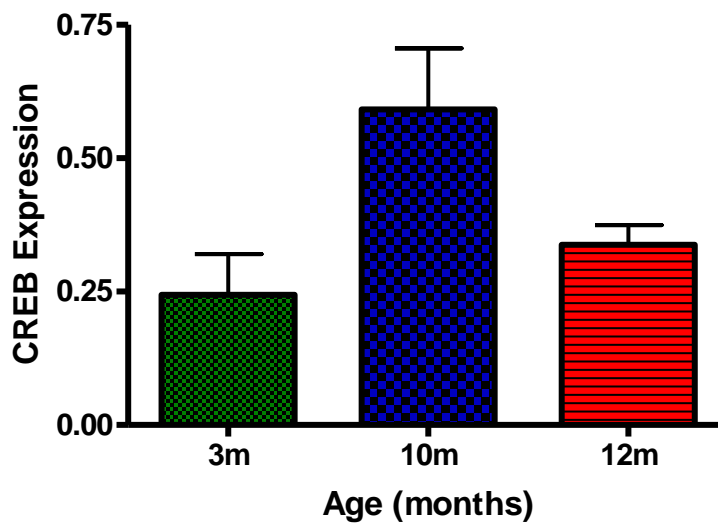
Figure 5-2: Age-dependent changes in CREB expression in 3, 10, and 12m old CD-1 mouse brain where A) is an Immunoblot representation where each lane represents an individual mouse and B) is a column graph showing the quantitative results of CREB expression from the immunoblot. Abbreviations: CREB, cAMP (cyclic adenosine monophosphate) response element binding. Mean values ± SEM, n = 3 for each group.

CD-1 mice at 12 months of age (n=3, 0.175 ± 0.088) showed significant decreased HSP27 (band 2) expression compared to mice at 10 months of age (0.6103 ± 0.1034, p<0.05) and a trend for decreased expression compared to 3 months (n=3, 0.784 ± 0.250, p<0.1). CD-1 mice at 10 months showed no difference in HSP27 expression compared to 3 month old mice (Figure 5-3).

A

B
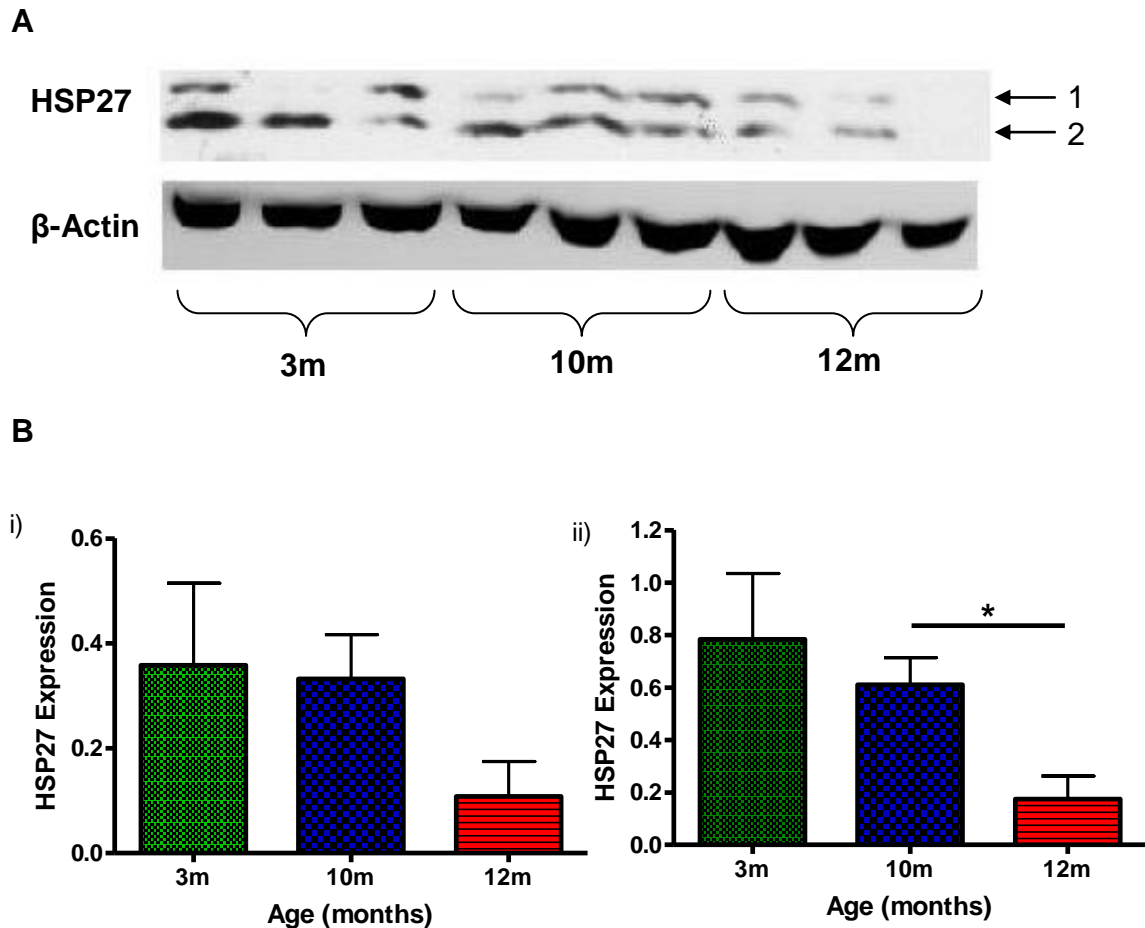
Figure 5-3: Age-dependent changes in HSP27 expression in 3, 10 and 12m old CD-1 mouse brain where A) is an Immunoblot representation where each lane represents an individual mouse, and B) is a column graph showing the quantitative results of i) band 1 and ii) band 2 of HSP27 expression. Abbreviations: HSP27, Heat Shock Protein 27. Mean values ± SEM, n = 3 for each group *p<0.05.

CD-1 mice at 12 months of age (n=3, 0.360 ± 0.090) showed a trend for decreased HSP90 expression compared to mice at 3 months of age (0.624 ± 0.032, p<0.1). CD-1 mice at 10 months of age (n=3, 0.498 ± 0.119) showed no difference in HSP90 expression compared to 3 month or 12 month old mice (Figure 5-4).

A
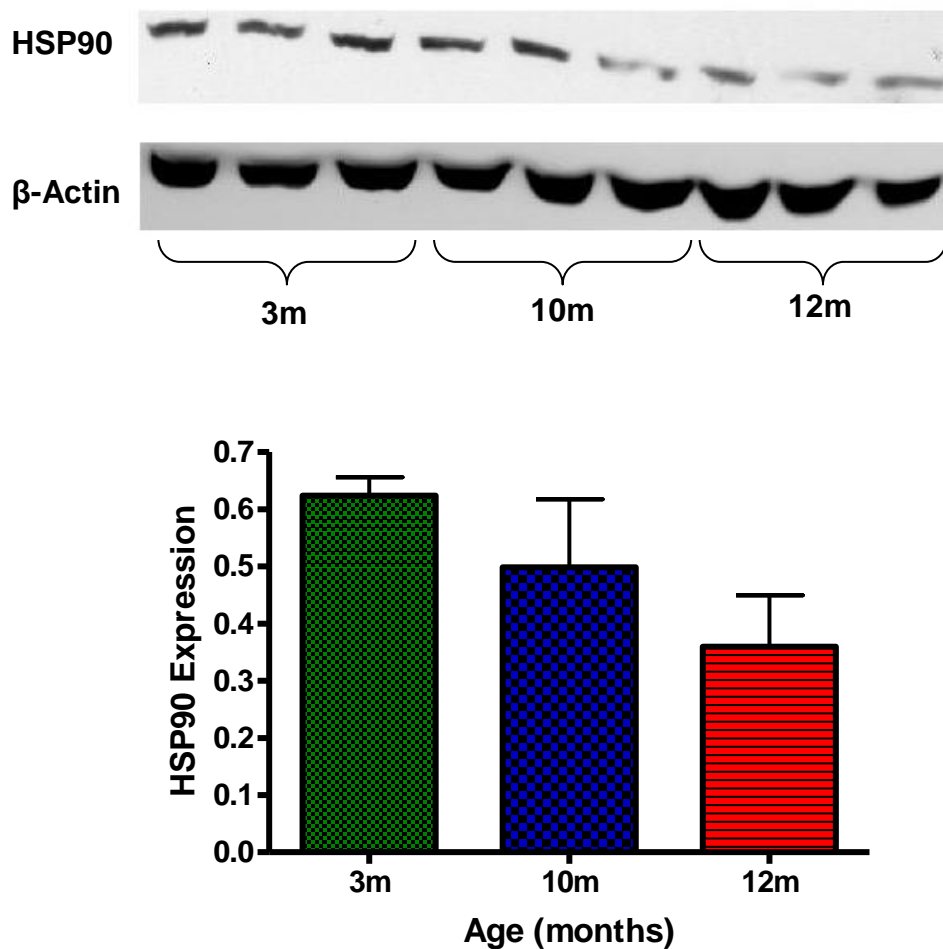
Figure 5-4: Age-dependent changes in HSP90 expression in 3, 10 and 12m old CD-1 mouse brain where A) is an Immunoblot representation where each lane represents an individual mouse, and B) is a column graph showing the quantitative results of HSP90 expression. Abbreviations: HSP90, Heat Shock Protein 90. Mean values ± SEM, n = 3 for each group.

5.2.2 CD-1 Age Timeline: Immunohistochemical analysis

Table 5-2: Summary table depicting immunohistochemical analysis of various protein expression in 3, 10, or 12 month old CD-1 mice. Arrows represent an increase (↑) or decrease (↓) in protein expression in older mice. Abbreviations; BDNF, Brain Deived Neurotrophic Factor; ERK1/2, Extracellular Signal-regulated Kinase; CREB, Cyclic Adenosine Monophosphate (AMP) Response Element Binding; AKT, Protein Kinase B; HSP, Heat Shock Protein. n=3 for each group.

Effect of Chronic IR1072 treatment on protein expression in CD-1 TL	
1º Ab	**Result**
BDNF	-
ERK1	-
ERK2	-
ERK1-P	-
ERK2-P	-
CREB	-
AKT	-
AKT-P	-
HSP27	↓
HSP40	-
HSP60	-
HSP70	-
HSP90	-
HSP105	-

A decrease in HSP27 expression in the cortex, CA2/3 and CA1 was observed in 3, 10, and 12 month old CD-1 mice (Figure 5-5).
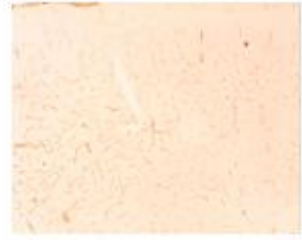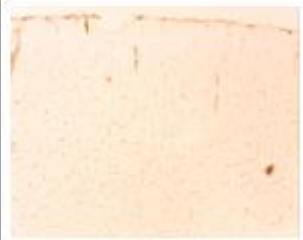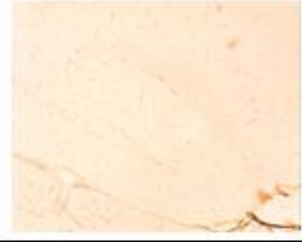
HSP27	3m	10m	12m
Ctx			
CA1			
CA2/3			
DG			
CPu			

Figure 5-5: Immunohistochemical representation of HSP27 expression in 3, 10, or 12 month old CD-1 mice in various brain regions. Abbreviations: BDNF; Ctx, cerebral cortex; CA (1/2/3), Cornu ammonis; DG, Dentate Gyrus; Cb, Cerebellum; CPu, Caudate Putamen. n=3 for each group, X100 magnification.

5.2.3 Chronic IR1072 Treatment: CD-1 mice

5.2.3.1 Chronic IR1072-preconditioning in 7 month old CD-1 mice: Immunoblot analysis

Protein levels were standardised using mouse β-actin primary antibody. Data were statistically analysed using a two tailed student t-test. Data represent mean ± SEM.

Table 5-3: Protein expression profile following chronic IR1072 treatment in 7 month old CD-1 mice compared to age-matched sham-treated CD-1 mice. Arrows represent an increase (↑) or decrease (↓) in protein expression in IR-treated CD-1 mice compared to age-matched sham controls, and respective figure numbers. Abbreviations; BDNF, Brain Deived Neurotrophic Factor; ERK1/2, Extracellular Signal-regulated Kinase; CREB, Cyclic Adenosine Monophosphate (AMP) Response Element Binding; AKT, Protein Kinase B; HSP, Heat Shock Protein. Data was statistically analysed using a two tailed student t-test. Pink cells represent significant results and blue cells represent a trend. n=4 for each group, *p<0.05, **p<0.01.

Effect of Chronic IR1072 treatment on protein expression in 7 month old CD-1 mice			
1º Ab	**p value**	**Result**	**Figure**
BDNF	***0.0026**	↑	**Figure 5-6**
ERK1	***0.0069**	↓	**Figure 5-7**
ERK2	****0.0006**	↓	**Figure 5-7**
ERK1-P	0.0799	↓	**Figure 5-8**
ERK2-P	0.1373	NS	Data not shown
CREB	0.6651	NS	Data not shown
AKT	*0.0498*	↓	**Figure 5-9**
AKT-P	0.1073	NS	Data not shown
HSP27	0.0843	↑	**Figure 5-10**
HSP40	0.4575	NS	Data not shown
HSP60	0.4271	NS	Data not shown
HSP70	*0.0108*	↓	**Figure 5-11**
HSP90	0.8165	NS	Data not shown
HSP105	0.7176	NS	Data not shown

IR1072-preconditioned 7 month old CD-1 mice (n=4, 1.302 ± 0.095) showed a significant increase in BDNF expression compared to age-matched sham controls (n=4, 0.798 ± 0.038, p<0.01) (Figure 5-6).
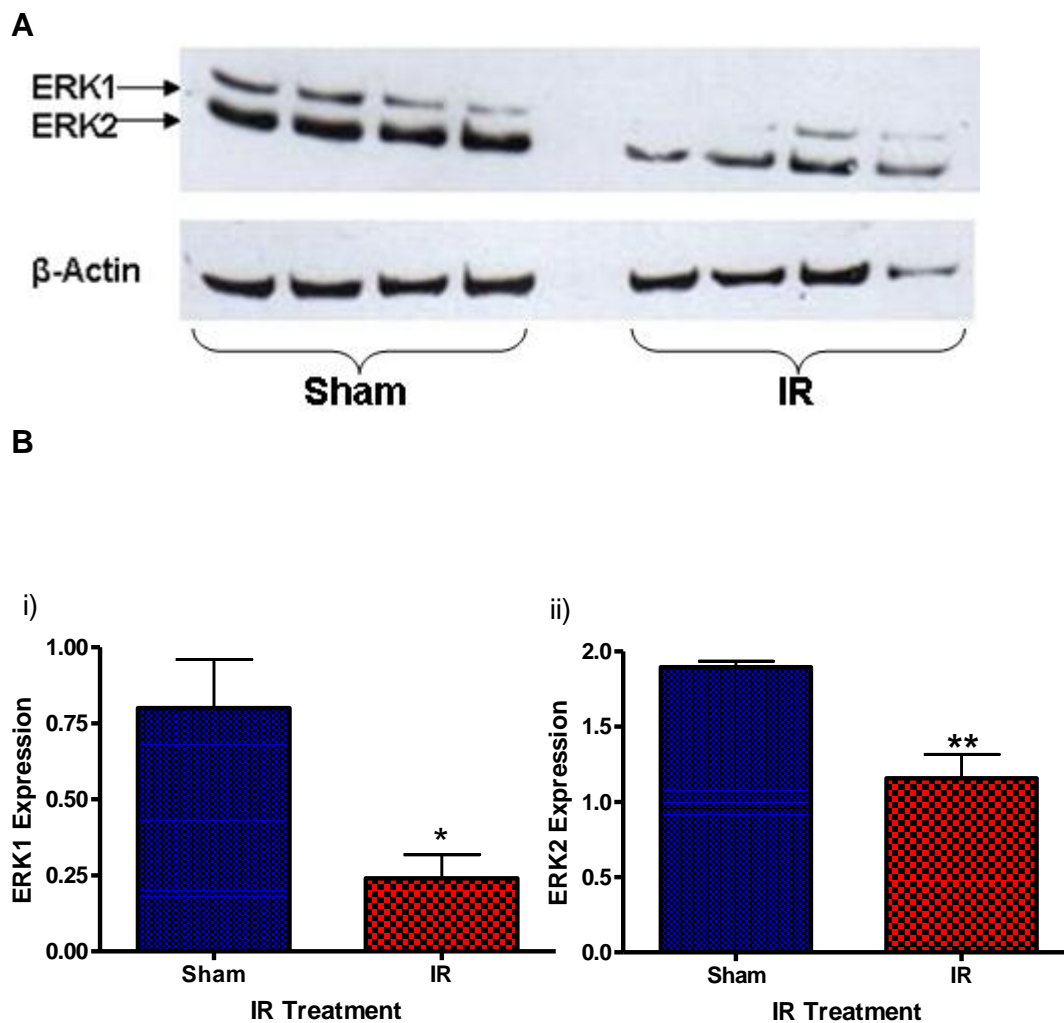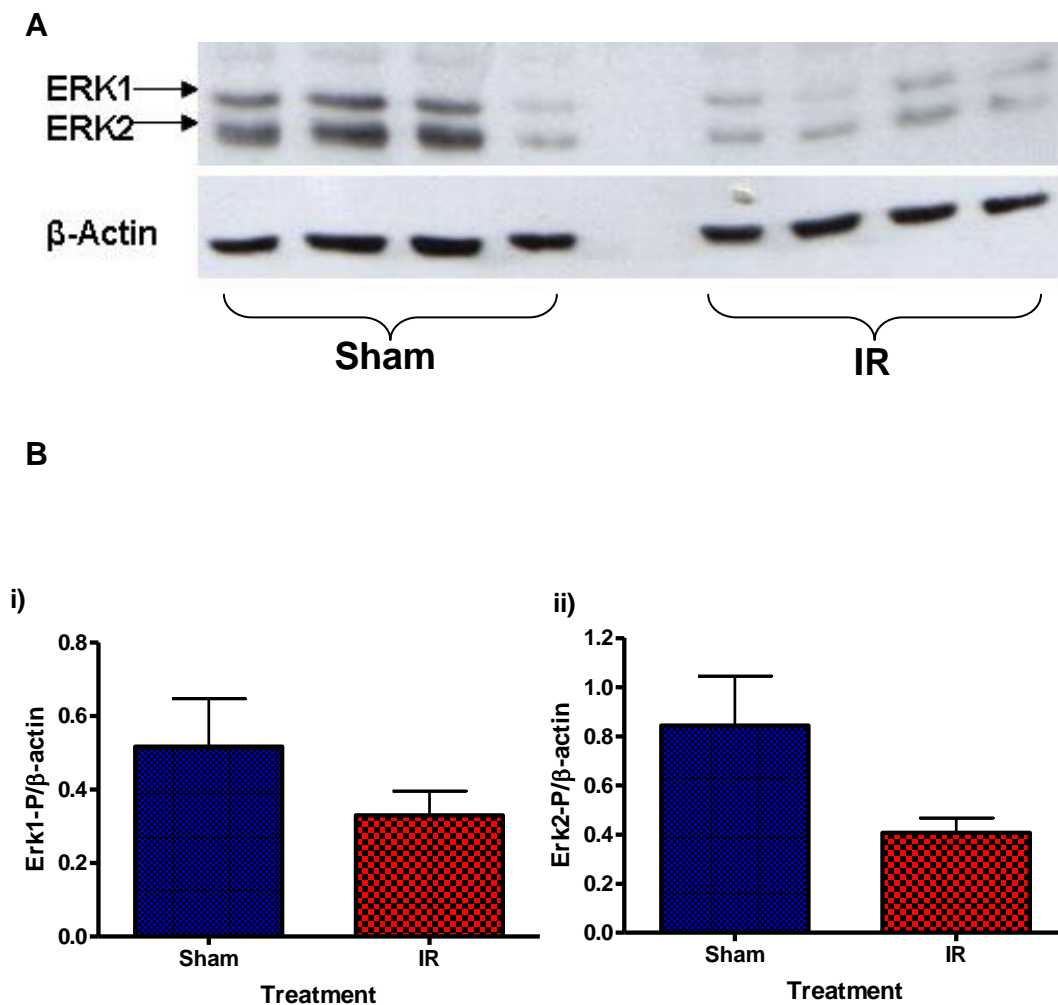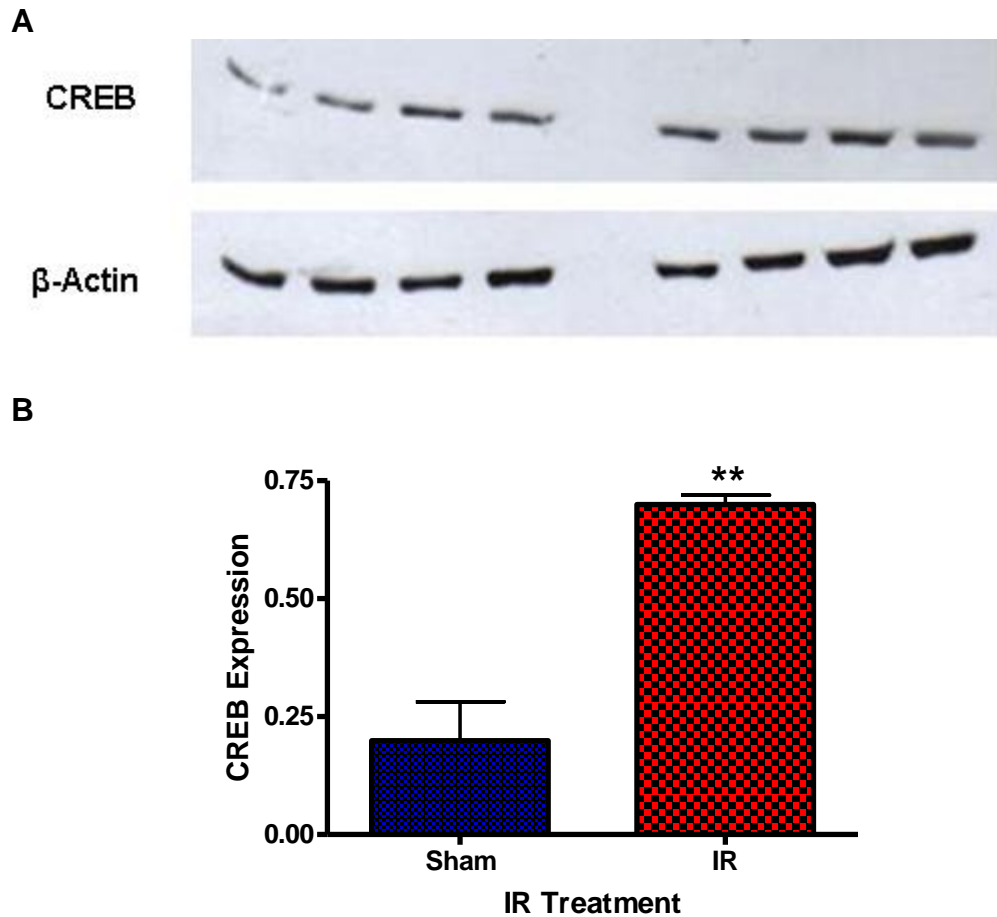
A
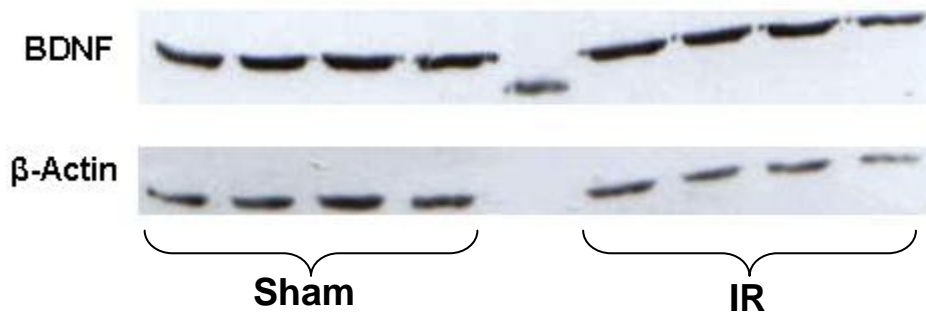
B
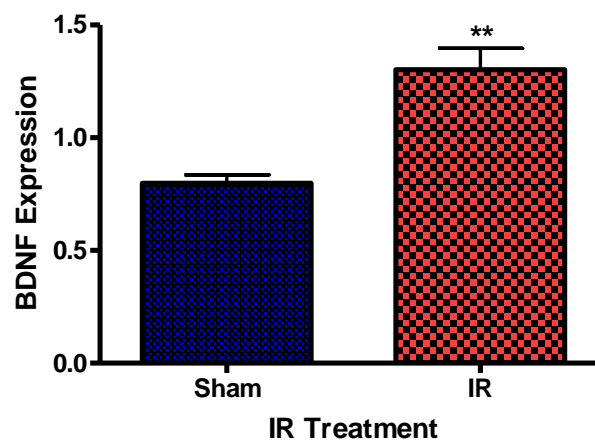
Figure 5-6: BDNF expression in chronically IR1072 treated (*in vivo*) 7 month old CD-1 mouse brain and age-matched sham controls where A) is an Immunoblot representation where each lane represents an individual mouse and B) is a column graph showing the quantitative results of BDNF expression. Protein expression were standardised to total β-actin levels. Abbreviations: BDNF, Brain Derived Neurotrophic Factor. Mean values ± SEM, n = 4 for each group, **p<0.01.

IR1072-preconditioned 7 month old CD-1 mice (n=4, 0.635 ± 0.164) showed a significant decrease in ERK1 expression compared to age-matched sham controls (n=4, 1.372 ± 0.081, $p<0.01$). IR1072-preconditioned 7 month old CD-1 mice (n=4, 1.459 ± 0.123) showed a significant decrease in ERK2 expression compared to age-matched sham controls (n=4, 2.778 ± 0.158, $p<0.001$) (Figure 5-7).
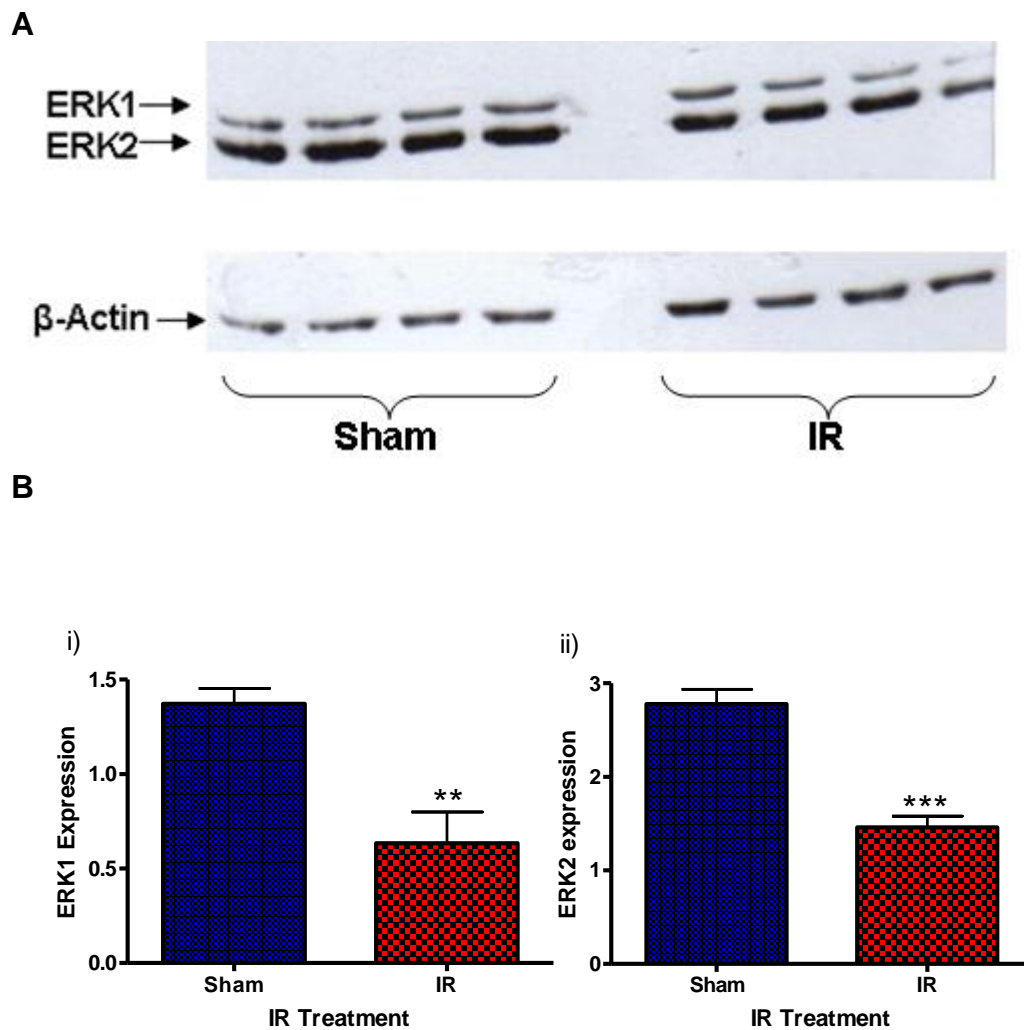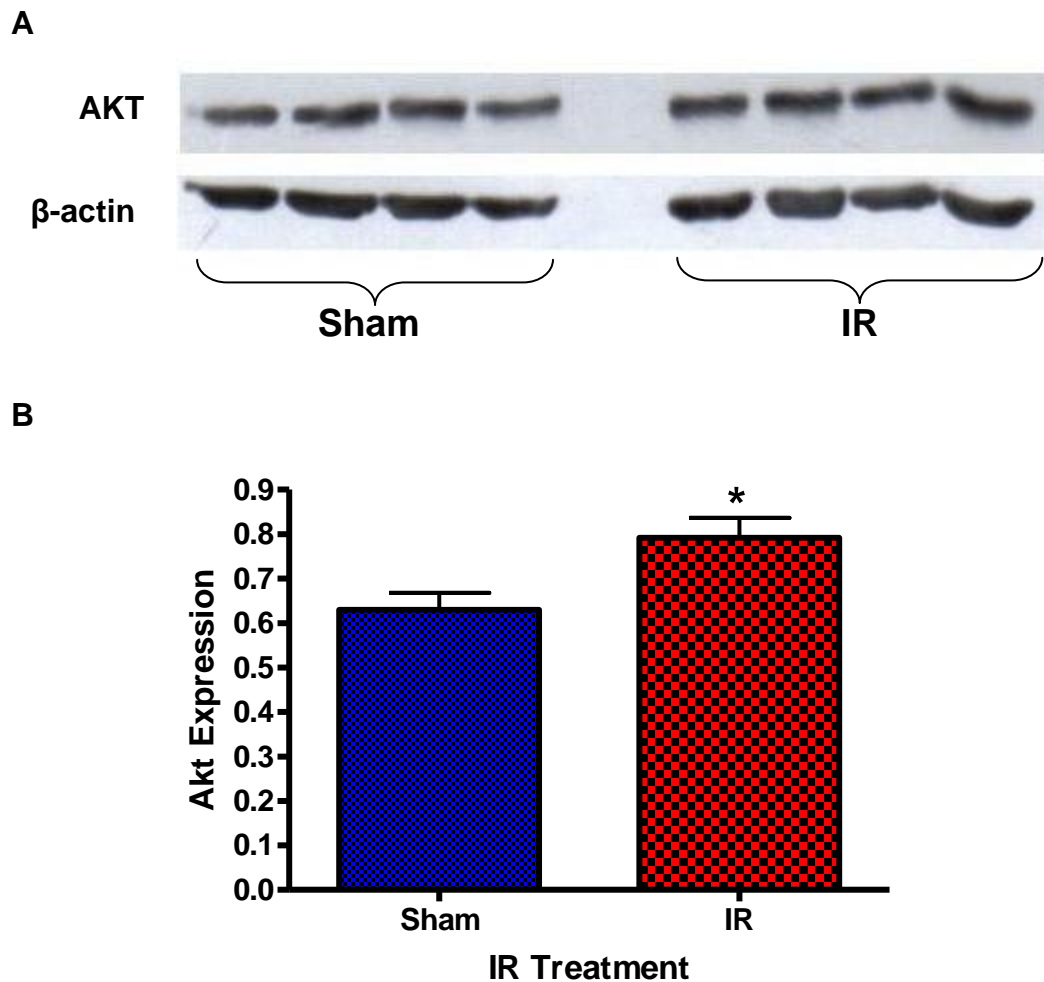

Figure 5-7: ERK1/2 expression in chronically IR1072 treated (*in vivo*) 7 month old CD-1 mouse brain and age-matched sham controls where A) is an Immunoblot representation where each lane represents an individual mouse, and B) is a column graph showing the quantitative results of i) ERK1 and ii) ERK2 expression. Protein expression were standardised

to total β-actin levels. Abbreviations: ERK1/2, Extracellular Signal-regulated Kinase 1 or 2. Mean values ± SEM, n = 4 for each group, **p<0.01, ***p<0.001.

IR1072-preconditioned 7 month old CD-1 mice (n=4, 0.359 ± 0.124) showed a trend for decreased ERK1-P expression compared to age-matched sham controls (n=4, 0.659 ± 0.071, p<0.1). IR1072-preconditioned 7 month old CD-1 mice (n=4, 0.613 ± 0.181) showed no significant difference in ERK2-P expression compared to age-matched sham controls (n=4, 0.979 ± 0.113) (Figure 5-8).
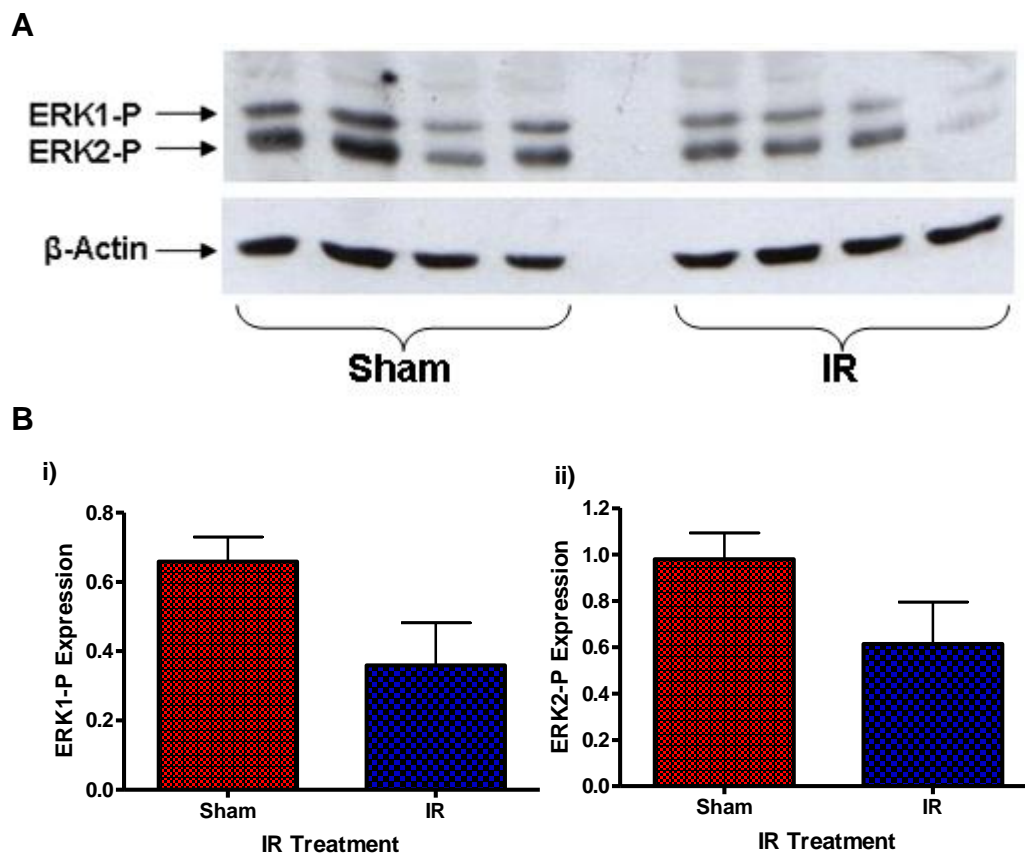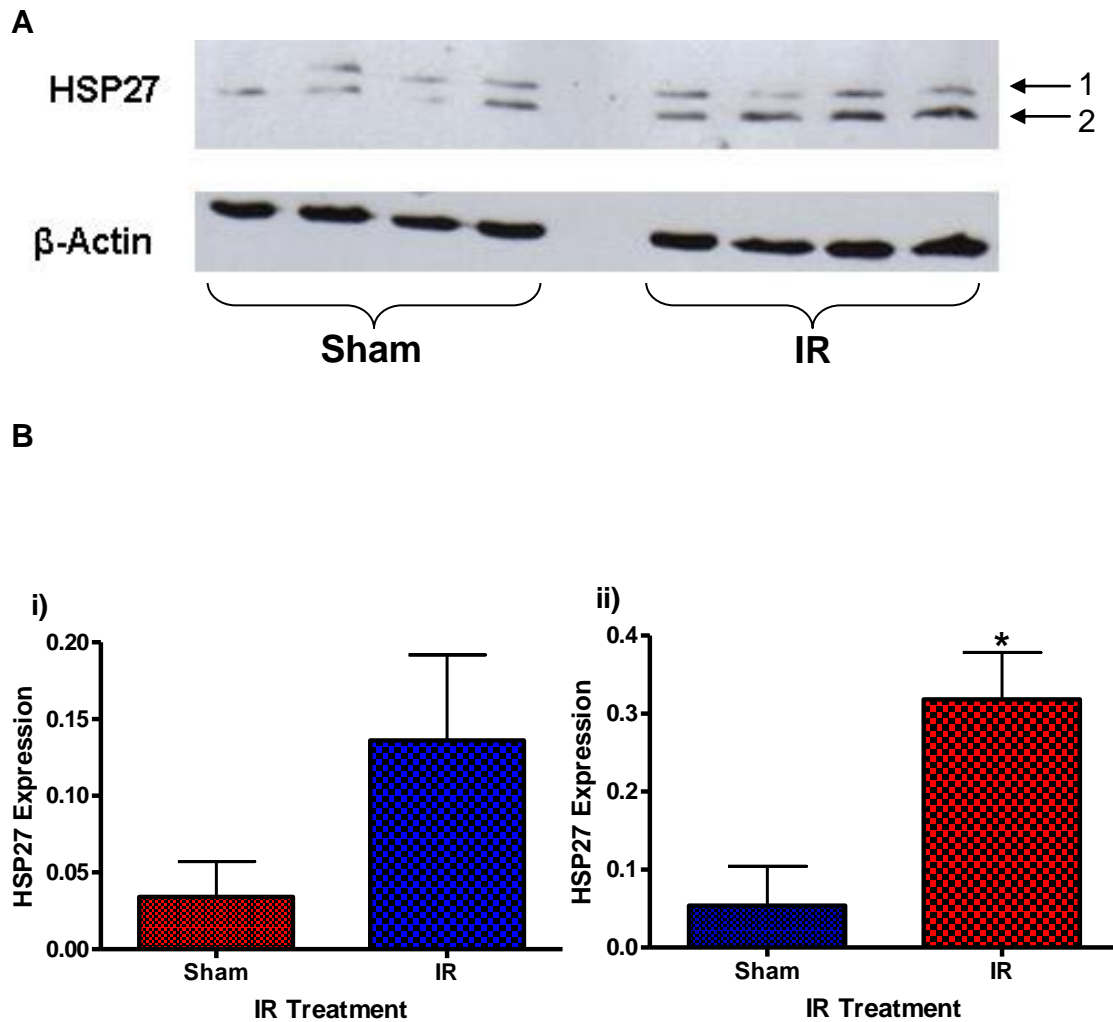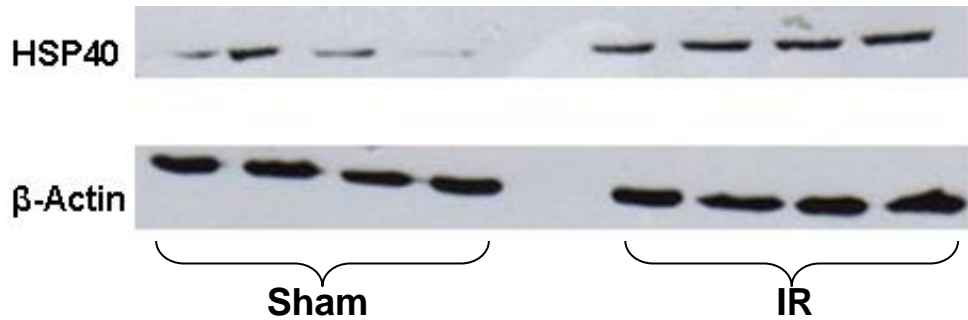

Figure 5-8: ERK1/2-P expression in chronically IR1072 treated (*in vivo*) 7 month old CD-1 mouse brain and age-matched sham controls where A) is an Immunoblot representation where each lane represents an individual mouse, and B) is a column graph showing the quantitative results of i) ERK1-P and ii) ERK2-P expression. Protein expression were standardised to total β-actin levels. Abbreviations: ERK1/2-P, Phosphorylated Extracellular Signal-regulated Kinase 1 or 2. Mean values ± SEM, n = 4 for each group.

IR1072-preconditioned 7 month old CD-1 mice (n=4, 0.788 ± 0.034) showed a significant decrease in AKT expression compared to age-matched sham controls (n=4, 1.049 ± 0.099, p<0.05) (Figure 5-9).
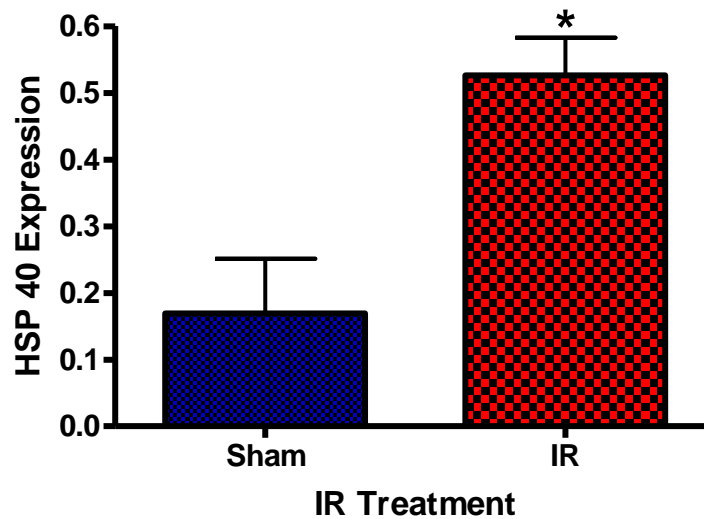
A

B
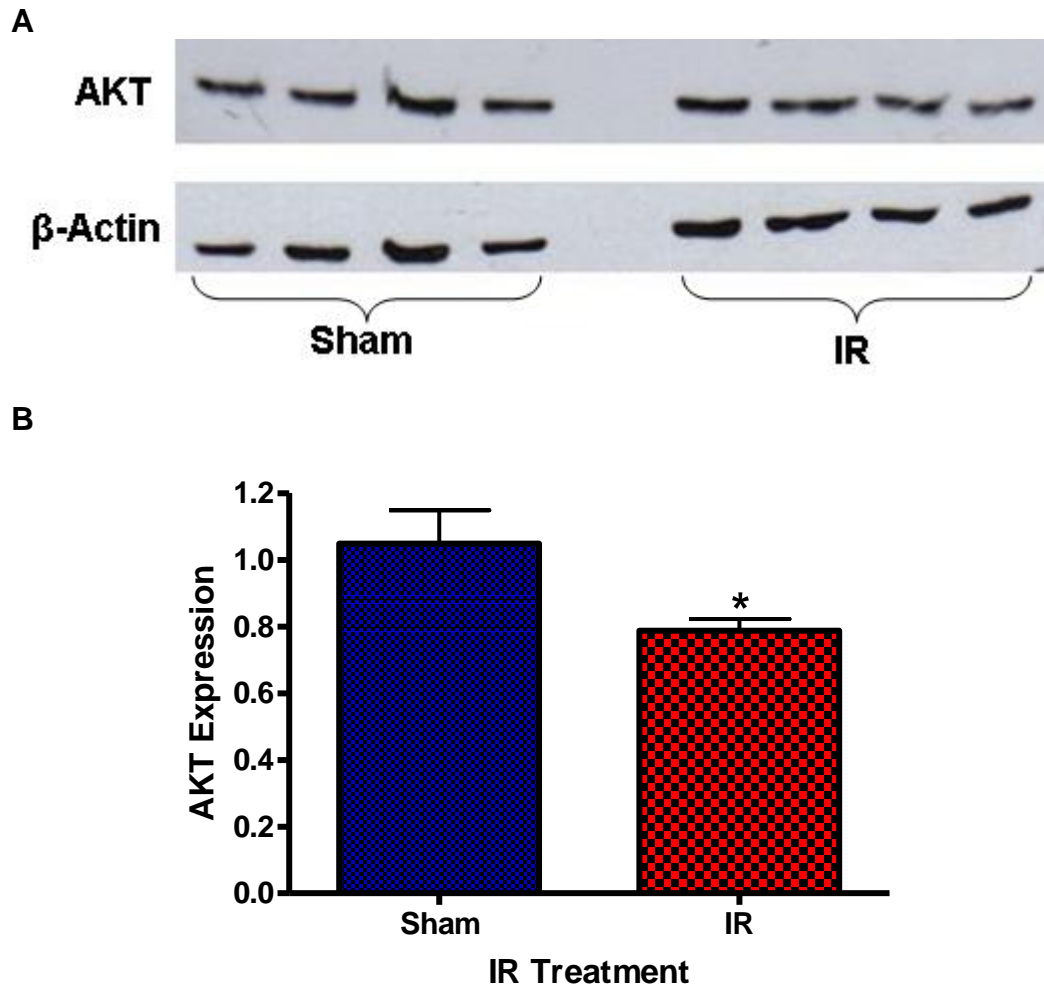
Figure 5-9: AKT expression in chronically IR1072 treated (*in vivo*) 7 month old CD-1 mouse brain and age-matched sham controls where A) is an Immunoblot representation where each lane represents an individual mouse, and B) is a column graph showing the quantitative results of AKT expression. Protein expression were standardised to total β-actin levels. Abbreviations: AKT, Protein Kinase B. Mean values ± SEM, n = 4 for each group, *p<0.05.

IR1072-preconditioned 7 month old CD-1 mice (n=4, 0.227 ± 0.080) showed a trend for increased HSP27 expression compared to age-matched sham controls (n=4, 0.041 ± 0.041, p<0.1) (Figure 5-10).
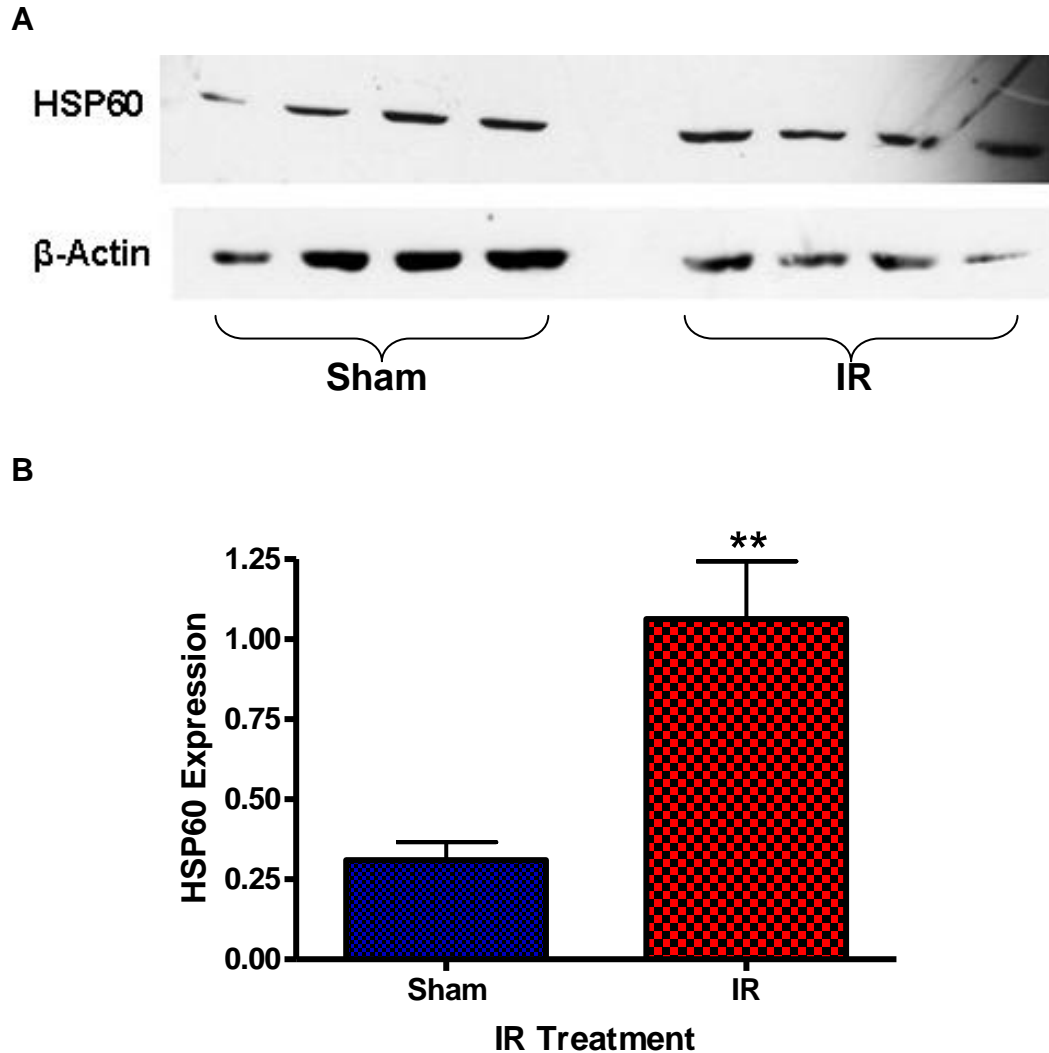
A
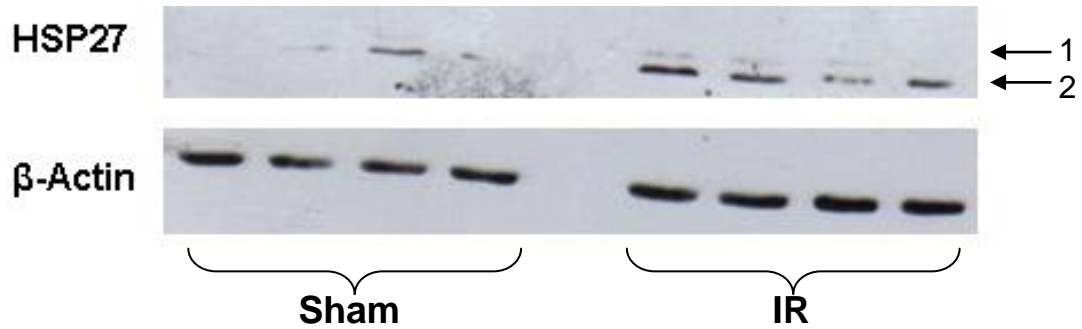
B
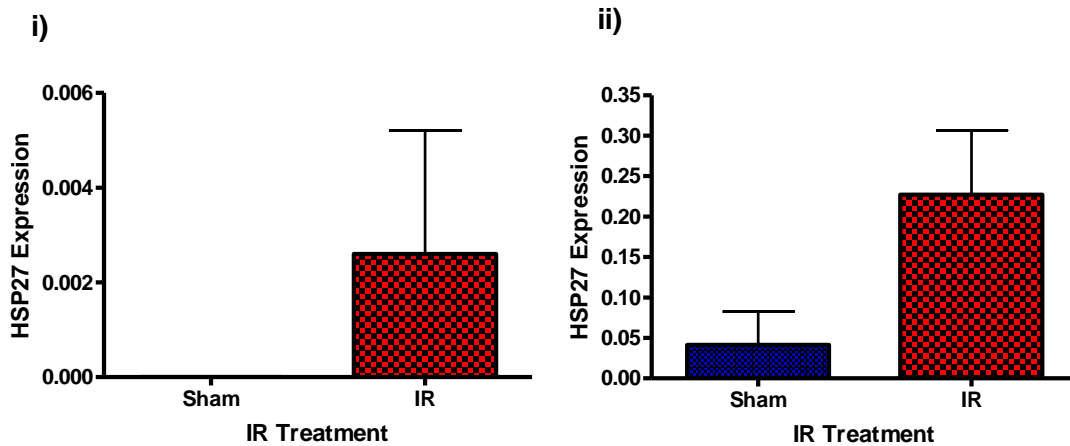
Figure 5-10: HSP27 expression in chronically IR1072 treated (*in vivo*) 7 month old CD-1 mouse brain and age-matched sham controls where A) is an Immunoblot representation where each lane represents an individual mouse, and B) is a column graph showing the quantitative results of i) band 1 and ii) band 2 HSP27 expression. Protein expression were standardised to total β-actin levels. Abbreviations: HSP27, Heat Shock Protein 27. Mean values ± SEM, n = 4 for each group.

IR1072-preconditioned 7 month old CD-1 mice (n=4, 0.719 ± 0.060) showed a trend for increased HSP70 expression compared to age-matched sham controls (n=4, 1.038 ± 0.063, p<0.05) (Figure 5-11).

A

B
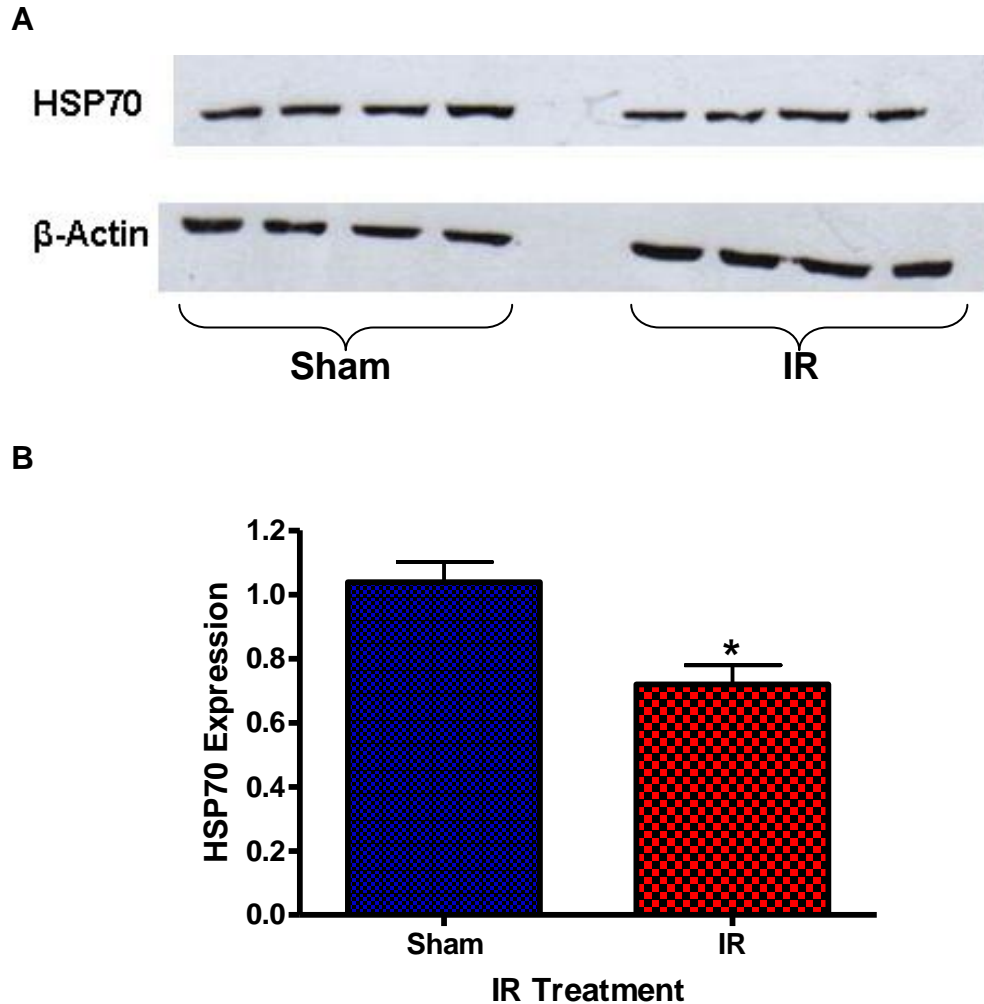
Figure 5-11: HSP70 expression in chronically IR1072 treated (*in vivo*) 7 month old CD-1 mouse brain and age-matched sham controls where A) is an Immunoblot representation where each lane represents an individual mouse, and B) is a column graph showing the quantitative results of HSP70 expression. Protein expression were standardised to total β-actin levels. Abbreviations: HSP70, Heat Shock Protein 70. Mean values ± SEM, n = 4 for each group, *p<0.05.

5.2.3.2 Chronic IR1072-preconditioning in 7 month old CD-1 mice: Immunohistochemical analysis

Immunohistochemical analysis did not reveal differences between groups IR1072-treated 7 month old CD-1 mice and age matched sham controls.

5.2.3.3 Chronic IR1072-preconditioning in 13 month old CD-1 mice: Immunoblot analysis

Protein levels were standardised using mouse β-actin primary antibody. Data was statistically analysed using a two tailed student t-test. Data represent mean ± SEM for n numbers.

Table 5-5: Protein expression profile in 13 month old CD-1 mouse brain following chronic IR1072 treatment compared to age-matched sham-treated controls. Arrows represent an increase (↑) or decrease (↓) in protein expression in IR-treated CD-1 mice compared to age-matched sham controls, and respective figure numbers. Abbreviations; BDNF, Brain Deived Neurotrophic Factor; ERK1/2, Extracellular Signal-regulated Kinase; CREB, Cyclic Adenosine Monophosphate (AMP) Response Element Binding; AKT, Protein Kinase B; HSP, Heat Shock Protein. Data were statistically analysed using a two tailed student t-test. Pink cells represent significant results (p<0.05) and blue cells represent a trend (p<0.1). n=4 for each group, *p<0.05, **p<0.01.

Effect of Chronic IR1072 treatment on protein expression in 13 month old CD-1 mice			
	CD-1_O		
1º	p value	Result	Figure
BDNF	0.1009	NS	Data not shown
ERK1	*0.0198	↓	Figure 5-12
ERK2	**0.0041	↓	
ERK1-P	0.2467	NS	Data not shown
ERK2-P	0.083	↓	Figure 5-13
CREB	**0.0011	↑	Figure 5-14
AKT	*0.0335	↑	Figure 5-15
AKT-P	0.5873	NS	Data not Shown
HSP27	*0.015	↑	Figure 5-16
HSP40	*0.0117	↑	Figure 5-17
HSP60	**0.0072	↑	Figure 5-18
HSP70	0.1392	NS	Data not shown
HSP90	0.9898	NS	Data not shown
HSP105			Incomplete

IR1072-preconditioned 13 month old CD-1 mice (n=4, 0.240 ± 0.079) showed a significant decrease in ERK1 expression compared to age-matched sham controls (n=4, 0.801 ± 0.160, p<0.05). IR1072-preconditioned 13 month old CD-1 mice (n=4, 1.157 ± 0.160) showed a significant decrease in ERK2 expression compared to age-matched sham controls (n=4, 1.896 ± 0.038, p<0.01) (Figure 5-12).

Figure 5-12: ERK1/2 expression in chronically IR1072 treated (*in vivo*) 13 month old CD-1 mouse brain and age-matched sham controls where A) is an Immunoblot representation where each lane represents an individual mouse, and B) is a column graph showing the quantitative results of ERK1/2 expression. Protein expression were standardised to total β-actin levels. Abbreviations: ERK1/2, Extracellular Signal-regulated Kinase 1 or 2. Mean values ± SEM, n = 4 for each group, *p<0.05, **p<0.01.

IR1072-preconditioned 13 month old CD-1 mice (n=4, 0.406 ± 0.060) showed a trend for decreased ERK2-P expression compared to age-matched sham controls (n=4, 0.843 ± 0.202, p<0.1). IR1072-preconditioned 13 month old CD-1 mice (n=4, 0.330 ± 0.066) showed no significant difference in ERK1-P expression compared to age-matched sham controls (n=4, 0.517 ± 0.130) (Figure 5-13).

Figure 5-13: ERK1/2-P expression in chronically IR1072 treated (*in vivo*) 13 month old CD-1 mouse brain and age-matched sham controls where A) is an Immunoblot representation where each lane represents an individual mouse, and B) is a column graph showing the quantitative results i) ERK1-P and ii) ERK2-P expression. Protein expression were standardised to total β-actin levels. Abbreviations: ERK1/2-P, phosphorylated Extracellular Signal-regulated Kinase 1 or 2. Mean values ± SEM, n = 4 for each group.

IR1072-preconditioned 13 month old CD-1 mice (n=4, 0.700 ± 0.0198) showed a significant increase in CREB expression compared to age-matched sham controls (n=4, 0.199 ± 0.083, p<0.01) (Figure 5-14).

A

B

Figure 5-14: CREB expression in chronically IR1072 treated (*in vivo*) 13 month old CD-1 mouse brain and age-matched sham controls where A) is an Immunoblot representation where each lane represents an individual mouse, and B) is a column graph showing the quantitative results CREB expression. Protein expression were standardised to total β-actin levels. Abbreviations: CREB, cAMP (cyclic adenosine monophosphate) response element binding. Mean values ± SEM, n = 4 for each group, **p<0.01.

IR1072-preconditioned 13 month old CD-1 mice (n=4, 0.791 ± 0.045) showed a significant increase in AKT expression compared to age-matched sham controls (n=4, 0.630 ± 0.038, p<0.05) (Figure 5-15).

A

B

Figure 5-15: Effects of BDNF expression in chronically sham or IR1072 treated 4 month old CD-1 mouse brain (*in vivo*) where A) is an Immunoblot representation where each lane represents an individual mouse, and B) is a column graph showing the quantitative results of BDNF expression from the immunoblot. Protein expression were standardised to total β-actin levels. Abbreviations: AKT, Protein Kinase B. Mean values ± SEM, n = 5 for each group, *p<0.05.

IR1072-preconditioned 13 month old CD-1 mice (n=4, 0.318 ± 0.060) showed a significant increase in HSP27 expression compared to age-matched sham controls (n=4, 0.054 ± 0.050, p<0.05) (Figure 5-16).

A

B

Figure 5-16: HSP27 expression in chronically IR1072 treated (*in vivo*) 13 month old CD-1 mouse brain and age-matched sham controls where A) is an immunoblot representation where each lane represents an individual mouse, and B) is a column graph showing the quantitative results HSP27 expression. Protein expression were standardised to total β-actin levels. Abbreviations: HSP27, Heat Shock Protein 27. Mean values ± SEM, n = 4 for each group, *p<0.05.

IR1072-preconditioned 13 month old CD-1 mice (n=4, 0.526 ± 0.057) showed a significant increase in HSP40 expression compared to age-matched sham controls (n=4, 0.169 ± 0.082, p<0.05) (Figure 5-17).

A

B

Figure 5-17: HSP40 expression in chronically IR1072 treated (*in vivo*) 13 month old CD-1 mouse brain and age-matched sham controls where A) is an immunoblot representation where each lane represents an individual mouse, and B) is a column graph showing the quantitative results HSP40 expression. Protein expression were standardised to total β-actin levels. Abbreviations: HSP40, Heat Shock Protein 40. Mean values ± SEM, n = 4 for each group, *p<0.05.

IR1072-preconditioned 13 month old CD-1 mice (n=4, 1.063 ± 0.180) showed a significant increase in HSP60 expression compared to age-matched sham controls (n=4, 0.3101 ± 0.056, p<0.01) (Figure 5-18).

A

B

Figure 5-18: HSP60 expression in chronically IR1072 treated (*in vivo*) 13 month old CD-1 mouse brain and age-matched sham controls where A) is an immunoblot representation where each lane represents an individual mouse, and B) is a column graph showing the quantitative results HSP60 expression. Protein expression were standardised to total β-actin levels. Abbreviations: HSP60, Heat Shock Protein 60. Mean values ± SEM, n = 4 for each group, **p<0.01.

5.2.3.4 Chronic IR1072-preconditioning in 13 month old CD-1 mice: Immunohistochemical analysis

Table5-6: Protein expression profile in the brain regions of 13 month old CD-1 mice following chronic IR1072 treatment. Arrows represent an increase (↑) or decrease (↓) in protein expression in IR-treated CD-1 mice compared to age-matched sham controls. n=4 for each group.

Effect of Chronic IR1072 treatment on protein expression in 13 month old CD-1 mice	
1º Ab	**Result**
BDNF	-
ERK1/2	**-**
ERK1/2-P	↓ Ctx, CA2/3, CA1
CREB	**-**
AKT	**-**
AKT-P	-
HSP27	↑ Ctx, DG
HSP27-P	↑ CA1, CA2/3
HSP40	↑ DG
HSP60	-
HSP70	-
HSP90	-
HSP105	↓ CA1

A decrease in ERK1/2-P expression in the cortex, CA2/3 and CA1 was observed in IR1072 treated 13 month old CD-1 mice compared to age matched sham controls (Figure 5-19).
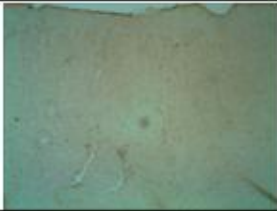

Figure 5-19: Immunohistochemical representation of ERK1/2-P expression in IR1072-treated 13m old CD-1 mice and age-matched sham controls in various brain regions. Abbreviations: ERK1/2-P, Extracellular Signal-regulated Kinase; Ctx, cerebral cortex; CA (1/2/3), Cornu ammonis; DG, Dentate Gyrus; Cb, Cerebellum; CPu, Caudate Putamen. n=4 for each group, X100 magnification.

An increase in HSP27 expression in the cortex and dentate gyrus was observed in IR1072 treated 13 month old CD-1 mice compared to age matched sham controls (Figure 5-20).
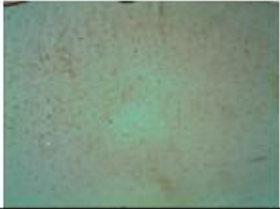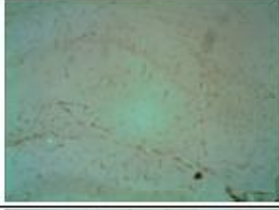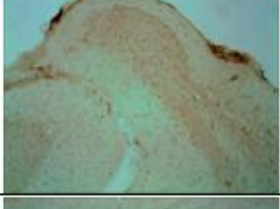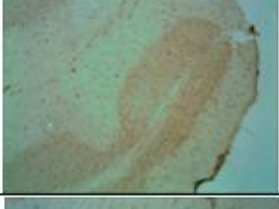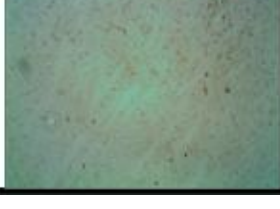
Figure 5-20: Immunohistochemical representation of HSP27 expression in IR1072-treated 13m old CD-1 mice and age-matched controls in various brain regions. Abbreviations: HSP27, Heat Shock Protein 27; Ctx, cerebral cortex; CA (1/2/3), Cornu ammonis; DG, Dentate Gyrus; Cb, Cerebellum; CPu, Caudate Putamen. n=4 for each group, X100 magnification.

An increase in HSP27-P expression in the CA2/3 and CA1 was observed in IR1072 treated 13 month old CD-1 mice compared to age matched sham controls (Figure 5-21).
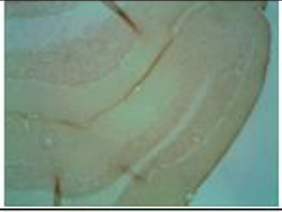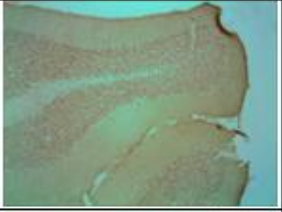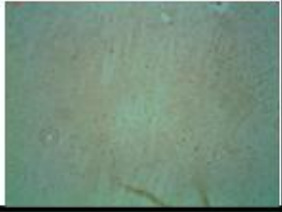
Figure 5-21: Immunohistochemical representation of HSP27-P expression in IR1072-treated 13m old CD-1 mice and age-matched sham controls in various brain regions. Abbreviations: HSP27-P, phosphorylated Heat Shock Protein 27; Ctx, cerebral cortex; CA (1/2/3), Cornu ammonis; DG, Dentate Gyrus; Cb, Cerebellum; CPu, Caudate Putamen. n=4 for each group, X100 magnification.

An increase in HSP40 expression in the dentate gyrus was observed in IR1072 treated 13 month old CD-1 mice compared to age matched sham controls (Figure 5-22).
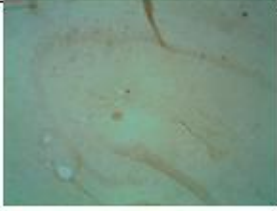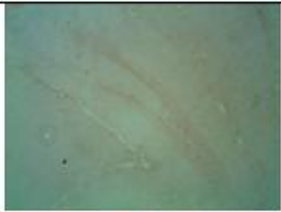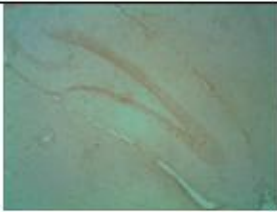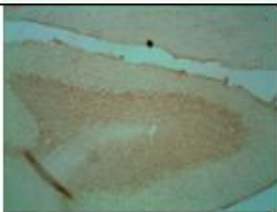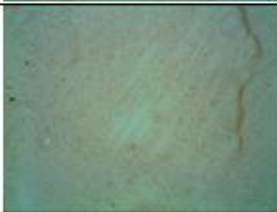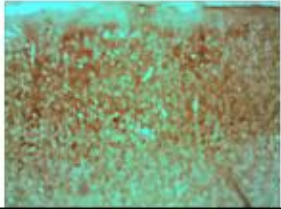

Figure 5-22: Immunohistochemical representation of HSP40 expression in IR1072-treated 13m old CD-1 mice and age-matched sham controls in various brain regions. Abbreviations: HSP40, Heat Shock Protein 40; Ctx, cerebral cortex; CA (1/2/3), Cornu ammonis; DG, Dentate Gyrus; Cb, Cerebellum; CPu, Caudate Putamen. n=4 for each group, X100 magnification.

An increase in HSP105 expression in the dentate gyrus was observed in IR1072 treated 13 month old CD-1 mice compared to age matched sham controls (Figure 5-23).
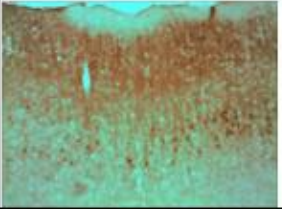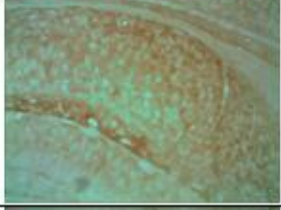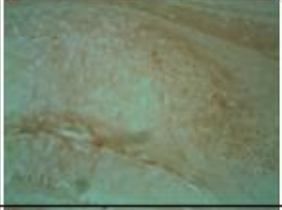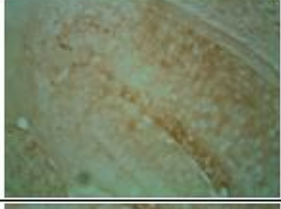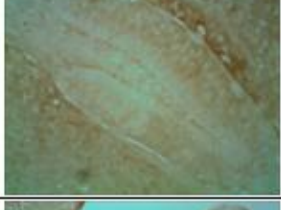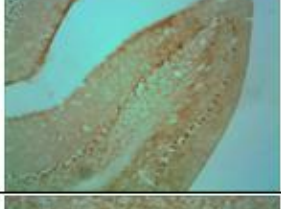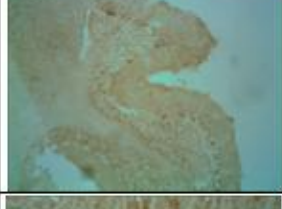

Figure 5-23: Immunohistochemical representation of HSP105 expression in IR1072-treated 13m old CD-1 mice age-matched sham controls in various brain regions. Abbreviations: HSP105, Heat Shock Protein 105; Ctx, cerebral cortex; CA (1/2/3), Cornu ammonis; DG, Dentate Gyrus; Cb, Cerebellum; CPu, Caudate Putamen. n=4 for each group, X100 magnification.

5.2.3.5 Ageing and chronic IR1072-preconditioning in CD-1 mice: AMPA receptor expression

There are three families of ionotropic glutamate receptors, NMDA, AMPA and kainate receptors (Kent et al., 2002; Bergink et al., 2004; Burroughs and French, 2007) which are mainly postsynaptic and regulate fast excitations and synaptic plasticity associated with the opening of cation-permeable ligand-gated ion channels (Meldrum, 2000; Kent et al., 2002; Burroughs and French, 2007). Depolarisation of the postsynaptic membrane by activation of other receptor subtypes, such as AMPA or kainate receptors, will remove the Mg^{2+} block from resting NMDA receptors, where activation of the NMDA receptor occurs subsequently resulting in the flow of Ca^{2+} and other ions through the NMDA receptor channel, a signal that has a role in synaptic plasticity (Bergink et al., 2004; Burroughs and French, 2007). AMPA and kainate receptors (non-NMDA receptors) are associated with voltage-independent channels that gate a depolarising current mainly carried by Na^+ ions, which in turn promote the activation of voltage-dependent NMDA receptor (Bergink et al., 2004; Burroughs and French, 2007).

AMPA receptors are composed of four subunits, each of which has a binding pocket for glutamate, and are postsynaptic mediators for fast excitatory neurotransmission are involved in learning and memory (Franciosi, 2001; Lynch, 2004; Mathew et al., 2008). Once glutamate binds to AMPA receptors, a conformational change occurs between the extracellular domain and transmembrane pore of the receptor, which opens the channel and allows

159

current to pass through the postsynaptic membrane (Lynch, 2004). When the transmitter is released from the binding pocket the current is terminated and the channel is in the deactivated state, or the extracellular domains produces a conformational change on the transmembrane channel, thus disrupting interaction between AMPA receptor subunits where the channel is prevented from reopening despite the bound transmitter still being present, resulting in a desensitized state of the receptor (Lynch, 2004). The size and shape of excitatory postsynaptic currents are regulated by these rapid desensitization and deactivation states of the receptor, where synthetic positive modulators of the AMPA receptors, such as ampakines, do not act on AMPA receptors directly but delay the receptor from deactivating or desensitizing in the presence of an agonist, thus prolonging the current flow (Lynch, 2004; Mathew et al., 2008). Ampakines act as positive modulators of the AMPA receptor, where they have been shown to facilitate synaptic transmission and formation of LTP in the hippocampus, thus aiding learning and memory (Lynch, 2004). Ampakines and other AMPA receptor positive modulators have been shown to increase BDNF production and the ERK1/2 signalling cascade, which is also heavily implicated in learning and memory. This study has performed AMPA receptor autoradiographical studies in CD-1 timeline at 3 months, 10 months and 12 months of age, and chronically treated IR1072 7 month or 13 month old CD-1 mice to determine whether IR1072 has any effect on modulation of AMPA receptor expression.
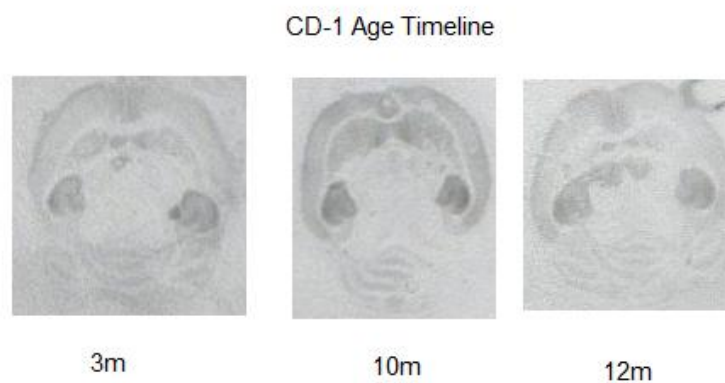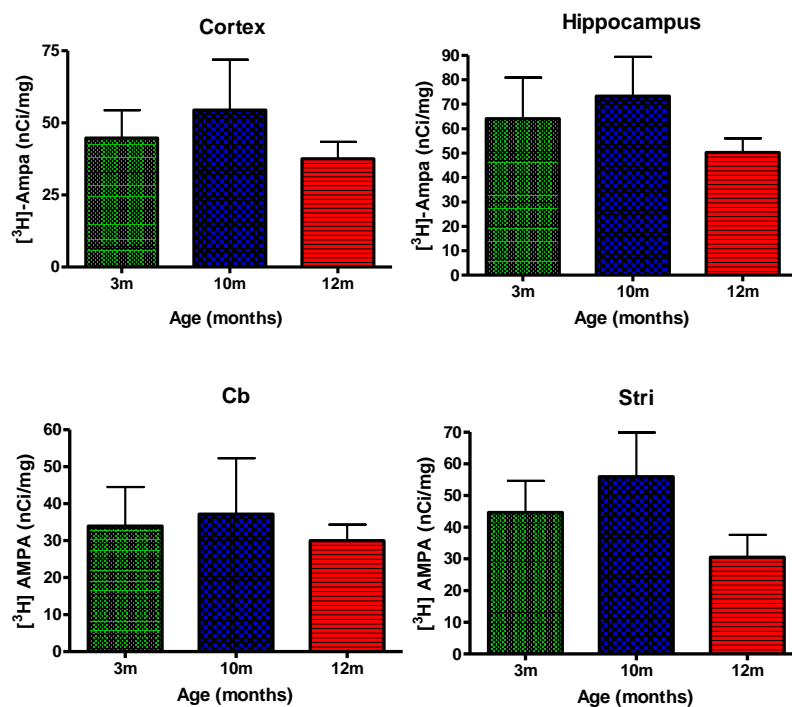
Figure 5-24: A) [³H]-AMPA autoradiographical images of CD-1 timeline showing anatomical AMPA receptor expression in brain structures as CD-1 mice age B) Quantification of AMPA receptor expression from autoradiographical images in various brain regions. Abbreviations: cb, cerebellum; stri, striatum. Mean values ± SEM, n = 3 per group, plus 3 replicates per n number.
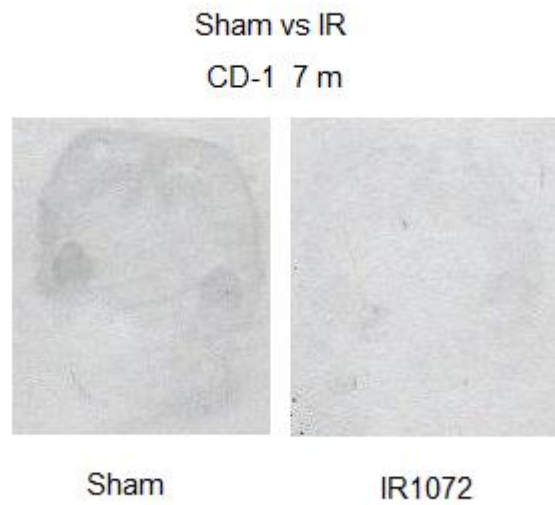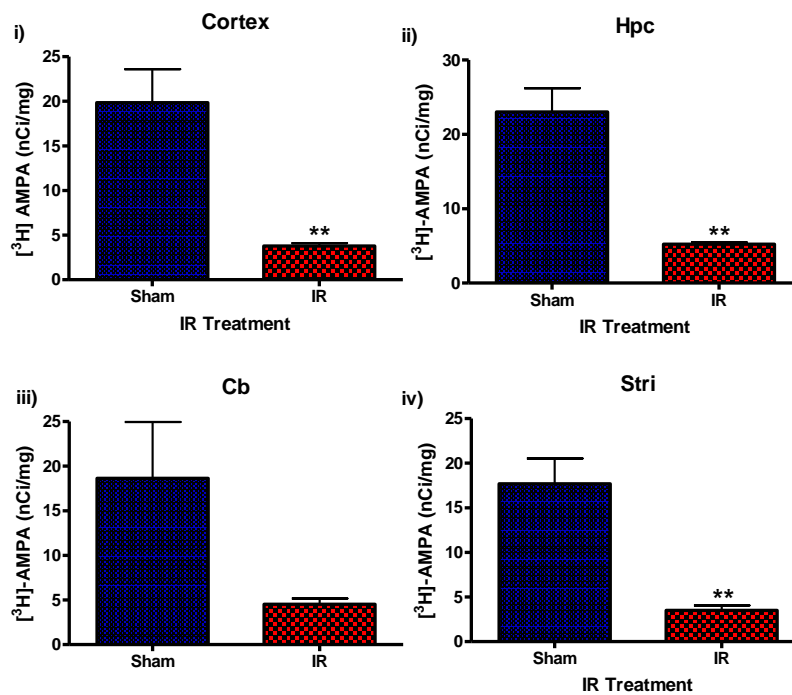
Figure 5-25: A) [³H]-AMPA autoradiographical image and B) the respective quantification of AMPA receptor expression in various brain regions in chronically IR1072-treated 7 month old CD-1 mice and age-matched sham controls. Abbreviations: IR, IR1072; Hpc, Hippocampus; cb, cerebellum; stri, striatum. Mean values ± SEM, n = 4 per group, plus 3 replicates per n number.

A

Sham vs IR
CD-1 13m

Sham   IR1072

B

Figure 5-26: A) [^{3}H]-AMPA autoradiographical image and B) the respective quantification of AMPA receptor expression in various brain regions in chronically IR1072-treated 13 month old CD-1 mice and age-matched sham controls. Abbreviations: IR, IR1072; Hpc, Hippocampus; cb, cerebellum; stri, striatum. Mean values ± SEM, n = 2 for sham, and n=3 for IR1072 group, plus 3 replicates per n number.

5.3 Discussion

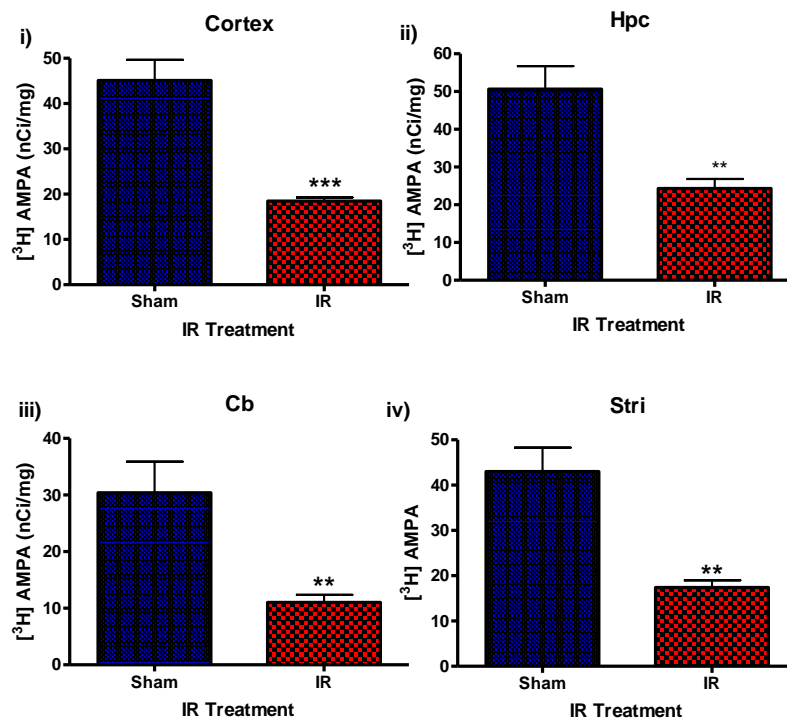The aim of this chapter was to establish the protein changes of ERK1/2 signalling, HSP or AMPA receptor expression that occur during ageing in CD-1 mice, and also to establish any long-term protein changes following chronic IR1072 treatment in 7 month old or 13 month old male CD-1 mice.

Table 5-7: Summary of the effects of ageing and IR1072 treatment on CD-1 mice. Abbreviations: CD-1TL, CD-1 age timeline; CD-1Y, sham vs IR1072 CD-1 7month old mice; CD-1O, sham vs IR1072 CD-1 13 month old mice; IR, IR 1072nm; BDNF; Brain Derived Neurotrophic Factor; ERK1/2 or ERK1/2-P, unphosphorylated or phosphorylated extracellular-signal regulated kinase 1 or 2, respectively; CREB, Cyclic Adenosine Monophosphate (AMP) Response Element Binding; HSP, Heat Shock Protein; PI3, Phosphatidylinositol 3-Kinase.

Pathways	Protein	CD-1TL (months)			Effects of Chronic IR on protein expression	
		3 vs 10	3vs12	10vs12	CD-1Y	CD-1O
ERK1/2	BDNF	↓	*↓	*↓	**↑	-
	ERK1/2	-	-	-	***↓	**↓
	ERK1/2-P				↓	↓
	CREB	↑	-	-	-	**↑
PI3	AKT	-	-	-	*↓	*↑
	AKT-P	-	-	-	-	-
Chaperones	HSP27		↓	*↓	↑	*↑
	HSP40	-	-	-	-	*↑
	HSP60	-	-	-	-	**↑
	HSP70	-	-	-	*↓	-
	HSP90	-	↓	-	-	-
	HSP105	-	-	-		

As discussed earlier, amyloidosis has been shown to be present in ageing CD-1 mice, however this study investigated circulating serum amyloid using an SAA assay (purchased from Life Diagnostics Inc.) but found no significant differences in serum amyloid in ageing CD-1 mice or chronically IR1072-treated CD-1 mice (data not shown). This could be due to the fact that studies

reporting these amyloid changes purchased the CD-1 mice from Charles Rivers, whereas the mice used in this study are the current in-house strain (housed for over two years), and also, more significantly, our CD-1 timeline was only up to 12 months of age. However premature death occurs at approximately 18 months of age in these CD-1 mice, and acute IR1072 induced effects were shown in 4 month old CD-1 mice, therefore chronic IR1072 investigations were warranted.

Many reports showing LILT eliciting a protective effect require an insult of some sort on a given *in vitro* or *in vivo* model, in order to generate sub-lethal effects, so any positive measures of LILT, as a preconditioning (preceding the insult) or neuroprotective (during the insult) therapy, to protect the model system can be determined. Most insults utilising *in vitro* or *in vivo* models are designed to induce stress on an experimental system to produce a sub-lethal decrease in tissue or cell viability and toxic signalling events. LILT has been shown to protect tissue or cells from sub-lethal insults, some of which include *in vivo* and *in vitro* models of ischemic damage (Ad and Oron, 2001; Whelan et al., 2001; Kolpakova et al., 2003), nutrition deprivation (Carnevalli et al., 2003; Ricci et al., 2009), diabetes (Lim et al., 2009), Parkinson's disease (Ying et al., 2008) and proactive physical load (swimming; Zubkova et al., 1995). In this present study, IR1072 was used during development where age was viewed as the "insult", and proteins involved in neuroprotection, and suggested to be decreased with age, were investigated.

BDNF plays an important role in neuroplasticity and promotes axonal growth, but its secretion declines with age (Kennedy et al., 2009). An age-dependant

reduction in BDNF occurred in CD-1 mouse brain whereby protein expression decreased as mice grew older. Gooney et al. (2004) infused young (2-4 months) and aged (20-24 months) Wistar rats with exogenous BDNF in order to induce LTP, which increases activation of TRKB and ERK signalling which in turn enhances evoked release of glutamate in synaptosomes. They found that in aged rats both BDNF induced LTP and the associated ERK signalling is reduced, suggesting the neuroprotective role of BDNF may be weakened with increasing age (Gooney et al., 2004; Sohrabji and Lewis, 2006). CD-1 mice, treated with IR1072 from 3 months to 7 months of age or 7 months to 13 months of age, show an increase or no change in BDNF expression, respectively. The increase in BDNF expression in the younger mice might lead to the assumption that ERK1/2 expression would increase, and similarly the unaltered BDNF expression shown in the older mice might lead to unaltered ERK1/2 expression, however an unexpected decrease in phosporylated and unphosphorylated ERK1/2 expression was found in both younger and older mice. Gooney also determined from the same set of experiments that aged rats appeared to have higher BDNF expression than younger rats, however the ERK1/2 signalling pathway was impaired despite the increase in BDNF, and concluded that TRKB and ERK is impaired with age, and this impairment must derive from age-related changes in TRKB receptor function (Gooney et al., 2004). Although BDNF expression is in disagreement with the ageing findings in this study, the increased BDNF expression and decreased ERK1/2 signalling seems to show a similar pattern in the IR1072 treated mice. These results suggest that IR1072 may be affecting the function of the TRKB receptor. There is a "dark side" as it were,

to ERK1/2 signalling, as well as a neuroprotective aspect. Sustained levels of ERK1/2 have been reported to promote cell death or promote cell survival in neurons depending upon the nature of the acute insult and the affected cell types (Chu et al., 2004). Some studies have shown that blocking ERK1/2 activation *in vivo*, led to decreased brain injury in mice and gerbils (Wang et al., 2004). These changes in ERK1/2 expression despite BDNF expression should be further investigated with phosphorylated TRKB receptor expression to conclude if IR1072 may be effecting the receptor numbers either directly or indirectly. Gooney (2004) also found that although the biochemical responses to BDNF infusion are impaired with age, the phosphorylation of CREB was not, indicating intact retrograde signalling, which may explain the trend for increased expression of CREB in 10 month old mice compared to 3 month old. However the present study looked at total CREB as the signal for CREB-P was never established, despite numerous attempts using various sample preparations and antibody concentrations/incubations to try to achieve a signal. Further investigations into the IR1072 ERK-independent increase in CREB expression are warranted.

An age-dependant decrease in HSP27 has been shown in 12month old CD-1 mice compared to 3 month old and 10 month old CD-1 mice. This correlates with previous data which has shown age-related changes in the heart and peripheral blood mono nuclear cell HSP27, where Colotti et al. (2005) demonstrated that age-related decreases occur in mRNA and protein expression of HSP27 HSP60, HSP72 in right atrium and left ventricle of the rat heart, and Njemini found basal levels of HSP27 expression decreased

during ageing (Colotti et al., 2005; Njemini et al., 2006). Decreased HSP27 expression as ageing increases may result in increased protein misfolding, inactivation of AKT signalling and hence cell survival pathways, and pro-apoptotic pathways activation with lessened inhibition from HSP27, resulting in an overall increase in apoptosis. This decrease in HSP27 at 10 and 12 months, and also a trend for decreased expression of HSP90 at 12 months, compared to 3 months of age, may contribute towards the learning deficits previously reported in CD-1 mice (Ennaceur et al., 2008).

A consistent and robust increase of HSP27 was shown in 7 month and 13 month old CD-1 mice irradiated with IR1072. HSPs have been shown to be upregulated in mouse models of stress following LILT. Novoselova et al. (2007) irradiated the thymus zone projection of male NMRI mice of stress, modelled by lipopolysaccharide injection. Stress alone induced a significant increase in several macrophage cytokines, IL-1alpha, IL-1beta, IL-6, IL-10 and TNF-alpha, where a single exposure of laser LILT (632.8nm) enhanced HSP25, HSP70, and HSP90 compared to sham controls and normalized the stress-induced cytokine production and suggested HSP normalised this stress response. This increase in HSP25 and 90 could have increased AKT signalling to promote cell survival, where HSP70 could be inhibiting the JNK signalling pathway in order to reduce pro-apoptotic proteins to be activated. Havasi et al. (2008) manipulated HSP27 expression in renal epithelial cells before transient metabolic stress, where it was demonstrated that enhanced HSP27 expression inhibited BAX activation, oligomerization, and translocation into mitochondria, reduced the leakage of both cytochrome c and AIF, and

significantly improved cell survival by more than 50% after stress, where decreased HSP27 expression activated BAX expression, induced mitochondrial injury and decreased cell survival. Interaction of BAX and HSP27 was not established before, during or after the insult, indicating that HSP27 acts on inhibiting BAX through an indirect pathway (Havasi et al., 2008). They concluded that HSP27 antagonizes BAX-mediated mitochondrial injury and apoptosis by promoting AKT activation via a PI3-kinase pathway (Havasi et al., 2008). This could explain the significant increase in HSP27 and AKT shown in 13 month old CD-1 mice treated with IR1072, however a decrease in AKT expression was shown in 7 month old CD-1 mice irradiated with IR1072 although there was a trend for increased HSP27 expression. This suggests there may be an age-dependent effect of IR1072 on AKT expression in CD-1 mice.

IR1072 appeared to induce HSP40 expression in 13 month old CD-1 mouse brains. Surprisingly, HSP70 was not induced which might be expected as HSP40 was induced and these proteins act in partnership, phosphorylating pro-apoptotic proteins and anti-apoptotic proteins to deactivate or activate, respectively, therefore preventing apoptosis. It has been proposed that HSP40 function as dimers and may bind and prime the non-native polypeptide into an extended conformation in preparation for the subsequent recognition and transference to HSP70 (Li et al., 2009). Perhaps an increase in HSP40 expression indicates an increase in the amount of mis-folded proteins bound in preparation for normal protein refolding or UPC disposal. Another possibility is HSP40 could be inhibiting the JNK MAPK "stress" pathway indirectly

preventing activation of pro-proapoptotic proteins, and/or by preventing pro-apoptotic protein translocation to the mitochondrial membrane directly whereby, in both instances, mitochondrial membrane permeabilisation and subsequent cytochrome c release is prevented, thus inhibiting apoptosis.

HSP60 activation was established in 13 month old CD-1 mice, where this HSP is thought to play an important role in protein mis-folding and transportation of mitochondrial proteins, and also activation of caspase-3, a protein involved in the initiation of apoptosis. HSP60 is not thought of initiating apoptosis itself, but acts as a feed-forward mechanism during the late-stages of apoptosis to ensure optimal caspase activation.

A significant decrease in AMPA receptor numbers were shown in both 7 month old and 13 month old IR1072 irradiated CD-1 mice. This correlates with a previous *in vitro* study investigation using microwaves on neuronal cultures. Wang et al. (2005) studied the effect of non-thermal low-intensity microwaves on AMPA GluR2 and the amount of intracellular calcium in rat cerebral cortical neurons, and showed that GluR2 receptor numbers were down-regulated in irradiated neurons, resulting in a raised calcium concentration (Wang et al., 2005). This effect of low intensity may indicate a photosensitive pathway that has yet to be explored. Several studies have suggested previously that calcium levels are increased following LILT (Alexandratou et al., 2002; Gao and Xing, 2009), however very little is known about LILT effects on AMPA receptor modulation, therefore further work to determine the effect of IR1072 on AMPA receptor down-regulation should becarried out.

Overall, these results indicate that IR1072 may participate in neuroprotective pathways involved in apoptosis, however age may influence the proteins in which IR1072 may directly or indirectly up-regulates or down-regulates.

Chapter 6: Age-dependant molecular changes in TASTPM mice: Effect of chronic IR1072 *(in vivo)* treatment

6.1 Introduction

6.1.1 Alzheimer's Disease

Alzheimer's disease (AD) is the most common cause of dementia in the Western world and the most prevelent neurodegenerative diseases (Gouras et al., 2005; Vardy et al., 2006). AD is characterized by progressive cognitive and behavioral decline, impacting on both sufferers and their carers (Vardy et al., 2006). Over a century ago, Alois Alzheimer described the pathological characteristics of Alzheimer's disease (AD) by the presence of extracellular Aβ plaques and intracellular neurofibrillary tangles in the brain (Richardson et al., 2003; Vardy et al., 2006; Howlett et al., 2008). Aβ is cleaved from the amyloid precursor protein (APP) by the 'amyloidogenic pathway', involving the enzymes β-secretase and γ-secretase (Vardy et al., 2006).

6.1.2 APP processing

APP receives two cleavages, one in the extracellular domain (β-secretase cleavage) and the other in the β transmembrane region (γ-secretase cleavage), are necessary to release varying isoforms of Aβ from the APP molecule (Figure 6-1) (Chiang et al., 2008; Thinakaran and Koo, 2008). APP processing by α-secretase (non-amyloidogenic pathway) results in the production of a single soluble secreted fragment (P3) and one non-amyloidogenic carboxy-terminal segment (Suzuki and Nakaya, 2008). The

processing of APP by β-secretase (amyloidogenic pathway) leads to the accumulation of Aβ fragments that make up amyloid plaques (Suzuki and Nakaya, 2008). The main components of Aβ plaques are $A\beta_{1-40}$ and $A\beta_{1-42}$ (Chiang et al., 2008) where $A\beta_{1-40}$ is the most prevalent species, whilst $A\beta_{1-42}$ is the most toxic (Melquiond et al., 2008).
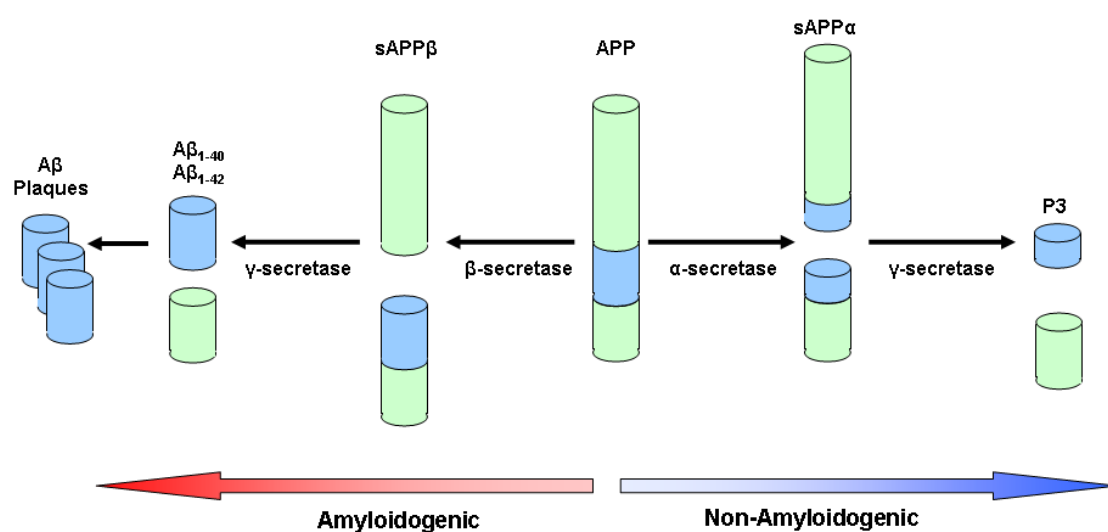

Figure 6-1: APP processing. Abbreviations: Aβ, β-amyloid; APP, Amyloid Precursor Protein.

6.1.3 Alzheimer's Disease animal model: TASTPM mice

Animal models of AD are a useful tool for exploring the pathological outcomes of the disease as well as preventative measures for disease acceleration, and therefore protection from irreversible neuronal loss, proposed to be caused by $A\beta_{42}$ plaques and neurofibrillary tangles. Transgenic (Tg) mice that overexpress high levels of human APP containing familial AD mutations (PDAPP, Tg2576 and APP23) have been previously shown to develop astrocytosis and microgliosis, and to produce high levels of total Aβ in the cortex and hippocampus from the age of 6 months, but little evidence of the development of neurofibrillary tangles (NFT) or neuronal loss (Games et al.,

1995; Hsiao et al., 1996; Sturchler-Pierrat et al., 1997; Moechars et al., 1999; Richardson et al., 2003).

The TASTPM mouse line has been shown to have increased Aβ levels at 3 months of age, Aβ plaques from 4 months of age and cognitive deficits from 6 months of age (Howlett et al., 2004; Howlett, 2006; Choudhry et al., 2008). The major criticisms of animal models of AD is the lack of NFT and neuronal loss, and, like other animal models of AD, TASTPM mice do not display signs of NFT but does, however, show significant neuronal loss with age (Howlett, 2006; Choudhry et al., 2008; Howlett et al., 2008). Howlett et al. (2006) immunolabelled and quantified neurons in TASTPM mouse brain of varying ages, and found a significant inverse correlation between Aβ load and neuronal counts and also between neuronal counts and animal age, where neuronal loss increased with age and Aβ deposition. Neuronal number in age-matched wild type (WT) controls did not change with age. In addition to this, immunohistochemical analysis revealed an incidence of astrocytes, phosphorylated tau, and cathepsin D, a protease enzyme implicated in the processing of APP and phosphorylation of tau (Benes et al., 2008), increased in parallel with the age of TASTPM mice and Aβ deposition (Howlett et al., 2008). Howlett et al. (2008) also showed that Aβ plaques in TASTPM mice consist of multiple forms of the peptide, including full length and N-terminally truncated, resembling those found in the human AD brain. Despite the lack of NFT formation, TASTPM mice would appear to model Alzheimer's disease reasonably well, as Aβ deposition, astrocytosis, phosphorylated tau and neuronal cell loss increase with age in this mouse model and therefore

provides a means of studying Aβ-associated neurodegeneration (Howlett, 2006). We have used this animal model of AD for our chronic studies using IR1072 irradiation as the pathological signs of AD in this mouse model have been validated and confirmed, and are apparent at a younger age than other mouse models, lending itself to a cost-effective chronic treatment protocol.

The aim of this chapter was to establish any protein changes in ERK1/2, AKT, or HSP signalling during ageing and/or following chronic IR1072 treatment in 7 month old TASTPM male and female mice. This study also investigated both $Aβ_{1-40}$ and $Aβ_{1-42}$ plaques together or $Aβ_{1-42}$ plaques alone.

6.2 Results

6.2.1 TASTPM Age Timeline: Immunoblot analysis

As this investigation is examining the effects of IR1072 on an animal model of AD, age and subsequent Aβ factors have a potential influence on protein expression, so naturally studying the effects of age on ERK1/2 and HSP protein expression is of interest in this study. Immunohistochemical analysis showed increase $A\beta_{40/42}$ and $A\beta_{42}$ deposits increased as the mice aged (Figure 6-9 and 6-10).

Protein levels were standardised using mouse β-actin primary antibody. Data were statistically analysed using a two tailed student t-test. Data represent mean ± SEM.

Table 6-1: Protein expression profile in 3, 7, or 12 month old TASTPM mice. Arrows represent an increase (↑) or decrease (↓) in protein expression. Data were statistically analysed using a two tailed student t-test. Pink cells represent significant results (p<0.05) and blue cells represent a trend (p<0.1). n=3 for each group, *p<0.05, **p<0.01. Abbreviations: ADTL, TASTPM age timeline; BDNF; Brain Derived Neurotrophic Factor; ERK1/2 or ERK1/2-P, unphosphorylated or phosphorylated extracellular-signal regulated kinase 1 or 2, respectively; CREB, Cyclic Adenosine Monophosphate (AMP) Response Element Binding; HSP, Heat Shock Protein; PI3, Phosphatidylinositol 3-Kinase.

| | AD TL (months) | | | | | |
| | 3mv7m | | 3mv12m | | 7mv12m | |
	p value	result	p value	result	p value	result
BDNF	0.0897	NS	*0.0341	12m↓	0.4509	NS
ERK1	0.698	NS	*0.0129	12m↓	*0.0441	12m↓
ERK2	0.1158	NS	*0.0117	12m↓	0.3416	NS
ERK1-P	0.0943	NS	0.2337	NS	0.3535	NS
ERK2-P	0.8478	NS	0.2983	NS	0.111	NS
CREB	0.4274	NS	0.3797	NS	0.8401	NS
CREB-P						
AKT	**0.0019	7m↑	*0.0212	12m↑	*0.0488	12m↓
AKT-P	0.6021	NS	0.2396	NS	0.1245	NS
HSP27						
HSP40	0.0793	NS	**0.0095	12m↓	*0.0338	12m↓
HSP60	0.1568	NS	0.5474	NS	0.2765	NS
HSP70	0.5401	NS	0.5654	NS	0.3277	NS
HSP90	0.199	NS	0.0715	NS	0.128	NS
HSP105	0.0949	NS	*0.0121	12m↓	0.2839	NS

TASTPM mice at 12 months of age (n=3, 0.435 ± 0.0486, p<0.05) showed significantly decreased BDNF expression compared to mice at 3 months of age (n=3, 0.6152 ± 0.030,) but no differences in BDNF expression when compared to mice at 7 months of age (n=3, 0.4916 ± 0.04691). TASTPM mice at 7 months of age showed a trend for decreased BDNF expression compared to 3 month old mice (Figure 6-2).
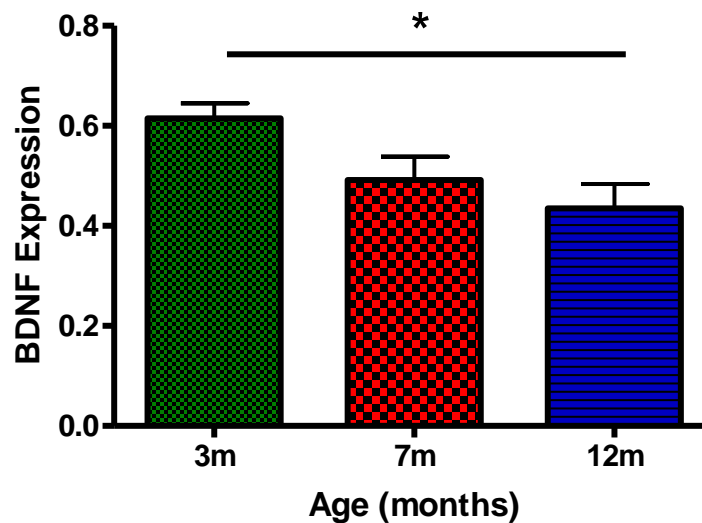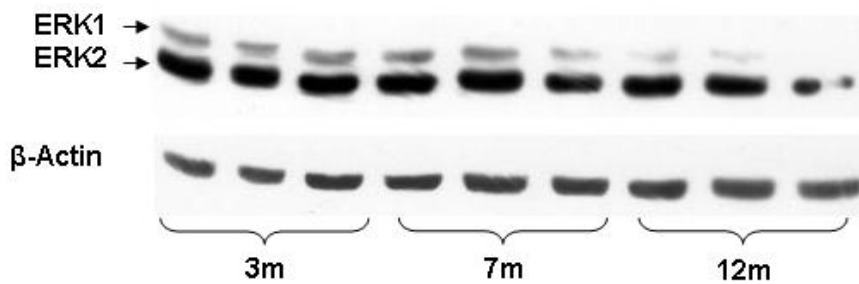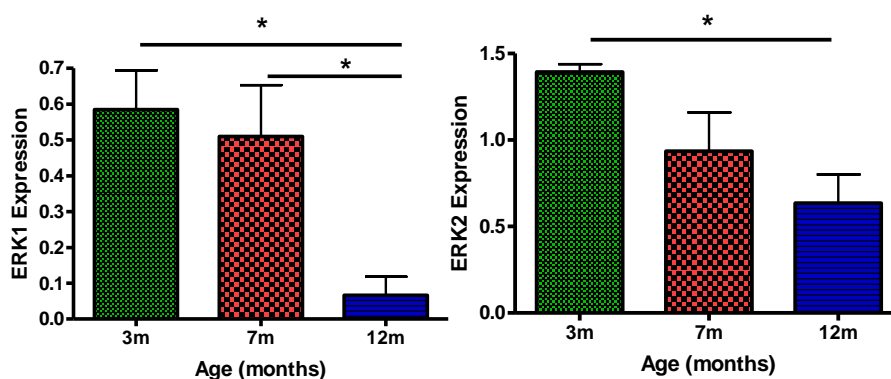
A
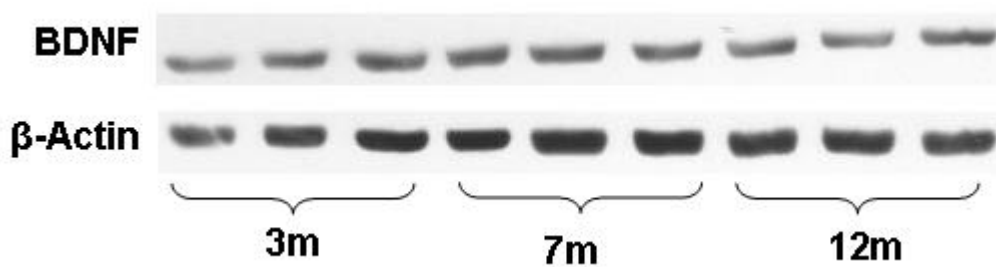
B

Figure 6-2: Age-dependant changes in BDNF expression in 3, 7, or 12 month old male TASTPM mice where A) is an Immunoblot representation where each lane represents an individual mouse and B) is a column graph showing the quantitative results of BDNF expression from the immunoblot. Protein expression were standardised to total β-actin levels. Abbreviations: BDNF, Brain Derived Neurotrophic Factor. Mean values ± SEM, n = 3 for each group, *p<0.05.

TASTPM mice at 12 months (n=3, 0.066 ± 0.0523) showed significantly decreased levels of ERK1 expression compared to mice aged 3 months (n=3, 0.585 ± 0.110, p<0.05) and 7 months (n=3, 0.510 ± 0.144, p<0.05). TASTPM mice at 3 months showed no differences in ERK1 expression compared to 7 months of age. TASTPM mice at 12 months (n=3, 0.635 ± 0.166) showed significantly decreased levels of ERK2 expression compared to mice aged 3 months (n=3, 1.393 ± 0.047, p<0.05) and 7 months (n=3, 0.935 ± 0.224, p<0.05). TASTPM mice at 3 months showed no differences in ERK1 expression compared to 7months of age (Figure 6-3).
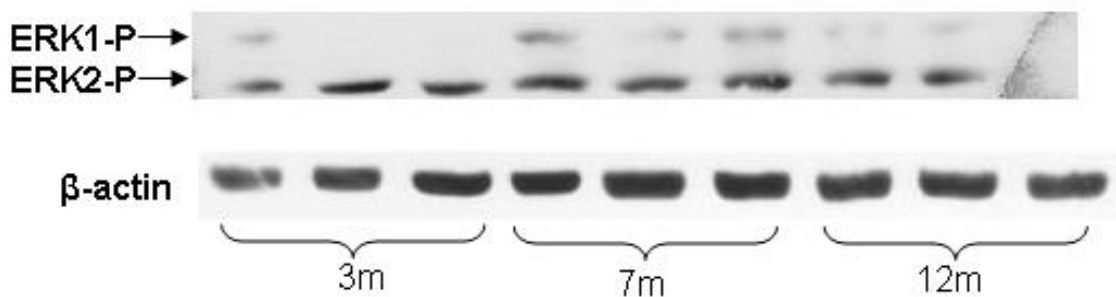
A

B

Figure 6-3: Age-dependant changes in ERK1/2 expression in 3, 7, or 12 month old male TASTPM mice where A) is an Immunoblot representation where each lane represents an individual mouse and B) is a column graph showing the quantitative results of ERK1/2 expression from the immunoblot. Abbreviations: ERK1/2, Extracellular Signal-regulated Kinase 1 or 2. Mean values ± SEM, n = 3 for each group, *p<0.05.

TASTPM mice at 7 months (n=3, 0.153 ± 0.0572) showed a trend for increased ERK1-P expression compared to 3 months (n=3, 0.020 ± 0.020, $p<0.1$) of age. TASTPM mice at 12 months (0.081 ± 0.038) showed no differences in ERK1-P expression compared to TASTPM mice at 3 or 7 months of age. No differences in ERK2-P expression was shown between TASTPM mice aged 3 months (n=3, 0.553 ± 0.131), 7 months (n=3, 0.582 ± 0.064) and 12 months (n=3, 0.367 ± 0.084) (Figure 6-4).
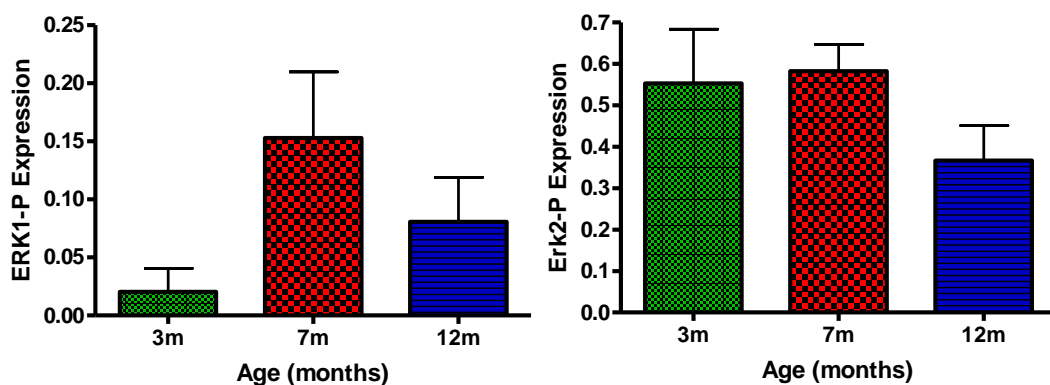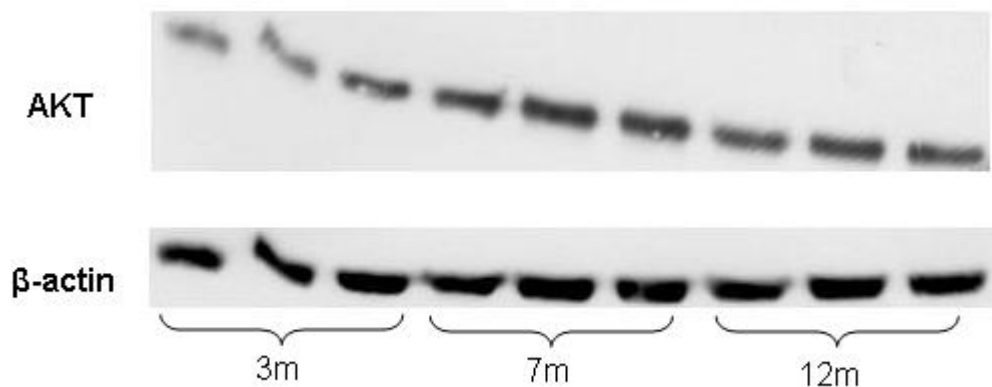
A

B

Figure 6-4: Age-dependant changes in phosphorylated ERK1/2 expression in 3, 7, or 12 month old male TASTPM mice where A) is an Immunoblot representation where each lane represents an individual mouse and B) is a column graph showing the quantitative results of ERK1/2 expression from the immunoblot. Protein expression were standardised to total β-actin levels. Abbreviations: ERK1/2, Extracellular Signal-regulated Kinase 1 or 2. Mean values ± SEM, n = 3 for each group.

TASTPM mice at 12 months (n=3, 0.5294 ± 0.021) showed significantly higher expression when compared to 3months (n=3, 0.410 ± 0.024, p<0.05) but significantly lower AKT expression compared to 7 months (n=3, 0.593 ± 0.007, p<0.05) of age. TASTPM mice at 7 months showed significantly higher AKT expression compared to mice at 3 months of age (p<0.01) (Figure 6-5).
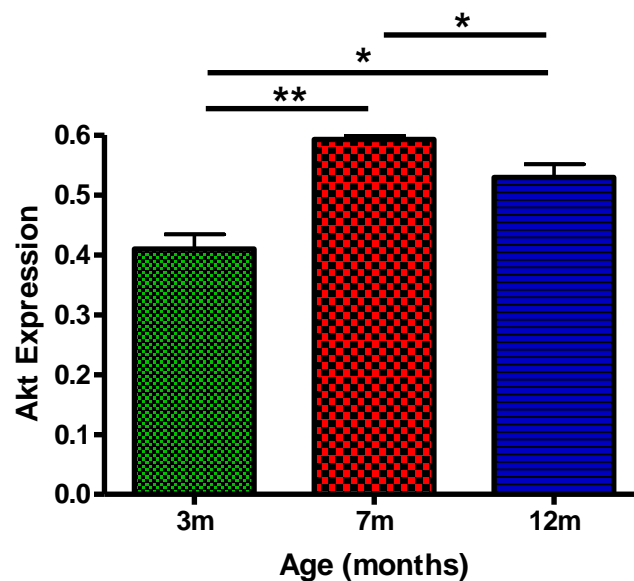
A

B

Figure 6-5: Age-dependant changes in AKT expression in 3,7, or 12 month old male TASTPM mice where A) is an Immunoblot representation where each lane represents an individual mouse and B) is a column graph showing the quantitative results of AKT expression from the immunoblot. Protein expression were standardised to total β-actin levels. Abbreviations: AKT, Protein Kinase B. Mean values ± SEM, n = 3 for each group, *p<0.05, **P<0.01.

TASTPM mice at 12 months old (n=3, 1.024 ± 0.103) displayed significantly lower HSP40 expression compared to 3 months (n=3, 4.014 ± 0.631, p<0.01) and 7 months (n=3, 2.29 ± 0.384, p<0.05) old mice. TASTPM mice at 7 months show a trend for decreased expression compared to 3 months old mice (p<0.1) (Figure 6-6).
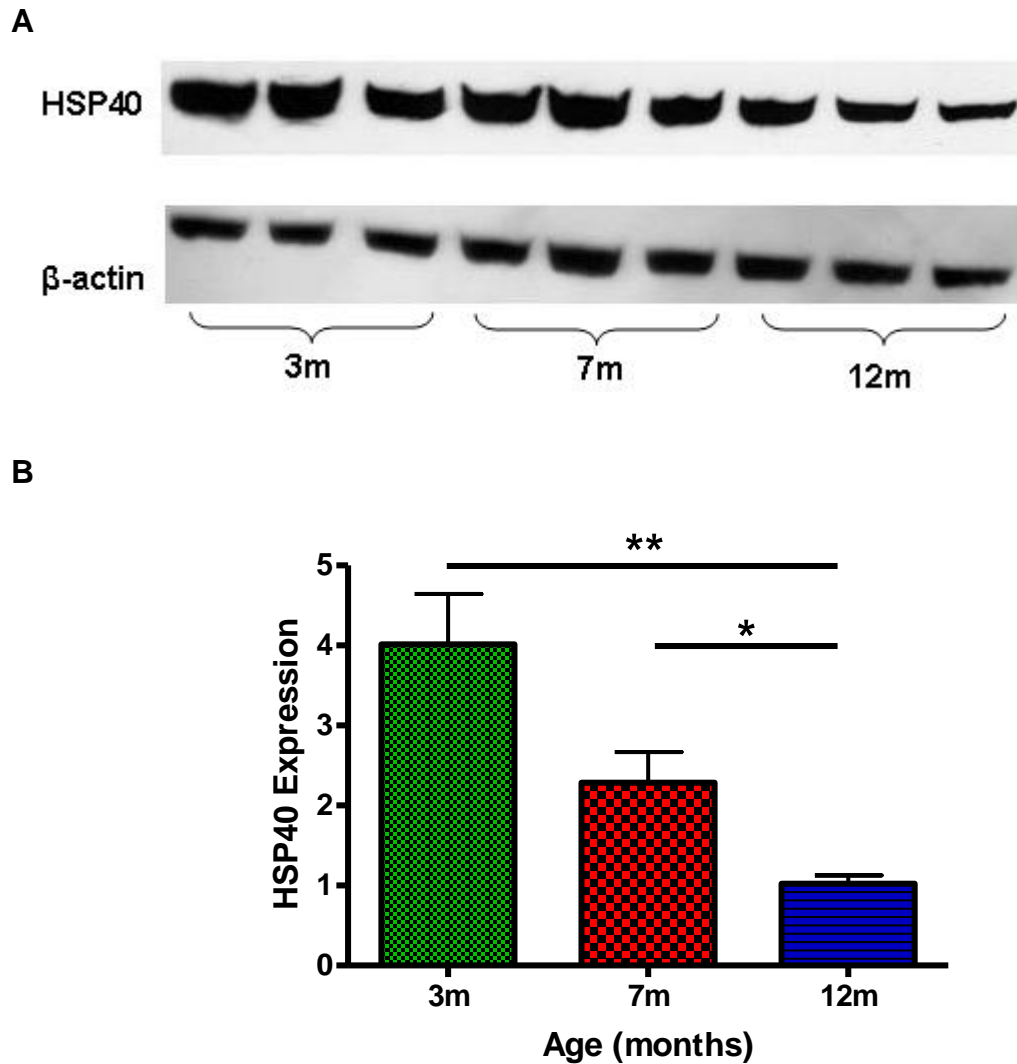
A

B

Figure 6-6: Age-dependant changes in HSP40 expression in 3,7, or 12 month old male TASTPM mice where A) is an Immunoblot representation where each lane represents an individual mouse and B) is a column graph showing the quantitative results of HSP40 expression from the immunoblot. Protein expression were standardised to total β-actin levels. Abbreviations: HSP40, Heat Shock Protein 40. Mean values ± SEM, n = 3 for each group, *p<0.05, **P<0.01.

TASTPM mice at 12 months old (n=3, 0.510 ± 0.0577) showed a trend for decreased HSP90 expression compared to 3 months (n=3, 0.734 ± 0.072, p<0.1), but no differences were seen when compared to 7 month old mice (n=3, 0.622 ± 0.011) old mice. TASTPM mice at 7 months displayed no differences when compared to 3 months old mice (Figure 6-7).
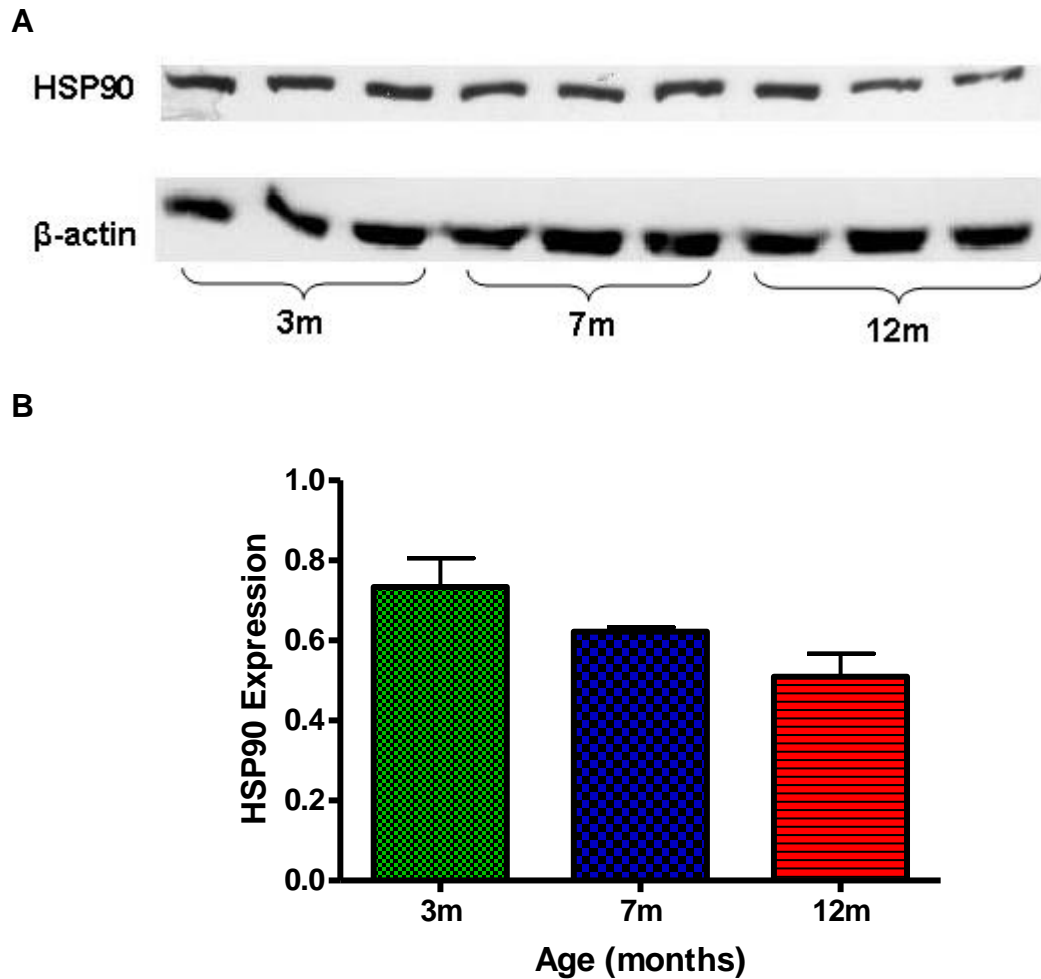
A

B

Figure 6-7: Age-dependant changes in HSP90 expression in 3,7, or 12 month old male TASTPM mice where A) is an Immunoblot representation where each lane represents an individual mouse, therefore one n number and B) is a column graph showing the quantitative results of HSP90 expression from the immunoblot. Protein expression were standardised to total β-actin levels. Abbreviations: HSP90, Heat Shock Protein 90. Mean values ± SEM, n = 3 for each group.

TASTPM mice at 12 months old (n=3, 1.496 ± 0.099) showed a significantly

decreased HSP105 expression compared to mice at 3 months old (n=3, 2.497

± 0.207, p<0.05), but no differences were seen when compared to 7 month

old mice (n=3, 1.812 ± 0.236) old mice. TASTPM mice at 7 months showed a

trend for decreased expression when compared to 3 months old mice (p<0.1)
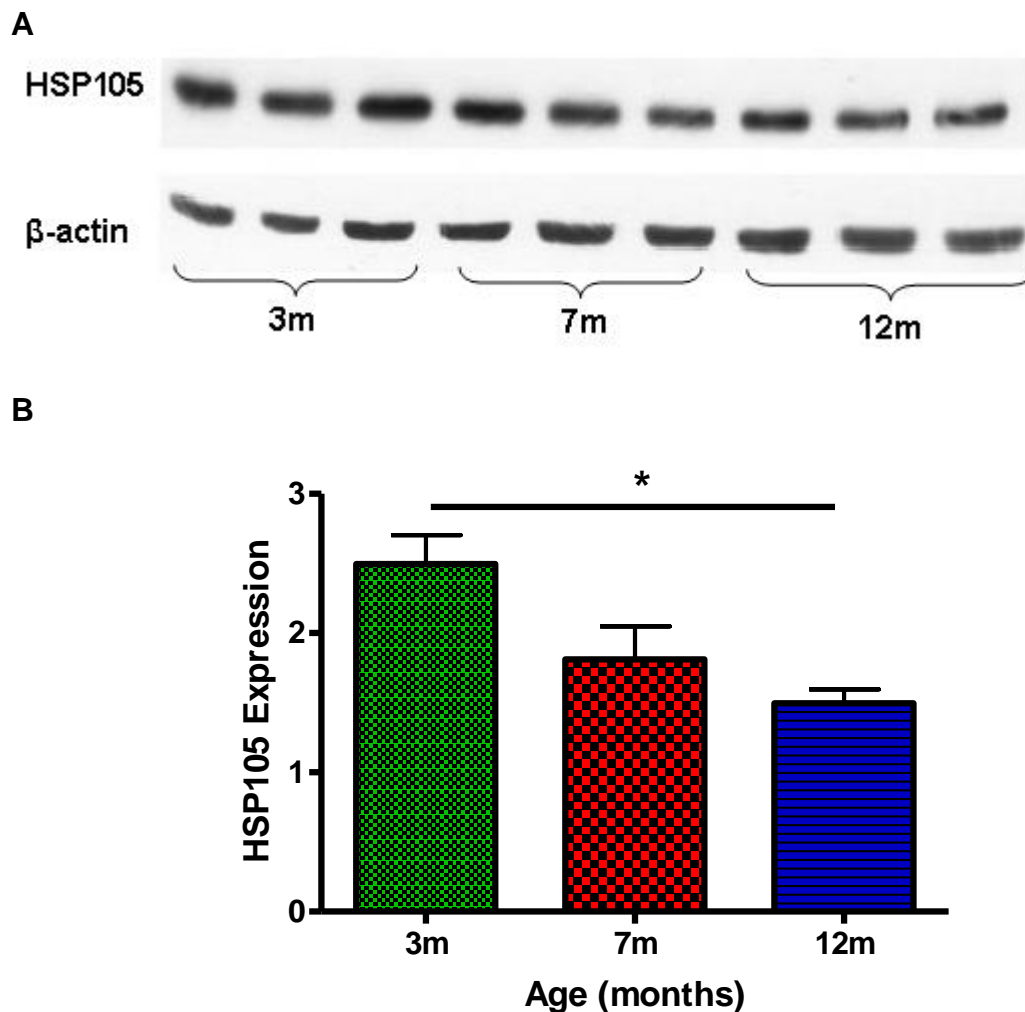
(Figure 6-8).

A

B

Figure 6-8: Age-dependant changes in HSP105 expression in 3,7, or 12 month old male

TASTPM mice where A) is an Immunoblot representation where each lane represents an

individual mouse and B) is a column graph showing the quantitative results of HSP105

expression from the immunoblot. Protein expression were standardised to total β-actin levels.

Abbreviations: HSP105, Heat Shock Protein 105. Mean values ± SEM, n = 3 for each group,

*p<0.05.

6.2.2 TASTPM Age Timeline: Immunohistochemical analysis

Table 6-2: Summary table depicting immunohistochemical analysis of various protein expression in 3, 7, or 12 month old TASTPM mice (n=3 for 3m old, 7m old and 12m old groups). Arrows represent an increase (↑) or decrease (↓) in protein expression in older mice and respective figure numbers. Abbreviations; BDNF, Brain Deived Neurotrophic Factor; ERK1/2, Extracellular Signal-regulated Kinase; CREB, Cyclic Adenosine Monophosphate (AMP) Response Element Binding; AKT, Protein Kinase B; HSP, Heat Shock Protein. n=3 for each group.

Cell signalling protein expression in ageing TASTPM mice	
1⁰ Ab	**Result**
BDNF	-
ERK1/2	-
ERK1/2-P	-
CREB	-
AKT	-
AKT-P	-
HSP27	
HSP40	-
HSP60	-
HSP70	-
HSP90	↓
HSP105	-
Aβ$_{40/42}$	↑
Aβ$_{42}$	↑

The TASTPM timeline immunohistochemistry showed a reduction in HSP90 as mice aged (Figure 6-9).
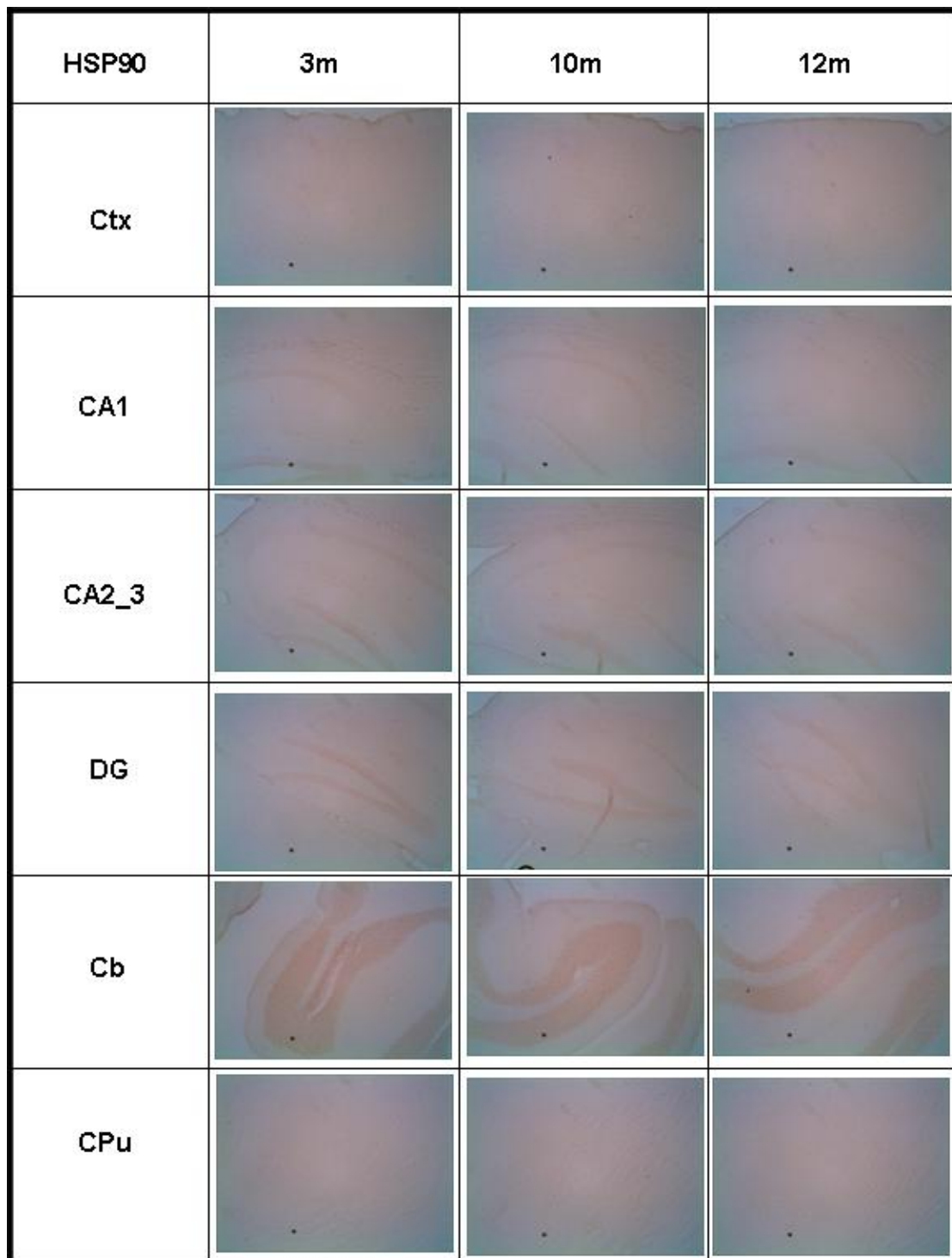

Figure 6-9: Immunohistochemical representation of HSP90 expression in 3, 7, or 12 month old TASTPM mice in various brain regions. Abbreviations: HSP90, Heat Shock Protein 90; Ctx, cerebral cortex; CA (1/2/3), Cornu ammonis; DG, Dentate Gyrus; Cb, Cerebellum; CPu, Caudate Putamen. n=3 for each group, X100 magnification.

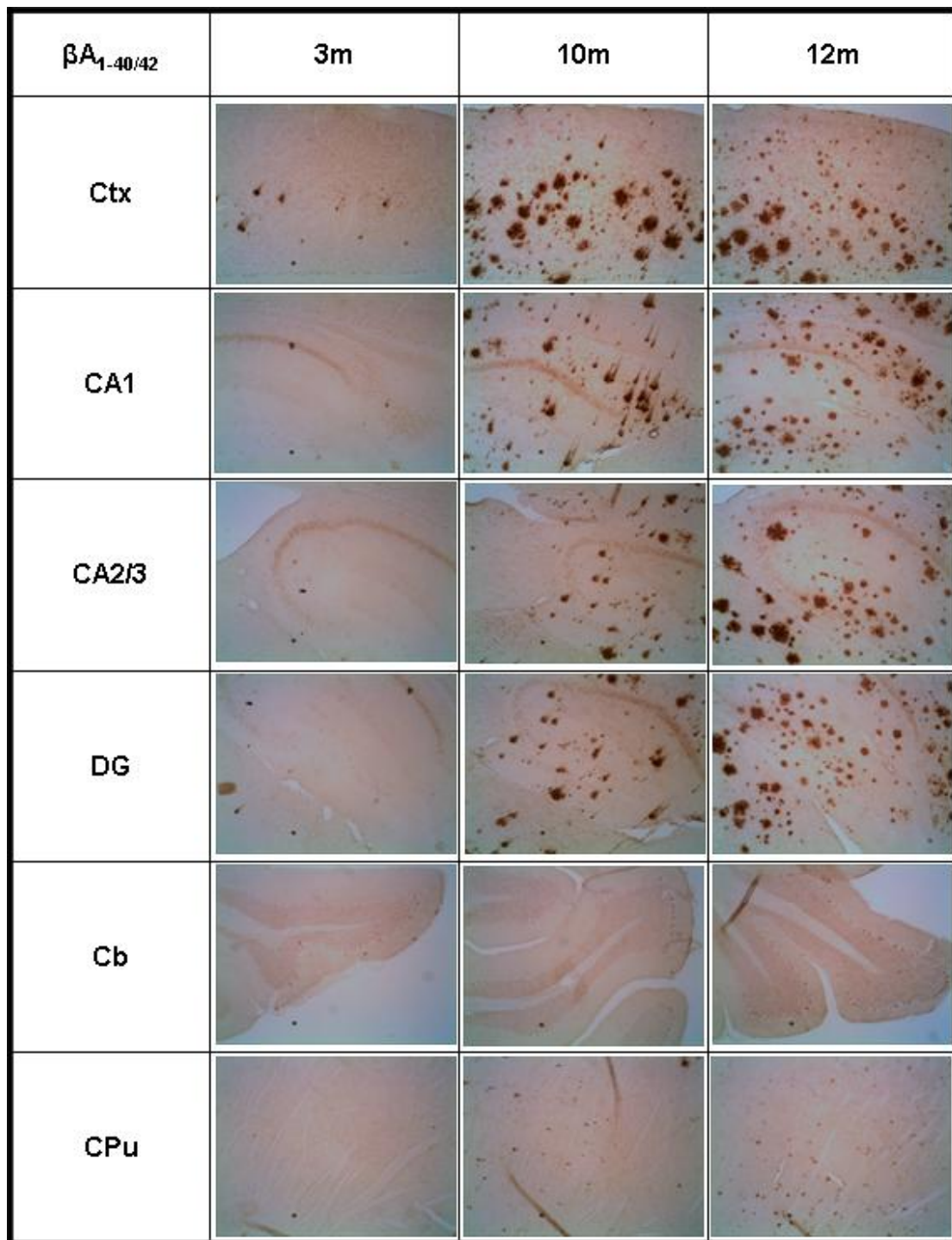The TASTPM timeline showed an increase in $A\beta_{1\text{-}40/42}$ deposits as mice aged (Figure 6-10).

$\beta A_{1\text{-}40/42}$	3m	10m	12m
Ctx			
CA1			
CA2/3			
DG			
Cb			
CPu			

Figure 6-10: Immunohistochemical representation of $A\beta_{1\text{-}40/42}$ expression in 3, 7, or 12 month old TASTPM mice in various brain regions. Abbreviations: $A\beta$, β-amyloid; Ctx, cerebral cortex; CA (1/2/3), Cornu ammonis; DG, Dentate Gyrus; Cb, Cerebellum; CPu, Caudate Putamen. n=3 for each group, X100 magnification.

The TASTPM timeline showed an increase in $A\beta_{1-42}$ deposits as mice aged (Figure 6-11).
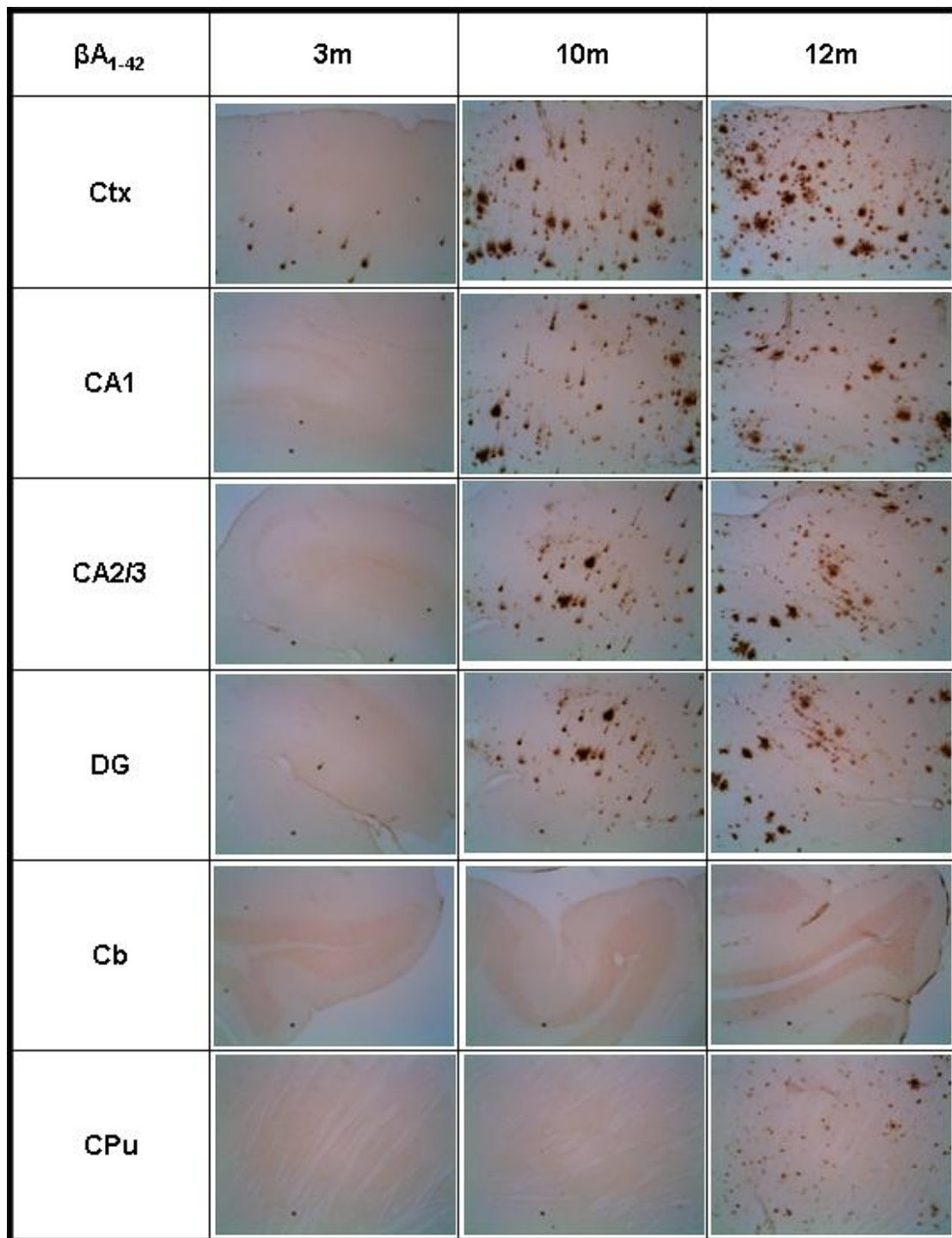

Figure 6-11: Immunohistochemical representation of $A\beta_{1-42}$ expression in 3, 7, or 12 month old TASTPM mice in various brain regions. Abbreviations: $A\beta$, β-amyloid, Ctx, cerebral cortex; CA (1/2/3), Cornu ammonis; DG, Dentate Gyrus; Cb, Cerebellum; CPu, Caudate Putamen. n=3 for each group, X100 magnification.

6.2.3 TASTPM Age Timeline: Serum Amyloid A Assay

A Serum Amyloid A (SAA) assay was performed in ageing TASTPM mice in order to establish any differences in serum amyloid as mice age. SAA assay kit purchased from Life diagnostics Inc., kit protocol was followed.

TASTPM mice at 7 months of aged (400.0 ± 9.200, n=3, $p<0.05$) showed a significant reduction in serum amyloid compared to 3 month old mice(487.6 ± 25.24, n=3) and 12 month old mice (451.3 ± 6.76, n=3, $p<0.05$). There were no significant differences found between 3 months and 12 months old TASTPM mice (Figure 6-11).

IR1072 and sham treated TASTPM mice revealed no significant differences in serum amyloid between groups (data not shown).
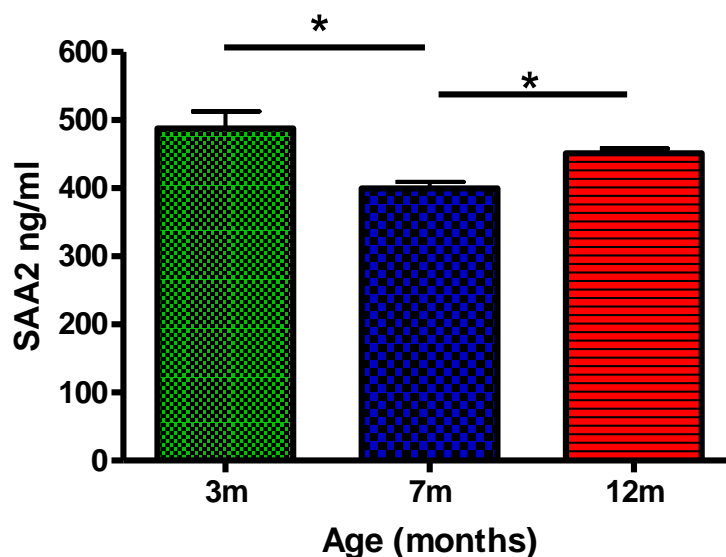

Figure 6-12: Graph showing decreased expression in serum amyloid during ageing in TASTPM mice. Abbreviations: SAA, Serum Amyloid A. Mean values $\pm$ SEM, n = 3 for each group, *$p<0.05$.

6.2.3 Chronic IR1072 Treatment: TASTPM mice

Difficulties maintaining TASTPM mice in the LSSU arose initially, where female mice were having difficulties giving birth to live pups, and life-span for all mice were reduced to 6 or 7 months of age, due to unknown causes. Therefore limited numbers and lifespan of TASTPM mice dictated the following experiments. TASTPM mice, age-matched female and male, were pooled together in order to make the required n number per group for behavioural studies (n=8), where both female and male mice were preconditioned with 6 minute sham or IR1072 treatments, biweekly from 2 months of age to 7 months of age. The following results show molecular changes in ERK1/2 signalling and HSP expression using quantitative immunoblotting and immunohistochemical analysis, where each sex was investigated separately.

6.2.3.1 Chronic IR1072 treatment in male TASTPM mice: Immunoblot analysis

Protein levels were standardised using mouse β-actin primary antibody. Data were statistically analysed using a two tailed student t-test. Data represent mean ± SEM.

Table 6-3: Protein expression profile in 7 month old male TASTPM mouse brain following chronic IR1072 treatment compared to age-matched sham-treated controls. Arrows represent an increase (↑) or decrease (↓) in protein expression in IR-treated TASTPM mice compared to age-matched sham controls, and respective figure numbers. Data were statistically analysed using a two tailed student t-test. Pink cells represent significant results (p<0.05) and blue cells represent a trend (p<0.1). n=4 for each group, **p<0.01. Abbreviations: BDNF; Brain Derived Neurotrophic Factor; ERK1/2 or ERK1/2-P, unphosphorylated or phosphorylated extracellular-signal regulated kinase 1 or 2, respectively; CREB, Cyclic Adenosine Monophosphate (AMP) Response Element Binding; HSP, Heat Shock Protein; PI3, Phosphatidylinositol 3-Kinase.

Effect of Chronic IR1072 treatment on protein expression in male 7 month old TASTPM mice			
1^0	pvalue	Result	Figure
BDNF	**0.0003	↓	Figure 6-12
ERK1	0.4139	NS	Data not shown
ERK2	0.3472	NS	Data not shown
ERK1-P	0.6549	NS	Data not shown
ERK2-P	0.0532	NS	Figure 6-13
CREB	**0.0034	↑	Figure6-14
AKT	0.4682	NS	Data not shown
AKT-P	0.49	NS	Data not shown
HSP27			Incomplete
HSP40	0.2347	NS	Data not shown
HSP60	**0.0051	↓	Figure 6-15
HSP70	0.7877	NS	Data not shown
HSP90	0.0818	NS	Figure 6-16
HSP105	0.6592	NS	Data not shown
$A\beta_{1\text{-}40/42}$-1	0.0038	**↓	Figure 6-17
$A\beta_{1\text{-}40/42}$-2	0.0186	*↓	
$A\beta_{1\text{-}40/42}$-3	0.0077	**↓	

IR1072-preconditioned male TASTPM mice (n=4, 0.328 ± 0.044) showed a significant decrease in BDNF expression compared to age-matched sham controls (n=4, 0.743 ± 0.032, p<0.001) (Figure 6-13).
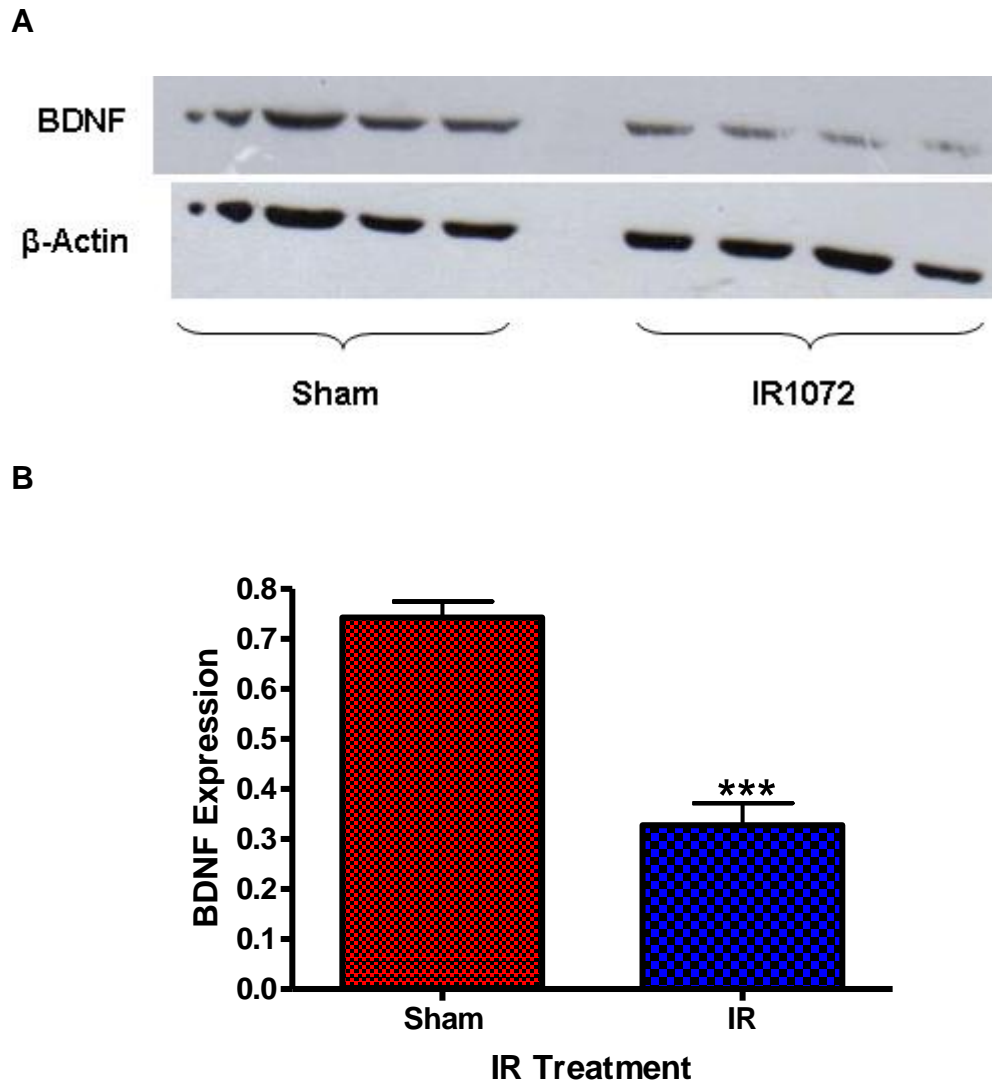
A

B

Figure 6-13: BDNF expression in chronically sham or IR1072 treated 7 month old TASTPM mouse brain (*in vivo*) where A) is an immunoblot representation where each lane represents an individual mouse and B) is a column graph showing the quantitative results of BDNF expression. Protein expression were standardised to total β-actin levels. Abbreviations: BDNF, Brain Derived Neurotrophic Factor. Mean values ± SEM, n = 4 for each group, ***p<0.001.

IR1072-preconditioned male TASTPM mice (n=4, 0.3689 ± 0.1786) showed no differences in ERK1-P expression compared to age-matched sham controls (n=4, 0.483 ± 0.163). However, IR1072-preconditioned male TASTPM mice (n=4, 0.358 ± 0.069) showed displayed a trend for increased ERK2-P expression compared to age-matched sham controls (n=4, 0.613 ± 0.081, p<0.1) (Figure 6-14).

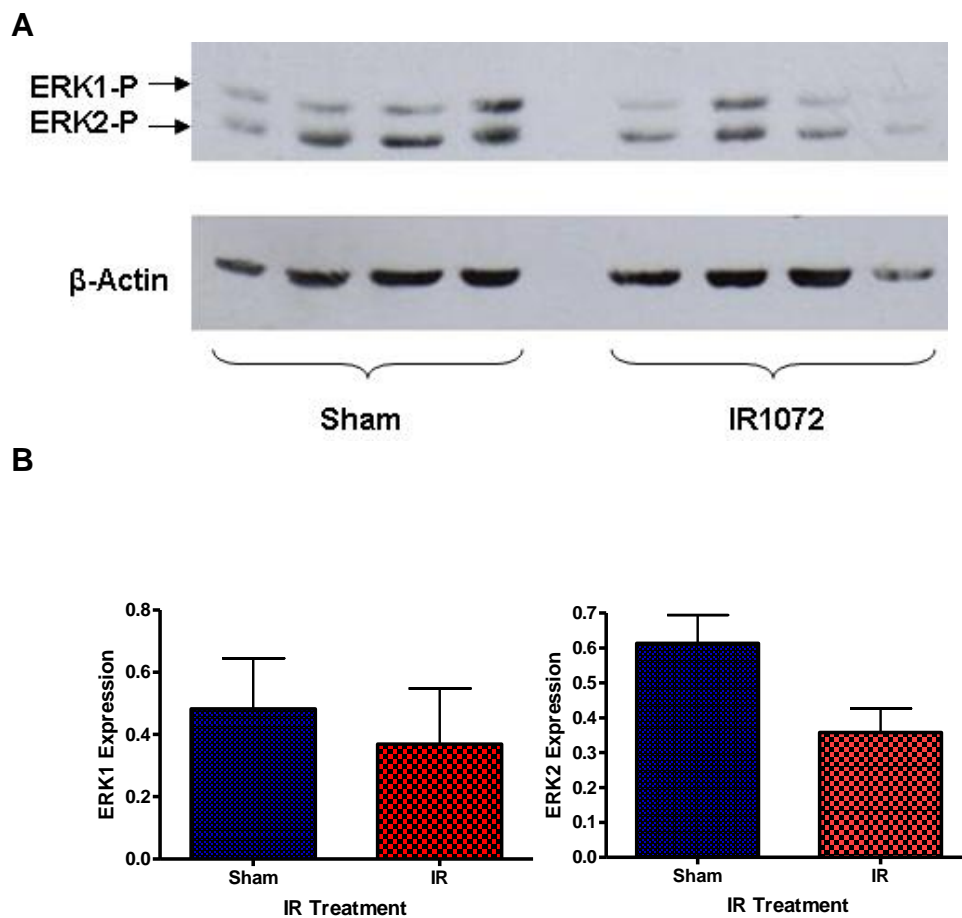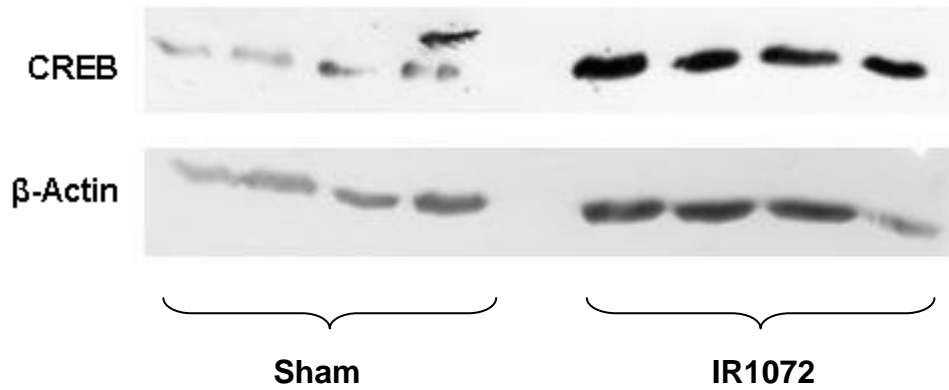**Figure 6-14:** ERK1/2-P expression in chronically sham or IR1072 treated 7 month old TASTPM mouse brain (*in vivo*) where A) is an immunoblot representation where each lane represents an individual mouse and B) is a column graph showing the quantitative results of phosphorylated ERK1/2-P expression. Protein expression were standardised to total β-actin levels. Abbreviations: ERK1/2-P, phosphorylated extracellular signal regulated kinase. Mean values ± SEM, n = 4 for each group.

IR1072-preconditioned male TASTPM mice (n=4, 1.432 ± 0.221) showed a significant increase in CREB expression compared to age-matched sham controls (n=4, 0.367 ± 0.057, p<0.01) (Figure 6-15).
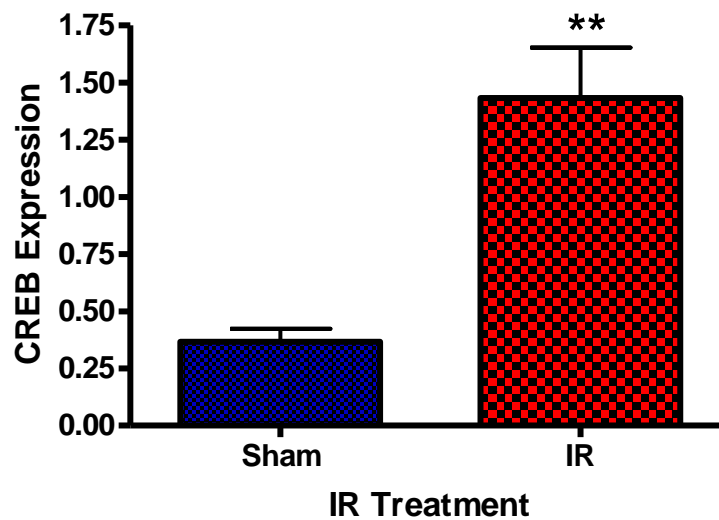
A

B

Figure 6-15: CREB expression in chronically sham or IR1072 treated 7 month old TASTPM mouse brain (*in vivo*) where A) is an immunoblot representation where each lane represents an individual mouse and B) is a column graph showing the quantitative results of phosphorylated CREB expression. Protein expression were standardised to total β-actin levels. Abbreviations: CREB, cAMP (cyclic adenosine monophosphate) response element binding. Mean values ± SEM, n = 4 for each group, **p<0.01.

IR1072-preconditioned male TASTPM mice (n=4, 0.606 ± 0.103) showed a significant decrease in HSP60 expression compared to age-matched sham controls (n=4, 1.590 ± 0.204, p<0.01) (Figure 6-16).
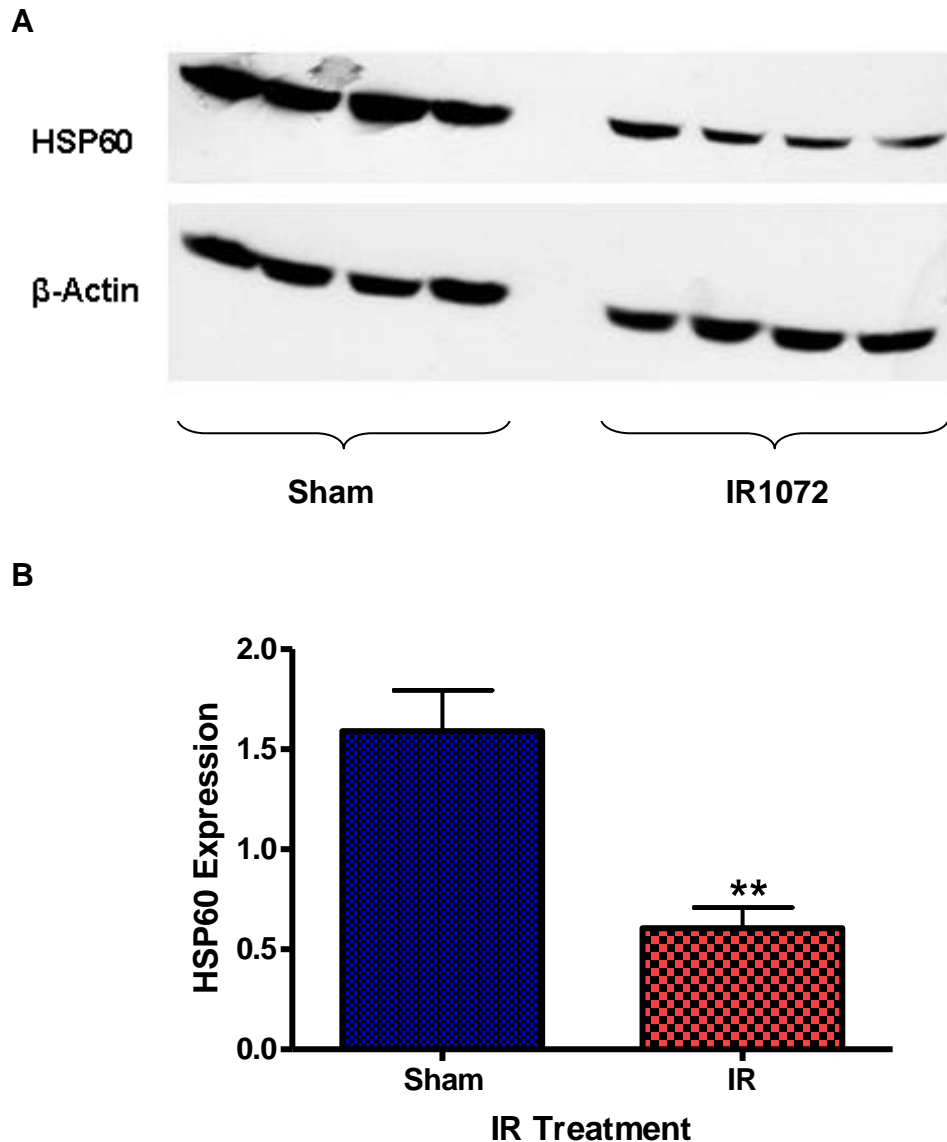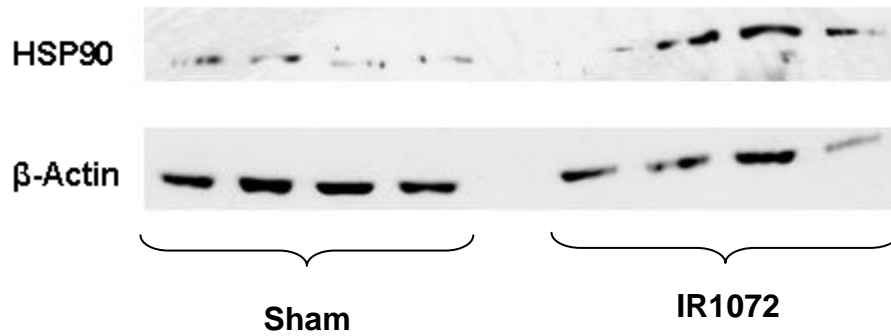
A

B

Figure 6-16: HSP60 expression in chronically sham or IR1072 treated 7 month old TASTPM mouse brain (*in vivo*) where A) is an immunoblot representation where each lane represents an individual mouse and B) is a column graph showing the quantitative results of phosphorylated HSP60 expression. Protein expression were standardised to total β-actin levels. Abbreviations: HSP, Heat Shock Protein 60. Mean values ± SEM, n = 4 for each group, **p<0.01.

IR1072-preconditioned male TASTPM mice (n=4, 0.915 ± 0.030) showed a trend toward increased in HSP90 expression compared to age-matched sham controls (n=4, 0.726 ± 0.085, p<0.1) (Figure 6-17).
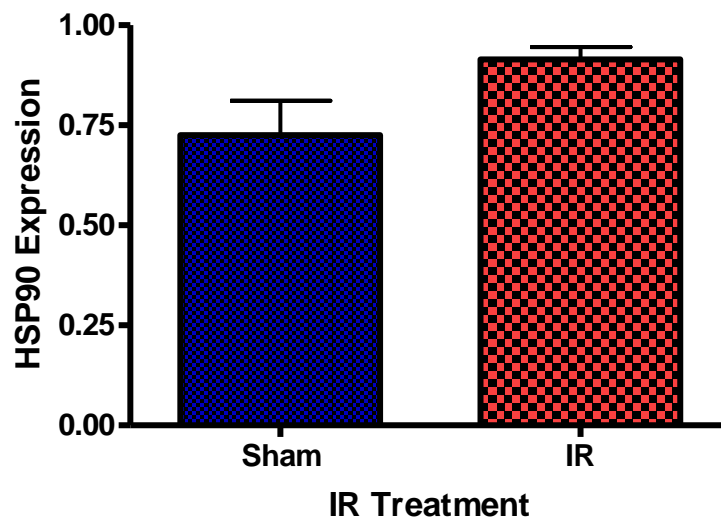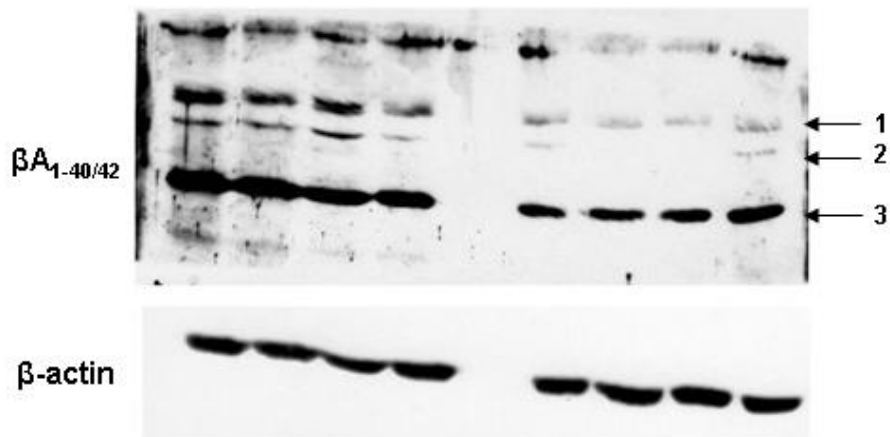
A

B

Figure 6-17: HSP90 expression in chronically sham or IR1072 treated 7 month old TASTPM mouse brain (*in vivo*) where A) is an immunoblot representation where each lane represents an individual mouse and B) is a column graph showing the quantitative results of phosphorylated HSP90 expression. Protein expression were standardised to total β-actin levels. Abbreviations: HSP90, Heat Shock Protein 90. Mean values ± SEM, n = 4 for each group.

IR1072-preconditioned male TASTPM mice (n=4, band 1: 0.128 ± 0.0289; band 2: 0.037 ± 0.0254; band 3: 0.448 ± 0.067) showed significant decreased $A\beta_{1-40/42}$ expression compared to age-matched sham controls (n=4, band 1: 0.743 ± 0.131; band 2: 0.510 ± 0.146; band 3: 1.015 ± 0.128) (Figure 6-18).
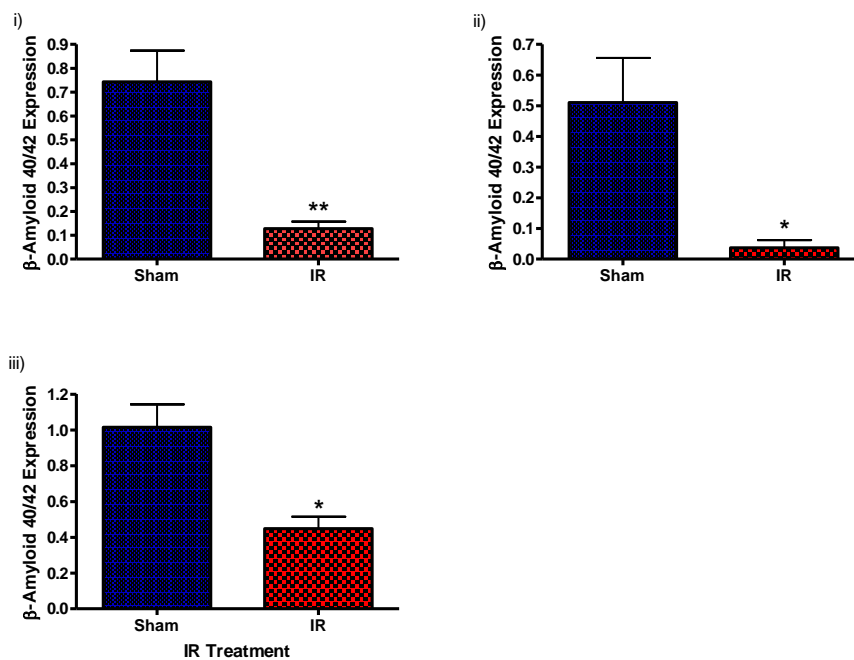
A

B

Figure 6-18: $A\beta_{1-40/42}$ expression in chronically sham or IR1072 treated 7 month old TASTPM mouse brain (*in vivo*) where A) is an immunoblot representation where each lane represents an individual mouse and B) is a column graph showing the quantitative results of i) band 1, ii) band 2 and iii) band 3 of β-amyloid expression. Protein expression were standardised to total β-actin levels. Mean values ± SEM, n = 4 for each group. *p<0.05, **p<0.01.

6.2.3.2 Chronic IR1072 treatment in male TASTPM mice: Immunohistochemical analysis

Table 6-4: Summary table depicting immunohistochemical analysis of various protein expression in IR1072-treated male TASTPM mice and sham-treated controls. Arrows represent an increase (↑) or decrease (↓) in protein expression in older mice. Abbreviations; BDNF, Brain Deived Neurotrophic Factor; ERK1/2, Extracellular Signal-regulated Kinase; CREB, Cyclic Adenosine Monophosphate (AMP) Response Element Binding; AKT, Protein Kinase B; HSP, Heat Shock Protein. n=3 for each group.

Cell signalling protein expression in sham or IR1072-treated male TASTPM mice	
1º Ab	**Result**
BDNF	↓ Ctx, CA1
ERK1/2	-
ERK1/2-P	↓ Ctx, CA1, CA2/3, Cb
CREB	-
AKT	-
AKT-P	-
HSP27	
HSP40	-
HSP60	-
HSP70	-
HSP90	
HSP105	-
A$\beta_{40/42}$	↓ Ctx
Aβ_{42}	-

IR1072-treated male TASTPM mice (n=4) showed a decrease in BDNF expression in the cortex and CA1 region of the hippocampus compared to age-matched sham controls (n=3) (Figure 6-19).

Figure 6-19: Immunohistochemical representation of BDNF expression in IR1072-treated male TASTPM mice compared to age-matched sham controls in various brain regions. Abbreviations: BDNF, Brain Deived Neurotrophic Factor; Ctx, cerebral cortex; CA (1/2/3), Cornu ammonis; DG, Dentate Gyrus; Cb, Cerebellum; CPu, Caudate Putamen. n=3 for sham and n=4 for IR groups, X100 magnification.

IR1072-treated male TASTPM mice (n=4) showed a decrease in ERK1/2 expression in the cortex, the CA1/2/3 regions of the hippocampus and the cerebellum compared to age-matched sham controls (n=3) (Figure 6-20).

ERK1/2	Sham	IR
Ctx		
CA1		
CA2_3		
DG		
Cb		
CPu		

Figure 6-20: Immunohistochemical representation of ERK1/2-P expression in IR1072-treated male TASTPM mice compared to age-matched sham controls in various brain regions. Abbreviations: Extracellular Signal-regulated Kinase 1 or 2; Ctx, cerebral cortex; CA (1/2/3), Cornu ammonis; DG, Dentate Gyrus; Cb, Cerebellum; CPu, Caudate Putamen. n=3 for sham and n=4 for IR groups, X100 magnification.

Quantification of Immunohistochemical staining of $A\beta_{1-40/42}$ and $A\beta_{1-42}$ expression showed that total $A\beta_{1-40/42}$ (27.75 ± 5.22, n=4, p<0.05) and small $A\beta_{1-40/42}$ plaque formation (17.00 ± 2.86, n=4, p<0.001) in IR1072 treated male TASTPM mice was significantly decreased in the cortex compared to age-matched sham controls age-matched sham controls (41.67 ± 3.52, n=4 and 32.000 ± 2.08, n=4, respectively) (Figure 6-21 - 6-23). All other parameters measured were statistically insignificant. IR1072 treated male TASTPM mice showed that $A\beta_{1-42}$ plaque formation was not statistically different from sham-treated TASTPM mice (Figure 6-24 - 6-26).

Figure 6-21: Immunohistochemical representation of Aβ$_{1-40/42}$ expression in IR1072-treated male TASTPM mice compared to age-matched sham controls in various brain regions. Abbreviations: Aβ, β-amyloid ; Ctx, cerebral cortex; CA (1/2/3), Cornu ammonis; DG, Dentate Gyrus; Cb, Cerebellum; CPu, Caudate Putamen. n=3 for sham and n=4 for IR groups, magnification.
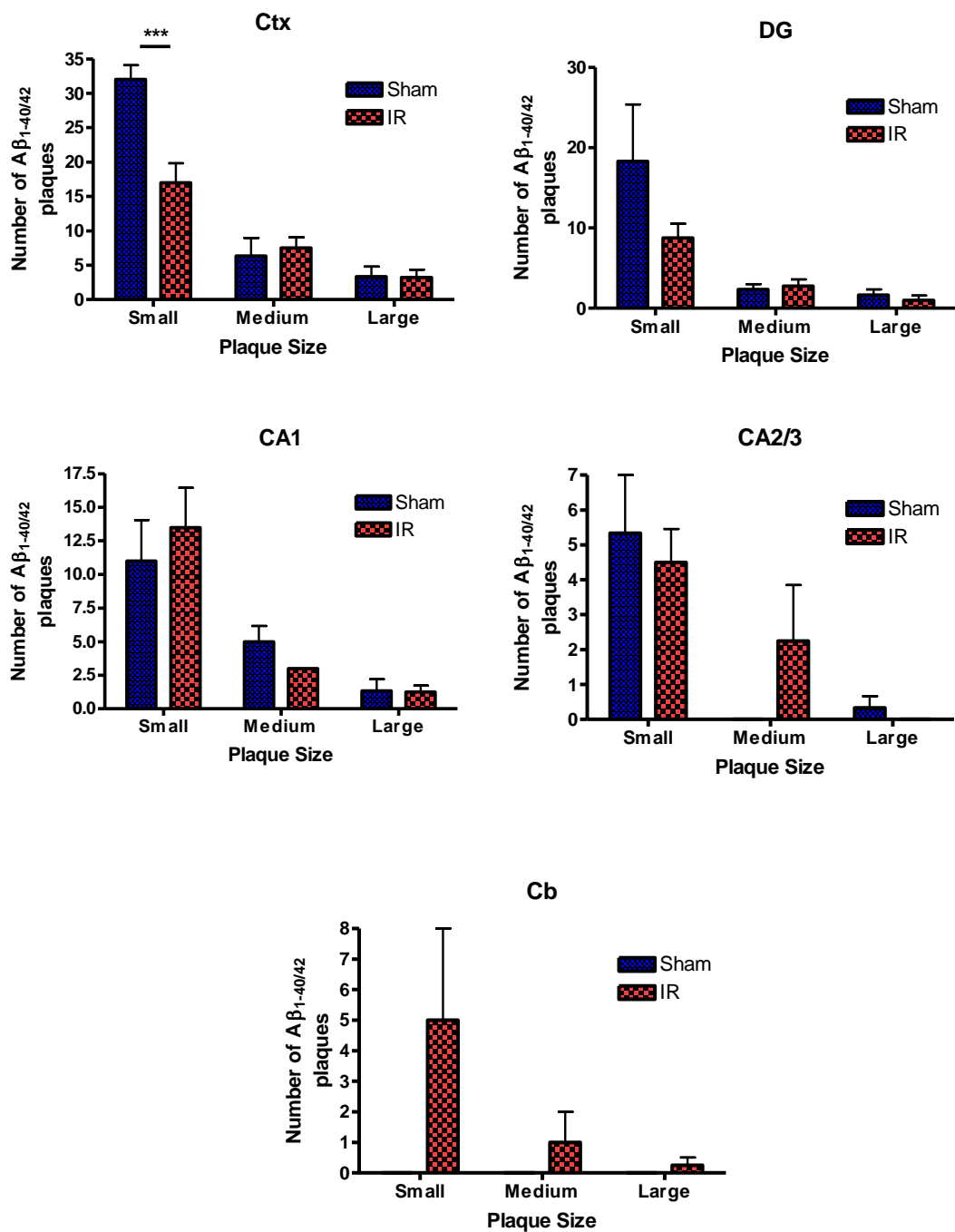
Figure 6-22: Quantification of immunohistochemical Aβ$_{1-40/42}$ expression data in IR1072-treated male TASTPM mice compared to age-matched sham controls in various brain regions. Abbreviations: Aβ, β-amyloid ; Ctx, cerebral cortex; CA (1/2/3), Cornu ammonis; DG, Dentate Gyrus; Cb, Cerebellum. n=3 for sham and n=4 for IR groups.
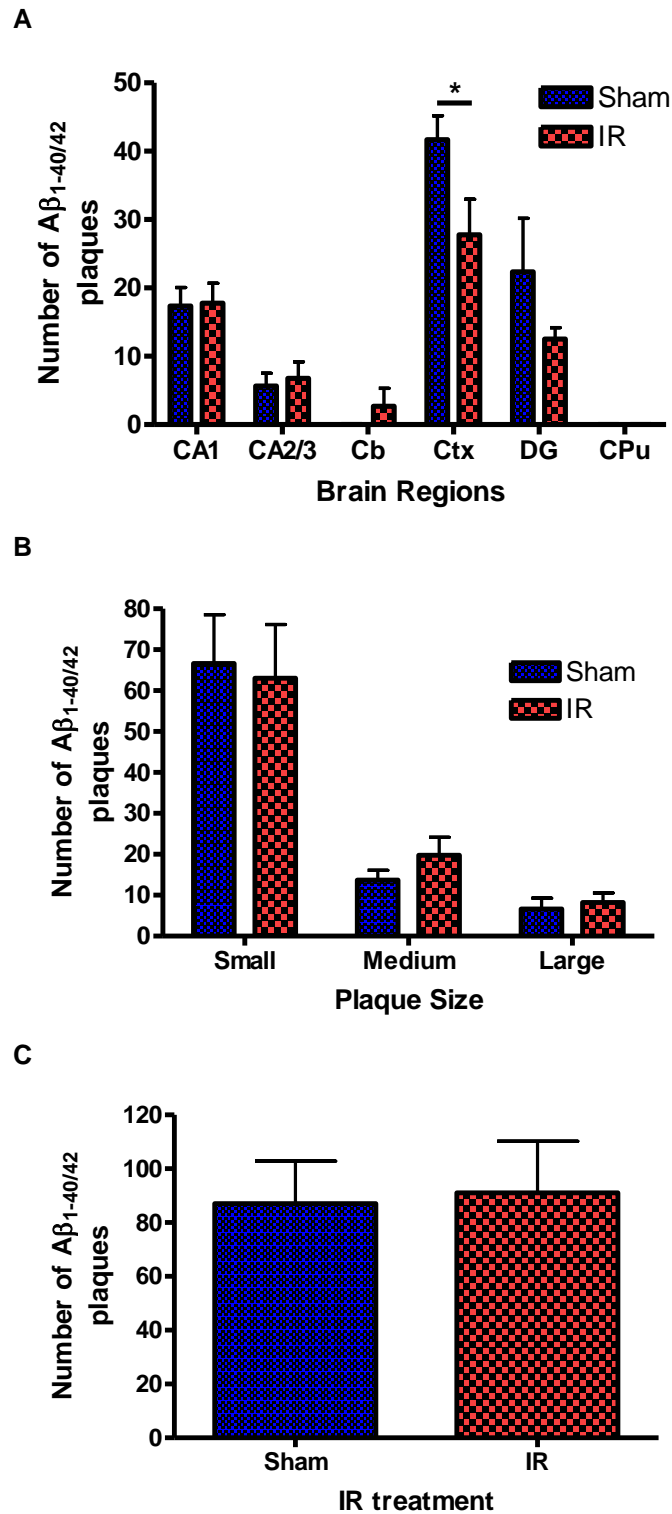
Figure 6-23: Quantification of immunohistochemical total $A\beta_{1-40/42}$ expression data in IR1072-treated male TASTPM mice compared to age-matched sham controls for A) various brain regions, B) plaque size C) total count. Abbreviations: $A\beta$, β-amyloid; Ctx, cerebral cortex; CA (1/2/3), Cornu ammonis; DG, Dentate Gyrus; Cb, Cerebellum; CPu, Caudate Putamen. n=3 for sham and n=4 for IR groups.
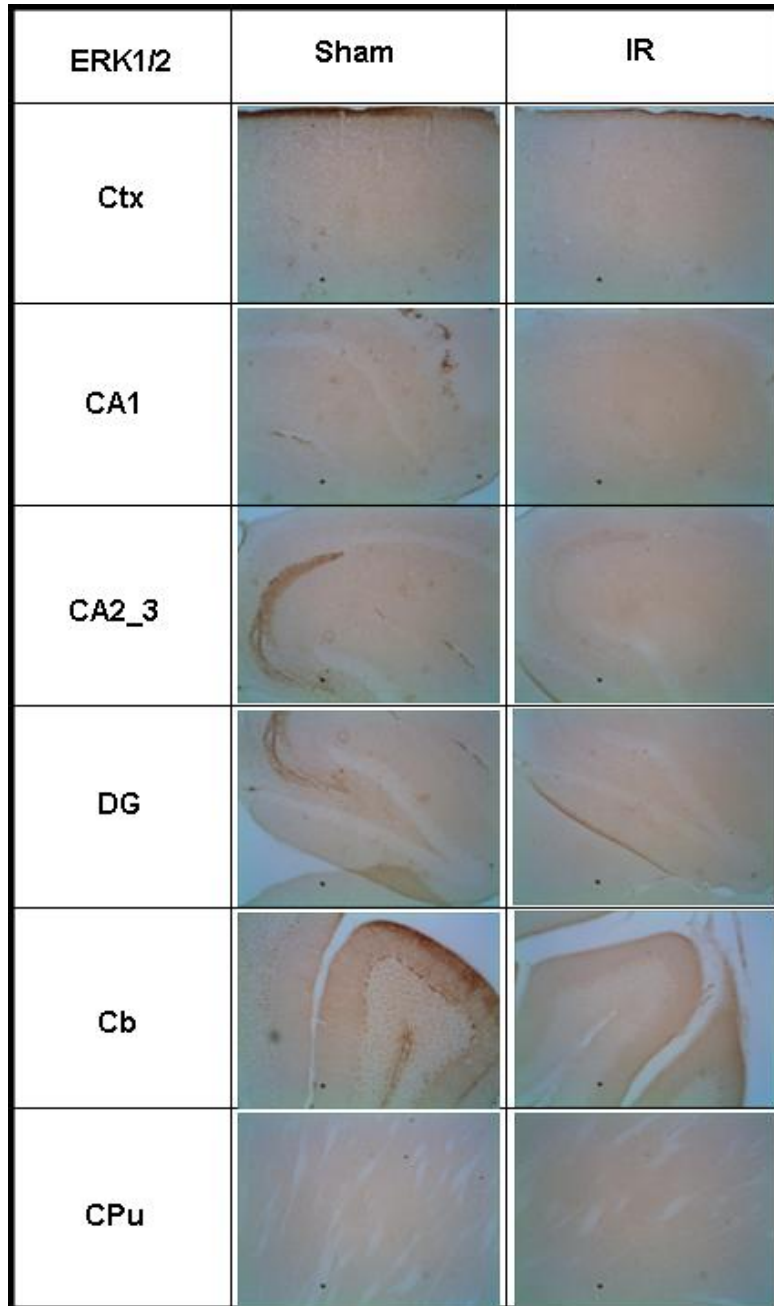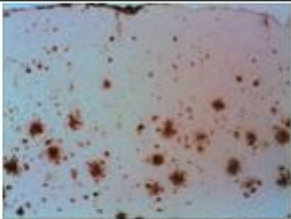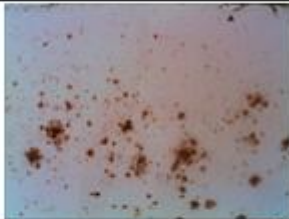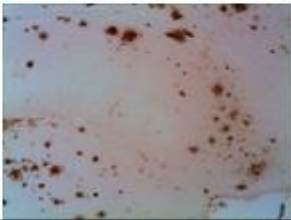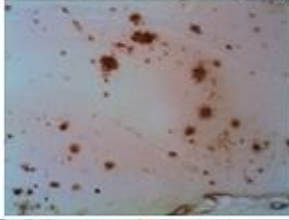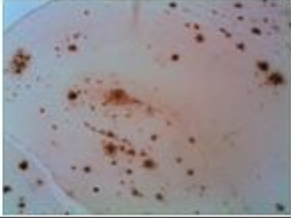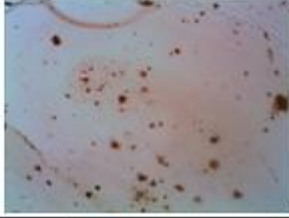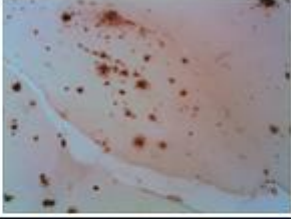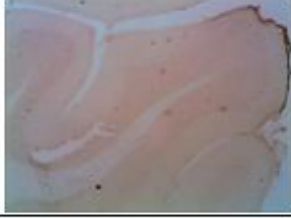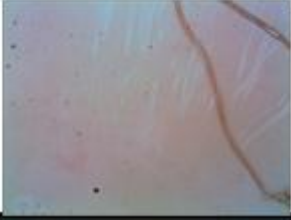
Figure 6-24: Immunohistochemical representation of $A\beta_{1-42}$ expression in IR1072-treated male TASTPM mice compared to age-matched sham controls in various brain regions. Abbreviations: $A\beta$, β-amyloid ; Ctx, cerebral cortex; CA (1/2/3), Cornu ammonis; DG, Dentate Gyrus; Cb, Cerebellum; CPu, Caudate Putamen. n=3 for sham and n=4 for IR groups, X100 magnification.
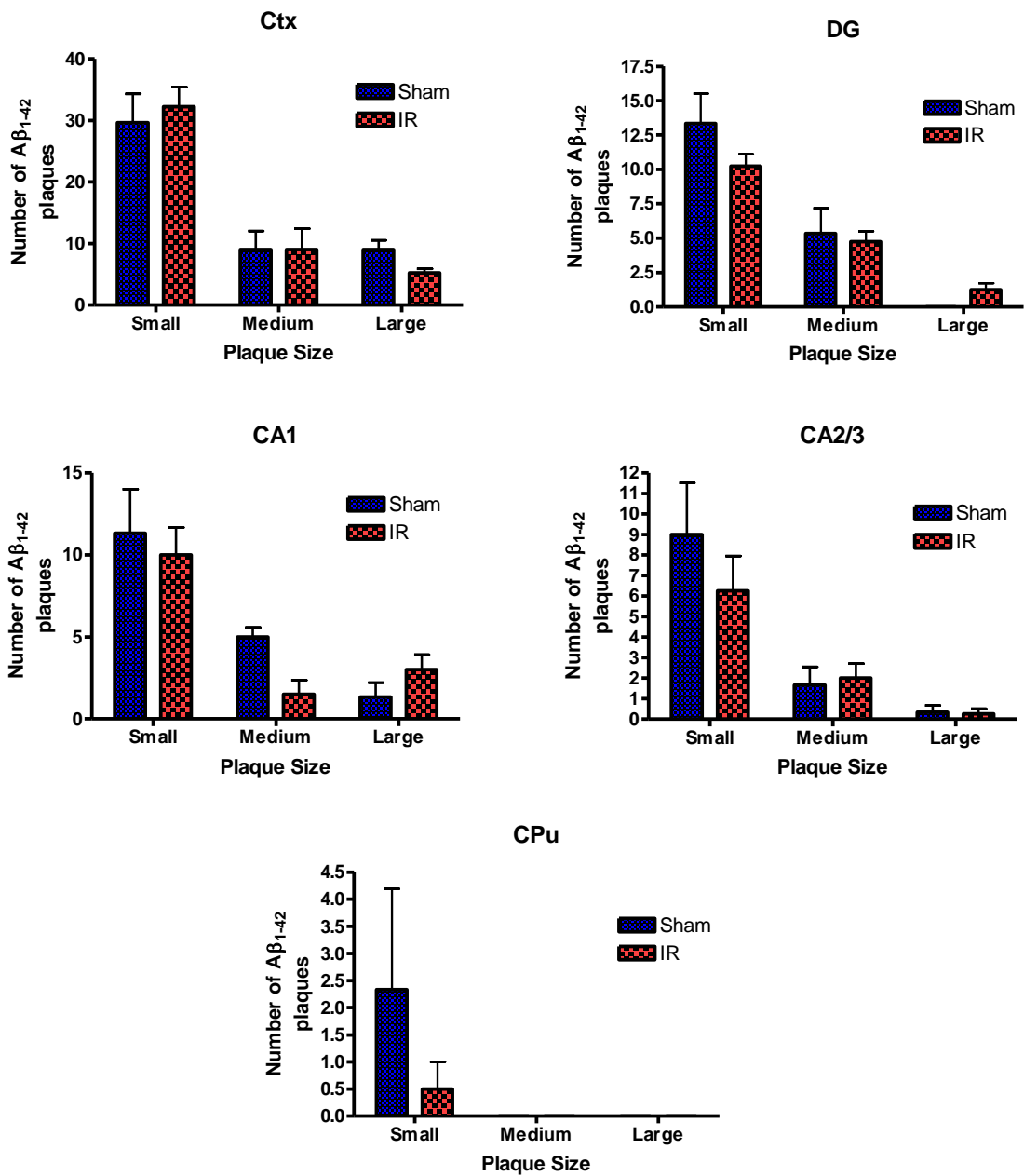
Figure 6-25: Quantification of immunohistochemical $A\beta_{1-42}$ expression data in IR1072-treated male TASTPM mice compared to age-matched sham controls in various brain regions. Abbreviations: Aβ, β-amyloid; Ctx, cerebral cortex; CA (1/2/3), Cornu ammonis; DG, Dentate Gyrus; CPu, Caudate Putamen. n=3 for sham and n=4 for IR groups.
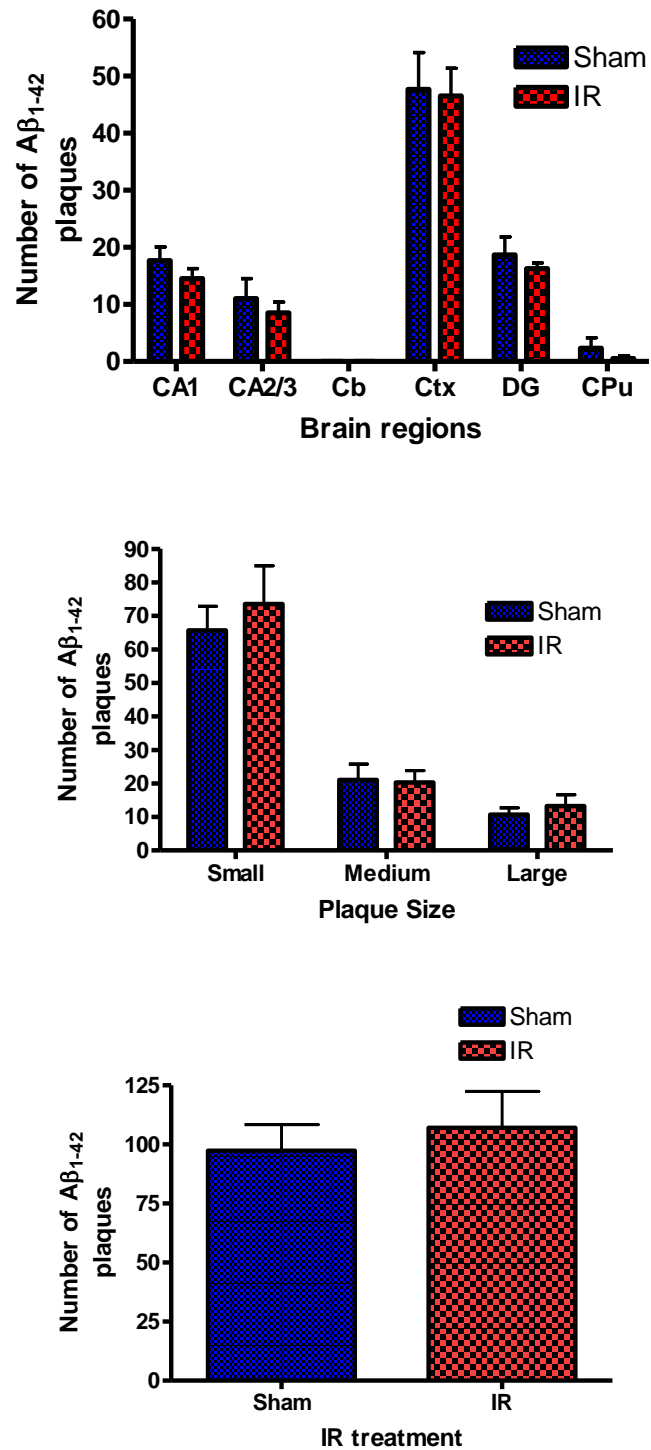
Figure 6-26: Quantification of immunohistochemical total $A\beta_{1-42}$ expression data in IR1072-treated male TASTPM mice compared to age-matched sham controls for A) various brain regions, B) plaque size C) total count. Abbreviations: $A\beta$, β-amyloid; Ctx, cerebral cortex; CA (1/2/3), Cornu ammonis; DG, Dentate Gyrus; Cb, Cerebellum; CPu, Caudate Putamen. n=3 for sham and n=4 for IR groups.

6.2.3.3 Chronic IR1072 treatment in female TASTPM mice: Immunoblot analysis

Protein levels were standardised using mouse β-actin primary antibody. Data were statistically analysed using a two tailed student t-test. Data represent mean ± SEM.

Table 6-5: Protein expression profile in 7 month old female TASTPM mouse brain following chronic IR1072 treatment compared to age-matched sham-treated controls. Arrows represent an increase (↑) or decrease (↓) in protein expression in IR-treated TASTPM mice compared to age-matched sham controls, and respective figure numbers. Data were statistically analysed using a two tailed student t-test. Pink cells represent significant results (p<0.05) and blue cells represent a trend (p<0.1). n=4 for each group, *p<0.05, **p<0.01. Abbreviations: BDNF; Brain Derived Neurotrophic Factor; ERK1/2 or ERK1/2-P, unphosphorylated or phosphorylated extracellular-signal regulated kinase 1 or 2, respectively; CREB, Cyclic Adenosine Monophosphate (AMP) Response Element Binding; HSP, Heat Shock Protein; PI3, Phosphatidylinositol 3-Kinase.

Effect of Chronic IR1072 treatment on protein expression in female 7 month old TASTPM mice			
1⁰	**p value**	**Results**	**Figure**
BDNF	*0.0171*	↓	**Figure 6-26**
ERK1	0.5005	NS	Data not shown
ERK2	0.0234	↑	**Figure 6-27**
ERK1-P	0.3395	NS	Data not shown
ERK2-P	0.864	NS	Data not Shown
CREB	0.0948	NS	**Figure 6-28**
AKT	0.1485	NS	Data not shown
AKT-P			Data not shown
HSP27	0.1712	NS	Incomplete
HSP40	0.1925	NS	Data not shown
HSP60	**0.0057**	↑	**Figure 6-29**
HSP70	0.2124	NS	Data not shown
HSP90	0.43	NS	Data not shown
HSP105	**0.0016**	↑	**Figure 6-30**
Aβ$_{1-40/42}$			Incomplete

IR1072-preconditioned female TASTPM mice (n=3, 0.482 ± 0.0422) showed a significant decrease in BDNF expression compared to age-matched sham controls (n=3, 0.820 ± 0.075, p<0.05) (Figure 6-27).

A
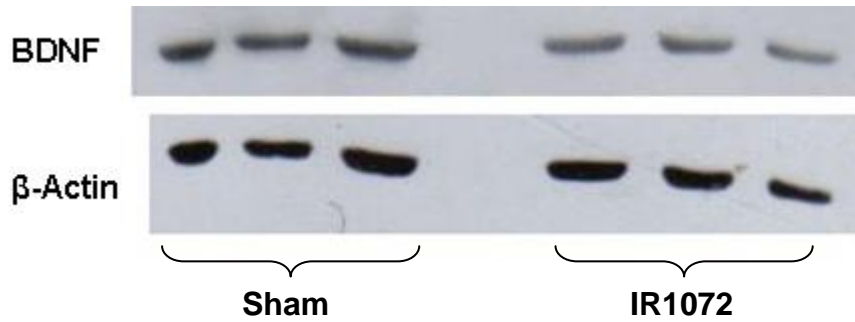
B
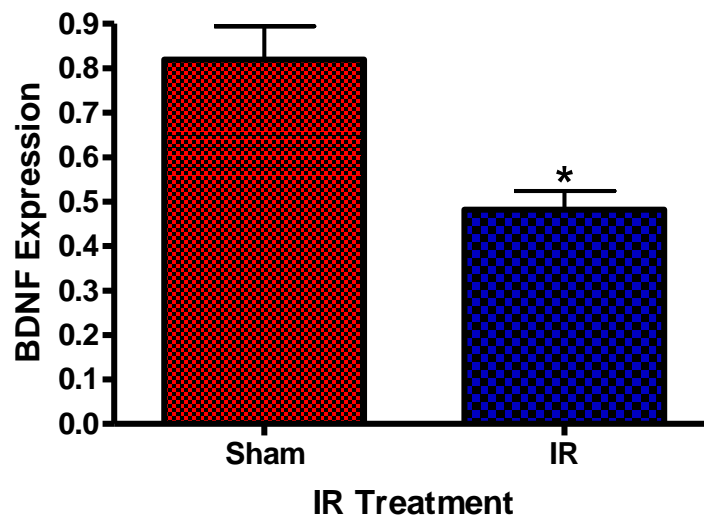
Figure 6-27: BDNF expression in chronically sham or IR1072 treated 7 month old TASTPM mouse brain (*in vivo*) where A) is an immunoblot representation where each lane represents an individual mouse and B) is a column graph showing the quantitative results of BDNF expression. Protein expression were standardised to total β-actin levels. Abbreviations: BDNF, Brain Derived Neurotrophic Factor. Mean values ± SEM, n = 3 for each group, *p<0.05.

IR1072-preconditioned female TASTPM mice (n=3, 0.372 ± 0.086) showed no differences in ERK1 expression compared to age-matched sham controls (n=3, 0.629 ± 0.095, p<0.05). However, IR1072-preconditioned female TASTPM mice (n=3, 1.412 ± 0.0367) showed significant increase in ERK2 expression compared to age-matched sham controls (n=3, 0.601 ± 0.225, p<0.05) (Figure 6-28).

A
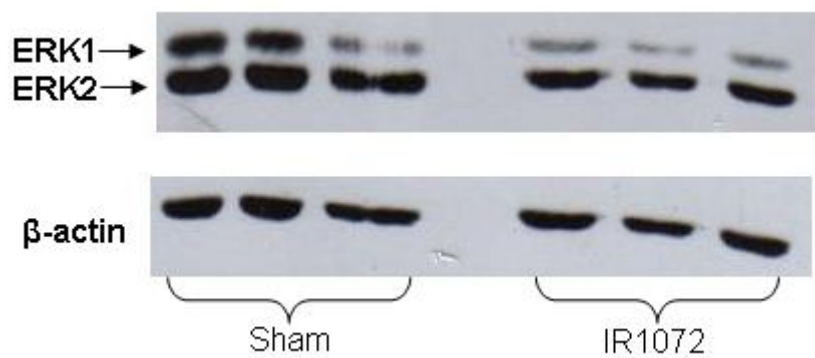
B
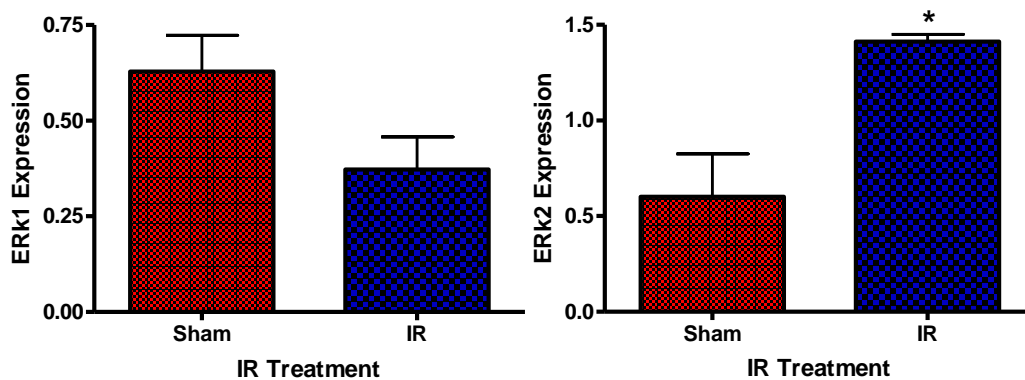
Figure 6-28: ERK1/2 expression in chronically sham or IR1072 treated 7 month old TASTPM mouse brain (*in vivo*) where A) is an immunoblot representation where each lane represents an individual mouse and B) is a column graph showing the quantitative results of ERK1/2 expression. Protein expression were standardised to total β-actin levels. Abbreviations: ERK1/2, Extracellular Signal-regulated Kinase 1 or 2. Abbreviations: Mean values ± SEM, n = 3 for each group, *p<0.05.

IR1072-preconditioned female TASTPM mice (n=3, 1.465 ± 0.027) showed a trend towards increased CREB expression compared to age-matched sham controls (n=3, 0.764 ± 0.320, p<1) (Figure 6-29).

A
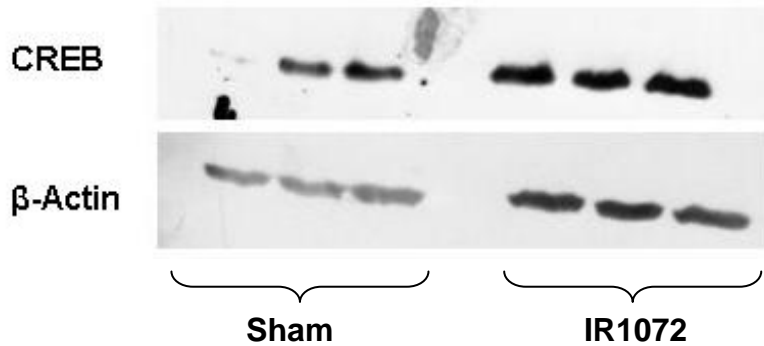
B
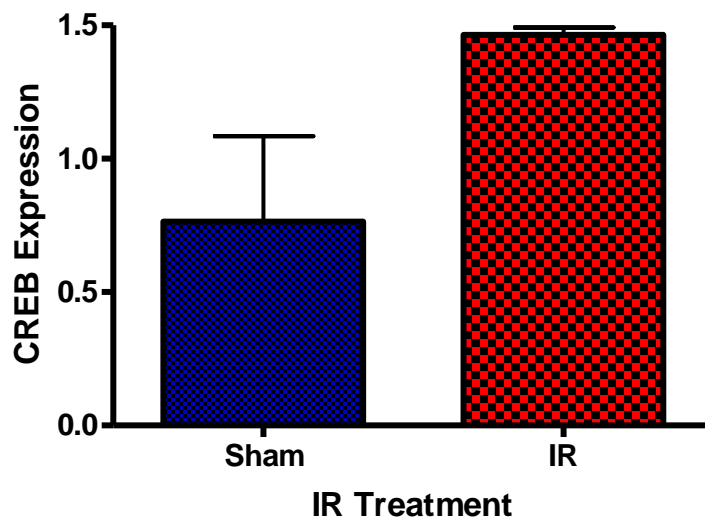
Figure 6-29: CREB expression in chronically sham or IR1072 treated 7 month old TASTPM mouse brain (*in vivo*) where A) is an immunoblot representation where each lane represents an individual mouse and B) is a column graph showing the quantitative results of CREB expression. Protein expression were standardised to total β-actin levels. Abbreviations: CREB, cAMP (cyclic adenosine monophosphate) response element binding. Mean values ± SEM, n = 3 for each group.

IR1072-preconditioned female TASTPM mice (n=3, 1.750 ± 0.078) showed significant increased HSP60 expression compared to age-matched sham controls (n=3, 0.7314 ± 0.1720, p<0.01) (Figure 6-30).

A
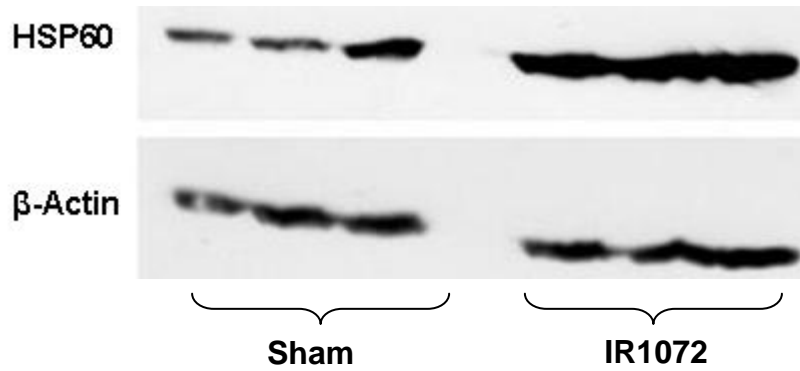
B
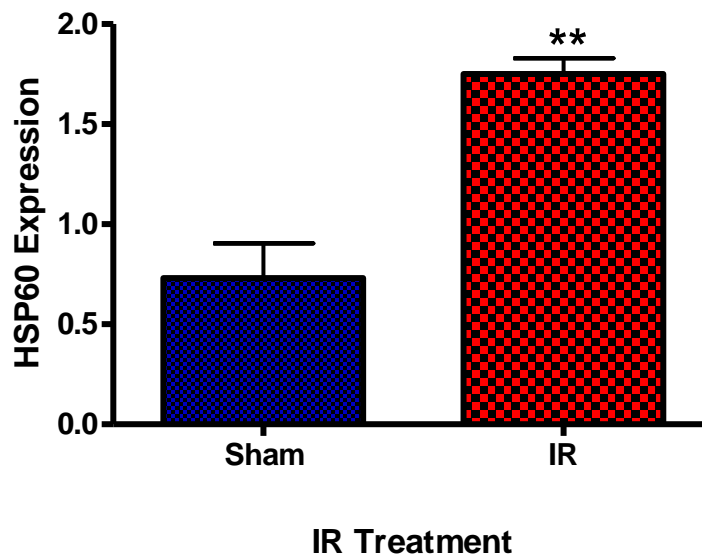
Figure 6-30: HSP60 expression in chronically sham or IR1072 treated 7 month old TASTPM mouse brain (*in vivo*) where A) is an immunoblot representation where each lane represents an individual mouse and B) is a column graph showing the quantitative results of HSP60 expression. Protein expression were standardised to total β-actin levels. Abbreviations: HSP60, Heat Shock Protein 60. Mean values ± SEM, n = 3 for each group. p<0.01.

IR1072-preconditioned female TASTPM mice (n=3, 1.256 ± 0.077) showed significant increased HSP105 expression compared to age-matched sham controls (n=3, 0.5259 ± 0.058, p<0.01) (Figure 6-31).

A
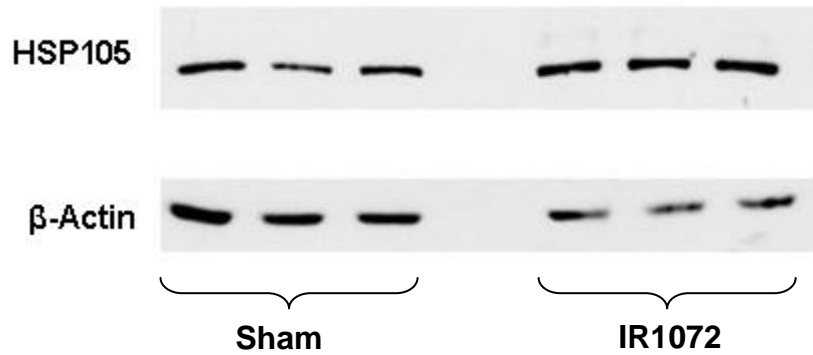
B
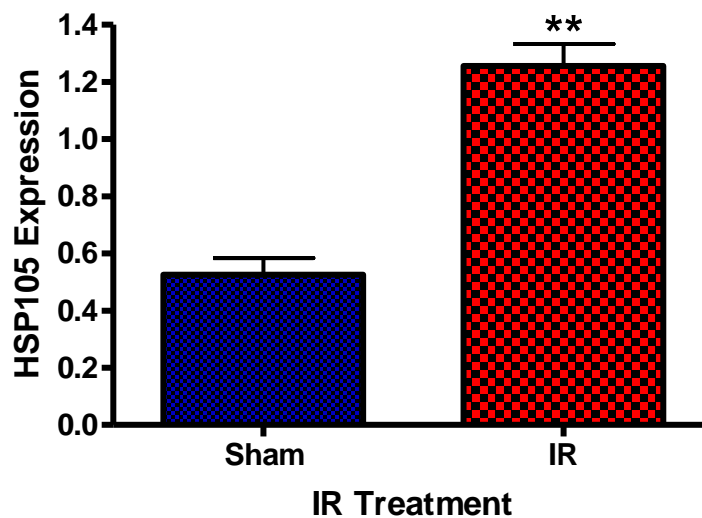
Figure 6-31: HSP105 expression in chronically sham or IR1072 treated 7 month old TASTPM mouse brain (*in vivo*) where A) is an immunoblot representation where each lane represents an individual mouse and B) is a column graph showing the quantitative results of HSP105 expression. Protein expression were standardised to total β-actin levels. Abbreviations: HSP105, Heat Shock Protein 105. Mean values ± SEM, n = 3 for each group. **p<0.01.

6.2.3.4 Chronic IR1072 treatment in female TASTPM mice: Immunohistochemical analysis

Table 6-6: Summary table depicting immunohistochemical analysis of various protein expression in IR1072-treated female TASTPM mice and sham-treated controls. Arrows represent an increase (↑) or decrease (↓) in protein expression. Abbreviations; BDNF, Brain Deived Neurotrophic Factor; ERK1/2, Extracellular Signal-regulated Kinase; CREB, Cyclic Adenosine Monophosphate (AMP) Response Element Binding; AKT, Protein Kinase B; HSP, Heat Shock Protein. n=3 for each group.

Cell signalling protein expression in sham or IR1072-treated female TASTPM mice	
1º Ab	**Result**
BDNF	↓ Ctx, CA1, CA2/3, DG
ERK1/2	-
ERK1/2-P	-
CREB	-
AKT	-
AKT-P	-
HSP27	-
HSP40	-
HSP60	-
HSP70	-
HSP90	
HSP105	↑CA1, CA2/3
Aβ$_{40/42}$	↓ DG, ↑ CPu
Aβ$_{42}$	↓Ctx

IR1072-treated female TASTPM mice (n=3) displayed a decrease in BDNF expression in the cortex, CA1/2/3 and dentate gyrus region of the hippocampus compared to age-matched sham controls (n=3)) (Figure 6-32).

Figure 6-32: Immunohistochemical representation of BDNF expression in IR1072-treated female TASTPM mice compared to age-matched sham controls in various brain regions. Abbreviations: BDNF, Brain Derived Neurotrophic Factor; Ctx, cerebral cortex; CA (1/2/3), Cornu ammonis; DG, Dentate Gyrus; Cb, Cerebellum; CPu, Caudate Putamen. n=3 for each group, X100 magnification.

IR1072-treated female TASTPM (n=3) mice showed an increased HSP105 expression in CA1/2/3 regions of the hippocampus compared to age-matched sham controls (n=3) (6-33).
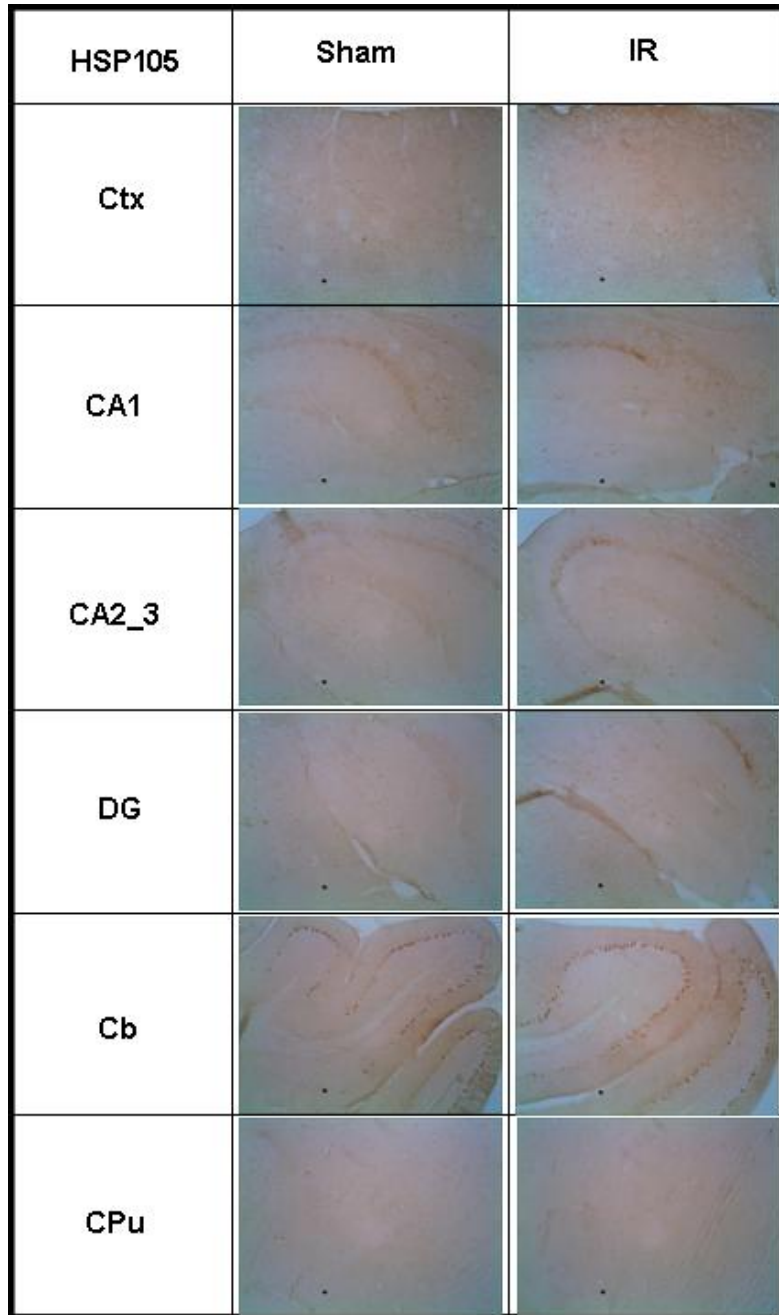
Figure 6-33: Immunohistochemical representation of HSP105 expression in IR1072-treated female TASTPM mice compared to age-matched sham controls in various brain regions. Abbreviations: HSP105, Heat Shock Protein 105; Ctx, cerebral cortex; CA (1/2/3), Cornu ammonis; DG, Dentate Gyrus; Cb, Cerebellum; CPu, Caudate Putamen. n=3 for each group, X100 magnification.

Results of immunohistochemical staining of $A\beta_{1-40/42}$ and $A\beta_{1-42}$ expression were quantified and revealed for IR1072 treated female TASTPM mice that total $A\beta_{1-40/42}$ (116.33 ± 5.93, n=3, p<0.001) and small plaque formation (35.67 ± 5.21, n=3, p<0.01) was significantly increased in the caudate putamen compared to age-matched sham controls (97.00 ± 8.62, n=3 and 12.00 ± 6.25, n=4, respectively). Small $A\beta_{1-40/42}$ plaque counts were significantly reduced in the dentate gyrus of IR1072-treated female mice (14.67 ± 4.33, n=3, p<0.05) compared to age-matched sham controls (22.33 ± 0.67) (Figure 6-33 - 6-35). Small $A\beta_{1-42}$ plaque counts were significantly reduced in the cortex of IR1072-treated mice (33.33 ± 1.86, n=3, p<0.05) compared to age matched sham controls (45.67 ± 2.96, n=3). Total small $A\beta_{1-42}$ plaque formation was significantly reduced in IR1072-treated female mice (83.00 ± 8.08, n=3, p<0.05) compared to age matched sham controls (107.67 ± 9.67, n=3) (Figure 6-36 - 6-38). All other parameters measured were statistically insignificant.
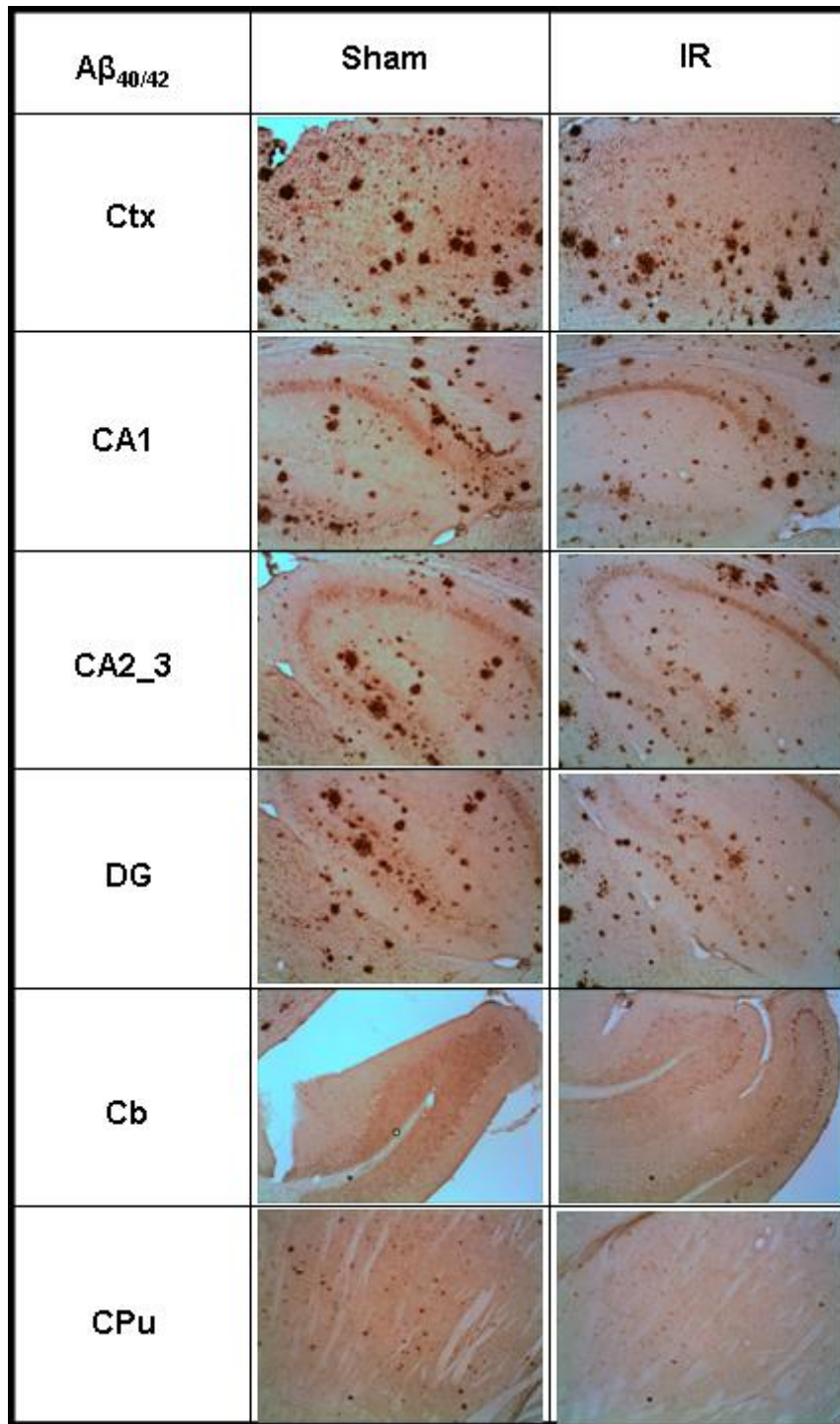
Figure 6-34: Immunohistochemical representation of Aβ$_{1-40/42}$ expression in IR1072-treated female TASTPM mice compared to age-matched sham controls in various brain regions. Abbreviations: Aβ, β-amyloid; Ctx, cerebral cortex; CA (1/2/3), Cornu ammonis; DG, Dentate Gyrus; Cb, Cerebellum; CPu, Caudate Putamen. n=3 for each group, X100 magnification.
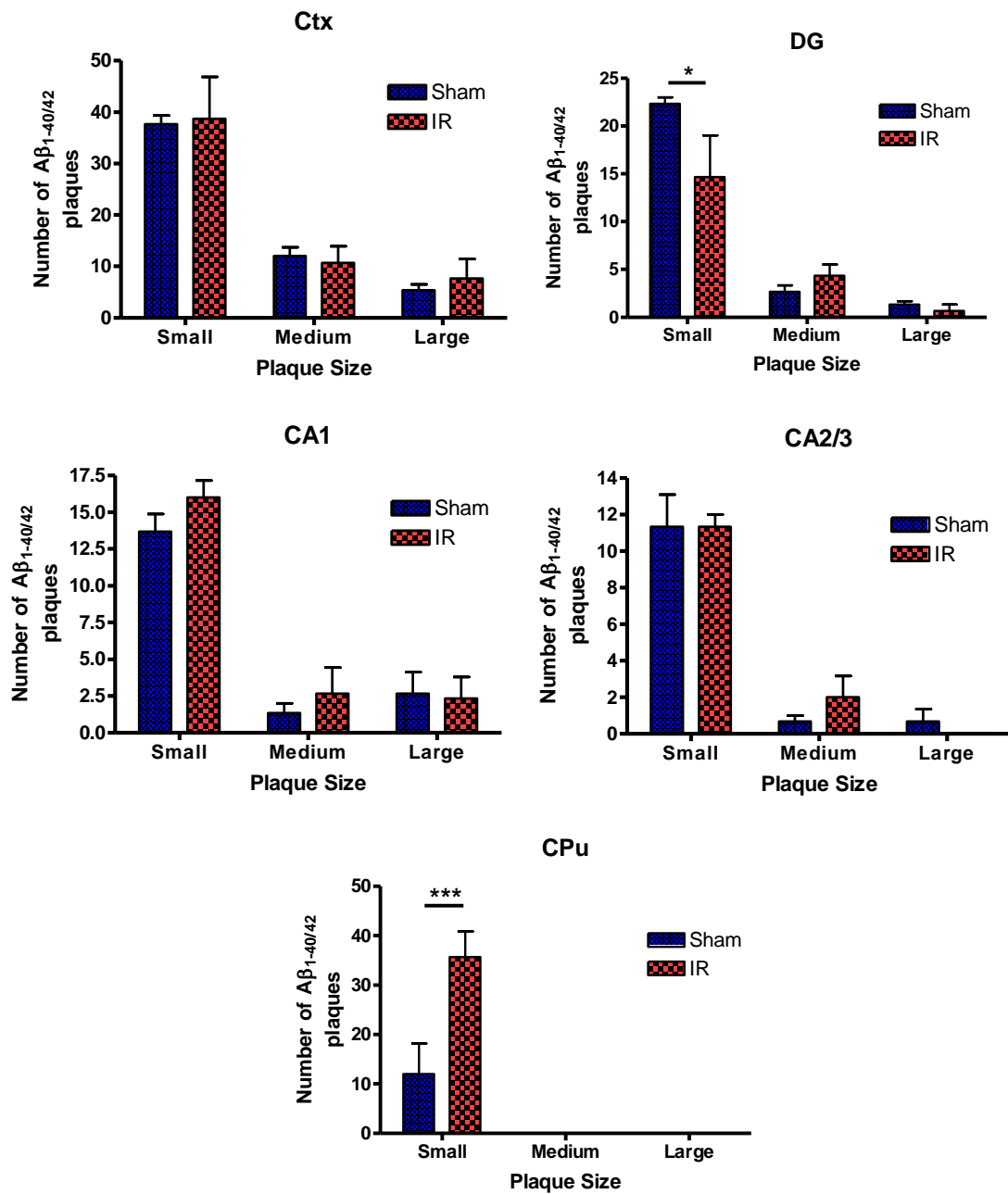
Figure 6-35: Quantification of immunohistochemical Aβ$_{1\text{-}40/42}$ expression data in IR1072-treated female TASTPM mice compared to age-matched sham controls in various brain regions. Abbreviations: Aβ, β-amyloid ; Ctx, cerebral cortex; CA (1/2/3), Cornu ammonis; DG, Dentate Gyrus; CPu, Caudate Putamen. n=3 for each groups.
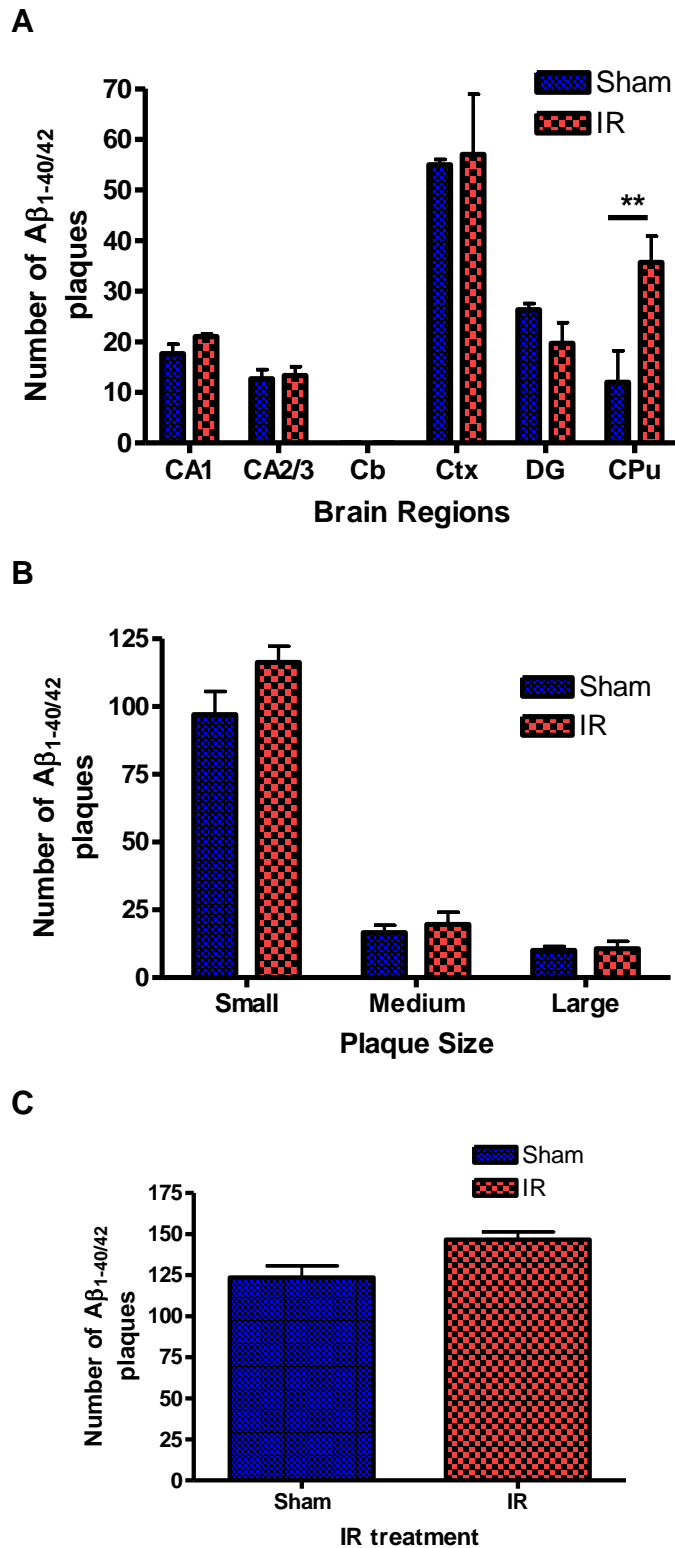
Figure 6-36: Quantification of immunohistochemical total $A\beta_{1-40/42}$ expression data in IR1072-treated female TASTPM mice compared to age-matched sham controls for A) various brain regions, B) plaque size C) total count. Abbreviations: $A\beta$, β-amyloid ; Ctx, cerebral cortex; CA (1/2/3), Cornu ammonis; DG, Dentate Gyrus; Cb, Cerebellum; CPu, Caudate Putamen. n=3 for each group.
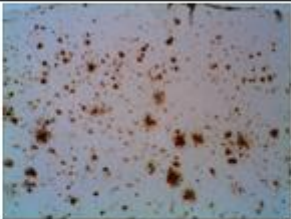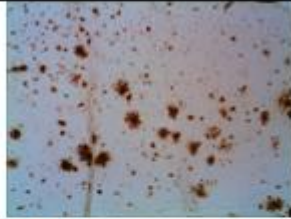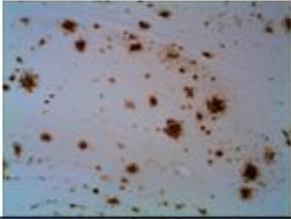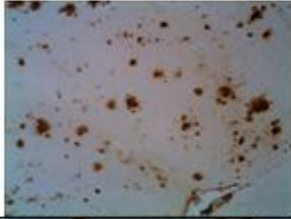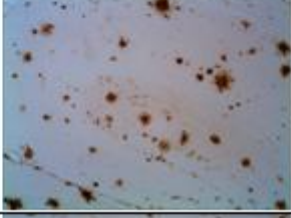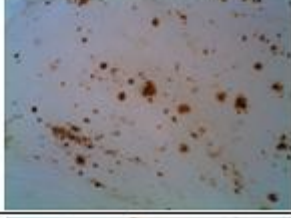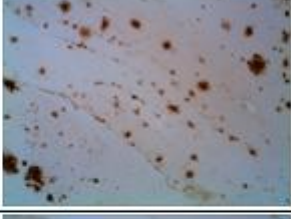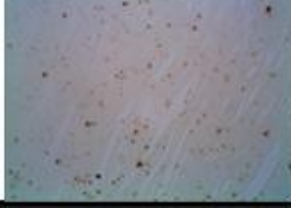
Figure 6-37: Immunohistochemical representation of $A\beta_{1-42}$ expression in IR1072-treated female TASTPM mice compared to age-matched sham controls in various brain regions. Abbreviations: $A\beta$, β-amyloid; Ctx, cerebral cortex; CA (1/2/3), Cornu ammonis; DG, Dentate Gyrus; Cb, Cerebellum; CPu, Caudate Putamen. n=3 for each group, X100 magnification.
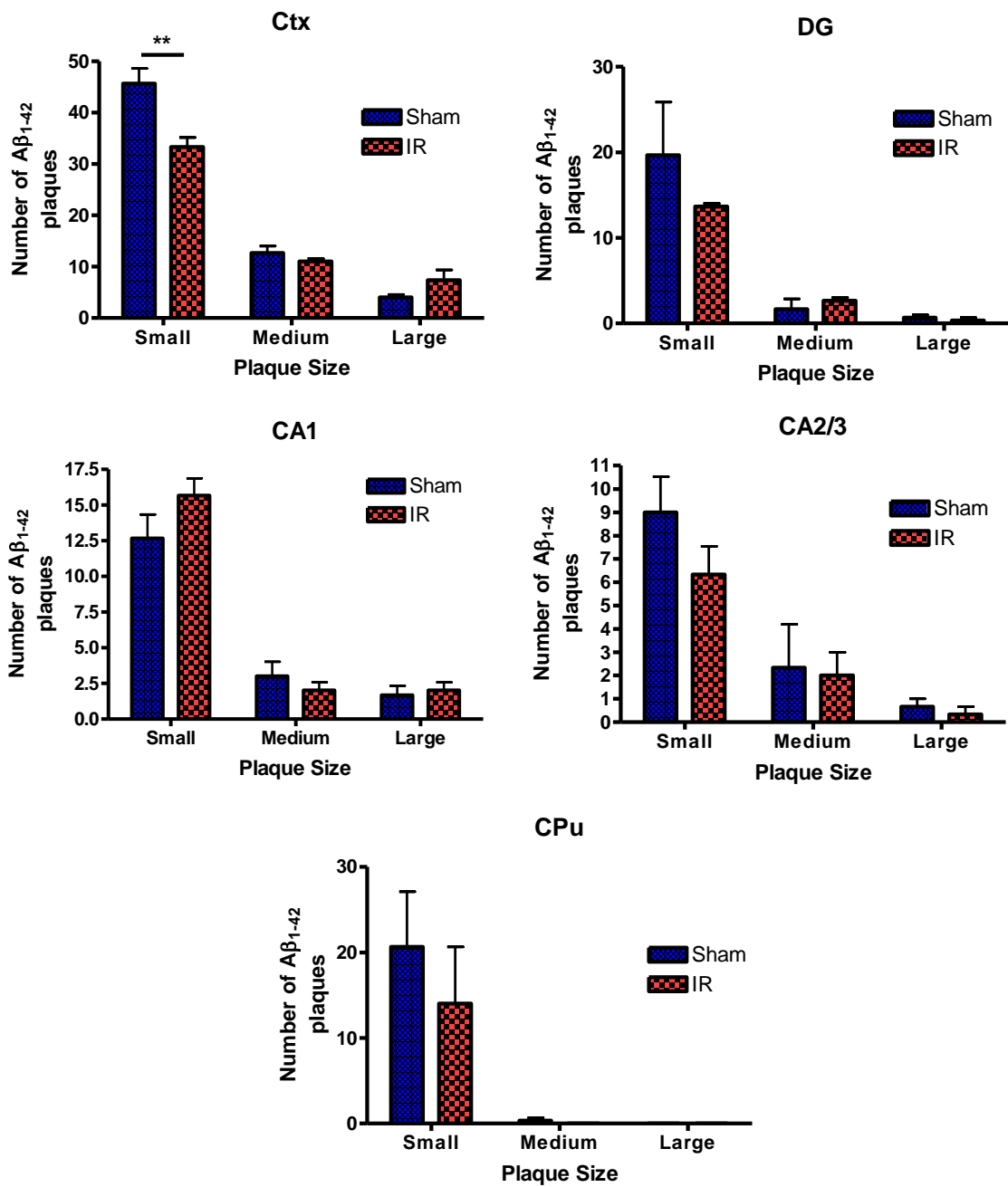
Figure 6-38: Quantification of immunohistochemical Aβ$_{1-42}$ expression data in IR1072-treated female TASTPM mice compared to age-matched sham controls in various brain regions. Abbreviations: Aβ, β-amyloid ; Ctx, cerebral cortex; CA (1/2/3), Cornu ammonis; DG, Dentate Gyrus; CPu, Caudate Putamen. n=3 for each groups.

A

B

C
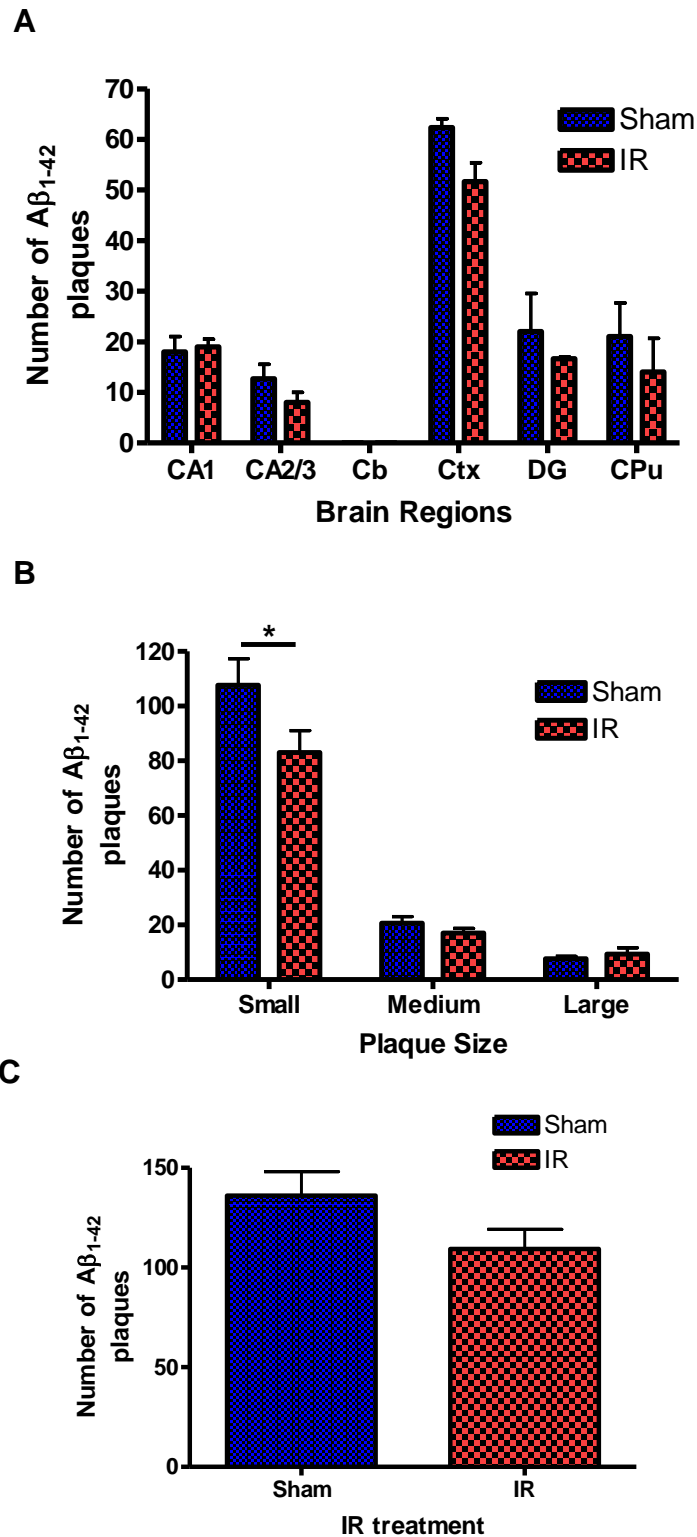
Figure 6-39: Quantification of immunohistochemical total Aβ$_{1-42}$ expression data in IR1072-treated female TASTPM mice compared to age-matched sham controls for A) various brain regions, B) plaque size C) total count. Abbreviations: Aβ, β-amyloid ; Ctx, cerebral cortex; CA (1/2/3), Cornu ammonis; DG, Dentate Gyrus; Cb, Cerebellum; CPu, Caudate Putamen. n=3 for each group.

6.4 Discussion

The aim of this chapter was to establish the protein changes of ERK1/2 signalling or HSP expression that occur during ageing in TASTPM animal model of AD, and also to establish any long-term protein changes following chronic IR1072 treatment in 7 month old TASTPM male and female mice.

Table 6-6: Summary of the effects of ageing and IR1072 treatment on TASTPM mice. Abbreviations: AD1TL, TASTPM age timeline; ADF, sham vs IR1072 female TASTPM 7month old mice; ADM, sham vs IR1072 male TASTPM 7 month old mice; IR, IR 1072nm; BDNF; Brain Derived Neurotrophic Factor; ERK1/2 or ERK1/2-P, unphosphorylated or phosphorylated extracellular-signal regulated kinase 1 or 2, respectively; CREB, Cyclic Adenosine Monophosphate (AMP) Response Element Binding; HSP, Heat Shock Protein; PI3, Phosphatidylinositol 3-Kinase.

Pathways	Protein	ADTL			Effects of chronic IR on protein expression	
		3 vs 7	3 vs 12	7 vs 12	ADF	ADM
ERK1/2	BDNF	↓	*↓	-	*↓	*↓
	ERK1/2	-	*↓	*↓	*↑	-
	ERK1/2-P	↑	*↓	-	-	-
	CREB	-	-	-	↑	**↑
PI3	AKT	*↑	*↑	*↓	-	-
	AKT-P	-	-	-	-	-
Chaperones	HSP27				-	-
	HSP40	↓	**↓	*↓	-	-
	HSP60	-	-	-	*↑	**↓
	HSP70	-	-	-	-	-
	HSP90	-	↓	-	-	↑
	HSP105	↓	*↓	-	*↑	-

Increased Aβ deposition, astrocytosis, phosphorylated tau and neuronal cell loss are the pathological hallmarks of AD, and appear to increase in TASTPM

mice as they age. Immunolabelling of Aβ deposition in ageing TASTPM mice bred and maintained at the University of Durham confirmed previously published reports of Aβ plaque formation in 3 month old TASTPM mice, albeit few, and subsequent increases in plaque population as the mice aged. High density of varying sized plaques was formed in the cortex, hippocampus (CA1-3) and the dentate gyrus of 7 month and 12 month old TASTPM mice.

An age-dependant decrease in BDNF and ERK1/2 protein expression occurred in TASTPM mouse brain whereby protein expression decreased as mice grew older. This decreased expression is likely to be caused by the high levels of Aβ plaques present in the older mice, as several studies show that even at low levels, Aβ interferes with downstream events that occur during various signalling cascades (Cotman, 2005; Chen et al., 2009). A reduction in neurotrophin levels has been shown to occur in some areas of the CNS of AD patients, and neurotrophic factors have begun to be used in clinical trials as therapeutic agents to prevent or reduce neuronal cell loss (Matrone et al., 2008). Chen et al. (2009), showed that non-lethal application of Aβ in rat cortical cultures partially blocked BDNF-induced upregulation of activity-regulated cytoskeleton-associated (Arc) protein, a protein involved in modulating synaptic plasticity. The Aβ blocking effect was proposed to act through the AKT or ERK1/2 signalling pathway, as Aβ prevented BDNF-induced phosphorylation of eukaryotic initiation factor 4E binding protein (4EBP) and activation markers downstream in these pathways (Chen et al., 2009). Tong et al. (2004) showed that low levels of Aβ in neuronal cultures interfered with BDNF signalling by suppressing ERK1/2 and PI3-K pathways

and BDNF activation of critical transcription factors, such as CREB, were significantly reduced, Aβ did not, however, effect basal levels of CREB or ERK1/2 expression in neuronal cultures. They showed that Aβ did not effect BDNF-induced PLCγ pathway activation or autophosphorylation of the TRKB receptor, indicating Aβ interferes at steps downstream of BDNF-induced signalling, possibly via the docking proteins that mediate signalling to ERK1/2 and AKT pathways (Tong et al., 2004). Mok et al. (2006) showed Aβ treatment on vascular smooth muscle cells reduced ERK1/2-P, and Poon et al. (2009) showed that Aβ reduced BDNF signalling by impairing axonal transport. However, in contrast to these studies enhanced and prolonged ERK1/2-P in sporadic and familial AD fibroblasts in response to bradykinin, but not in age-matched controls, was shown in a study conducted by Zhao et al. (2002). They also report that bradykinin-induced CREB activation was no different between AD and age-matched controls (Zhao et al., 2002). As a reduction in BDNF occured, it is natural to assume that ERK1/2 expression may occur as BDNF stimulates the ERK signalling pathway. However this reduction in ERK expression did not occur in the aged CD-1 mice even though BDNF was reduced, so this may suggest that Aβ may be influencing the regulation of ERK1/2 protein expression with age in TASTPM mice.

This study showed an age-dependent effect of AKT expression, whereby AKT expression increased from 3 months to 7 months, where levels were significantly reduced by the time mice reached 12 months of age. A similar expression pattern, however insignificant, was seen in activated AKT-P (data not shown). Chen et al. (2009), found that Aβ slightly increased AKT activity,

that was similar to the effect of the on PC12 and SH-SY5Y neuroblastoma cells from previous studies proposed to be caused by oxygen derived free radicals (Martin et al., 2001; Wei et al., 2002). Shay and Hagen (2009) found basal phospho-Ser473 AKT is 30% lower in aged rat hepatocytes when compared to young rat hepatocytes (Shay and Hagen, 2009). Activated caspases and accumulation of caspase cleavage products has been detected in postmortem AD brains, it has been suggested that once Aβ toxicity goes beyond a critical threshold, an apoptotic pathological cascade is initiated (Tong et al., 2004) Perhaps at 7 months old, the cell survival AKT pathway is increased in order to attempt to rescue and repair neurons from Aβ toxicity, but once Aβ accumulation tips the balance in favour of cell death at 12 months old, the apoptotic caspase cascade is initiated and BDNF, ERK1/2 and PI3K/AKT pathways are affected.

An age-dependant decrease of HSP40 was seen in male TASTPM mice. Previous studies found an inverse correlation between tau and levels of HSP 27, 40, 90 and alpha-crystallin in human AD brain samples, where it was proposed that HSP regulate the levels of soluble tau levels, but once the chaperone system has been saturated, granular tau oligomers form unabated and HSP levels are decreased (Sahara et al., 2007). Evans et al. (2006) showed the addition of HSP70/40 and HSP90 to pre-formed oligomers and fibrils caused structural changes in oligomers but had little effect on fibrils, suggesting that chaperones present in the same cellular compartment in which Aβ is produced, may suppress the early stages of self-assembly, but are not as effective once fibrils are formed, suggesting again that once the chaperone system is overloaded their functionality is limited. Kovacs et al.

(2006) demonstrated that heat shock alone was sufficient to induce PS1 aggresome formation and HSP70 expression, where the presence of the heat-shock proteins HSP70 in aggresomes suggested chaperone-mediated transport of PS1 into the ER (Kovacs et al., 2006). They suggested malfunctioning of the proteasome or heat-shock stress response in the AD brain may lead to the accumulation of stable aggresomes of PS1, perhaps contributing to neurodegeneration. Although there was no significant changes in HSP70 expression in ageing TASTPM mice, it is well known that HSP40 proteins have been shown to facilitate the folding of polypeptides through their interaction and regulation of partner HSP70 proteins (Nicoll et al., 2006), therefore a reduction in HSP40 seen in aging TASTPM mice may contribute towards malfunctioning of the HSP70 stress response.

This study showed a significant decease in expression of HSP105 as TASPTM mice aged. As HSP105 has been shown to inhibit the JNK pathway, a decrease in HSP105 may reflect a higher amount of pro-apoptotic proteins being phosphorylated and therefore activated, where translocation to the mitochondrial membrane would result in the initiation of apoptosis and neuronal in these AD mouse models.

IR1072 treatment appeared to show differences between male and female TASTPM mice. Howlett et al. (2004) investigated the differences between age, Aβ load and cognitive impairment in male and female TASTPM mice, and found that at all ages investigated, the Aβ load, in female TASTPM mice was greater than that in males, however there was no sex difference in the cognitive impairment demonstrated by TASTPM mice in the object recognition

task. They proposed that the Aβ deposition must reach a certain threshold before cognitive impairment is apparent, where the behavioural test used may not be sensitive enough to reveal graded impairments (Howlett et al., 2004). Another possibility is that the cognitive impairment may be more due to location of the Aβ deposits, their composition or the response of respective brain structures, rather than total Aβ load (Howlett et al., 2004). So differences in sex between male and female mice in response to IR1072 treatment may be due to the Aβ deposition reported previously.

A reduction in BDNF expression in both female and male TASTPM mice following chronic IR1072 treatments was found, where ERK1/2 levels were increased in females however no difference in ERK levels occurred in males which underwent the same treatment. Previous studies have reported that estrogen may play a role in ERK1/2 signalling, particularly ERK1/2 protein expression. Svegliati-Baroni (2006) showed that biliary-digestive diversion determined a marked reduction of ERK1/2 phosphorylation in cholangiocytes, which was reversed by the administration of 17β-estradiol (Svegliati-Baroni et al., 2006). Thordarson et al. (2004) found that enhanced expression of ERK1/2 and ERK1/2-P were associated with an increase in mammary tumorigenesis, where expression of the estrogen receptor-α (ERα) was also significantly elevated (Thordarson et al., 2004). However, this study did not show an increase in ERK1/2-P. Although the results differ from the IR1072 CD-1 data, BDNF expression, in both mouse stains, does not reflect the ERK1/2 protein expression in each respective experimental model. This could again suggest that IR1072 influences the function of the TRKB receptor,

where the differences may be dependant on the presence or absence of Aβ deposition.

Increased CREB was shown in both female and male TASTPM mice. This implies that CREB activation may be increasing cell survival via the upregulation of Bcl-2. As with the aged CD-1 mice, the male and female TASTPM mice showed no alterations in phophorylated ERK1/2 signalling following LILT, however CREB was increased in both sexes therefore CREB expression may be through a mitochondria-related pathway. But again, the present study probed for total CREB therefore further work is needed to show whether active CREB is altered following LILT.

An interesting clear differential response to IR was seen with HSP60. Female TASTPM mice showed an increase in HSP60, whereas male TASTPM mice showed a decrease in HSP60 expression. Previous studies have shown HSP60 expression were similar in skeletal muscle and liver in males and females except in the kidney, where HSP60 expression was twice as much in females compared to males (Voss et al., 2003). The brain was not investigated, however this difference in HSP60 expression could again be due to estrogen influences.

Female mice treated with IR1072 showed an increase in HSP105. This increase in HSP105 may be inhibiting the JNK pathway and therefore decreasing the amount of pro-apoptotic proteins being phosphorylated and activated, therefore indirectly inhibiting the initiation of apoptosis. Male

TASTPM mice irradiated with IR1072, however, did not show any detectable differences in HSP105 expression. Male mice showed an increase in HSP90 following IR1072 treatment however female mice showed no detectable difference in expression following irradiation. Previous studies showed that HSP90 was in fact present in lower levels in female hearts than in male hearts (Voss et al., 2003). This shows that at basal levels, there are sex differences in HSP90 expression, therefore IR1072 behaviour in mice may be dictated by hormonal differences between the sexes. Or another possibility may be that, if Aβ load is higher in female mice than male mice, this may be influencing the behaviour of IR1072 in TASTPM mice.

TASTPM mice showed a decrease in $A\beta_{1-40/42}$ expression following IR1072 irradiation. Immunohistochemical analysis confirmed $A\beta_{1-42}$ and $A\beta_{1-40/42}$ are present in both female and male 7 month old mice (Figure 6-33 and 6-36, respectively). The plaques were divided in to classes dependent on size: small (<5μm), medium (5-20μm) and large (>20μm), and quantified by an individual impartial to this investigation. Data showed that the total number of $A\beta_{1-40/42}$ plaques present in the cortex of AD male mice was decreased following chronic IR1072 irradiation, where it was shown that the number of small plaques present was particularly decreased. The dentate gyrus also showed a trend for decreased expression following IR1072 irradiation. A trend for decreased formation of medium sized $A\beta_{1-40/42}$ and $A\beta_{1-42}$ plaques in the CA1 region of the hippocampus has been shown in male mice following irradiation. A significant decrease of small sized $A\beta_{1-40/42}$ plaques was shown in the dentate gyrus of female TASTPM mice chronically treated with IR1072

irradiation. However an increase in $A\beta_{1-40/42}$ plaques, particularly small plaques, was shown following IR1072 irradiation. IR1072 irradiation appeared to reduce small $A\beta_{1-42}$ plaques located in the cortex of female TASTPM mice. The total number of small $A\beta_{1-42}$ plaques in all brain regions was significantly reduced following in female TASTPM mice chronically treated with IR1072. This significant decrease in $A\beta$ plaques in both male and female TASTPM mice, confirmed by both immunoblotting and immunohistochemistry, could be an extremely important and significant finding in relation to IR1072 irradiation, suggesting a potential non-invasive and non-pharmacological therapy for AD. Very little or no plaques are presented in the cerebellum or caudate putamen. Total $A\beta_{1-42}$ and $A\beta_{1-40/42}$ load appeared to remain the same for both male and female IR1072-treated mice and age-matched sham controls.

A signal was never accomplished with HSP27 for male TASTPM mice or $A\beta$ for female TASTPM IR1072 treated mice, despite attempts using varying protocols, but due to time constraints and limited antibody availability this was never achieved, therefore further investigations in to whether this is a sex-dependant effect are warranted.

Chapter 7: Overall Discussion and Future Work

The aim of this project was to determine whether LED IR1072 LILT has any neuroprotective effects in pure neuronal cultures (*in vitro*) and behavioural or molecular beneficial effects in ageing CD-1 and TASTPM mice (*in vivo*). Some of the approaches to address these objectives are detailed in figure 7-1.
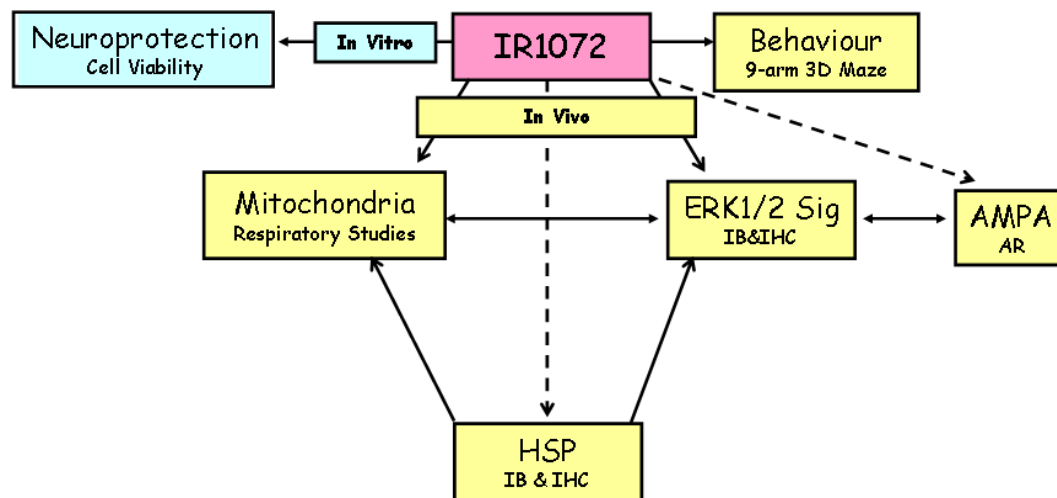
Figure 7-1: Primary aims to establish the effect of IR1072 on *in vitro* and *in vivo* systems. Blue boxes represents *in vitro* treatment and yellow boxes represent *in vivo* treatment. Abbreviations: ERK1/2, Extracellular Signal-regulated Kinase 1 or 2; HSP, Heat Shock Protein; AMPA, α-amino-3-hydro-5-methyl-4-isoxazole Proprionate.

Previous results showed IR1072 treated human lymphocytes had the highest cell viability compared to viability following irradiation with other wavelengths, where IR1072 was also shown to partially protect human lymphocytes from UVA toxicity (Bradford et al., 2005), which led to the question "does IR1072 have beneficial effects in other cell types"? Investigations into cell viability following excitotoxicity in sham or IR1072-treated pure neuronal cultures proved a insult-dependant protection of IR1072. As described earlier, the

233

proposed mechanism of LILT is primary acceptance of light in the red to near-IR region is through photoacceptors located in the mitochondrion, namely cytochrome *c* oxidase. Through respiratory assays conducted in this study, it was shown that acute *in vivo* irradiation of IR1072 in CD-1 mice appears to increase respiration of the ETC via the complex II enzyme in the brain and liver, as well as having beneficial effects via signalling molecules in young CD-1 brain. This confirmed previous findings of increased mitochondrial respiration following LILT (Alexandratou et al., 2002; Zhang et al., 2009) which guided the project to determine the protective effects of IR1072 on signalling pathways related to mitochondrial retrograde signalling on naturally occurring toxic events that takes place during the ageing process. Some key proteins involved in LILT-related signalling processes, detailed in figure 7-2, were investigated in this study.

The key findings in ageing CD-1 and TASTPM mice in the presence or absence of IR1072 are detailed in figures 7-3 and 7-4, respectively.

Ageing CD-1 mice showed a reduction in BDNF, HSP27 and HSP90. This correlates with previous studies showing decreases in these key signalling molecules and has been assumed to be due to cells losing the capacity to activate transcriptional pathways leading to HSP and/or growth factor synthesis. In the presence of IR1072, ageing CD-1 mice showed an increase in BDNF, several HSP i.e. 27, 40 and 60, cell survival proteins AKT and CREB, despite a decrease in ERK1/2 signalling, where a reduction in AMPA receptors was also shown. Ageing TASTPM mice showed a decrease in

BDNF, ERK1/2, AKT, and several HSP i.e. 40, 90, and 105. In the presence of IR1072 during ageing, an increase in ERK1/2, AKT and CREB was shown, despite decreases in BDNF, and several HSP i.e. HSP60, 90 and 105 were induced. These results suggest that IR1072 treatment may be working with reparation mechanisms of the cell in order to restore homeostasis for optimal cellular function.
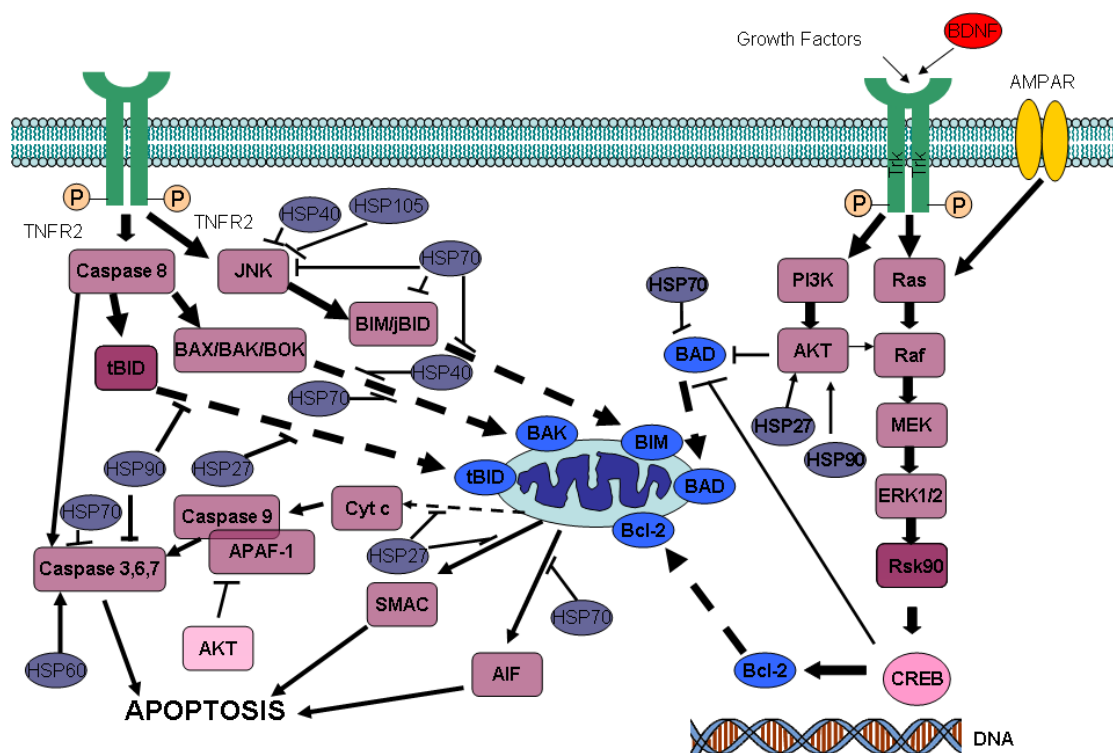
Figure 7-2: Overall signalling pathways aimed to study in this investigation. Abbreviations: BDNF, Brain Deived Neurotrophic Factor; MEK, MAPK/ERK Kinase; ERK1/2, Extracellular Signal-regulated Kinase; Rsk90, 90kDa Ribosomal Protein S6 Kinases; CREB, Cyclic Adenosine Monophosphate (AMP) Response Element Binding; Bcl-2, B-cell Lymphoma 2; BAD, Bcl-2 Associated Death Factor; P, Phosphate; DNA, Deoxyribonucleic Acid AKT, Protein Kinase B; TRKs, Tyrosine Kinase Receptors; PI3K, Phosphatidylinositol 3-Kinase; BAD, Bcl-2-associated Death Promoter; TNF, Tumour Necrosis Factor; TNFR1 or 2, Tumour Necrosis Factor 1 or 2; JNK, c-Jun N-terminal Kinase; BIM/jBID, BH3-only proteins; BAX/BAK/BOK/tBID, Bcl-2 family pro-apoptotic proteins; SMAC, Second Mitochondrial-derived Activator of Caspases; Cyto c; cytochome c; AIF, Apoptosis Inducing Factor; HSP, Heat Shock Protein; AMPA, α-amino-3-hydro-5-methyl-4-isoxazole Proprionate; P, phosphate.
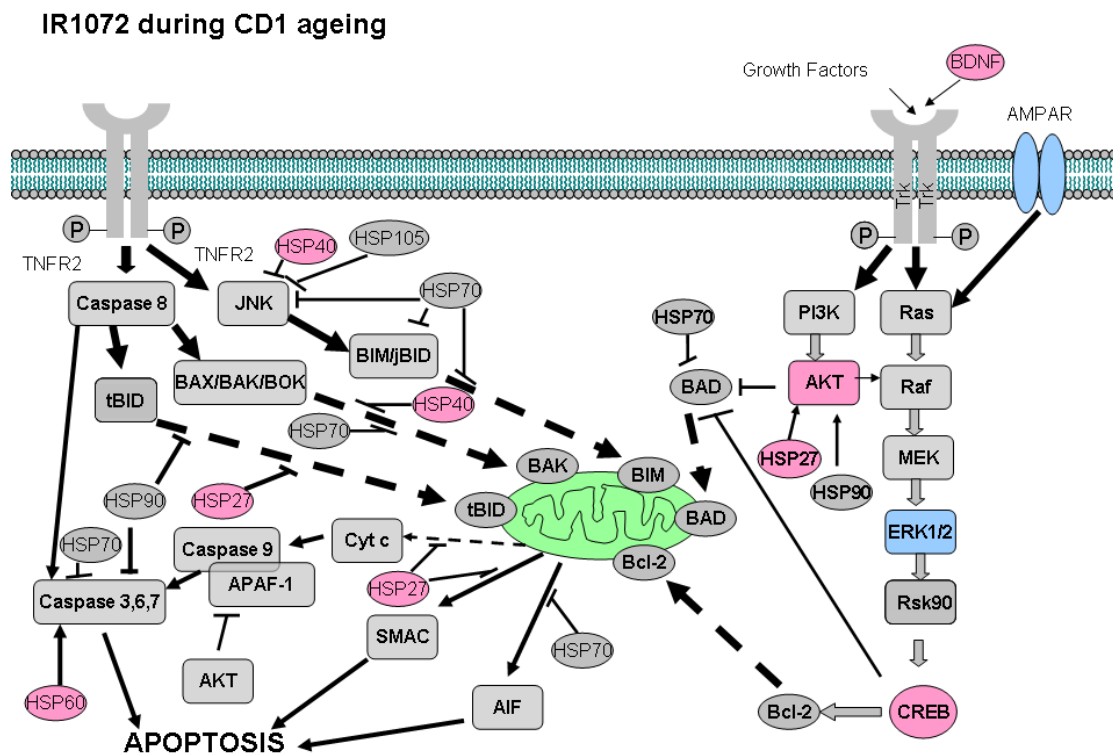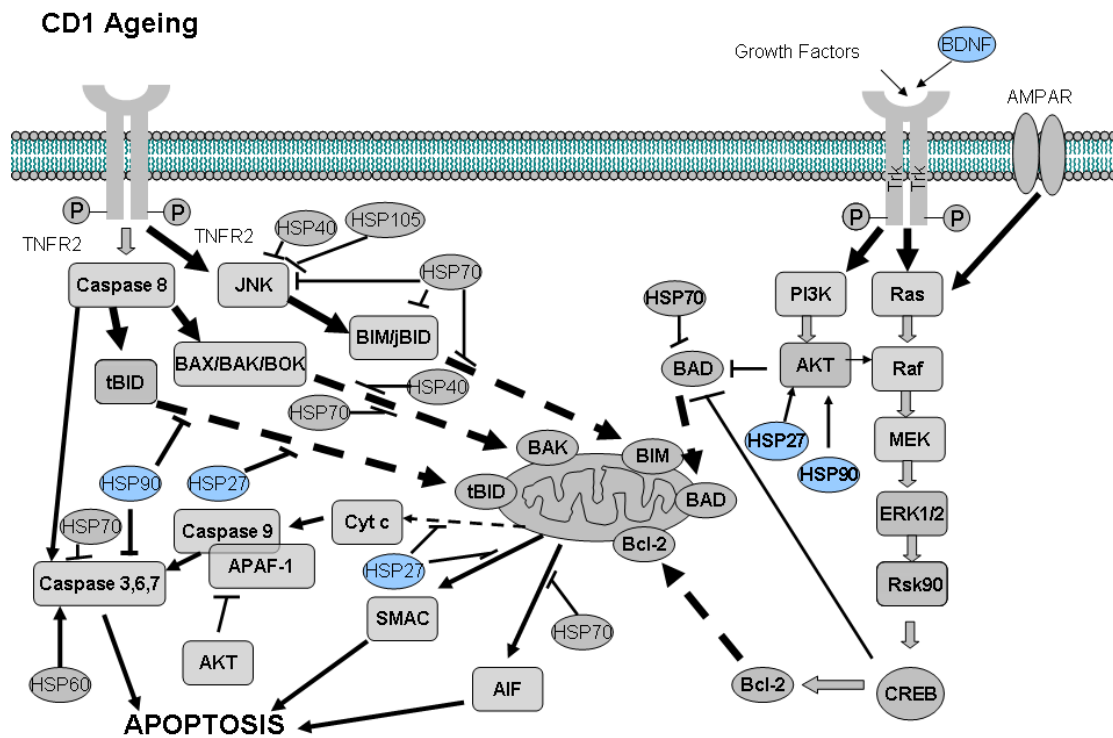
Figure 7-3: Summary of molecular effects of ageing in CD-1 mice in the presence or absence of IR1072 irradiation, where blue highlights represent decrease in protein expression and pink represents increases in protein expression, where green represents increased acitivity. Dashed lines represent translocation. Abbreviations: as described in figure 7-2.
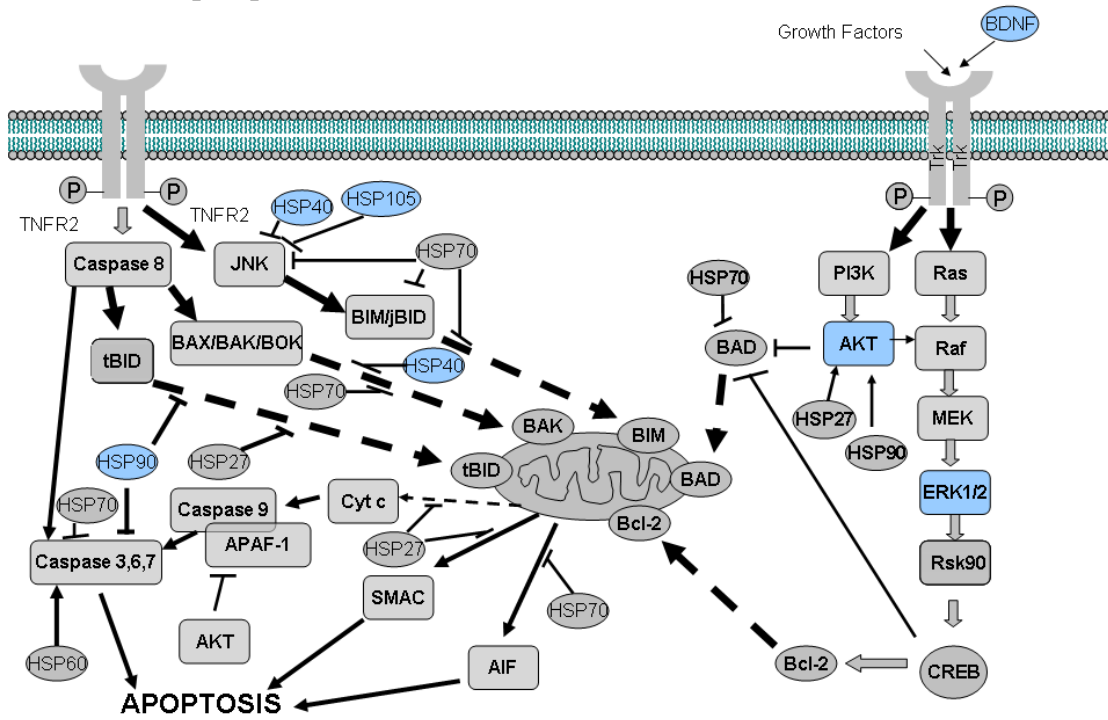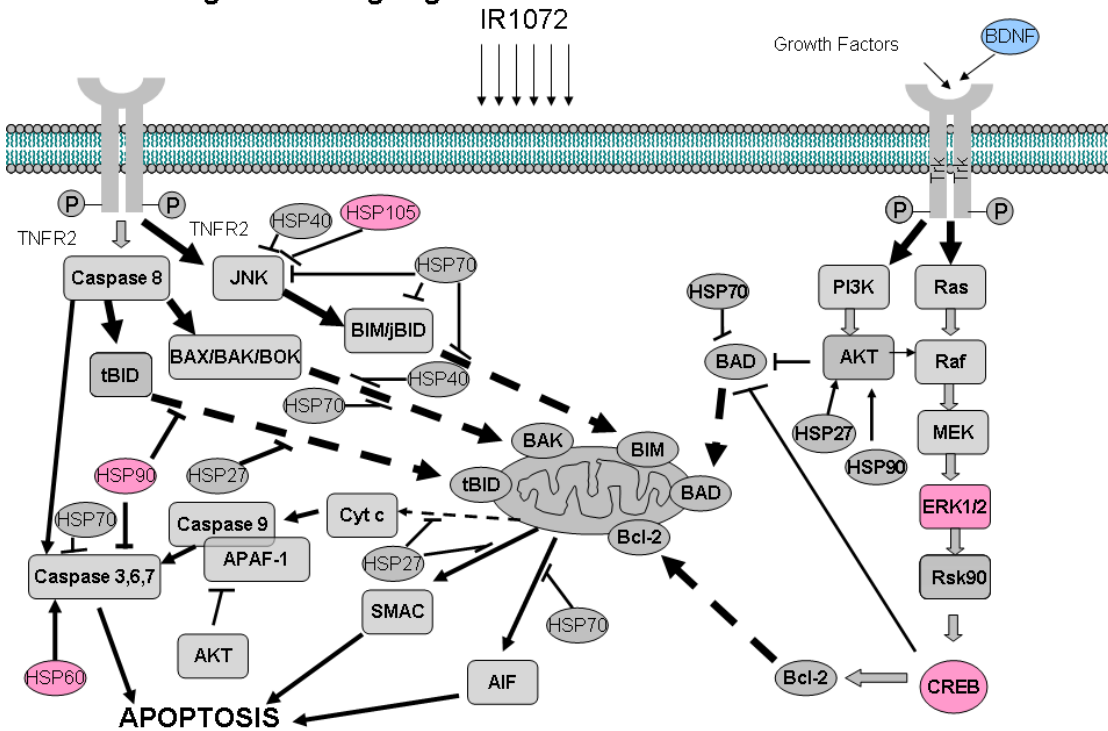
Figure 7-4: Summary of molecular effects of ageing in TASTPM mice in the presence or absence of IR1072 irradiation, where blue highlights represent decrease in protein expression and pink represents increases in protein expression. Dashed lines represent translocation. Abbreviations: as described in figure 7-2.

It is important to note that ageing TASTPM have increased Aβ deposition and increased neuronal loss compared to ageing CD-1 mice, which may go some way to explaining the differences in protein changes that have occurred in these mouse models following chronic IR1072 irradiation.

It has been reported that during LILT excitation of electronic states, a fraction of the excitation energy is converted to heat, which causes a local increase in the temperature of the absorbing chromophores (Karu et al., 1995). This local rise in temperature may contribute to the induction of HSP and other molecules seen following IR1072 irradiation, however bare in mind that this local transient heating of absorbing molecules is not the same as average heating of the whole cell, which does not occur during the doses and intensities used in this study (Karu et al., 1995).

Several studies have shown a rise in reactive oxygen species following LILT in cellular systems, some of which include cardiac and sperm cells with a 400-500nm halogen lamp (Eichler et al., 2005) and in bacteria using 400-800 white light (Lipovsky et al., 2008). Alexandratou et al. (2002) irradiated human foetal foreskin fibroblasts with 670nm laser and, by using specific fluorescent vital probes, observed a alkalinization of the cytosolic pH, an increase in mitochondrial membrane potential, generation of ROS and recurrent spikes of intracellular calcium concentration, where non-irradiated cells produced no such changes (Alexandratou et al., 2002). This may be an important find in explaining the mechanistic nature of LILT and the effects shown in this study.

A proposed mechanism of how IR1072 may be having an effect on certain cell types has been proposed (see figure 7-5).

In most cell types, mitochondria appear to represent one of the major sources of generation of free radicals or ROS (Duchen, 2004). Complex I and cytochrome c oxidase of the mitochondrial ETC are the two major contributors to ROS production in the cell, where nitric oxide is produced in the cell by nitric oxide synthase (NOS) located in the inner mitochondrial membrane (Brookes et al., 2002).
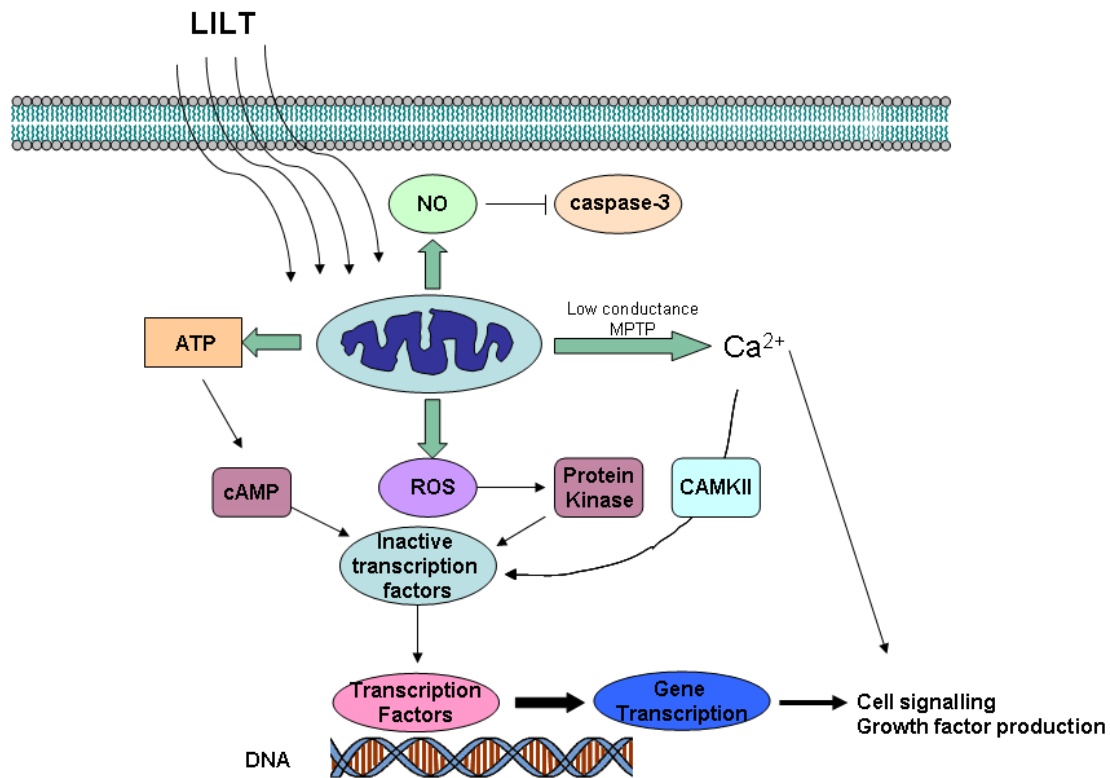
Figure 7-5: Possible mechanism of LILT. Abbreviations: LILT, Low Intensity Light Therapy; NO, Nitric Oxide; ATP, Adenosine Triphosphate; ROS, Reactive Oxygen Species; CAMKII, Calcium/calmodulin-dependent Protein Kinase II, DNA, Deoxyribonucleic Acid (Figure based on Huang et al., 2009).

Although ROS and NO are generally considered to have destructive effects, when present at low, physiologically relevant concentrations, they can also participate in initiation of redox signalling events that regulate a variety of molecular mechanisms, including stimulation of tyrosine residue phosphorylation of membrane receptors and thereby triggering cell signalling cascades (Salvi et al., 2005). Photosensitized generation of ROS in the cytoplasm of some cells induces a free-radical activation of synthesis of proteins, the most significant being the de novo synthesis of inducible NO-synthase (iNOS), superoxide dismutase, and various cytokines (Vladimirov Iu et al., 2004). ROS can induce several redox-sensitive transcription factors, which in turn activates transcription of gene products involved in cytoprotection (Huang et al., 2009).

In addition to demonstrating IR1072 being most beneficial in human lymphocytes, Bradford et al. (2005) showed a significant increase in iNOS expression following IR1072 treatment in human lymphocytes, where nitric oxide is a potent inhibitor of apoptosis. The up-regulation of NO in several reports for various wavelengths and tissue types have been confirmed, including endothelial and sperm cells (Ankri et al., 2009) in cardiomyocytes (Zhang et al., 2009) monocytes/macrophages (Novoselova et al., 2006; Gavish et al., 2008) and skin tissue (Glushkov et al., 2006). suggesting LILT may act through NO mechanisms involving the inactivation or inhibition of caspase-3-like protease enzyme, a key enzyme regulating apoptotic programmed cell death.

As discussed previously, a rise in ATP following LILT has been repeatedly reported and has been suggested to be induced in order to power metabolic processes such as synthesising DNA, RNA, proteins, enzymes, and other biological materials needed to repair or regenerate cell and tissue components to restore homeostasis (Enwemeka, 2004). The perinuclear localization of the mitochondria following LILT has been shown, which has been suggested to facilitate ATP access to repairing damaged nuclear components (Hallmann et al., 2004; Pires Oliveira et al., 2008). LILT has been reported to cause cAMP elevation, presumably due to increased ATP production following LILT, which may contribute to inducing activator protein-1 (AP-1) activity and therefore activating transcription factors, in turn stimulating both DNA and RNA synthesis (Karu, 1987; Gao and Xing, 2009). This could be related to the changes in protein expression shown following IR1072 treatment.

Intracellular stores of Ca^{2+} in the mitochondrion and endoplasmic reticulum are thought to be regulated by multiple cellular components including ATP, H^+, Ca^{2+}, protein kinases, ROS and NO species (Hidalgo, 2005). Intracellular increases in Ca^{2+} can be mediated through extracellular influx (NMDA receptors) as well as intracellular stores (Ryanodine receptors, MPTP). Alexandratou (2002) suggested that their findings of intracellular spikes of Ca^{2+} following LILT may be due to the opening of the mitochondria permeability transition pore (MPTP) and suggested that LILT operates the MPTP in the low conductance state. MPTP is a channel of the inner mitochondrial membrane that appears to operate two distinct pathways: 1)

Ca^{2+} signalling during the lifespan of the cell (low conductance state) and 2) the effector signal of the apoptotic cascade during Ca^{2+} dependent cell death (high conductance state; Alexandratou et al., 2002). During the low conductance state, the diffusion of small ions such as Ca^{2+} ions is pH-controlled, promoting spontaneous closure of the channel, whereas high conductance, promotes the unselective diffusion of big molecules into the mitochondrial matrix which in turn disrupts the mitochondrial structure and causes the release of cytochrome *c* thus initiating apoptosis (Alexandratou et al., 2002). Increases in intracellular Ca^{2+} can initiate and modulate different cellular events including short-term responses, such as muscle contraction and secretion, as well as long-term responses including cell growth and proliferation and the expression of genes required for memory acquisition and learning (Hidalgo, 2005). The increased calcium concentration activates key enzymes such as CaMKII, which eventually results in the modulation of AMPA receptors (Manabe, 2008). Calcium signalling has been implicated in the initiation of signalling cascades required for LTP, including ERK1/2, so if a change in intracellular Ca^{2+} has occurred following IR1072, this may contribute to the protein changes shown in this study.

Current influx through AMPA receptors provides the depolarizing drive to open NMDA receptors for extracellular Ca^{2+} influx, and the amplitudes of synaptic potentials are generally thought to reflect the number of AMPA receptors at each synapse, where AMPA receptors are regulated by protein kinases and phosphatases (Carvalho et al., 2000; Bloodgood and Sabatini, 2008), therefore the decreased AMPA receptor expression shown in this

study may reflect a decrease in synaptic potentials in IR1072 treated CD-1 mice. As discussed previously, calcium excitotoxicity has been implicated as a major player in neuronal loss which takes place during ageing and neurodegenerative diseases. If IR1072 does work by restoring homeostasis to the cellular environment, this indirect or direct reduction in AMPA receptors may restore the cellular levels of intracellular Ca^{2+} to resting concentrations. Investigations into the mechanisms towards IR1072-AMPAR reduction are warranted.

As described previously, a proton leak or uncoupling of the ETC as ageing occurs could lead to an increased production of ROS. This excessive ROS production, and therefore free radical species, may damage the nuclear DNA and therefore contribute to the inability of the ageing cell to transcribe important signalling factors involved in cell survival. In light of these results, it may be appropriate to suggest that varying amounts of ATP, ROS, Ca^{2+} and NO produced during various wavelength and treatment protocols in differing *in vitro* e.g. neuronal cultures, lymphocytes, and *in vivo* e.g. CD-1 mice, TASTPM mice, are determinants of the effect of LILT treatment. Future experiments should include a protocol for ROS, ATP, Ca^{2+} and NO generation following IR1072 treatments in order to determine a baseline of these products, as they are emerging as key regulators involved in LILT-induced cell signalling. This may help towards proposal of a mechanism for the beneficial effects reported following LILT treatment.

7.1 Future work and direction

Investigations into varying the frequencies of IR1072 treatments in chronic protocols: As this study employed a chronic *in vivo* IR1072 protocol not previously tested, it would be interesting to see whether varying frequencies of treatment would elicit differing effects i.e. weekly treatments, daily treatments. Also, if IR1072 treatments were carried out until the last day of behavioural experiments, short-term and long-term protein changes would have been observed, so this change in protocol would be beneficial in future experiments.

Investigations in to mitochondrial photoacceptors: There is much published data stating that red to near-IR light at wavelengths 600-850nm is primarily accepted through the ETC chain in mitochondria, however there is very little evidence establishing the photoacceptor for IR light acceptance at 1072nm. Extensive experiments in to the primary photoacceptor of IR1072 are warranted, in order to achieve a basis to the mechanistic nature of LILT.

Extensive investigations in to the signalling pathways and related receptors: Further studies into the signalling pathways, proteins and receptors described in this study are required, particularly into the TRKB receptor as BDNF expression and ERK1/2 expression do not reflect one another in both animal models used, suggesting the TRKB receptor may be altered following LILT. Also, stress pathways and anti- or pro-apoptotic

proteins should be investigated to get an overall picture of how IR1072 in influencing cellular function.

ROS/NO/ATP/Ca^{2+} basal levels: As stated previously, basal levels of these ROS/NO/ATP/Ca^{2+} should be established as these components have been repeatedly reported to be increased following LILT, therefore high or low basal levels in differing mouse models, or parameters within a mouse model i.e. age or gender, may determine the therapeutic output of IR1072.

References

Ad, N. and Oron, U. (2001). "Impact of low level laser irradiation on infarct size in the rat following myocardial infarction." Int J Cardiol *80* (2-3): 109-116.

Akaike, A. (1994). "[Glutamate neurotoxicity and neuroprotective factors]." Nippon Yakurigaku Zasshi *103* (5): 193-201.

Akbar, M., Calderon, F., Wen, Z. and Kim, H. Y. (2005). "Docosahexaenoic acid: a positive modulator of Akt signaling in neuronal survival." Proc Natl Acad Sci U S A *102* (31): 10858-10863.

Alexandratou, E., Yova, D., Handris, P., Kletsas, D. and Loukas, S. (2002). "Human fibroblast alterations induced by low power laser irradiation at the single cell level using confocal microscopy." Photochem Photobiol Sci *1* (8): 547-552.

Andera, L. (2009). "Signaling activated by the death receptors of the TNFR family." Biomed Pap Med Fac Univ Palacky Olomouc Czech Repub *153* (3): 173-180.

Ankri, R., Friedman, H., Savion, N., Kotev-Emeth, S., Breitbart, H. and Lubart, R. (2009). "Visible light induces no formation in sperm and endothelial cells." Lasers Surg Med.

Arya, R., Mallik, M. and Lakhotia, S. C. (2007). "Heat shock genes - integrating cell survival and death." J Biosci *32* (3): 595-610.

Barolet, D. (2008). "Light-emitting diodes (LEDs) in dermatology." Semin Cutan Med Surg *27* (4): 227-238.

Barolet, D., Roberge, C. J., Auger, F. A., Boucher, A. and Germain, L. (2009). "Regulation of skin collagen metabolism in vitro using a pulsed 660 nm LED light source: clinical correlation with a single-blinded study." J Invest Dermatol *129* (12): 2751-2759.

Batschauer, A., Ed. (2003). "Photoreceptors and Light Signalling". COMPREHENSIVE SERIES IN PHOTOCHEMISTRY & PHOTOBIOLOGY. Marburg, Germany, The Royal Society of Chemistry.

Beere, H. M. (2004). ""The stress of dying": the role of heat shock proteins in the regulation of apoptosis." J Cell Sci *117* (Pt 13): 2641-2651.

Benes, P., Vetvicka, V. and Fusek, M. (2008). "Cathepsin D--many functions of one aspartic protease." Crit Rev Oncol Hematol *68* (1): 12-28.

Benn, S. C. and Woolf, C. J. (2004). "Adult neuron survival strategies-- slamming on the brakes." Nat Rev Neurosci *5* (9): 686-700.

Bergink, V., van Megen, H. J. and Westenberg, H. G. (2004). "Glutamate and anxiety." Eur Neuropsychopharmacol *14* (3): 175-183.

Berlin, A. L., Hussain, M., Phelps, R. and Goldberg, D. J. (2007). "Treatment of photoaging with a very superficial Er:YAG laser in combination with a broadband light source." J Drugs Dermatol *6* (11): 1114-1118.

Bernardi, P., Scorrano, L., Colonna, R., Petronilli, V. and Di Lisa, F. (1999). "Mitochondria and cell death. Mechanistic aspects and methodological issues." Eur J Biochem *264* (3): 687-701.

Blaya, D. S., Guimaraes, M. B., Pozza, D. H., Weber, J. B. and de Oliveira, M. G. (2008). "Histologic study of the effect of laser therapy on bone repair." J Contemp Dent Pract *9* (6): 41-48.

Bloodgood, B. L. and Sabatini, B. L. (2008). "Regulation of synaptic signalling by postsynaptic, non-glutamate receptor ion channels." J Physiol *586* (6): 1475-1480.

Bradford, A., Barlow, A. and Chazot, P. L. (2005). "Probing the differential effects of infrared light sources IR1072 and IR880 on human lymphocytes: evidence of selective cytoprotection by IR1072." J Photochem Photobiol B *81* (1): 9-14.

Bratic, I. and Trifunovic, A. "Mitochondrial energy metabolism and ageing." Biochimica et Biophysica Acta (BBA) - Bioenergetics *In Press, Uncorrected Proof.*

Bratic, I. and Trifunovic, A. "Mitochondrial energy metabolism and ageing." Biochimica et Biophysica Acta (BBA) - Bioenergetics *In Press, Corrected Proof.*

Brawn, P. R. and Kwong-Hing, A. (2007). "Histologic comparison of light emitting diode phototherapy-treated hydroxyapatite-grafted extraction sockets: a same-mouth case study." Implant Dent *16* (2): 204-211.

Bree, R. T., Stenson-Cox, C., Grealy, M., Byrnes, L., Gorman, A. M. and Samali, A. (2002). "Cellular longevity: role of apoptosis and replicative senescence." Biogerontology *3* (4): 195-206.

Brondon, P., Stadler, I. and Lanzafame, R. J. (2005). "A study of the effects of phototherapy dose interval on photobiomodulation of cell cultures." Lasers Surg Med *36* (5): 409-413.

Brookes, P. S., Levonen, A. L., Shiva, S., Sarti, P. and Darley-Usmar, V. M. (2002). "Mitochondria: regulators of signal transduction by reactive oxygen and nitrogen species." Free Radic Biol Med *33* (6): 755-764.

Burroughs, S. and French, D. (2007). "Depression and anxiety: Role of mitochondria." Current Anaesthesia & Critical Care *18* (1): 34-41.

Byrnes, K. R., Barna, L., Chenault, V. M., Waynant, R. W., Ilev, I. K., Longo, L., Miracco, C., Johnson, B. and Anders, J. J. (2004). "Photobiomodulation improves cutaneous wound healing in an animal model of type II diabetes." Photomed Laser Surg *22* (4): 281-290.

Byrnes, K. R., Waynant, R. W., Ilev, I. K., Wu, X., Barna, L., Smith, K., Heckert, R., Gerst, H. and Anders, J. J. (2005a). "Light promotes regeneration and functional recovery and alters the immune response after spinal cord injury." Lasers Surg Med *36* (3): 171-185.

Byrnes, K. R., Wu, X., Waynant, R. W., Ilev, I. K. and Anders, J. J. (2005b). "Low power laser irradiation alters gene expression of olfactory ensheathing cells in vitro." Lasers Surg Med *37* (2): 161-171.

Calderwood, S. K., Murshid, A. and Prince, T. (2009). "The shock of aging: molecular chaperones and the heat shock response in longevity and aging--a mini-review." Gerontology *55* (5): 550-558.

Campello, A. P., Voss, D. O., Freire, S. A. and Bacila, M. (1964). "The Role Of Citrate On The Respiratory Control Of Isolated Rat Heart Sarcosomes." J Biol Chem *239*: 3842-3846.

Canzoniero, L. M. and Snider, B. J. (2005). "Calcium in Alzheimer's disease pathogenesis: too much, too little or in the wrong place?" J Alzheimers Dis *8* (2): 147-154; discussion 209-115.

Carnevalli, C. M., Soares, C. P., Zangaro, R. A., Pinheiro, A. L. and Silva, N. S. (2003). "Laser light prevents apoptosis in Cho K-1 cell line." J Clin Laser Med Surg *21* (4): 193-196.

Carvalho, A. L., Duarte, C. B. and Carvalho, A. P. (2000). "Regulation of AMPA receptors by phosphorylation." Neurochem Res *25* (9-10): 1245-1255.

Chance, B. and Williams, G. R. (1956). "The respiratory chain and oxidative phosphorylation." Adv Enzymol Relat Subj Biochem *17*: 65-134.

Charney, D. S. and Manji, H. K. (2004). "Life stress, genes, and depression: multiple pathways lead to increased risk and new opportunities for intervention." Sci STKE *2004* (225): re5.

Chazot, P. L., Godukhin, O. V., McDonald, A. and Obrenovitch, T. P. (2002). "Spreading depression-induced preconditioning in the mouse cortex: differential changes in the protein expression of ionotropic nicotinic acetylcholine and glutamate receptors." J Neurochem *83* (5): 1235-1238.

Chen, T. J., Wang, D. C. and Chen, S. S. (2009). "Amyloid-beta interrupts the PI3K-Akt-mTOR signaling pathway that could be involved in brain-derived neurotrophic factor-induced Arc expression in rat cortical neurons." J Neurosci Res *87* (10): 2297-2307.

Chen, X. J., Kovacevic, N., Lobaugh, N. J., Sled, J. G., Henkelman, R. M. and Henderson, J. T. (2006). "Neuroanatomical differences between mouse strains as shown by high-resolution 3D MRI." Neuroimage *29* (1): 99-105.

Chiang, P. K., Lam, M. A. and Luo, Y. (2008). "The many faces of amyloid beta in Alzheimer's disease." Curr Mol Med *8* (6): 580-584.

Choudhry, F., Francis, P. T., Howlett, D. R., Richardson, J. R. C. and Williams, R. J. (2008). "P1-065: Oxidative load regulates amyloid burden in vitro and in vivo in an APP X PS1 transgenic mouse model of Alzheimer's disease." Alzheimer's and Dementia *4* (4, Supplement 1): T225-T225.

Chu, C. T., Levinthal, D. J., Kulich, S. M., Chalovich, E. M. and DeFranco, D. B. (2004). "Oxidative neuronal injury. The dark side of ERK1/2." Eur J Biochem *271* (11): 2060-2066.

Chung, T. Y., Peplow, P. V. and Baxter, G. D. (2009). "Laser Photobiomodulation of Wound Healing in Diabetic and Non-Diabetic Mice: Effects in Splinted and Unsplinted Wounds." Photomed Laser Surg.

Colotti, C., Cavallini, G., Vitale, R. L., Donati, A., Maltinti, M., Del Ry, S., Bergamini, E. and Giannessi, D. (2005). "Effects of aging and anti-aging caloric restrictions on carbonyl and heat shock protein levels and expression." Biogerontology *6* (6): 397-406.

Conley, K. E., Jubrias, S. A., Amara, C. E. and Marcinek, D. J. (2007). "Mitochondrial dysfunction: impact on exercise performance and cellular aging." Exerc Sport Sci Rev *35* (2): 43-49.

Conner, M. W., Conner, B. H., Fox, J. G. and Rogers, A. E. (1983). "Spontaneous Amyloidosis in Outbred CD-1 Mice." Pathology and Immunopathology Research *1* (1-2): 67-78.

Coss, R. A., Sedar, A. W., Sistrun, S. S., Storck, C. W., Wang, P. H. and Wachsberger, P. R. (2002). "Hsp27 protects the cytoskeleton and nucleus from the effects of 42 degrees C at pH 6.7 in CHO cells adapted to growth at pH 6.7." Int J Hyperthermia *18* (3): 216-232.

Cotman, C. W. (2005). "The role of neurotrophins in brain aging: a perspective in honor of Regino Perez-Polo." Neurochem Res *30* (6-7): 877-881.

Croll, S. D., Ip, N. Y., Lindsay, R. M. and Wiegand, S. J. (1998). "Expression of BDNF and trkB as a function of age and cognitive performance." Brain Res *812* (1-2): 200-208.

Datta, S. R., Dudek, H., Tao, X., Masters, S., Fu, H., Gotoh, Y. and Greenberg, M. E. (1997). "Akt Phosphorylation of BAD Couples Survival Signals to the Cell-Intrinsic Death Machinery." Cell *91* (2): 231-241.

de Bock, F., Derijard, B., Dornand, J., Bockaert, J. and Rondouin, G. (1998). "The neuronal death induced by endotoxic shock but not that induced by excitatory amino acids requires TNF-alpha." Eur J Neurosci *10* (10): 3107-3114.

Deriabin, E. I. (1997). "[The effect of noncoherent infrared radiation on the bone tissue reparation of the mandible in an experiment]." Stomatologiia (Mosk) *76* (2): 24-25.

Dougal, G. and Kelly, P. (2001). "A pilot study of treatment of herpes labialis with 1072 nm narrow waveband light." Clin Exp Dermatol *26* (2): 149-154.

Dubois-Dauphin, M., Pfister, Y., Vallet, P. G. and Savioz, A. (2001). "Prevention of apoptotic neuronal death by controlling procaspases? A point of view." Brain Res Brain Res Rev *36* (2-3): 196-203.

Duchen, M. R. (2004). "Roles of mitochondria in health and disease." Diabetes *53 Suppl 1*: S96-102.

Eells, J. T., Henry, M. M., Summerfelt, P., Wong-Riley, M. T., Buchmann, E. V., Kane, M., Whelan, N. T. and Whelan, H. T. (2003). "Therapeutic photobiomodulation for methanol-induced retinal toxicity." Proc Natl Acad Sci U S A *100* (6): 3439-3444.

Eells, J. T., Wong-Riley, M. T., VerHoeve, J., Henry, M., Buchman, E. V., Kane, M. P., Gould, L. J., Das, R., Jett, M., Hodgson, B. D., Margolis, D. and Whelan, H. T. (2004). "Mitochondrial signal transduction in accelerated wound and retinal healing by near-infrared light therapy." Mitochondrion *4* (5-6): 559-567.

Eichler, M., Lavi, R., Shainberg, A. and Lubart, R. (2005). "Flavins are source of visible-light-induced free radical formation in cells." Lasers Surg Med *37* (4): 314-319.

Einat, H., Yuan, P. and Manji, H. K. (2005). "Increased anxiety-like behaviors and mitochondrial dysfunction in mice with targeted mutation of the Bcl-2 gene: further support for the involvement of mitochondrial function in anxiety disorders." Behav Brain Res *165* (2): 172-180.

Engel, K., Ahlers, A., Brach, M. A., Herrmann, F. and Gaestel, M. (1995). "MAPKAP kinase 2 is activated by heat shock and TNF-alpha: in vivo phosphorylation of small heat shock protein results from stimulation of the MAP kinase cascade." J Cell Biochem *57* (2): 321-330.

Engelhardt, J. A., Gries, C. L. and Long, G. G. (1993). "Incidence of spontaneous neoplastic and nonneoplastic lesions in Charles River CD-1 mice varies with breeding origin." Toxicol Pathol *21* (6): 538-541.

Ennaceur, A., Michalikova, S. and Chazot, P. L. (2006a). "Models of anxiety: Responses of rats to novelty in an open space and an enclosed space." Behavioural Brain Research *171* (1): 26-49.

Ennaceur, A., Michalikova, S., van Rensburg, R. and Chazot, P. L. (2006b). "Models of anxiety: responses of mice to novelty and open spaces in a 3D maze." Behav Brain Res *174* (1): 9-38.

Ennaceur, A., Michalikova, S., van Rensburg, R. and Chazot, P. L. (2008). "Detailed analysis of the behavior and memory performance of middle-aged male and female CD-1 mice in a 3D maze." Behav Brain Res *187* (2): 312-326.

Enwemeka, C. S. (2004). "Therapeutic light." Rehab Manag *17* (1): 20-25, 56-27.

Ernster, L. (1993). "P/O ratios--the first fifty years." Faseb J *7* (15): 1520-1524.

Evans, C. G., Wisen, S. and Gestwicki, J. E. (2006). "Heat shock proteins 70 and 90 inhibit early stages of amyloid beta-(1-42) aggregation in vitro." J Biol Chem *281* (44): 33182-33191.

Ferrer, I., Marin, C., Rey, M. J., Ribalta, T., Goutan, E., Blanco, R., Tolosa, E. and Marti, E. (1999). "BDNF and full-length and truncated TrkB expression in Alzheimer disease. Implications in therapeutic strategies." J Neuropathol Exp Neurol *58* (7): 729-739.

Franciosi, S. (2001). "AMPA receptors: potential implications in development and disease." Cell Mol Life Sci *58* (7): 921-930.

Freddo, A. L., Rodrigo, S. M., Massotti, F. P., Etges, A. and de Oliveira, M. G. (2009). "Effect of low-level laser therapy after implantation of poly-L-lactic/polyglycolic acid in the femurs of rats." Lasers Med Sci *24* (5): 721-728.

Frith, C. H. and Chandra, M. (1991). "Incidence, distribution, and morphology of amyloidosis in Charles Rivers CD-1 mice." Toxicol Pathol *19* (2): 123-127.

Frödin, M. and Gammeltoft, S. (1999). "Role and regulation of 90 kDa ribosomal S6 kinase (RSK) in signal transduction." Molecular and Cellular Endocrinology *151* (1-2): 65-77.

Gabai, V. L., Mabuchi, K., Mosser, D. D. and Sherman, M. Y. (2002). "Hsp72 and stress kinase c-jun N-terminal kinase regulate the bid-dependent pathway in tumor necrosis factor-induced apoptosis." Mol Cell Biol *22* (10): 3415-3424.

Gabai, V. L., Meriin, A. B., Yaglom, J. A., Wei, J. Y., Mosser, D. D. and Sherman, M. Y. (2000a). "Suppression of stress kinase JNK is involved in HSP72-mediated protection of myogenic cells from transient energy deprivation. HSP72 alleviates the stewss-induced inhibition of JNK dephosphorylation." J Biol Chem *275* (48): 38088-38094.

Gabai, V. L., Yaglom, J. A., Volloch, V., Meriin, A. B., Force, T., Koutroumanis, M., Massie, B., Mosser, D. D. and Sherman, M. Y. (2000b). "Hsp72-mediated suppression of c-Jun N-terminal kinase is implicated in development of tolerance to caspase-independent cell death." Mol Cell Biol *20* (18): 6826-6836.

Games, D., Adams, D., Alessandrini, R., Barbour, R., Berthelette, P., Blackwell, C., Carr, T., Clemens, J., Donaldson, T., Gillespie, F. and et al. (1995). "Alzheimer-type neuropathology in transgenic mice overexpressing V717F beta-amyloid precursor protein." Nature *373* (6514): 523-527.

Gao, X. and Hu, H. (2008). "Quality control of the proteins associated with neurodegenerative diseases." Acta Biochim Biophys Sin (Shanghai) *40* (7): 612-618.

Gao, X. and Xing, D. (2009). "Molecular mechanisms of cell proliferation induced by low power laser irradiation." J Biomed Sci *16*: 4.

Gavish, L., Perez, L. S., Reissman, P. and Gertz, S. D. (2008). "Irradiation with 780 nm diode laser attenuates inflammatory cytokines but upregulates nitric oxide in lipopolysaccharide-stimulated macrophages: implications for the prevention of aneurysm progression." Lasers Surg Med *40* (5): 371-378.

Gerbi, M. E., Marques, A. M., Ramalho, L. M., Ponzi, E. A., Carvalho, C. M., Santos Rde, C., Oliveira, P. C., Noia, M. and Pinheiro, A. L. (2008). "Infrared laser light further improves bone healing when associated with bone morphogenic proteins: an in vivo study in a rodent model." Photomed Laser Surg *26* (1): 55-60.

Glushkov, O. V., Novoselova, E. G., Cherenkov, D. A., Novoselova, T. V., Khrenov, M. O., Lunin, S. M., Chudnovskii, V. M., Iusupov, V. I. and Fesenko, E. E. (2006). "[Effects of exposure of different skin areas to low-power laser light]." Biofizika *51* (1): 123-135.

Gonzaga Ribeiro, M. A., Cavalcanti de Albuquerque, R. L., Santos Barreto, A. L., Moreno de Oliveira, V. G., Santos, T. B. and Freitas Dantas, C. D. (2009). "Morphological analysis of second-intention wound healing in rats submitted to 16 J/cm 2 lambda 660-nm laser irradiation." Indian J Dent Res *20* (3): 390.

Gooney, M., Messaoudi, E., Maher, F. O., Bramham, C. R. and Lynch, M. A. (2004). "BDNF-induced LTP in dentate gyrus is impaired with age: analysis of changes in cell signaling events." Neurobiol Aging *25* (10): 1323-1331.

Gordon, S. A. and Surrey, K. (1960). "RED AND FAR-RED ACTION ON OXIDATIVE PHOSPHORYLATION." Journal Name: Radiation Research; Journal Volume: Vol: 12; Other Information: Orig. Receipt Date: 31-DEC-60: Medium: X; Size: Pages: 325-339.

Gotoh, T., Terada, K., Oyadomari, S. and Mori, M. (2004). "hsp70-DnaJ chaperone pair prevents nitric oxide- and CHOP-induced apoptosis by inhibiting translocation of Bax to mitochondria." Cell Death Differ *11* (4): 390-402.

Gouras, G. K., Almeida, C. G. and Takahashi, R. H. (2005). "Intraneuronal Abeta accumulation and origin of plaques in Alzheimer's disease." Neurobiol Aging *26* (9): 1235-1244.

Gruys, E., Tooten, P. C. J. and Kuijpers, M. H. M. (1996). "Lung, ileum and heart are predilection sites for AApoAII amyloid deposition in CD-1 Swiss mice used for toxicity studies. Pulmonary amyloid indicates AApoAII." Lab Anim *30* (1): 28-34.

Hahn, G. M. and Li, G. C. (1982). "Thermotolerance and heat shock proteins in mammalian cells." Radiat Res *92* (3): 452-457.

Hallmann, A., Milczarek, R., Lipinski, M., Kossowska, E., Spodnik, J. H., Wozniak, M., Wakabayashi, T. and Klimek, J. (2004). "Fast perinuclear clustering of mitochondria in oxidatively stressed human choriocarcinoma cells." Folia Morphol (Warsz) *63* (4): 407-412.

Hansson, O., Nylandsted, J., Castilho, R. F., Leist, M., Jaattela, M. and Brundin, P. (2003). "Overexpression of heat shock protein 70 in R6/2 Huntington's disease mice has only modest effects on disease progression." Brain Res *970* (1-2): 47-57.

Harazaki, M., Hayakawa, K., Fukui, T., Isshiki, Y. and Powell, L. G. (2001). "The Nd-YAG laser is useful in prevention of dental caries during orthodontic treatment." Bull Tokyo Dent Coll *42* (2): 79-86.

Hargis, M. T., Storck, C. W., Wickstrom, E., Yakubov, L. A., Leeper, D. B. and Coss, R. A. (2004). "Hsp27 anti-sense oligonucleotides sensitize the microtubular cytoskeleton of Chinese hamster ovary cells grown at low pH to 42 degrees C-induced reorganization." Int J Hyperthermia *20* (5): 491-502.

Harman, D. (1956). "Aging: a theory based on free radical and radiation chemistry." J Gerontol *11* (3): 298-300.

Harrison, A. P. and Pierzynowski, S. G. (2008). "Biological effects of 2-oxoglutarate with particular emphasis on the regulation of protein, mineral and lipid absorption/metabolism, muscle performance, kidney function, bone formation and cancerogenesis, all viewed from a healthy ageing perspective state of the art--review article." J Physiol Pharmacol *59 Suppl 1*: 91-106.

Hartung, T., Balls, M., Bardouille, C., Blanck, O., Coecke, S., Gstraunthaler, G. and Lewis, D. (2002). "Good Cell Culture Practice. ECVAM Good Cell Culture Practice Task Force Report 1." Altern Lab Anim *30* (4): 407-414.

Hatayama, T., Yamagishi, N., Minobe, E. and Sakai, K. (2001). "Role of hsp105 in protection against stress-induced apoptosis in neuronal PC12 cells." Biochem Biophys Res Commun *288* (3): 528-534.

Havasi, A., Li, Z., Wang, Z., Martin, J. L., Botla, V., Ruchalski, K., Schwartz, J. H. and Borkan, S. C. (2008). "Hsp27 inhibits Bax activation and apoptosis via a phosphatidylinositol 3-kinase-dependent mechanism." J Biol Chem *283* (18): 12305-12313.

Hawkins, D. H. and Abrahamse, H. (2006). "The role of laser fluence in cell viability, proliferation, and membrane integrity of wounded human skin fibroblasts following helium-neon laser irradiation." Lasers Surg Med *38* (1): 74-83.

Heimbach, J. K., Reznikov, L. L., Calkins, C. M., Robinson, T. N., Dinarello, C. A., Harken, A. H. and Meng, X. (2001). "TNF receptor I is required for induction of macrophage heat shock protein 70." Am J Physiol Cell Physiol *281* (1): C241-247.

Hidalgo, C. (2005). "Cross talk between Ca2+ and redox signalling cascades in muscle and neurons through the combined activation of ryanodine receptors/Ca2+ release channels." Philos Trans R Soc Lond B Biol Sci *360* (1464): 2237-2246.

Holsinger, R. M., Schnarr, J., Henry, P., Castelo, V. T. and Fahnestock, M. (2000). "Quantitation of BDNF mRNA in human parietal cortex by competitive reverse transcription-polymerase chain reaction: decreased levels in Alzheimer's disease." Brain Res Mol Brain Res *76* (2): 347-354.

Howlett, D. R. (2006). "P1-034: Quantification of cortical neurodegeneration in APP X PS1 transgenic mice." Alzheimer's and Dementia *2* (3, Supplement 1): S104-S104.

Howlett, D. R., Bowler, K., Soden, P. E., Riddell, D., Davis, J. B., Richardson, J. C., Burbidge, S. A., Gonzalez, M. I., Irving, E. A., Lawman, A., Miglio, G., Dawson, E. L., Howlett, E. R. and Hussain, I. (2008). "Abeta deposition and related pathology in an APP x PS1 transgenic mouse model of Alzheimer's disease." Histol Histopathol *23* (1): 67-76.

Howlett, D. R., Richardson, J. C., Austin, A., Parsons, A. A., Bate, S. T., Davies, D. C. and Gonzalez, M. I. (2004). "Cognitive correlates of Abeta deposition in male and female mice bearing amyloid precursor protein and presenilin-1 mutant transgenes." Brain Res *1017* (1-2): 130-136.

Hsiao, K., Chapman, P., Nilsen, S., Eckman, C., Harigaya, Y., Younkin, S., Yang, F. and Cole, G. (1996). "Correlative memory deficits, Abeta elevation, and amyloid plaques in transgenic mice." Science *274* (5284): 99-102.

Huang, E. J. and Reichardt, L. F. (2003). "Trk receptors: roles in neuronal signal transduction." Annu Rev Biochem *72*: 609-642.

Huang, H. and Manton, K. G. (2004). "The role of oxidative damage in mitochondria during aging: a review." Front Biosci *9*: 1100-1117.

Huang, Y., Chen, A. and Hamblin, M. (2009). Low-level laser therapy: an emerging clinical paradigm, SPIE Newsroom.

Hubler, R., Blando, E., Gaiao, L., Kreisner, P. E., Post, L. K., Xavier, C. B. and de Oliveira, M. G. (2009). "Effects of low-level laser therapy on bone formed after distraction osteogenesis." Lasers Med Sci.

Huen, N. Y., Wong, S. L. and Chan, H. Y. (2007). "Transcriptional malfunctioning of heat shock protein gene expression in spinocerebellar ataxias." Cerebellum *6* (2): 111-117.

Iijima-Ando, K., Wu, P., Drier, E. A., Iijima, K. and Yin, J. C. (2005). "cAMP-response element-binding protein and heat-shock protein 70 additively suppress polyglutamine-mediated toxicity in Drosophila." Proc Natl Acad Sci U S A *102* (29): 10261-10266.

Ishihara, K., Yamagishi, N., Saito, Y., Adachi, H., Kobayashi, Y., Sobue, G., Ohtsuka, K. and Hatayama, T. (2003). "Hsp105alpha suppresses the aggregation of truncated androgen receptor with expanded CAG repeats and cell toxicity." J Biol Chem *278* (27): 25143-25150.

Johnson, L. N. (2009). "The regulation of protein phosphorylation." Biochem Soc Trans *37* (Pt 4): 627-641.

Kadenbach, B. (2003). "Intrinsic and extrinsic uncoupling of oxidative phosphorylation." Biochim Biophys Acta *1604* (2): 77-94.

Karabudak, O., Dogan, B. and Baloglu, H. (2008). "Histologic evidence of new collagen formation using a Q-switched Nd:YAG laser in periorbital rhytids." J Dermatolog Treat: 1-5.

Karu, T. (1999). "Primary and secondary mechanisms of action of visible to near-IR radiation on cells." J Photochem Photobiol B *49* (1): 1-17.

Karu, T. (2003). Low-Power Laser Therapy, Biomedical Photonics Handbook. *1116:* 1-26.

Karu, T., Pyatibrat, L. and Kalendo, G. (1995). "Irradiation with He-Ne laser increases ATP level in cells cultivated in vitro." J Photochem Photobiol B *27* (3): 219-223.

Karu, T. I. and Kolyakov, S. F. (2005). "Exact action spectra for cellular responses relevant to phototherapy." Photomed Laser Surg *23* (4): 355-361.

Karu, T. I. T., O. A.; Lukpanova, G. G.; Parkhomenko, I. M. (1987). "Effect of irradiation with monochromatic visible light on cAMP content in Chinese hamster fibroblasts." Il Nuovo Cimento D *9* (10): 1245-1251.

Keezer, S. M., Ivie, S. E., Krutzsch, H. C., Tandle, A., Libutti, S. K. and Roberts, D. D. (2003). "Angiogenesis inhibitors target the endothelial cell cytoskeleton through altered regulation of heat shock protein 27 and cofilin." Cancer Res *63* (19): 6405-6412.

Keller, E., Ishihara, H., Nadler, A., Niederer, P., Seifert, B., Yonekawa, Y. and Frei, K. (2002). "Evaluation of brain toxicity following near infrared light exposure after indocyanine green dye injection." J Neurosci Methods *117* (1): 23-31.

Keller, J. M., Escara-Wilke, J. F. and Keller, E. T. (2008). "Heat stress-induced heat shock protein 70 expression is dependent on ERK activation in zebrafish (Danio rerio) cells." Comp Biochem Physiol A Mol Integr Physiol *150* (3): 307-314.

Kennedy, K. M., Rodrigue, K. M., Land, S. J. and Raz, N. (2009). "BDNF Val66Met polymorphism influences age differences in microstructure of the Corpus Callosum." Front Hum Neurosci *3*: 19.

Kent, J. M., Mathew, S. J. and Gorman, J. M. (2002). "Molecular targets in the treatment of anxiety." Biol Psychiatry *52* (10): 1008-1030.

Kolpakova, M. E., Vlasov, T. D., Petrishchev, N. N. and Vislobokov, A. I. (2003). "[Effect of the He-Ne laser irradiation on resistance of the isolated heart to the ischemic and reperfusion injury]." Ross Fiziol Zh Im I M Sechenova *89* (12): 1496-1502.

Konishi, H., Matsuzaki, H., Tanaka, M., Takemura, Y., Kuroda, S., Ono, Y. and Kikkawa, U. (1997). "Activation of protein kinase B (Akt/RAC-protein kinase) by cellular stress and its association with heat shock protein Hsp27." FEBS Lett *410* (2-3): 493-498.

Korzeniewski, B. (2001). "Theoretical studies on the regulation of oxidative phosphorylation in intact tissues." Biochimica et Biophysica Acta (BBA) - Bioenergetics *1504* (1): 31-45.

Kostenko, S. and Moens, U. (2009). "Heat shock protein 27 phosphorylation: kinases, phosphatases, functions and pathology." Cell Mol Life Sci *66* (20): 3289-3307.

Kovacs, I., Lentini, K. M., Ingano, L. M. and Kovacs, D. M. (2006). "Presenilin 1 forms aggresomal deposits in response to heat shock." J Mol Neurosci *29* (1): 9-19.

Kreisler, M., Christoffers, A. B., Willershausen, B. and d'Hoedt, B. (2003a). "Effect of low-level GaAlAs laser irradiation on the proliferation rate of human periodontal ligament fibroblasts: an in vitro study." J Clin Periodontol *30* (4): 353-358.

Kreisler, M., Christoffers, A. B., Willershausen, B. and d'Hoedt, B. (2003b). "Low-level 809 nm GaAlAs laser irradiation increases the proliferation

rate of human laryngeal carcinoma cells in vitro." Lasers Med Sci *18* (2): 100-103.

Lambot, M. A., Peny, M. O., Fayt, I., Haot, J. and Noel, J. C. (2000). "Overexpression of 27-kDa heat shock protein relates to poor histological differentiation in human oesophageal squamous cell carcinoma." Histopathology *36* (4): 326-330.

Laske, C., Stransky, E., Leyhe, T., Eschweiler, G. W., Wittorf, A., Richartz, E., Bartels, M., Buchkremer, G. and Schott, K. (2006). "Stage-dependent BDNF serum concentrations in Alzheimer's disease." J Neural Transm *113* (9): 1217-1224.

Latchman, D. S. (2005). "HSP27 and cell survival in neurones." Int J Hyperthermia *21* (5): 393-402.

Lawrence, M. C., Jivan, A., Shao, C., Duan, L., Goad, D., Zaganjor, E., Osborne, J., McGlynn, K., Stippec, S., Earnest, S., Chen, W. and Cobb, M. H. (2008). "The roles of MAPKs in disease." Cell Res *18* (4): 436-442.

Li, J., Qian, X. and Sha, B. (2009). "Heat shock protein 40: structural studies and their functional implications." Protein Pept Lett *16* (6): 606-612.

Liang, H. L., Whelan, H. T., Eells, J. T., Meng, H., Buchmann, E., Lerch-Gaggl, A. and Wong-Riley, M. (2006). "Photobiomodulation partially rescues visual cortical neurons from cyanide-induced apoptosis." Neuroscience *139* (2): 639-649.

Lim, J., Ali, Z. M., Sanders, R. A., Snyder, A. C., Eells, J. T., Henshel, D. S. and Watkins, J. B., 3rd (2009). "Effects of low-level light therapy on hepatic antioxidant defense in acute and chronic diabetic rats." J Biochem Mol Toxicol *23* (1): 1-8.

Lin, C. H., Chen, P. S. and Gean, P. W. (2008). "Glutamate preconditioning prevents neuronal death induced by combined oxygen-glucose deprivation in cultured cortical neurons." Eur J Pharmacol *589* (1-3): 85-93.

Lipovsky, A., Nitzan, Y. and Lubart, R. (2008). "A possible mechanism for visible light-induced wound healing." Lasers Surg Med *40* (7): 509-514.

Lopes, C. B., Pinheiro, A. L., Sathaiah, S., Da Silva, N. S. and Salgado, M. A. (2007). "Infrared laser photobiomodulation (lambda 830 nm) on bone tissue around dental implants: a Raman spectroscopy and scanning electronic microscopy study in rabbits." Photomed Laser Surg *25* (2): 96-101.

Lowry, O. H., Rosebrough, N. J., Farr, A. L. and Randall, R. J. (1951). "Protein measurement with the Folin phenol reagent." J Biol Chem *193* (1): 265-275.

Luo, G. R., Chen, S. and Le, W. D. (2007). "Are heat shock proteins therapeutic target for Parkinson's disease?" Int J Biol Sci *3* (1): 20-26.

Lynch, G. (2004). "AMPA receptor modulators as cognitive enhancers." Curr Opin Pharmacol *4* (1): 4-11.

Mailhos, C., Howard, M. K. and Latchman, D. S. (1993). "Heat shock protects neuronal cells from programmed cell death by apoptosis." Neuroscience *55* (3): 621-627.

Maiman, T. H. (1960). "Stimulated Optical Radiation in Ruby." Nature *187* (4736): 493-494.

Manabe, T. (2008). "[Molecular mechanisms for memory formation]." Brain Nerve *60* (7): 707-715.

Markham, A., Cameron, I., Franklin, P. and Spedding, M. (2004). "BDNF increases rat brain mitochondrial respiratory coupling at complex I, but not complex II." Eur J Neurosci *20* (5): 1189-1196.

Martin, D., Salinas, M., Lopez-Valdaliso, R., Serrano, E., Recuero, M. and Cuadrado, A. (2001). "Effect of the Alzheimer amyloid fragment Abeta(25-35) on Akt/PKB kinase and survival of PC12 cells." J Neurochem *78* (5): 1000-1008.

Mathew, S. J., Manji, H. K. and Charney, D. S. (2008). "Novel drugs and therapeutic targets for severe mood disorders." Neuropsychopharmacology *33* (9): 2080-2092.

Matrone, C., Ciotti, M. T., Mercanti, D., Marolda, R. and Calissano, P. (2008). "NGF and BDNF signaling control amyloidogenic route and Abeta production in hippocampal neurons." Proc Natl Acad Sci U S A *105* (35): 13139-13144.

Mattson, M. P., Maudsley, S. and Martin, B. (2004a). "BDNF and 5-HT: a dynamic duo in age-related neuronal plasticity and neurodegenerative disorders." Trends Neurosci *27* (10): 589-594.

Mattson, M. P., Maudsley, S. and Martin, B. (2004b). "A neural signaling triumvirate that influences ageing and age-related disease: insulin/IGF-1, BDNF and serotonin." Ageing Res Rev *3* (4): 445-464.

May, L. T. and Hill, S. J. (2008). "ERK phosphorylation: Spatial and temporal regulation by G protein-coupled receptors." The International Journal of Biochemistry & Cell Biology *40* (10): 2013-2017.

Mearow, K. M., Dodge, M. E., Rahimtula, M. and Yegappan, C. (2002). "Stress-mediated signaling in PC12 cells - the role of the small heat shock protein, Hsp27, and Akt in protecting cells from heat stress and nerve growth factor withdrawal." J Neurochem *83* (2): 452-462.

Medrado, A. P., Soares, A. P., Santos, E. T., Reis, S. R. and Andrade, Z. A. (2008). "Influence of laser photobiomodulation upon connective tissue remodeling during wound healing." J Photochem Photobiol B *92* (3): 144-152.

Meireles, G. C., Santos, J. N., Chagas, P. O., Moura, A. P. and Pinheiro, A. L. (2008). "Effectiveness of laser photobiomodulation at 660 or 780 nanometers on the repair of third-degree burns in diabetic rats." Photomed Laser Surg *26* (1): 47-54.

Meirelles, G. C., Santos, J. N., Chagas, P. O., Moura, A. P. and Pinheiro, A. L. (2008). "A comparative study of the effects of laser photobiomodulation on the healing of third-degree burns: a histological study in rats." Photomed Laser Surg *26* (2): 159-166.

Meldrum, B. (1990). "Protection against ischaemic neuronal damage by drugs acting on excitatory neurotransmission." Cerebrovasc Brain Metab Rev *2* (1): 27-57.

Meldrum, B. S. (2000). "Glutamate as a neurotransmitter in the brain: review of physiology and pathology." J Nutr *130* (4S Suppl): 1007S-1015S.

Melquiond, A., Dong, X., Mousseau, N. and Derreumaux, P. (2008). "Role of the region 23-28 in Abeta fibril formation: insights from simulations of the monomers and dimers of Alzheimer's peptides Abeta40 and Abeta42." Curr Alzheimer Res *5* (3): 244-250.

Mese, H., Sasaki, A., Nakayama, S., Yoshioka, N., Yoshihama, Y., Kishimoto, K. and Matsumura, T. (2002). "Prognostic significance of heat shock protein 27 (HSP27) in patients with oral squamous cell carcinoma." Oncol Rep *9* (2): 341-344.

Mester, E., Ludany, G., Selyei, M., Szende, B. and Total, G. J. (1968). "THE STIMULATING EFFECT OF LOW POWER LASER RAYS ON BIOLOGICAL SYSTEMS." Journal Name: Laser Rev., 1: 3(Mar. 1968).; Other Information: Orig. Receipt Date: 31-DEC-69; Bib. Info. Source: UK (United Kingdom (sent to DOE from)): Medium: X.

Mester, E., Spiry, T., Szende, B. and Tota, J. G. (1971). "Effect of laser rays on wound healing." Am J Surg *122* (4): 532-535.

Michalikova, S., Ennaceur, A., van Rensburg, R. and Chazot, P. L. (2008). "Emotional responses and memory performance of middle-aged CD1 mice in a 3D maze: effects of low infrared light." Neurobiol Learn Mem *89* (4): 480-488.

Michalikova, S., van Rensburg, R., Chazot, P. L. and Ennaceur, A. (2009). "Anxiety responses in Balb/c, c57 and CD-1 mice exposed to a novel open space test." Behav Brain Res.

Mitchell, P. (1961). "Coupling of phosphorylation to electron and hydrogen transfer by a chemi-osmotic type of mechanism." Nature *191*: 144-148.

Miura, T. A., Morris, K., Ryan, S., Cook, J. L. and Routes, J. M. (2003). "Adenovirus E1A, not human papillomavirus E7, sensitizes tumor cells to lysis by macrophages through nitric oxide- and TNF-alpha-dependent mechanisms despite up-regulation of 70-kDa heat shock protein." J Immunol *170* (8): 4119-4126.

Mizumori, S. J., Rosenzweig, M. R. and Kermisch, M. G. (1982). "Failure of mice to demonstrate spatial memory in the radial maze." Behav Neural Biol *35* (1): 33-45.

Mochizuki-Oda, N., Kataoka, Y., Cui, Y., Yamada, H., Heya, M. and Awazu, K. (2002). "Effects of near-infra-red laser irradiation on adenosine triphosphate and adenosine diphosphate contents of rat brain tissue." Neurosci Lett *323* (3): 207-210.

Moechars, D., Dewachter, I., Lorent, K., Reverse, D., Baekelandt, V., Naidu, A., Tesseur, I., Spittaels, K., Haute, C. V., Checler, F., Godaux, E., Cordell, B. and Van Leuven, F. (1999). "Early phenotypic changes in transgenic mice that overexpress different mutants of amyloid precursor protein in brain." J Biol Chem *274* (10): 6483-6492.

Mok, S. S., Losic, D., Barrow, C. J., Turner, B. J., Masters, C. L., Martin, L. L. and Small, D. H. (2006). "The beta-amyloid peptide of Alzheimer's disease decreases adhesion of vascular smooth muscle cells to the basement membrane." J Neurochem *96* (1): 53-64.

Morimoto, Y., Arai, T., Kikuchi, M., Nakajima, S. and Nakamura, H. (1994). "Effect of low-intensity argon laser irradiation on mitochondrial respiration." Lasers Surg Med *15* (2): 191-199.

Mosmann, T. (1983). "Rapid colorimetric assay for cellular growth and survival: Application to proliferation and cytotoxicity assays." Journal of Immunological Methods *65* (1-2): 55-63.

Murphy, E., Imahashi, K. and Steenbergen, C. (2005). "Bcl-2 regulation of mitochondrial energetics." Trends Cardiovasc Med *15* (8): 283-290.

Nagappan, G. and Lu, B. (2005). "Activity-dependent modulation of the BDNF receptor TrkB: mechanisms and implications." Trends Neurosci *28* (9): 464-471.

Nakagami, Y. (2004). "Inhibitors beta-amyloid-induced toxicity by modulating the Akt signaling pathway." Drug News Perspect *17* (10): 655-660.

Nicholls, D. G. and Budd, S. L. (2000). "Mitochondria and neuronal survival." Physiol Rev *80* (1): 315-360.

Nicola, R. A., Jorgetti, V., Rigau, J., Pacheco, M. T., dos Reis, L. M. and Zangaro, R. A. (2003). "Effect of low-power GaAlAs laser (660 nm) on bone structure and cell activity: an experimental animal study." Lasers Med Sci *18* (2): 89-94.

Nicoll, W. S., Boshoff, A., Ludewig, M. H., Hennessy, F., Jung, M. and Blatch, G. L. (2006). "Approaches to the isolation and characterization of molecular chaperones." Protein Expression and Purification *46* (1): 1-15.

Nie, K., Yu, J. C., Fu, Y., Cheng, H. Y., Chen, F. Y., Qu, Y. and Han, J. X. (2009). "Age-related decrease in constructive activation of Akt/PKB in SAMP10 hippocampus." Biochem Biophys Res Commun *378* (1): 103-107.

Njemini, R., Lambert, M., Demanet, C. and Mets, T. (2006). "The effect of aging and inflammation on heat shock protein 27 in human monocytes and lymphocytes." Exp Gerontol *41* (3): 312-319.

Novoselova, E. G., Cherenkov, D. A., Glushkova, O. V., Novoselova, T. V., Chudnovskii, V. M., Iusupov, V. I. and Fesenko, E. E. (2006). "[Effect of low-intensity laser radiation (632.8 nm) on immune cells isolated from mice]." Biofizika *51* (3): 509-518.

Oliveira, P. C., Meireles, G. C., dos Santos, N. R., de Carvalho, C. M., de Souza, A. P., dos Santos, J. N. and Pinheiro, A. L. (2008). "The use of light photobiomodulation on the treatment of second-degree burns: a histological study of a rodent model." Photomed Laser Surg *26* (4): 289-299.

Ow, Y. P., Green, D. R., Hao, Z. and Mak, T. W. (2008). "Cytochrome c: functions beyond respiration." Nat Rev Mol Cell Biol *9* (7): 532-542.

Park, H. S., Lee, J. S., Huh, S. H., Seo, J. S. and Choi, E. J. (2001). "Hsp72 functions as a natural inhibitory protein of c-Jun N-terminal kinase." EMBO J *20* (3): 446-456.

Parmigiani, S., Palanza, P., Rogers, J. and Ferrari, P. F. (1999). "Selection, evolution of behavior and animal models in behavioral neuroscience." Neurosci Biobehav Rev *23* (7): 957-969.

Passarella, S., Casamassima, E., Molinari, S., Pastore, D., Quagliariello, E., Catalano, I. M. and Cingolani, A. (1984). "Increase of proton electrochemical potential and ATP synthesis in rat liver mitochondria irradiated in vitro by helium-neon laser." FEBS Lett *175* (1): 95-99.

Pastore, D., Greco, M. and Passarella, S. (2000). "Specific helium-neon laser sensitivity of the purified cytochrome c oxidase." Int J Radiat Biol *76* (6): 863-870.

Paul, C., Manero, F., Gonin, S., Kretz-Remy, C., Virot, S. and Arrigo, A. P. (2002). "Hsp27 as a negative regulator of cytochrome C release." Mol Cell Biol *22* (3): 816-834.

Pereira, A. N., Eduardo Cde, P., Matson, E. and Marques, M. M. (2002). "Effect of low-power laser irradiation on cell growth and procollagen synthesis of cultured fibroblasts." Lasers Surg Med *31* (4): 263-267.

Pinheiro, A. L. and Gerbi, M. E. (2006). "Photoengineering of bone repair processes." Photomed Laser Surg *24* (2): 169-178.

Piotrowicz, R. S., Hickey, E. and Levin, E. G. (1998). "Heat shock protein 27 kDa expression and phosphorylation regulates endothelial cell migration." FASEB J *12* (14): 1481-1490.

Pires Oliveira, D. A., de Oliveira, R. F., Zangaro, R. A. and Soares, C. P. (2008). "Evaluation of low-level laser therapy of osteoblastic cells." Photomed Laser Surg *26* (4): 401-404.

Poon, W. W., Blurton-Jones, M., Tu, C. H., Feinberg, L. M., Chabrier, M. A., Harris, J. W., Jeon, N. L. and Cotman, C. W. (2009). "beta-Amyloid impairs axonal BDNF retrograde trafficking." Neurobiol Aging.

Pugliese, L. S., Medrado, A. P., Reis, S. R. and Andrade Zde, A. (2003). "The influence of low-level laser therapy on biomodulation of collagen and elastic fibers." Pesqui Odontol Bras *17* (4): 307-313.

Ricci, R., Pazos, M. C., Borges, R. E. and Pacheco-Soares, C. (2009). "Biomodulation with low-level laser radiation induces changes in endothelial cell actin filaments and cytoskeletal organization." J Photochem Photobiol B *95* (1): 6-8.

Richardson, J. C., Kendal, C. E., Anderson, R., Priest, F., Gower, E., Soden, P., Gray, R., Topps, S., Howlett, D. R., Lavender, D., Clarke, N. J., Barnes, J. C., Haworth, R., Stewart, M. G. and Rupniak, H. T. (2003). "Ultrastructural and behavioural changes precede amyloid deposition in a transgenic model of Alzheimer's disease." Neuroscience *122* (1): 213-228.

Rogers, D. C., Jones, D. N. C., Nelson, P. R., Jones, C. M., Quilter, C. A., Robinson, T. L. and Hagan, J. J. (1999). "Use of SHIRPA and discriminant analysis to characterise marked differences in the behavioural phenotype of six inbred mouse strains." Behavioural Brain Research *105* (2): 207-217.

Roka, F., Freissmuth, M. and Nanoff, C. (2000). "G protein-dependent signalling and ageing[small star, filled]." Experimental Gerontology *35* (2): 133-143.

Rust, W., Kingsley, K., Petnicki, T., Padmanabhan, S., Carper, S. W. and Plopper, G. E. (1999). "Heat shock protein 27 plays two distinct roles in controlling human breast cancer cell migration on laminin-5." Mol Cell Biol Res Commun *1* (3): 196-202.

Ruttiger, L., Panford-Walsh, R., Schimmang, T., Tan, J., Zimmermann, U., Rohbock, K., Kopschall, I., Limberger, A., Muller, M., Fraenzer, J. T., Cimerman, J. and Knipper, M. (2007). "BDNF mRNA expression and protein localization are changed in age-related hearing loss." Neurobiol Aging *28* (4): 586-601.

Sahara, N., Maeda, S., Yoshiike, Y., Mizoroki, T., Yamashita, S., Murayama, M., Park, J. M., Saito, Y., Murayama, S. and Takashima, A. (2007). "Molecular chaperone-mediated tau protein metabolism counteracts the formation of granular tau oligomers in human brain." J Neurosci Res *85* (14): 3098-3108.

Salvi, M., Brunati, A. M. and Toninello, A. (2005). "Tyrosine phosphorylation in mitochondria: a new frontier in mitochondrial signaling." Free Radic Biol Med *38* (10): 1267-1277.

Samali, A., Cai, J., Zhivotovsky, B., Jones, D. P. and Orrenius, S. (1999). "Presence of a pre-apoptotic complex of pro-caspase-3, Hsp60 and Hsp10 in the mitochondrial fraction of jurkat cells." EMBO J *18* (8): 2040-2048.

Santos, A. E., Carvalho, A. L., Lopes, M. C. and Carvalho, A. P. (2001). "Differential postreceptor signaling events triggered by excitotoxic stimulation of different ionotropic glutamate receptors in retinal neurons." J Neurosci Res *66* (4): 643-655.

Santos, N. R., Dos Santos, J. N., Sobrinho, J. B., Ramalho, L. M., Carvalho, C. M., Soares, L. G. and Pinheiro, A. L. (2009). "Effects of Laser Photobiomodulation on Cutaneous Wounds Treated with Mitomycin C: A Histomorphometric and Histological Study in a Rodent Model." Photomed Laser Surg.

Sato, S., Fujita, N. and Tsuruo, T. (2000). "Modulation of Akt kinase activity by binding to Hsp90." Proc Natl Acad Sci U S A *97* (20): 10832-10837.

Schafer, C., Clapp, P., Welsh, M. J., Benndorf, R. and Williams, J. A. (1999). "HSP27 expression regulates CCK-induced changes of the actin cytoskeleton in CHO-CCK-A cells." Am J Physiol *277* (6 Pt 1): C1032-1043.

Schaffer, M., Bonel, H., Sroka, R., Schaffer, P. M., Busch, M., Reiser, M. and Duhmke, E. (2000a). "Effects of 780 nm diode laser irradiation on blood microcirculation: preliminary findings on time-dependent T1-weighted contrast-enhanced magnetic resonance imaging (MRI)." J Photochem Photobiol B *54* (1): 55-60.

Schaffer, M., Bonel, H., Sroka, R., Schaffer, P. M., Busch, M., Sittek, H., Reiser, M. and Duhmke, E. (2000b). "Magnetic resonance imaging (MRI) controlled outcome of side effects caused by ionizing radiation, treated with 780 nm-diode laser -- preliminary results." J Photochem Photobiol B *59* (1-3): 1-8.

Scheffler, I. E. (2001). "A century of mitochondrial research: achievements and perspectives." Mitochondrion *1* (1): 3-31.

Schloesser, R. J., Huang, J., Klein, P. S. and Manji, H. K. (2007). "Cellular Plasticity Cascades in the Pathophysiology and Treatment of Bipolar Disorder." Neuropsychopharmacology *33* (1): 110-133.

Schmitz, K. J., Lang, H., Wohlschlaeger, J., Sotiropoulos, G. C., Reis, H., Schmid, K. W. and Baba, H. A. (2007). "AKT and ERK1/2 signaling in intrahepatic cholangiocarcinoma." World J Gastroenterol *13* (48): 6470-6477.

Schwartz, J. A., Shetty, A. M., Price, R. E., Stafford, R. J., Wang, J. C., Uthamanthil, R. K., Pham, K., McNichols, R. J., Coleman, C. L. and Payne, J. D. (2009). "Feasibility study of particle-assisted laser ablation of brain tumors in orthotopic canine model." Cancer Res *69* (4): 1659-1667.

Shay, K. P. and Hagen, T. M. (2009). "Age-associated impairment of Akt phosphorylation in primary rat hepatocytes is remediated by alpha-lipoic acid through PI3 kinase, PTEN, and PP2A." Biogerontology *10* (4): 443-456.

Shefer, G., Oron, U., Irintchev, A., Wernig, A. and Halevy, O. (2001). "Skeletal muscle cell activation by low-energy laser irradiation: a role for the MAPK/ERK pathway." J Cell Physiol *187* (1): 73-80.

Sherman, M. Y. and Goldberg, A. L. (2001). "Cellular defenses against unfolded proteins: a cell biologist thinks about neurodegenerative diseases." Neuron *29* (1): 15-32.

Shimura, H., Miura-Shimura, Y. and Kosik, K. S. (2004). "Binding of tau to heat shock protein 27 leads to decreased concentration of hyperphosphorylated tau and enhanced cell survival." J Biol Chem *279* (17): 17957-17962.

Sicaeros, B. and O'Dowd, D. K. (2007). "Preparation of neuronal cultures from midgastrula stage Drosophila embryos." J Vis Exp(5): 226.

Silveira, P. C., Streck, E. L. and Pinho, R. A. (2007). "Evaluation of mitochondrial respiratory chain activity in wound healing by low-level laser therapy." J Photochem Photobiol B *86* (3): 279-282.

Simon, M. M., Reikerstorfer, A., Schwarz, A., Krone, C., Luger, T. A., Jaattela, M. and Schwarz, T. (1995). "Heat shock protein 70 overexpression affects the response to ultraviolet light in murine fibroblasts. Evidence for increased cell viability and suppression of cytokine release." J Clin Invest *95* (3): 926-933.

Sinsimer, K. S., Gratacos, F. M., Knapinska, A. M., Lu, J., Krause, C. D., Wierzbowski, A. V., Maher, L. R., Scrudato, S., Rivera, Y. M., Gupta, S., Turrin, D. K., De La Cruz, M. P., Pestka, S. and Brewer, G. (2008). "Chaperone Hsp27, a novel subunit of AUF1 protein complexes, functions in AU-rich element-mediated mRNA decay." Mol Cell Biol *28* (17): 5223-5237.

Skaper, S. D., Facci, L. and Strijbos, P. J. (2001). "Neuronal protein kinase signaling cascades and excitotoxic cell death." Ann N Y Acad Sci *939*: 11-22.

Sohrabji, F. and Lewis, D. K. (2006). "Estrogen-BDNF interactions: implications for neurodegenerative diseases." Front Neuroendocrinol *27* (4): 404-414.

Sturchler-Pierrat, C., Abramowski, D., Duke, M., Wiederhold, K. H., Mistl, C., Rothacher, S., Ledermann, B., Burki, K., Frey, P., Paganetti, P. A., Waridel, C., Calhoun, M. E., Jucker, M., Probst, A., Staufenbiel, M. and Sommer, B. (1997). "Two amyloid precursor protein transgenic mouse models with Alzheimer disease-like pathology." Proc Natl Acad Sci U S A *94* (24): 13287-13292.

Sunyer, B., An, G., Kang, S. U., Hoger, H. and Lubec, G. (2009). "Strain-dependent hippocampal protein levels of GABA(B)-receptor subunit 2 and NMDA-receptor subunit 1." Neurochem Int *55* (4): 253-256.

Suzuki, T. and Nakaya, T. (2008). "Regulation of amyloid beta-protein precursor by phosphorylation and protein interactions." J Biol Chem *283* (44): 29633-29637.

Svegliati-Baroni, G., Ghiselli, R., Marzioni, M., Alvaro, D., Mocchegiani, F., Saccomanno, S., Sisti, V., Ugili, L., Orlando, F., Alpini, G., Saba, V. and Benedetti, A. (2006). "Estrogens maintain bile duct mass and reduce apoptosis after biliodigestive anastomosis in bile duct ligated rats." J Hepatol *44* (6): 1158-1166.

Sweetman, A. J. and Weetman, D. F. (1969). "Polarographic assay of monoamine oxidase." Br J Pharmacol *37* (2): 550P.

Takahashi-Horiuchi, Y., Sugiyama, K., Sakashita, H. and Amano, O. (2008). "Expression of heat shock protein 27 with the transition from proliferation to differentiation of acinar precursor cell in regenerating submandibular gland of rats." Tohoku J Exp Med *214* (3): 221-230.

Taniguchi, D., Dai, P., Hojo, T., Yamaoka, Y., Kubo, T. and Takamatsu, T. (2009). "Low-energy laser irradiation promotes synovial fibroblast proliferation by modulating p15 subcellular localization." Lasers Surg Med *41* (3): 232-239.

Thinakaran, G. and Koo, E. H. (2008). "Amyloid precursor protein trafficking, processing, and function." J Biol Chem *283* (44): 29615-29619.

Thordarson, G., Semaan, S., Low, C., Ochoa, D., Leong, H., Rajkumar, L., Guzman, R. C., Nandi, S. and Talamantes, F. (2004). "Mammary tumorigenesis in growth hormone deficient spontaneous dwarf rats; effects of hormonal treatments." Breast Cancer Res Treat *87* (3): 277-290.

Tong, L., Balazs, R., Thornton, P. L. and Cotman, C. W. (2004). "Beta-amyloid peptide at sublethal concentrations downregulates brain-derived neurotrophic factor functions in cultured cortical neurons." J Neurosci *24* (30): 6799-6809.

Trautinger, F., Kindas-Mugge, I., Barlan, B., Neuner, P. and Knobler, R. M. (1995). "72-kD heat shock protein is a mediator of resistance to ultraviolet B light." J Invest Dermatol *105* (2): 160-162.

Trelles, M. A. and Allones, I. (2006). "Red light-emitting diode (LED) therapy accelerates wound healing post-blepharoplasty and periocular laser ablative resurfacing." J Cosmet Laser Ther *8* (1): 39-42.

Trounce, I. (2000). "Genetic control of oxidative phosphorylation and experimental models of defects." Hum Reprod *15 Suppl 2*: 18-27.

Ueda, Y. and Shimizu, N. (2003). "Effects of pulse frequency of low-level laser therapy (LLLT) on bone nodule formation in rat calvarial cells." J Clin Laser Med Surg *21* (5): 271-277.

Van Houten, B., Woshner, V. and Santos, J. H. (2006). "Role of mitochondrial DNA in toxic responses to oxidative stress." DNA Repair (Amst) *5* (2): 145-152.

Van Remmen, H. and Richardson, A. (2001). "Oxidative damage to mitochondria and aging." Exp Gerontol *36* (7): 957-968.

van Rensburg, R., Errington, D. R., Ennaceur, A., Lees, G., Obrenovitch, T. P. and Chazot, P. L. (2009). "A new model for the study of high-K(+)-induced preconditioning in cultured neurones: role of N-methyl-d-aspartate and alpha7-nicotinic acetylcholine receptors." J Neurosci Methods *177* (2): 311-316.

Vardy, E. R., Hussain, I. and Hooper, N. M. (2006). "Emerging therapeutics for Alzheimer's disease." Expert Rev Neurother *6* (5): 695-704.

Vekshin, N. L. and Mironov, G. P. (1982). "[Flavin-dependent oxygen uptake in mitochondria under illumination]." Biofizika *27* (3): 537-539.

Vietor, I. and Vilcek, J. (1994). "Pathways of heat shock protein 28 phosphorylation by TNF in human fibroblasts." Lymphokine Cytokine Res *13* (5): 315-323.

Vinck, E. M., Cagnie, B. J., Cornelissen, M. J., Declercq, H. A. and Cambier, D. C. (2003). "Increased fibroblast proliferation induced by light emitting diode and low power laser irradiation." Lasers Med Sci *18* (2): 95-99.

Vladimirov Iu, A., Klebanov, G. I., Borisenko, G. G. and Osipov, A. N. (2004). "[Molecular and cellular mechanisms of the low intensity laser radiation effect]." Biofizika *49* (2): 339-350.

Voss, M. R., Stallone, J. N., Li, M., Cornelussen, R. N. M., Knuefermann, P. and Knowlton, A. A. (2003). "Gender differences in the expression of heat shock proteins: the effect of estrogen." Am J Physiol Heart Circ Physiol *285* (2): H687-692.

Wang, H., Lin, G. and Zhang, Z. (2007). "ATF5 promotes cell survival through transcriptional activation of Hsp27 in H9c2 cells." Cell Biol Int *31* (11): 1309-1315.

Wang, Q. and Bag, J. (2008). "Induction of expression and co-localization of heat shock polypeptides with the polyalanine expansion mutant of poly(A)-binding protein N1 after chemical stress." Biochem Biophys Res Commun *370* (1): 11-15.

Wang, Q., Cao, Z. J. and Bai, X. T. (2005). "[Effect of 900Mhz electromagnetic fields on energy metabolism in postnatal rat cerebral cortical neurons]." Wei Sheng Yan Jiu *34* (2): 155-158.

Wang, X. and Lin, Y. (2008). "Tumor necrosis factor and cancer, buddies or foes?" Acta Pharmacol Sin *29* (11): 1275-1288.

Wang, Z. Q., Wu, D. C., Huang, F. P. and Yang, G. Y. (2004). "Inhibition of MEK/ERK 1/2 pathway reduces pro-inflammatory cytokine interleukin-1 expression in focal cerebral ischemia." Brain Res *996* (1): 55-66.

Wei, W., Wang, X. and Kusiak, J. W. (2002). "Signaling events in amyloid beta-peptide-induced neuronal death and insulin-like growth factor I protection." J Biol Chem *277* (20): 17649-17656.

Whelan, H. T., Connelly, J. F., Hodgson, B. D., Barbeau, L., Post, A. C., Bullard, G., Buchmann, E. V., Kane, M., Whelan, N. T., Warwick, A. and Margolis, D. (2002). "NASA light-emitting diodes for the prevention of oral mucositis in pediatric bone marrow transplant patients." J Clin Laser Med Surg *20* (6): 319-324.

Whelan, H. T., Smits, R. L., Jr., Buchman, E. V., Whelan, N. T., Turner, S. G., Margolis, D. A., Cevenini, V., Stinson, H., Ignatius, R., Martin, T., Cwiklinski, J., Philippi, A. F., Graf, W. R., Hodgson, B., Gould, L., Kane, M., Chen, G. and Caviness, J. (2001). "Effect of NASA light-emitting diode irradiation on wound healing." J Clin Laser Med Surg *19* (6): 305-314.

Wilden, L. and Karthein, R. (1998). "Import of radiation phenomena of electrons and therapeutic low-level laser in regard to the mitochondrial energy transfer." J Clin Laser Med Surg *16* (3): 159-165.

Wilhelmus, M. M., de Waal, R. M. and Verbeek, M. M. (2007). "Heat shock proteins and amateur chaperones in amyloid-Beta accumulation and clearance in Alzheimer's disease." Mol Neurobiol *35* (3): 203-216.

Wong-Riley, M. T., Bai, X., Buchmann, E. and Whelan, H. T. (2001). "Light-emitting diode treatment reverses the effect of TTX on cytochrome oxidase in neurons." Neuroreport *12* (14): 3033-3037.

Yamada, K. (1991). "Biological effects of low power laser irradiation on clonal osteoblastic cells (MC3T3-E1)." Nippon Seikeigeka Gakkai Zasshi *65* (9): 787-799.

Yamashita, H., Kawamata, J., Okawa, K., Kanki, R., Nakamizo, T., Hatayama, T., Yamanaka, K., Takahashi, R. and Shimohama, S. (2007). "Heat-shock protein 105 interacts with and suppresses aggregation of mutant Cu/Zn superoxide dismutase: clues to a possible strategy for treating ALS." J Neurochem *102* (5): 1497-1505.

Yeager, R. L., Franzosa, J. A., Millsap, D. S., Angell-Yeager, J. L., Heise, S. S., Wakhungu, P., Lim, J., Whelan, H. T., Eells, J. T. and Henshel, D. S. (2005). "Effects of 670-nm phototherapy on development." Photomed Laser Surg *23* (3): 268-272.

Yeager, R. L., Franzosa, J. A., Millsap, D. S., Lim, J., Hansen, C. M., Jasevicius, A. V., Heise, S. S., Wakhungu, P., Whelan, H. T., Eells, J. T. and Henshel, D. S. (2006a). "Brief report: embryonic growth and hatching implications of developmental 670-nm phototherapy and dioxin co-exposure." Photomed Laser Surg *24* (3): 410-413.

Yeager, R. L., Franzosa, J. A., Millsap, D. S., Lim, J., Heise, S. S., Wakhungu, P., Whelan, H. T., Eells, J. T. and Henshel, D. S. (2006b). "Survivorship and mortality implications of developmental 670-nm phototherapy: dioxin co-exposure." Photomed Laser Surg *24* (1): 29-32.

Yeager, R. L., Lim, J., Millsap, D. S., Jasevicius, A. V., Sanders, R. A., Whelan, H. T., Watkins, J. B., 3rd, Eells, J. T. and Henshel, D. S. (2006c). "670 nanometer light treatment attenuates dioxin toxicity in the developing chick embryo." J Biochem Mol Toxicol *20* (6): 271-278.

Yenari, M. A. (2002). "Heat shock proteins and neuroprotection." Adv Exp Med Biol *513*: 281-299.

Ying, R., Liang, H. L., Whelan, H. T., Eells, J. T. and Wong-Riley, M. T. (2008). "Pretreatment with near-infrared light via light-emitting diode provides added benefit against rotenone- and MPP+-induced neurotoxicity." Brain Res *1243*: 167-173.

Young, A. E., Germon, T. J., Barnett, N. J., Manara, A. R. and Nelson, R. J. (2000). "Behaviour of near-infrared light in the adult human head: implications for clinical near-infrared spectroscopy." Br J Anaesth *84* (1): 38-42.

Yu, W., Chi, L. H., Naim, J. O. and Lanzafame, R. J. (1997a). "Improvement of host response to sepsis by photobiomodulation." Lasers Surg Med *21* (3): 262-268.

Yu, W., Naim, J. O. and Lanzafame, R. J. (1997b). "Effects of photostimulation on wound healing in diabetic mice." Lasers Surg Med *20* (1): 56-63.

Zezell, D. M., Boari, H. G., Ana, P. A., Eduardo Cde, P. and Powell, G. L. (2009). "Nd:YAG laser in caries prevention: a clinical trial." Lasers Surg Med *41* (1): 31-35.

Zhang, R., Mio, Y., Pratt, P. F., Lohr, N., Warltier, D. C., Whelan, H. T., Zhu, D., Jacobs, E. R., Medhora, M. and Bienengraeber, M. (2009). "Near infrared light protects cardiomyocytes from hypoxia and reoxygenation injury by a nitric oxide dependent mechanism." J Mol Cell Cardiol *46* (1): 4-14.

Zhao, W. Q., Ravindranath, L., Mohamed, A. S., Zohar, O., Chen, G. H., Lyketsos, C. G., Etcheberrigaray, R. and Alkon, D. L. (2002). "MAP kinase signaling cascade dysfunction specific to Alzheimer's disease in fibroblasts." Neurobiol Dis *11* (1): 166-183.

Zhou, X., Tron, V. A., Li, G. and Trotter, M. J. (1998). "Heat shock transcription factor-1 regulates heat shock protein-72 expression in human keratinocytes exposed to ultraviolet B light." J Invest Dermatol *111* (2): 194-198.

Zhu, Y., O'Neill, S., Saklatvala, J., Tassi, L. and Mendelsohn, M. E. (1994). "Phosphorylated HSP27 associates with the activation-dependent cytoskeleton in human platelets." Blood *84* (11): 3715-3723.

Zubkova, S. M., Mikhailik, L. V. and Chabanenko, S. S. (1995). "[The stress-limiting action of pulsed infrared laser radiation]." Vopr Kurortol Fizioter Lech Fiz Kult(1): 3-4.

Zungu, I. L., Hawkins Evans, D. and Abrahamse, H. (2009). "Mitochondrial responses of normal and injured human skin fibroblasts following low level laser irradiation--an in vitro study." Photochem Photobiol *85* (4): 987-996.

}